Probing 2D Materials using Capacitance Measurements

A Thesis submitted for the Degree of

Master of Technology

by

Akshay Patil
Quantum Technology
Indian Institute of Science

Under the Guidance of,

Prof. Chandni Usha

Department of Instrumentation and Applied Physics

Indian Institute Of Science
BANGALORE - 560012
July 2023

Declaration

I hereby declare that the work presented in this thesis titled Project title, is the result of the investigations carried out by me under the supervision of Prof. Chandni Usha at the Department of Instrumentation and Applied Physics, Indian Institute of Science, Bangalore, India, and that it has not been submitted elsewhere for the conferment of any degree or diploma of any Institute or University. Keeping with the general practice, due acknowledgements have been made wherever the work described is based on other investigations.

Akshay Patil
July 2023

Department of Instrumentation and Applied Physics,
Indian Institute of Science,
Bangalore-560012,
India.

Publications Based on this Thesis

High Possibilities in the Future...

Acknowledgements

Many thanks to my Project advisor Dr.Chandni Usha for offering me a project to work on knowing that I only had six months to work on this project and believing in me that I will be able to pull it off and guiding me.Thanks to my lab mates Satyarth S who introduced and helped me with my first transfer process in the Nano-scale Lab, Suvronil Dutta for fabricating the devices of the samples in CENSE and Physics Department,IISc and also helped me in exfoliation process of graphene and hBN and making of PPC,Pragya for guiding me with her experience on plasma cleaning and exfoliation processes,Radhika Soni for some helpful discussions and sharing her experience related to transfer process and other in lab processes,Saisab for helping with Measurement process in cryocan,Prabhat for having some cheerful discussions and Mrutunjay for his experienced opinions on contrast changes of the flakes of hBN and Graphene with its thickness on microscope.I would like to thank my batch-mates,colleagues Anurag, Avinash, Rajiv, Uday, Naipunnya, Sukhsagar , Chaitali and Vivek, Sacheet, Pavan, Vishal, Sibi, Sangeet, Vaishnav, Jacob, Kishore ,PD block and many more (the list can go on but would like to stop it here) for making this 1.5 years stay pleasant and helped me at some point or another at IISc.

I also would like to thank me for always believing in myself and moving forward.Lastly,but most importantly I would like to thank my family i.e my parents and my brother without them and their constant support and encouraging I wouldn't be here today.

Abstract

2D materials holds exciting electronic,mechanical,optical properties as opposed to their 3D counter parts.They can potentially help us realize the fascinating phenomenon that physicists have been dreaming since at least a decade such as Superconductivity at Room Temperature and Room Pressure,Quantum Computing of more than 70 Logical Qubits,Negative Quantum Capacitance,Quantum Memory Devices and many other applications based on the outstanding world of phenomenons such as Magnetism (orbital and Spin),Spin Orbit Coupling and Quantum Hall Effect,Quantum Anamolous Hall Effect,Quantum Spin Hall Effect,Co-related,Mott Insulators,Topological Insulators,Fractional Chern Insulators,Charge Density Wave Fluctuations,Nemacity,Pomeranchuk Effect etc. they show electrically ! But to realize these epitomes practically we will have to probe these 2D materials and extract out the physical quantities that make us understand how these 2D materials behave electrically.

In this thesis we will probe the in plane resistance of the 2D material for applied transverse electric field from which we will extract out the quantum capacitance of the 2D material and discuss a universal simple novel approach for the same.First we will begin with introduction of the 2D materials in which we will discuss a road-map of how we can realize the dreamy outlooks practically,followed by learning to characterize these 2D materials using microscopy techniques to get more optical,Band-diagram,surface and volume defects etc,insights on 2D material,then discuss a universal simple and novel procedure to extract out the quantum capacitance from the 2D material and then extraction of close to 15 quantities which can help one to completely characterize/parameterize the electron transport in 2D material,moving forward to how to make these hetero-structure consisting of dielectric-2D material-dielectric sandwich on Si-SiO_2 substrate and on to it's fabrication to take electrical contacts out and finally the general analysis and measurements of this van der waal Hetero-structure.

Hope this will be a fun read for all users/readers! Enjoy!

Contents

List Of Figures

Keywords

Quantum Capacitance,Van Der Waal Heterostructure,2D material

Notations And Abbrevations

Wherever notations are used in this document its meaning is clearly explained there itself. Again same goes for abbreviations.

And I have used we,our as a pronoun to include the reader who will read the thesis just to make him feel inclusive while reading,but wherever credits are due to my lab-mates I have given them,so the we here mostly means the work done in thesis by me.

Chapter 1

Introduction of 2D materials

1.1 Introduction

The field of 2D material first boomed with the exfoliation of graphene in year 2004 which was previously thought not possible due to unstability of 2D materials at ambient conditions. So let's begin out thesis with introduction of this 2D material - Graphene.

Now, In graphene the carbon atom undergoes sp_2 hybridization i.e it's 2s orbital wave function and $2p_x$ and $2p_y$ orbital wave-functions undergo intermixing to form a sp_2 hybridization and leaving the $2p_z$ orbital wave-function unhybridized. Now the 2s shell in ground state of carbon atom's sp_2 hybridization contains 2 electrons in spin up and spin down state as per the Pauli-Exclusion principle and then p_x and p_y as per Hund's Rule of filling after sp_2 hybridization should both contain one spin up electron each i.e the electronic configuration of the carbon atom after sp_2 hybridization is $1s^2\,|\uparrow\downarrow\rangle$,$2sp_2^2\,|\uparrow\downarrow\rangle$,$2sp_2^1\,|\uparrow\rangle$,$2sp_2^1\,|\uparrow\rangle$,$2p_z^0$. But for sp_2 hybridization of carbon atom to form 3 sigma in plane bonds to form graphene mono-layer ,all the three sp_2 hybridizations should have only one electron each so that it can form sigma bond with neighbouring carbon by sharing one electron each to fill the sp_2 orbital and hence this bonding is only possible when the carbon atom's sp_2 hybridization is in excited state,so one can conclude that the carbon's sp_2 hybridization's excited state's in plane sigma bonds is the ground state of the graphene carbon atom. Therefore the graphene carbon atom's ground state is, $1s^2\,|\uparrow\downarrow\rangle$,$2sp_2^1\,|\uparrow\rangle$,$2sp_2^1\,|\uparrow\rangle$,$2sp_2^1\,|\uparrow\rangle$,$2p_z^1\,|\uparrow\rangle$.The one electron from the unhybridized p_z orbital is responsible for the conduction via electron transport in graphene.

Now moving to Band structure of graphene, We know from special relativity (1905) $E = mc^2$ and therefore a relativistic particle moving with a velocity $V \leq C$ is E=c$\sqrt{p^2 + (mc)^2}$. For V=C and m=0, E=pc.

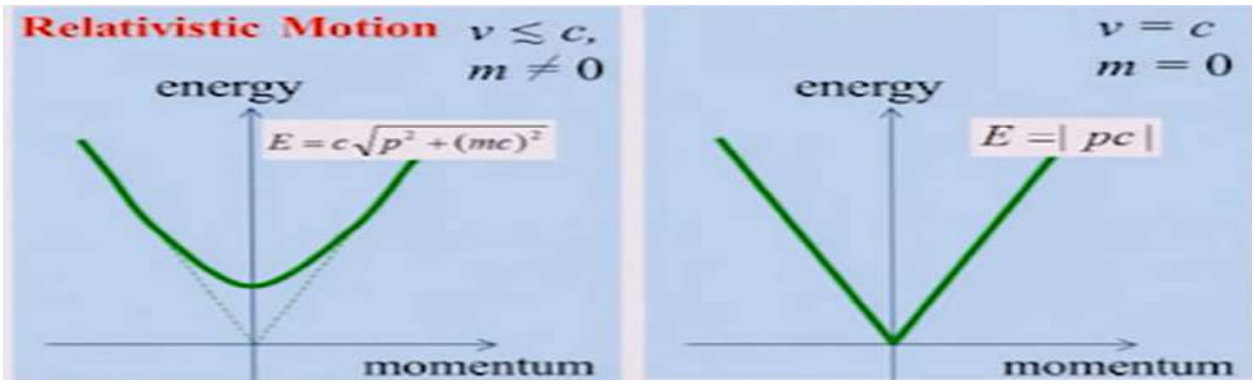

Figure 1.1: Relativistic Energy vs Momentum Diagram [3]

Now from Schrodinger Equation (1926) we know

i$\hbar \frac{\partial \psi}{\partial t}$= -$\frac{\hbar^2}{2m} \bigtriangledown^2 \psi$ + Vψ

Paul Dirac combined the Quantum Mechanics given by SE and Relativistic Physics given by Einstein to give Relativistic Quantum Mechanics.Now,Graphene's band structure follows relativistic Quantum Mechanics mathematics despite not having velocity of electrons in graphene equal to speed of light(2-3 percent of speed of light) as the effective mass of electron is considered to be zero in graphene.Hence the term used when Relativistic Quantum Mechanics is applied to charge carriers in Graphene is Quasi Relativistic Quantum Mechanics. Now the dirac equation is

(i$\gamma^\mu \frac{\partial}{\partial \mu}$ - m)$\psi = 0$

Dirac's Equation in 2D for massless particles is,

H$\psi = E\psi$

$\hbar$v$_f \bar{k}.\bar{\sigma} \begin{bmatrix} \alpha_k \\ \beta_k \end{bmatrix} = E\bar{(k)} \begin{bmatrix} \alpha_k \\ \beta_k \end{bmatrix}$

E > 0 are solutions of Conduction Band and E < 0 are solutions of Valence Band.

Also other ways to find transport Hamiltonian are nearest neighbour hopping,Hatree Fock Method etc.

Relativistic Electrons (or Fermions) are chiral i.e electron spin becomes parallel to momentum as shown in the figure below.

Note-The chirality of electron wavefunctions in graphene reduces the back scattering of electrons when incident on a barries to zero i.e the tunnelling transmission coefficient is 100 % for electrons in Graphene .The solutions of Dirac equations follows a linear dispersion relation with zero band gap,such a cone formed is known as Dirac Cone. Graphene as follows the same maths as relativistic Quantum Mechanics has the same band structure with no band gap with conduction band and valence band intersecting at dirac point at 6 different point at zero/ground energy level as shown in figure below.

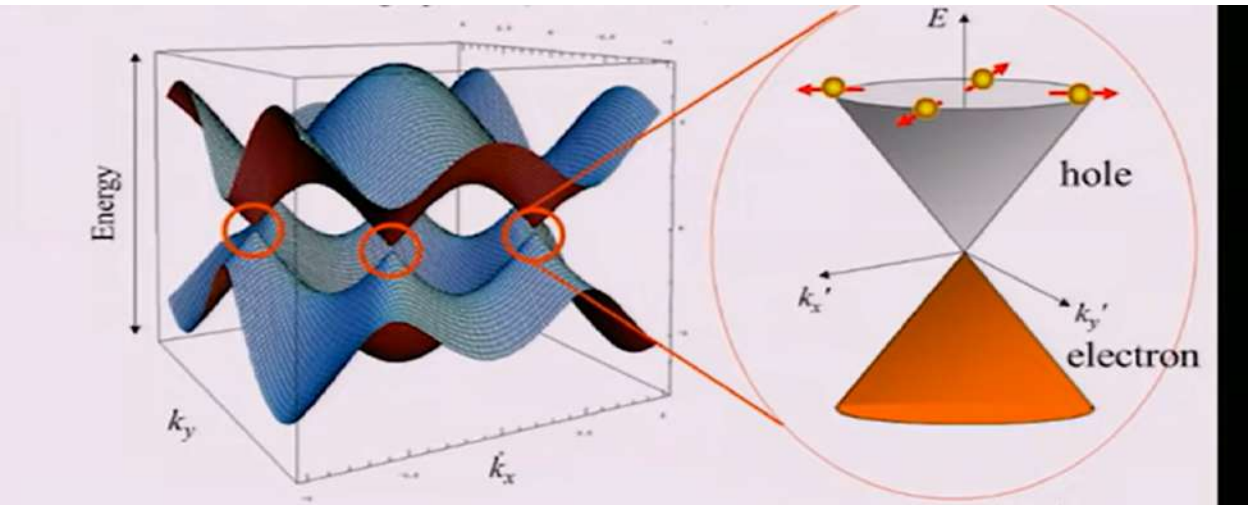

Figure 1.2: Graphene Band Structure And Dirac Cone [3]

Graphite is a 3D bulk material having parabolic dispersion relation whereas Graphene is a 2D bulk material having linear dispersion relation.

Fermions (electrons) in Graphene has to turn twice in the orbit before it comes back to its own original spin as the orbit the electron follows is like a mobius strip.

Figure 1.3: Mobius strip [3]

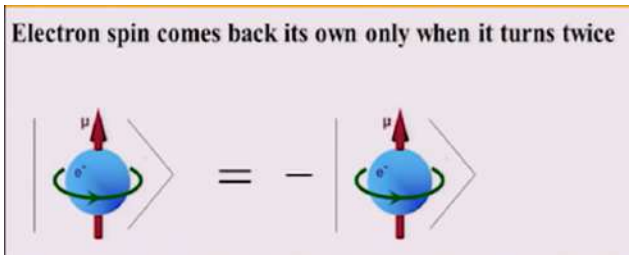

Figure 1.4: Negative Global Phase Factor After 1 rotation of electron in mobius Strip[3]

There are two spin degeneracies(spin up and spin down) due to electrons and two valley degeneracies(k and $k^{'}$) as the reciprocal lattice vector cannot trace the whole graphene unit cell in one go i.e different reciprocal lattice vectors are needed and hence the two valleys whose electrons cannot hop inter-valley during transport.The unit cell of Graphene is hexagonal in shape i.e Lattice structure is hexagonal with 3 corners having spin up configuration of electron i.e the sublattice A and remaining 3 corners having spin down configuration of electron i.e the sublattices B. Hence the maximum doping/removal of electrons allowed in Graphene is 4 electrons.

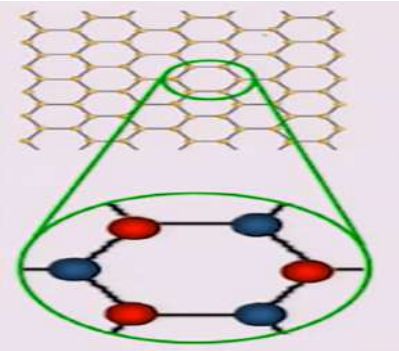

Figure 1.5: Graphene Hexagonal Lattice [3]

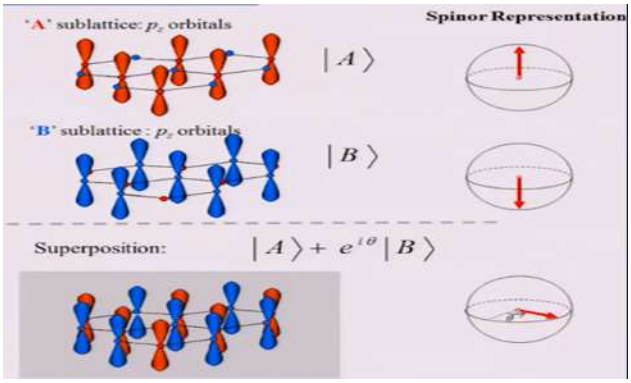

Figure 1.6: A and B sublattices in Graphene [3]

Now let us consider some important properties of Graphene,

1.High Speed Graphene Electrons-

Graphene is a semiconductor that gives the best electron mobility of around 70000 cm^2 per sec

2.Optically Almost Transparent-

Graphene is optically almost transparent as it is one atomic layer thick i.e T $\approx 100\%$

3.Mechanical Properties of Graphene-

1.Young's Modulus of Graphene = 1 TPa (very high stiffness as steel has Young's Modulus nearly equal to 0.2 TPa)

2.Lateral Strain = 25%

Graphene has many applications in Semiconductor Industries,Printable Inks,Composites,Heat Discipation,etc with a main one being transparent screen mobile or laptop which is yet to be launched in the market.

Now if stack monolayer of graphene on top of monolayer of graphene we get a bilayer graphene which depending the stacking order can be A-A or A-B stacking,and if we twist the two monolayers on top of each other then we a structure that is repeated over larger periods known as the moire patterns which opens a pathway to fascinating physical phenomenons observed in Twisted Bilayer Graphene as Superconductivity,Magnetism (orbital and Spin),Spin Orbit Coupling and Quantum Hall Effect,Corelated,Mott Insulators,Topological Insulators,Fractional Chern Insulators,Charge Density Wave Fluctuations,Nemacity,Pomeranchuk Effect, Many Body Interactions effect etc. with etc indicating more to be explored.

Monolayers of Graphene can be created by using exfoliation techniques,CVD's and plethora of other techniques.These layers can teared and pickup'd using dry transfer techniques and then twisted to create a twisted Bilayer graphene of required angles.More details on this are explained in the later chapter 4 of this thesis.

1.2 Possible Applications/Outlooks/Impacts In Quantum Technologies

1.2.1 Superconductivity At Room Temperature and Room Pressure Mathematical Machine Learning Model and then above Room Temperature Superconductivity - (my own original Idea and Work)

Superconductivity at Room Temperature was,is,will be a dream of almost every physicist when it first came in to existence by discovery of Dutch physicist Heike Kamerlingh Onnes's in mercury in 1911 by cooling it to near zero Kelvin temperature by using Helium gas as a refrigerent. Superconductivity at room temperature using my idea will at least take a 5 years worth time i.e a full time duration research of PhD student,so I will just discuss the road-map that one can take to achieve this.Superconductivity is phenomenon in which the resistance of the material becomes zero and hence there is no power discipation from the material i.e the current once passed through it can flow for infinite amount of time which can also be characterized by Meissner effect i.e a superconductor does not allow magnetic field to pass through it,i.e a superconductor levitates on the magnet ,a concept on which the Maglaev Bullet trains are based on.Superconductivity in material can be described by electron forming an attractive pair with another electron via a intermediate quasi-particle mediation ,if the mediatory particle responsible for e-e pair formation is phonon then this phenomenon is conventional superconductivity and can be explained by BCS theory. If the mediatory particle is other than phonon than we can categorize it as unconventional superconductor.So if we define a Hamiltonian to get the idea of the electron pair formation and flow pattern by nearest neighbour hopping we will require 4 operators in a single term i.e 2 creation,2 anhilation operators of the electron pair.The exact solving of this equation is computationally impossible for now but can be approximated by density mean field theory to give an approximate value of the 4 elements of the two by two matrix through which the superconductivity in the material can be characterized completely.But in case of unconventional superconductors density mean field approximation does not give in good results and are deviated from required results. So this is where my idea comes in, to identify the weak dependent parameters of known pristine materials,elements,compounds that affect the superconductivity in the materials. A naive set of parameters would be atomic weight of material,atomic number,Fermi Energy,Band Structure,number of free electrons available for conduction,Lattice Constant of material,Resistance of material,Scattering Mechanisms,Mean Free Path,Symmetry breakings,Phase Transitions,chemical composition of the material (for compounds) etc.The point here is that Superconductivity in material as it is material property should be weakly or strongly dependent on the material properties/constants/quantities that physically,chemically,atomically describe a material and one should be able to completely define it with use of these parameters though a physics mathematical model for same will be so complex that it is not available till date.So the first step of the road map is to identify these common parameters by reviewing each material,each element in the periodic table,every compound,2D material that shows superconductivity at specific temperature and specific pressures.This will not be an easy task as one should carefully review every research paper/article/video published till date on superconductivity for every material/element/compound/2D material to identify/interpret/deduce/intuit these

weak dependent parameters of material on which the superconductivity depends.The accuracy of the machine learning model will depend on exact identification of these parameters (more parameters one can exactly identify the better the accuracy of prediction by machine learning model will be).Once the identification of these set of parameters is done the next step will be quantification i.e assigning a mathematical number value to every parameter if it doesn't have one already. So these parameters will be our constant values for a particular material , and the temperature and pressure will be the variable quantities but for particular material it will be its critical temperature and pressure and can be considered as constant.The number of materials known to show superconductivity are in hundreds hence we will have at least have 100 sets of these parameters. Now second step is to apply supervised machine learning model that through mathematical nonlinear relations can identify in background(will not be known to us) the dependence of these parameters on the critical temperature and pressure below which material shows superconductivity.The role of the machine learning model will be to give us these parameters for a material at room temperature and pressure by performing background nonlinear mathematical relationship of these parameters with temperature and pressure .Once we get these parameters the next step is to research whether it is possible to (chemically/mechanically or any process) synthesize such a material capable of realizing these parameters or looking if already known materials have the potential of realizing these parameters.If it is possible to synthesize then there you have it a room temperature and room pressure superconductor.The main work and accuracy of this model is to carefully identify the weak and the strong parameters exactly of material on which superconductivity depends.Even if we don't observe it in one cycle of process one can study the synthesized material and reverse engineer to further understand the physics and identify and update the set of parameters again. To achieve this model one will require in detail knowledge of solid state/condensed matter physics,quantum mechanics, and superconductivity in particular, basic chemistry,basic machine learning,Material Science and a good intuition.

Why it relates to this work?

This outlook is discussed here as TBG is one of the unconventional superconductors and can form one set of parameters for our research .I strongly believe that someone in our generation will synthesize,discover the superconductor at room temperature and room pressure.

Also the ballistic transport in Graphene is shown to exceed 10 μm at room temperature i.e the electron transport regime in which the scattering is null i.e resistance of the 2D material is zero which be probed by Quantum Capacitance measurements in 2D materials.

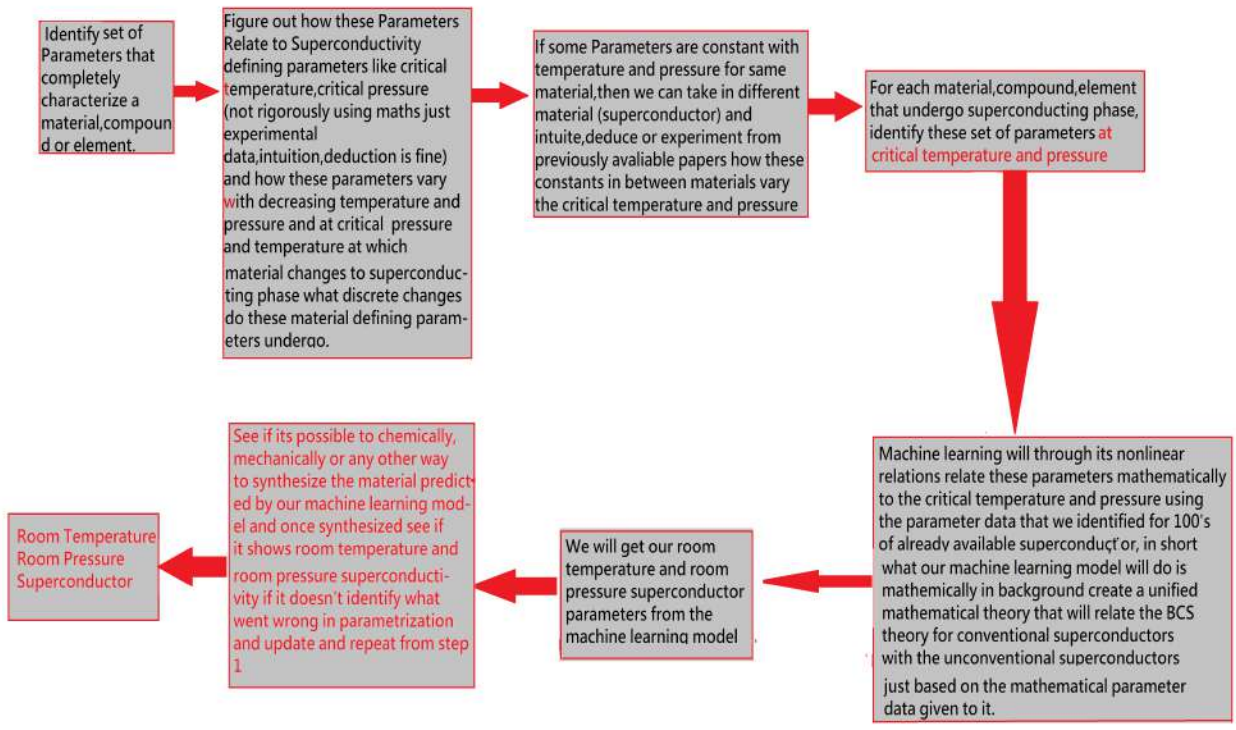

Figure 1.7: Road-Map to Room Temperature and Room Pressure Superconductivity

1.2.2 Quantum Circuit and Computing In Graphene Nano-ribbons at Room Temperature due to its Long Range Ballistic Transport Regime and realizing a Quantum Computer capable of Performing a task equivalent of at least 70 Logical Qubits (Equivalent Power of Classical Computer) and then further scaling it up to more logical Qubits.

I would like to discuss a road map of realizing scaled quantum computing using 2D materials ,in particular graphene.Before going in to that let's discuss what is mean free path of an electron.Again this is my road-map for scaling the 2D material's application in quantum computing, depending on the understanding of the hardware I have till now so can be tweaked a little as per one's understanding and as the field further progresses.So as per my understanding mean free path is the length, the electron can hop into or travel in a material without being backscattered,i.e without changing it's direction by doing a 180 degree out flip from the direction which it travelling earlier in.As calculated in later sections the maximum mean free path for graphene is in the range of few micrometer i.e 5 μm at low temperatures by the calculations discussed here in the thesis.So we call this region in which there is no backscattering of the electron during its transport as ballistic transport regime.So theoretically in this regime there is no resistance to flow of electrons i.e it graphene behaves as a no resistance material.This concept of ballistic transport in graphene can be used for realizing Quantum Circuits in graphene,we just have to scale down the graphene's electron transport to 1D i.e minimizing its width so that it can have only one hexagonal Lattice

perpendicular to transport i.e width in the orders of lattice constant of graphene.So as we already are aware of, that this electron transporting will have a particular wavefunction associated with it that can be represented as zero or one state.So if we pass a current through this nano-ribbon then it will generate a transport wave-function for a input length.Then what we require is a Y shaped distributor of nano-ribbon acting as a beam splitter in case of photonic computing that will split the electrons in to two channels let's say zero and one state,depending on the length and width of the channel we can modulate the amplitude probability of these states and later unify the two channels in to one bridge of length $L_{interference}$ and $W_{interference}$ which facilitates the interference between the two wave-functions of the electrons and we get a superposed state of zero and one.If the length and width of the two Y channels is equal and the interfering bridge length and width is adjusted accordingly we can get a Hadamard superposed state out of this i.e having equal superposition of zero and one at the end.This one gate can amount to a length of 20 to 30 nm and this will form a single qubit line.So using similar technique by adjusting the width and the length of the Y channel and the bridge ,we can construct a set of universal Quantum gates of Pauli Rotation gates,Hadamard Gate,CNOT gate and T gate through which we can construct by approximation any quantum algorithm that can be thought of.But the depth of the circuit i.e the number of circuit one can construct along it's length is limited to mean free path of graphene for single qubit line (let's call it one graphene cell box) i.e in orders of micrometer. So the depth we can go upto will amount for approximately 250 quantum gates in total before the backscattering in graphene starts which essentially means loss of the coherence of the electron wave-function.So this is where we can introduce a quantum memory/quantum repeater that stores the probability amplitude of the state by a physical phenomenon of energy fluctuations in atomic state of the quantum repeater that stores it at the end of one mean free path of single qubit line and then produces the state at the start of the first qubit line which will again start with fresh coherence length start from zero to mean free path of the next graphene cell box (for example graphene nano-drums or quantum memory devices from TBG's).So this system can be physically repeated up to required depth of the quantum algorithm in principle.Similarly we can construct as many of the qubit lines we want at a in plane transverse distance from this qubit line.A physical qubit as in this case the electron transport in graphene nanoribbon can deviate from the actual quantum state due to discrepencies in fabrication,external noise,measurement errors,state preparation errors etc.So we should repeat these physical qubits until we get a sufficient repeatitions of required circuit i.e the so called quantum error correction,1 Logical qubit i.e error free quantum computation of the state essentially amounts to 1000's of physical qubits computation whose clustering can amount to one qubit line of logical error free computations.So let's say we want a qubit lines of 200 logical qubits i.e we will require at least 200000 physical qubit lines i.e 200000* [40 nm (width of single qubit line) + 20 nm](extra distance if required for constructing C-Not gate for example in between two qubit lines) = 12mm length so whole of the error corrected quantum computer for that particular algorithm will be just a 12 mm Width by L(Length depending of the number of graphene ballistic cells and the length of quantum repeator/memory + the length of the readout (1 graphene ballistic cell is equal to 250 quantum gates) you want as per the depth of the circuit) which will again be not more than 100 mm so that's a pretty small chip capable of performing a single quantum algorithm capable of performing computations greater than the number of atoms in the universe that is $2^{\text{the size of the logical qubits (200)}}$.So if we consider all the quan-

tum algorithms available in theory, the whole of these chips can be not more than a 1000 cm's.The only problem which this computation is we have to hard fabricate the circuit and we cannot tune it electrically,so if you want to make changes in the circuit one will have to hard fabricate it again from scratch.The remaining concerns are the fidelities of the quantum repeators,read out and the fabrication errors.Getting to fabricate/sythesize such systems will require atomic level precision which the nano-scale industry is lacking at the moment as far as I know and hence if we try to construct/fabricate these ribbons with present fabrication techniques it will affect the fidelities of these circuits.

If one wants to dwelve more in to how to physically realize a single quantum gate as that's where this field is now then one can refer [1,2].Also one can begin with classical simulations of these circuits to tweak around and see how these circuits behave under varying depth and width of the Y channel.

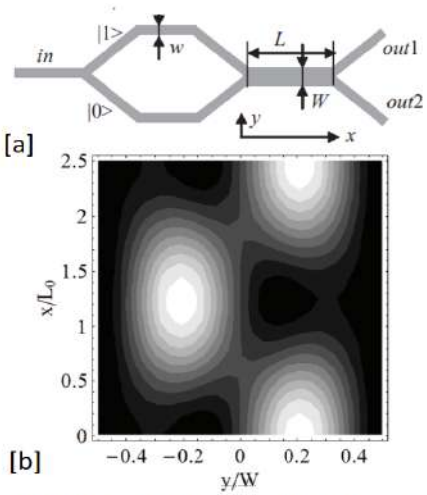

[a]Hadamard Quantum Circuit/Gate Realization via Electron Transport in Graphene.
[b] Transmission Probabilities observed in the Electron Transport of the Ballistic region of the 2D material i.e Graphene in this case which shows that Gate is Hadamard due to equal transmission probabilities in the interfering region of length L and width W.

Figure 1.8: Quantum Gate Realization in Ballistic Transport Regime of Graphene [1]

Also the passing of the current and getting the readout from the chip,we will be requiring connections taken out from the gold contacts of the graphene nanoribbons so for the space required to take its contacts out and measure will be proportional to number of qubit lines used.So I think at present we will require at least a floor of a institutional building to keep the instruments/equipments as in source meter's,coaxial cable,Lock in amplifier's tec.,to realize the Fault tolerant Quantum Computer fully.

Why it relates to this work?

The number of modes and the mean free path as well as the type of scattering mechanisms can be mathematically extracted by probing Quantum Capacitance of 2D material and hence it

can identify whether a 2D material is an ideal/potential candidate for recognizing Fault Tolerant Quantum Computer design in the Quantum Materials Domain of the Hardware.

1.2.3 Industrially Synthesizing the Large Sheets of Monolayers of Graphene to Explore and Realize it's Practical Real World Applications.

Graphene with Graphene has a layer adhesion energy in the range of 0.15 J/m^2.So to exfoliate monolayer graphene from the graphite crystal we will require a adhesion energy of monolayer graphene with another material/metal greater than 0.15 J/m^2 but less than 0.30 J/m^2.So if we look at various metals that can be thermally evaporated under pressure on the graphite crystal then gold,Selenium and other materials can be explored which can satisfy the requirement of adhering with monolayer graphene in this range.Once the materials that show these adhesion ranges are identified,next step is to exfoliate the graphene by first thermally evaporating that material on the graphite crystal and then lifting the gold film off of the graphite flake with one monolayer adhered to it ,followed by transfering the exfoliated graphene to desired substrate and then chemical cleaning to remove the material if any on the substrate and get the monolayer flake of graphene on substrate.So by this concept we can get large area of exfoliated graphene depending on the size and surface roughness of the graphite crystals.So what one can do is to optimize these sets of parameters (pressure of the deposited film,thickness,time,temperature of the deposited film etc) experimentally to obtain large area flakes at most the size of the graphite flake that it has been exfoliated off of.Now the next step is to perform lap joint in between the two exfoliated graphene flakes by gas laser assisted joining methods with minimum overlapping region.So one will have to transfer the two monolayers with minimum overlap on top of each other followed by electrically transport wise joining the two by laser technique.This joining may or may not be required as just transfering the graphene on graphene with minimum overlap also forms lap joint due to the inherent adhering between the two.So in theory we can create large sheets of graphene to upto the length that we desire just by exfoliating large sized flakes of monolayer graphene followed by transfering it on top of each other.So once we have large sheets of monolayer graphene we can practically realize the optical,mechanical and electrical properties of graphene and implement it to commercial use. We can try this approach of lap joining by just transfering or transfering followed by gas laser joining with Chemical Vapour Deposition technique grown graphene as well.This technique can also be scaled industrially by complete automation of the processes involved.

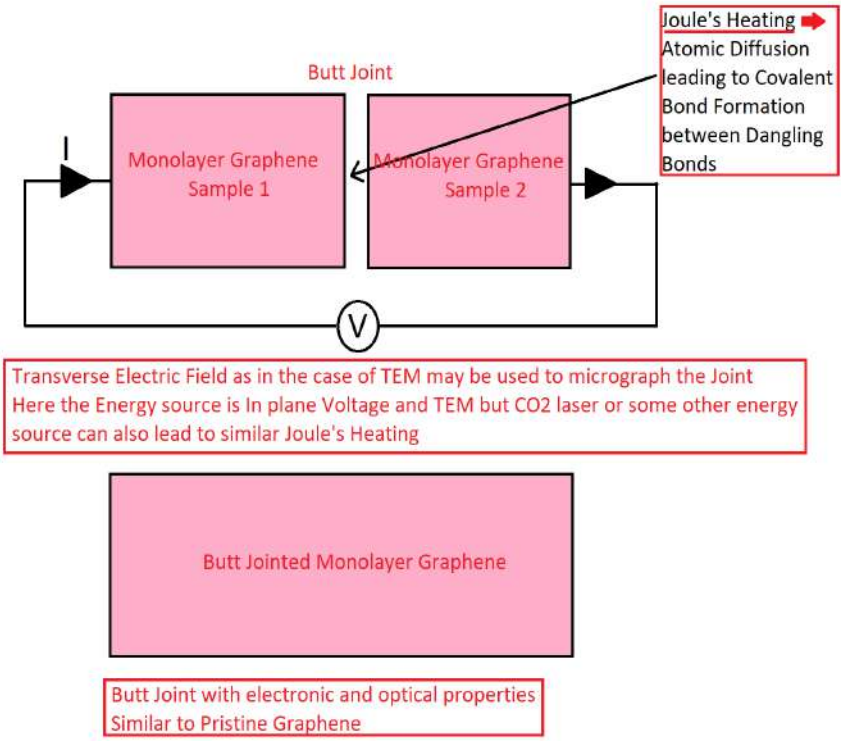

Figure 1.9: Butt Jointed Monolayer Graphene

Why it relates to this work?

We have tried the Exfoliation of graphene by conventional manufacturing way which results in size of the flake in the order of micro-meters but no surity of seeing monolayer graphene on $Si - SiO_2$ substrate but still provided a way to optimize the parameters to increase its probability of exfoliating , so this outlook is to realize another production method which can be used to scale graphene's size to realize its applications such as a optically transparent and conducting mobile screen,its young's modulus is greater than that of steel so in defense applications etc.

1.2.4 Negative Quantum Capacitance (Negative Compressibility)

One can in theory exceed the 1.Boltzmann Limit that limits the sub-threshold swing S i.e (slope of the gate voltage vs log scale Drain Current) to 60 mV/decade.

2.The dimensional size of channel which cannot be reduced below a certain range to avoid the kicking in of the tunnelling effects than the already existing CMOS Technology in transistors

by realizing the concept of negative Quantum capacitance in graphene i.e it's negative compressibility.

Previous studies have observed Negative Compressibilities in Graphene by applying a transverse magnetic field at low temperatures and adding in impurities in monolayer. So if we can research in this field and tune in the on and off gate voltage in this negative compressibility region of graphene in a graphene transistor setups then we can essentially exceed the Boltzmann Limit and Equivalent Oxide Thickness Fundamental limits which arises from laws of Quantum Mechanics.

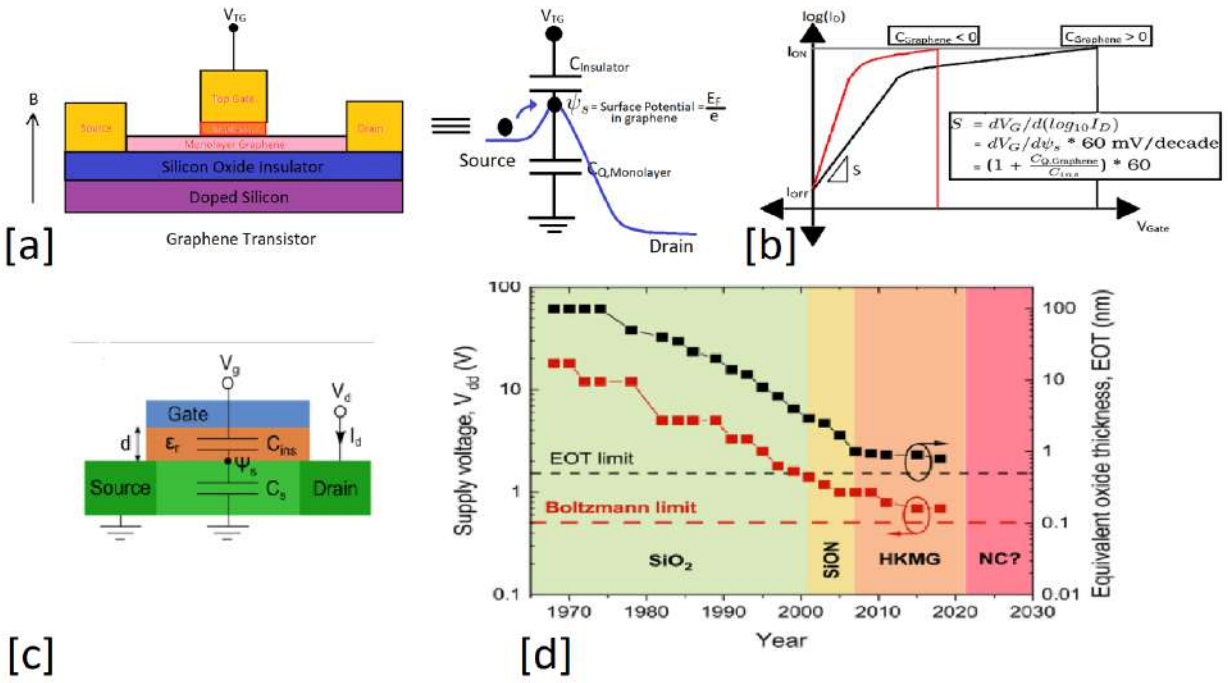

Figure 1.10: Negative Quantum Capacitance In Graphene [a] Graphene Transistor and it's equivalent Capacitance model [b] Subthreshold swing S can be less than 60 mV/decade by realizing Negative Quantum Capacitances in Graphene. [c] Conventional Complementory Metal Oxide Semiconductor Transisitor [d] EOT and Boltzmann Limits in CMOS Technology [4].

For more basic details on negative capacitances in general I suggest refering to [4].

Why it relates to this work?

By making changes i.e adding impurities in the graphene and subjecting it to transverse magnetic field we can realize negative quantum capacitances in graphene and to probe this compressibilities of graphene or any 2D material for that matter , this thesis presents novel and simplest of the ways.

1.2.5 Quantum Memory Devices made from Graphene.

In Twisted Bilayer Graphene we can flip magnetism with a small DC current which suggests that we can create a quantum memory out of this concept.But why do we require a quantum memory that works only at few kelvins? As from this system we require a current density that is 10^4 times lower than the conventional used spin orbital torque memory i.e we can get a power efficient quantum memory which can act as an control and read out interface for quantum computer.[3] .Another option to explore is in the field of graphene nano-drums.

1.2.6 Future Scope of this Work can be out of Plane Tunnelling Current Measurement to Probe the Quantum Capacitance of the 2D material.

When we apply an AC voltage gate modulation then charge flows across the hetero-structure,charge flows across the hetero-structure and at equilibrium its values can be taken as en_{total},due to this charge flow owing to applied AC gate modulation the tunnelling current flow across the structure,which can be measured by taking contacts out from top and bottom of the 2D material,this process involves fabrication in between transfer and hence it is difficult to create such a device,but this can be future scope of this thesis.More theoretical details related to this outlook is discussed in section [3.2] and figure [3.9].

1.2.7 Mathematical Machine Learning Models for Various Phenomenon Observed In 2D materials

Again similar idea as discussed in section [1.6.1] can be adapted for various phenomenons observed in 2D materials by parameterizing the phenomenons with material properties that can completely characterize a material and further specifically design such materials chemically to give the required phenomenons at desired temperatures and pressures ,which can further be used in that specific phenomenon oriented applications.

Why it relates to this work?

Because the phenomenons observed in conducting 2D materials can be probed by its Quantum Capacitances measurements as will be discussed in the Interpretation section [5.4] in some time if possible in the future .

1.2.8 Updating Theoretical Hamiltonian From Experimentally Extracted Quantum Capacitance.

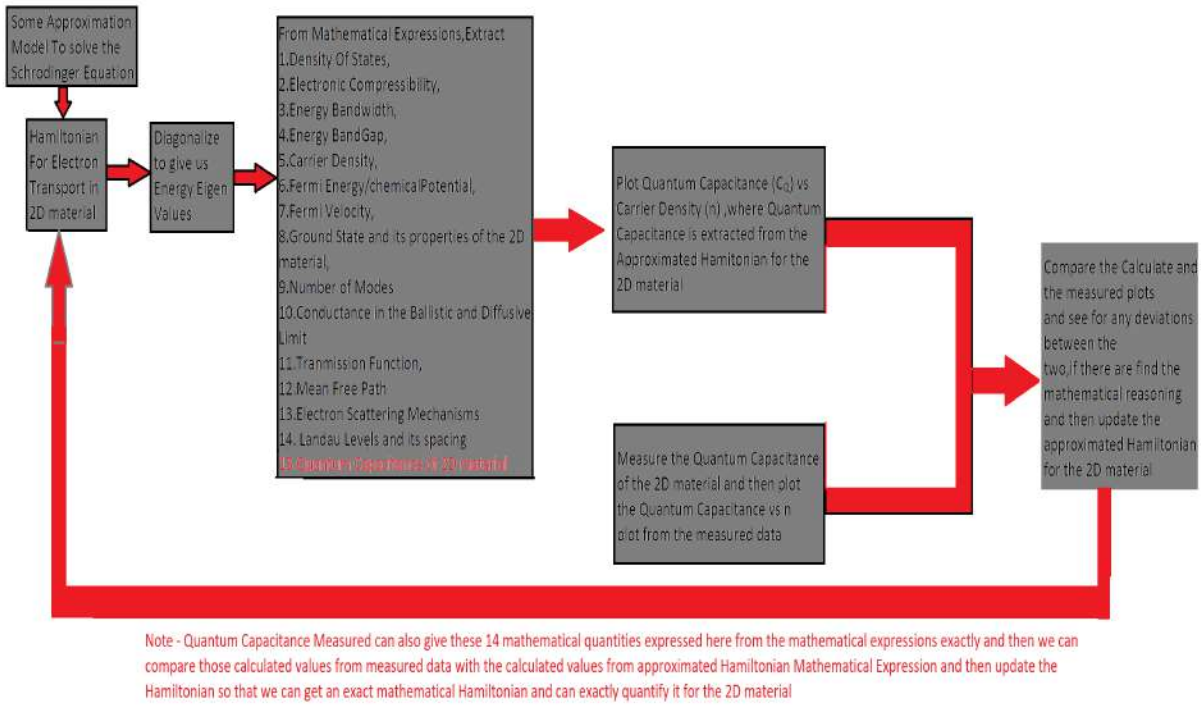

Figure 1.11: Quantum Capacitance Measured Data Process flow Schematic to exactly quantify the Hamiltonian of the 2D material and hence exactly understand the electronic transport in 2D material

Chapter 2

Probing/Characterization of 2D materials using Microscopy and Spectroscopy Techniques.

Microscopy techniques can be used to characterize the 2D materials, in general identify the number of layers,check quality of the 2D material,the band structure,Fermi Energy,cutting the 2D materials to get 1D nanoribbons,various corelated phenomenons etc.Let us explore the microscopy techniques one by one in particular for 2D materials hBN,Graphene,Bilayer Graphene and Twisted Bilayer Graphene.

2.1 Angle Resolved Photo-electron Spectroscopy (ARPES)

-

2.1.1 ARPES Basics

Angle Resolved Photoemmision Spectroscopy is a technique to experimentally obtain crystal momentums K_x,K_y and K_z i.e the Band Structure of the material by measuring the Intensity,Kinetic Energy of Emitted Electrons ,Fermi Function,Resolution,Angle of Emission of the electrons, in particular the spectral function captures the band structure and the co-related interations such as electron-electron,electron-photon,electron-plasmon etc.

[a] 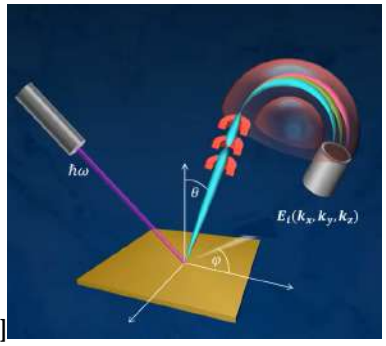

[b] 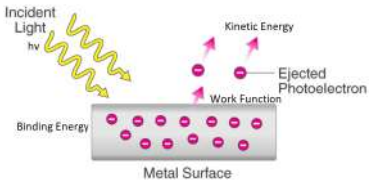

[c] 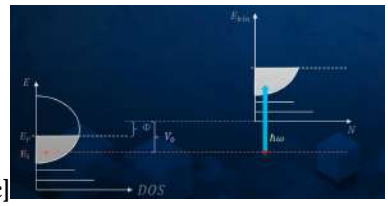

Figure 2.1: (a)Schematic Of ARPES [1] (b) Photoelectric Effect (c) E vs DOS showing Photo-excitation of the electron,travel to surface,escape in to vaccum [1]

ARPES is based on the principle of photoelectric effect i.e when light of particular frequency is shone on the material it emits electron from its surface with particular kinetic Energy.

By Conservation of Energy, E_{kin} = hν - E_{Bin} - ϕ

ARPES is a three step process, as shown in fig 1[a]

a.Photo-excitation of the electron in the bulk

b.Travel of the excited electron to the surface => governed by mean free path

c.Escape of the electrons in to vaccum by overcoming the work potential.

a.Photo-excitation of the electron in the bulk

When photon of energy hν is incident on the material at some angle the electrons in the materials at the surface at energy E_i or little below the surface states gain energy to overcome the Fermi energy as the work function Φ of the surface of the material and leaves the surface at some emmission angles θ and ϕ with kinetic energy given by conservation law of energy as, E_{Kin} = hν - E_i - Φ.

Now the lattice translation symmetry is preserved in the x and y direction (no defects) but it breaks in the z direction (vertical direction),hence crystal momentum is equal to linear momentum of the electrons in the x and y direction as the momentum is conserved in the x and y direction but breaks in the z direction.

By conservation of the momentum in x,y direction,

P_x = $\sqrt{2mE_{Kin}}cos\phi sin\theta$ = hk_x

P_y = $\sqrt{2mE_{Kin}}sin\theta$sin$\phi$ = hk_y

P_z = $\sqrt{2mE_{Kin}}sin\theta$sin$\phi \neq$ hk_z

k_z = $\frac{1}{h}$ $\sqrt{2mE_{kin}cos^2\theta - h\nu - E_i - \Phi}$

b.Travel of Electrons to the Surface.

1.In bulk materials,once the electrons leave its state in the material it can undergo scattering,which can be due to phonons,electrons,ions collision etc and once it undergoes scattering we cannot retrieve the electron from the surface.

2.Scattering events of electrons are typically governed by its mean free path.

3.Typical photon energies used for ARPES is 6-6000 eV,so it generally has a penetration depth of some nanometers,hence only those electrons are excited which are in the unit cells near surface of the materials,hence ARPES can be recognized as Surface Spectroscopy phenonmenon.

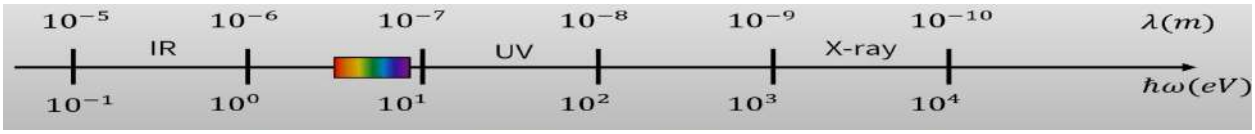

Figure 2.2: Incident Photon Spectrum From 6 to 6000eV [1]

4.Now,the typical electron mean free path is independent of the material and only depends on the excitation energy,hence typical mean free path of the electrons is 0.5 to 10 nm depending on the excitation energy as shown in the graph below.

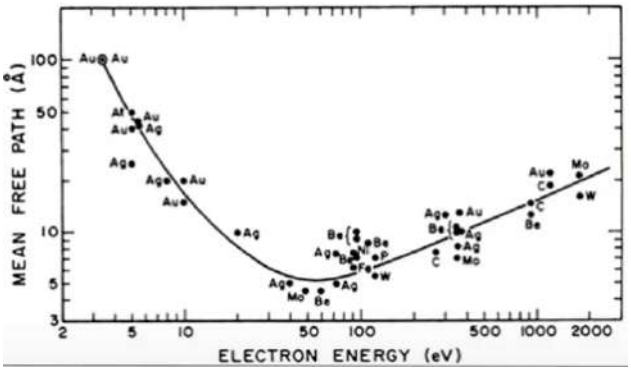

Figure 2.3: Mean Free Path of the electron independent of Material [4]

5.Hence,as 2D materials are only atomic size thick ($\approx$ 0.75 nm) ARPES can act as a perfect candidate for probing 2D materials.

c.Escape of the electrons in to vaccum by overcoming the work potential-

1.Electron apriori to escape from the surface has to overcome the work function of the material,hence loses its kinetic energy of escape by magnitude of the work function Φ of the material.

2.Probability of transition (given by Fermi Golden Rule) of electron from its initial state to final state depends on the incident frequency of the photon and work function Φ of the material.

Once the electron escape from the surface , the electron path of movement is focussed by using an analyzer in ultra-high vaccum and then the detector measures the E_{kin},emission angles θ and ϕ to give us crystal momentum's k_x,k_y and k_z of the material.

Intensity of photo-emission of electron in ARPES experiment, I(k,E) having k momentum,E energy is given by the product of Amplitude Intensity I_o,fermi function of electron f(E), electron spectral function A(k,E)and Energy Resolution R($\triangle$k ,$\triangle E$)

I(k,E) = I_of(E)A(k,E)R($\triangle$k ,$\triangle$E)

The Electron Spectral Function A(k,E) captures the Band Structures and interaction of the electrons in the materials.

A(k,E) = $\frac{-1}{\pi}\frac{Im(\sum(k,E)}{(E-E_K-Re(\sum(k,\nu)))^2+Im(\sum(k,E)^2}$

where the E_K is the bare band energy term without any interactions i.e only the dispersion relation accounting the electron interaction with periodic potential of lattice,the self energy term $\sum$(k,E) captures the (kink or non-linearity) band position in the real term and the line-width or lifetime and interactions(scattering rate) in the imaginary term.

Sharpness of the dispersion relation curve can be increased by tuning the momentum resolution for the same energy resolution [3].

The temperature of ARPES experiment governs the f(E) term of the electron ,broader for room temperature and step response for low temperature,but room temperature means more occupied states in the system hence more electrons to probe for ARPES.But higher temperature also means thermal broadening and hence we can't observe the quantum effects as well as the interaction effects in the band structure.Hence temperature of ARPES experiment can typically range from few mK to 400 K depending on what phenomenons we want to probe.

Hence ARPES acts as a perfect probe to probe the occupied states of 2D materials upto its Fermi Energy and experimentally study its electronic band structure and the many body effects and compare with the thereotical models for verifying model's validity.

2.1.2 ARPES of hBN,Graphene,Bilayer and Twisted Bilayer Graphene

1. A 2007 ARPES study of graphene on SiC substrate showed a band gap in the dirac dispersion cone as graphene on SiC breaks the sublattice symmetry and hence the band gap at Dirac Point as shown in the figure below.

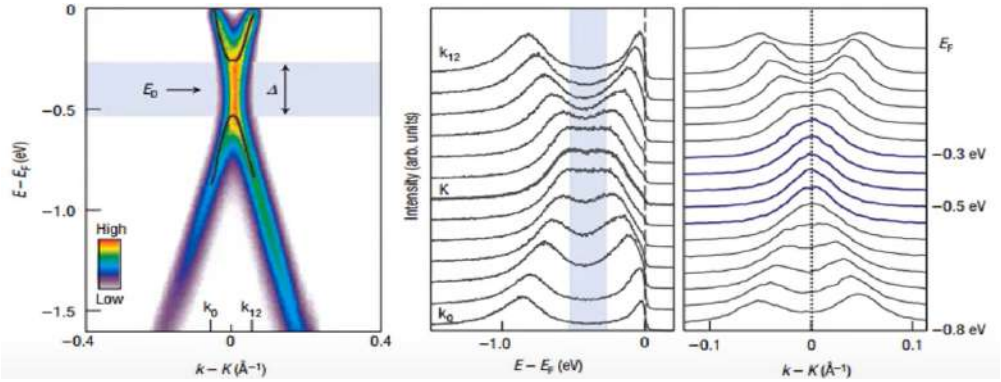

Figure 2.4: Band Dispersion Relation and Energy and Momentum Distribution Curve (EDC's and MDC's) by ARPES of of Graphene on SiC substrate [4]

2.SiO_2 on Si Wafer with hBN as a dielectric for graphene is conventional used hetero-structure for probing graphene as hBN forms smooth interface with graphene,gives better charge carrier mobilities than other dielectrics and also has low electronic screening.

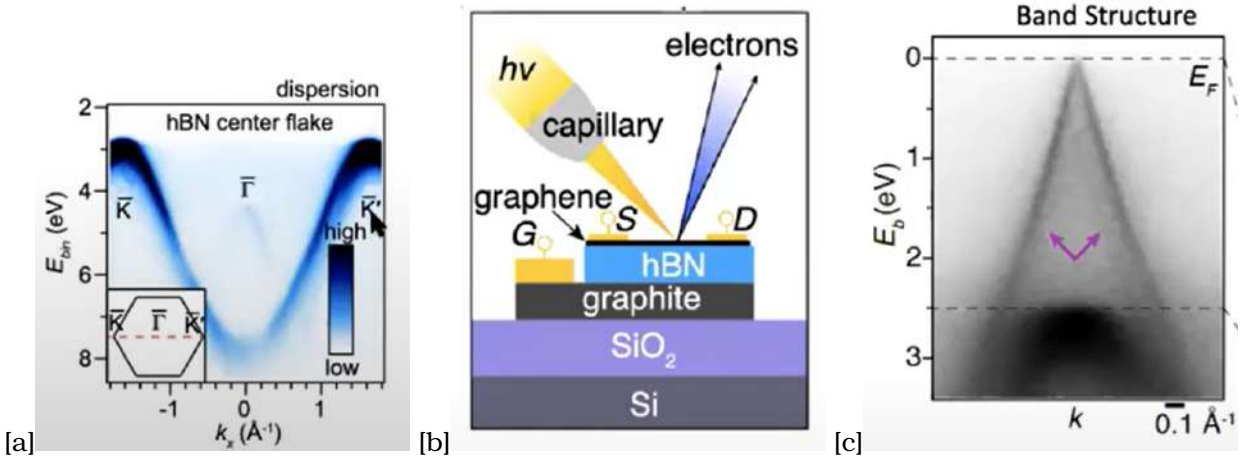

Figure 2.5: (a) ARPES of hBN [5] (b) ARPES Schematic of Graphene hBN with graphite gate device [5] (c) Band Structure of Graphene with ARPES [5]

3.ARPES of Graphene on hBN with graphite gate on SiO_2-Si substrate.

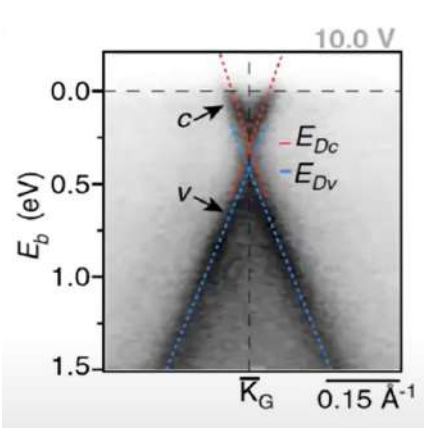

Figure 2.6: Quantum Many body Interaction effects on Graphene's Band Structure [5]

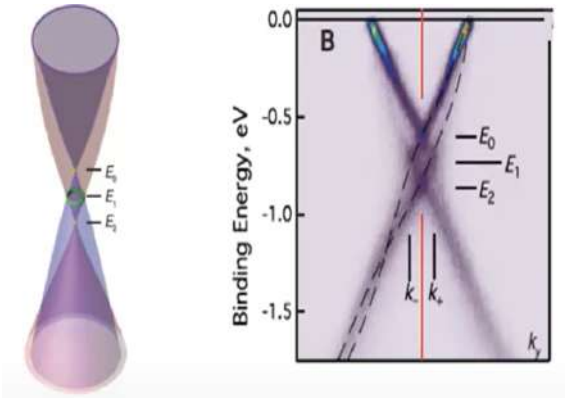

Figure 2.7: Unidentification of Dirac Point Exactly in Graphene due to Interaction Effects [5]

The pink arrow in figure 9 indicates fine lines in the dispersion relation which are present due to a small twist of 2 degrees of Graphene lattice to hBN lattice. From Figures 10 and 11 we can see that the dirac point in Band Structure cannot be clearly located,it is due to manybody electron interactions that take place in graphene which are tunable by gating i.e changing the carrier concentration density in graphene.

By plotting imaginary part of self energy term A(k,E) vs the carrier concentration density (n) we can also identify the type of electron scattering in the graphene as shown in the figure below which is usually short range scattering (Fermi Radius has a $\sqrt{n}$ dependence) which is due to electron electron and electron phonon interactions.

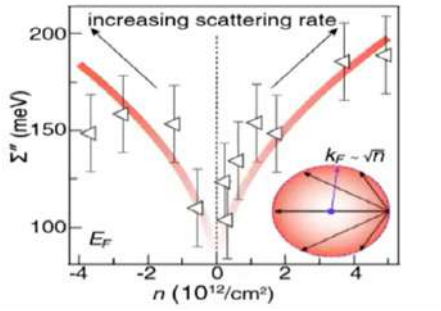

Figure 2.8: Imaginary term of self energy A(k,E) vs n indicating short range scattering of electrons in Graphene [5]

Electron in material can be, 1.Free from any localization i.e in electron gas 2.Having Electron-Electron Interactions which are not seen at higher charge carrier(electron) concentrations due to screening effect. 3.Electron-phonon interactions,electron-plasmon interactions,electron-impurity scattering,electron hole interactions and electron-other quasi-particle interactions.

All these interactions mentioned in 2 and 3 above causes the electron in the material to deviate from its free behaviour.In band structure we consider the electron experiencing potential due to lattice structure,but the actual band structure of the material will always have deviations from the ideal case and these deviations are captured from ARPES of material.

If we consider ARPES of Graphene on SiC as shown the figure below,there are two main deviations in the band structure from ideal case,

1.At 0.2eV we observe kink which can be attributed to electron-phonon interactions and which does not change with doping .(The Kink and the momentum linewidths can be clearly seen if we take 90 degree rotation of the ARPES photoemitted spectrum image)

2.Dirac Point is a small region which follows the E_D with doping which can be attributed to mainly electron-plasmon and other electron - quasi-particle interactions.

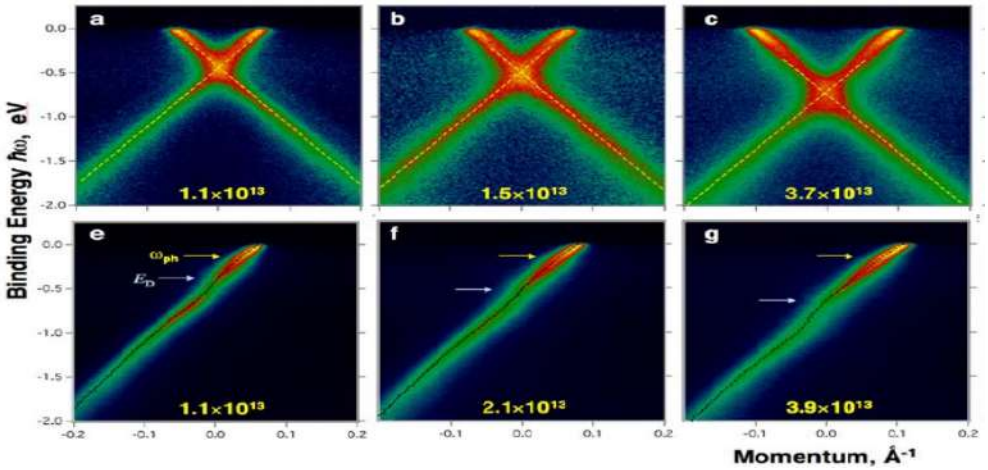

Figure 2.9: (a),(b),(c) => ARPES generated band Structure of Graphene on SiC for three dopings and (d),(e),(f) => a 90 degree rotated image of the ARPES spectra with axis parallel to Binding energy as axis of rotation[9]

Thereotical models to study the many body effects in graphene can be done from such ARPES measurement and the AB initio simulations are published in [1] and [9].A schematic of the same is shown in the figure below.[9]

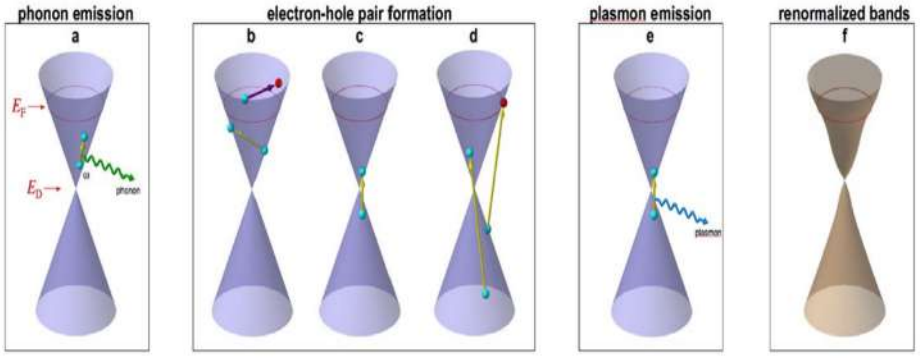

Figure 2.10: Electron Decay and Scattering processes in Graphene giving rise to renormalized bands in graphene [9]

If we plot the Momentum Line Widths vs Energy of photo-emmision as shown below then we can model the experimental results for various doping into 4 regions (for more details on energy range with the type of interaction refer [9]) of electron-quasi-particle interactions depending on the energy of the incident photon.

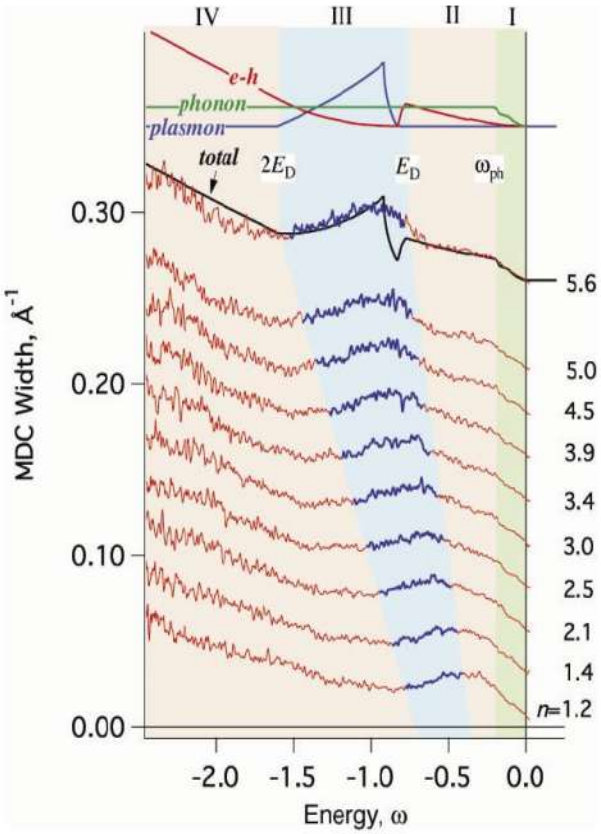

Figure 2.11: MDC width vs Energy for various doping showing 4 modelled regions in experimentally obtained values,with I region showing electron-phonon interaction,II region showing Electron-hole pair formation,III region of electron plasmon interaction and IV of electron-hole pair [9]

Note - Reference [9] has assumed MDC width as proportional to Imaginary self energy term i.e independent of momentum of particle and also the multi-interactions in the same energy range is not considered hence there are deviations in the theoretically predicted and experimentally probed band structure.

By ARPES probing we can also get the band structure of the Bilayer Graphene and Twisted Bilayer Graphene as shown in the figures below for twist angle of 12 degrees,and also VHS dipersion , Flat band Dispersion and finally the gate dependence of VHS and flat bands.[5]

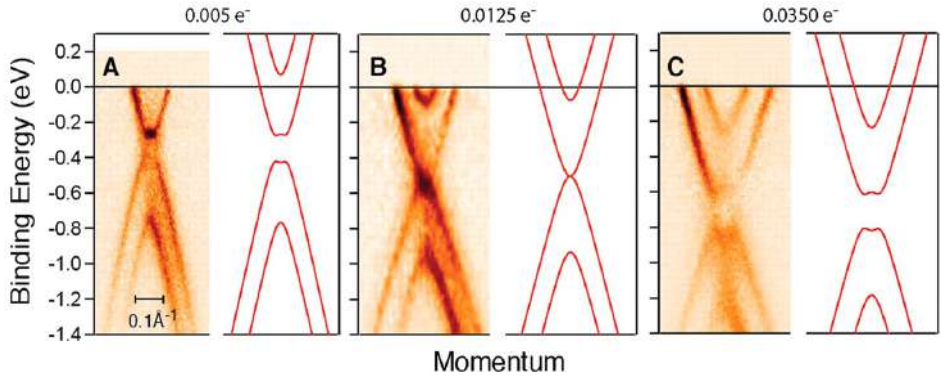

Figure 2.12: ARPES Band Structure of Bilayer Graphene on SiC substrate for 3 Potassium Dopings [6]

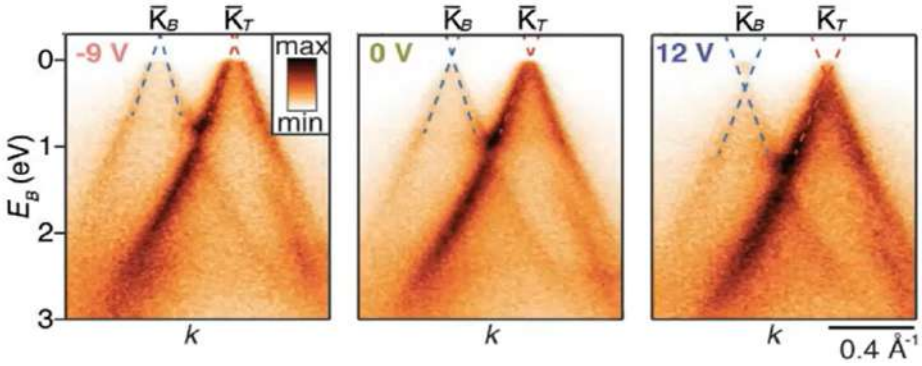

Figure 2.13: ARPES Band Structure of TBG for a twist of 12 degrees at three gating voltages [5]

2.2 Optical Microscopy (OM)

-

Optical Microscope uses light in visible region and a system of lenses to magnify the images of small samples ,such a characterization of small samples to visually see the magnified image of sample in real time is optical microscopy.It can be used to identify the number of layers of the 2D materials,the quality of the 2D flake,checking the quality of the heterostructure device after and before fabrication etc.

Main problem with seeing graphene on SiO_2 substrate under optical microscope is that it has low contrast and hence can be easily missed when checking for it on the substrate,also more magnification can require longer seeing times per sample and can cause straining in the eye.Hence the parameters of optical microscope as well as the thickness of the SiO_2 should be optimally designed to get maximum contrast of the graphene under optical microscope. Note - Contrast can be defined as relative intensity of the reflected light in presence and absence of graphene.

Graphene's Visibility contrast on Optical Microscope depends on,

1.SiO_2 substrate thickness

2.Incident Wavelength of the photons controlled by narrow band pass filter [1]

Relation between the optical contrast with the substrate thickness and incident light wavelength can be theoritically studied by using principles of Fresnel's Law but it slightly overestimates the contrast than experimental as discussed in the reference [1].

Monolayer Graphene on SiO_2 having thickness nearly equal 300 nm when viewed in the optical microscope with white light introduces optical path difference producing sufficient but eye straining optical contrast to visually differentiate monolayer graphene of depth d_1 from SiO_2 substrate of depth d_2.As shown in the figure below the incident visible white light photon is reflected from the graphene surface and refracted in to graphene which further interacts with the π orbital electrons (shown by red dot at depth x) and then again is reflected from the SiO_2 substrate and refracted into the substrate to finally reflect from the bottom of SiO_2 substrate.These reflected photons interfere to visually give an optical contrast to graphene on SiO_2/Si substrate.[2]

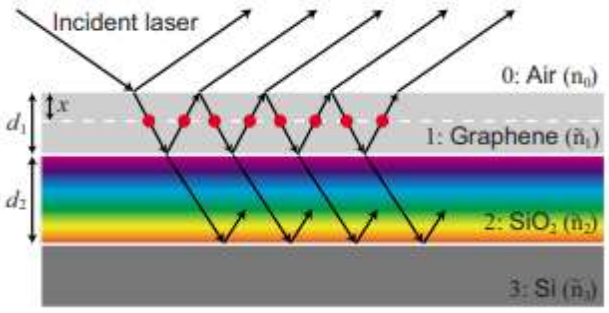

Figure 2.14: Multiple Reflection Interference in Graphene on SiO_2/Si substrate [2].

The reference [1] studies the optical contrast of graphene under microscope for 90 nm,200 nm and 300 nm thicknesses of SiO_2 on Si wafer for various wavelengths from 400 to 700 nm in the optical region controlled by narrow band pass filters both experimentally and thereotically (by using Fresnel's Laws) and the finally the reference has shown that the contrast of the graphene when observed under Microscope can be used as a quantitative tool for defining the number of graphene layers on the SiO_2 substrate.

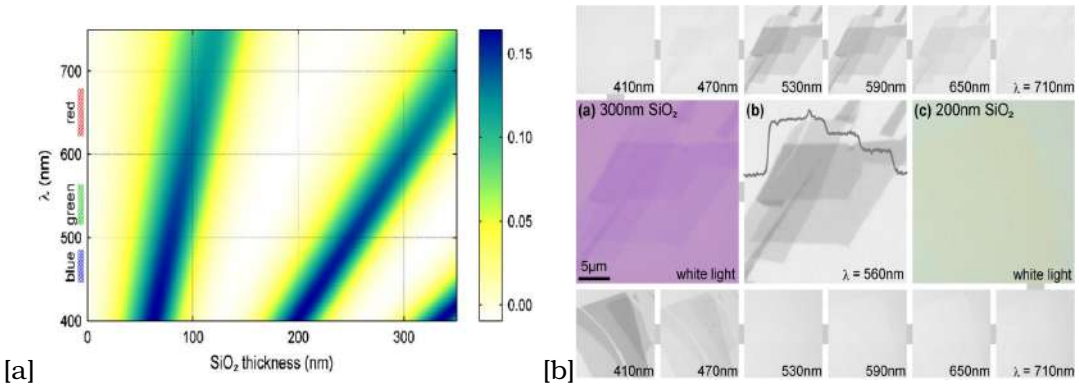

Figure 2.15: (a)Incident Wavelength vs SiO_2 thickness with colour indicating the optical contrast of graphene on SiO_2 substrate. (b) Optical Micrograph of Monolayer Graphene on SiO_2 substrate for two thicknesses 200 nm and 300 nm of SiO_2 and for different wavelength filters with green(blue) light filter showing better optical contrast than white light at 300nm(200nm)as clearly seen in colour plot[a] and also this optical contrast can act as a quantitative tool to define the number of layers as shown by line variation in middle micrograph [1].

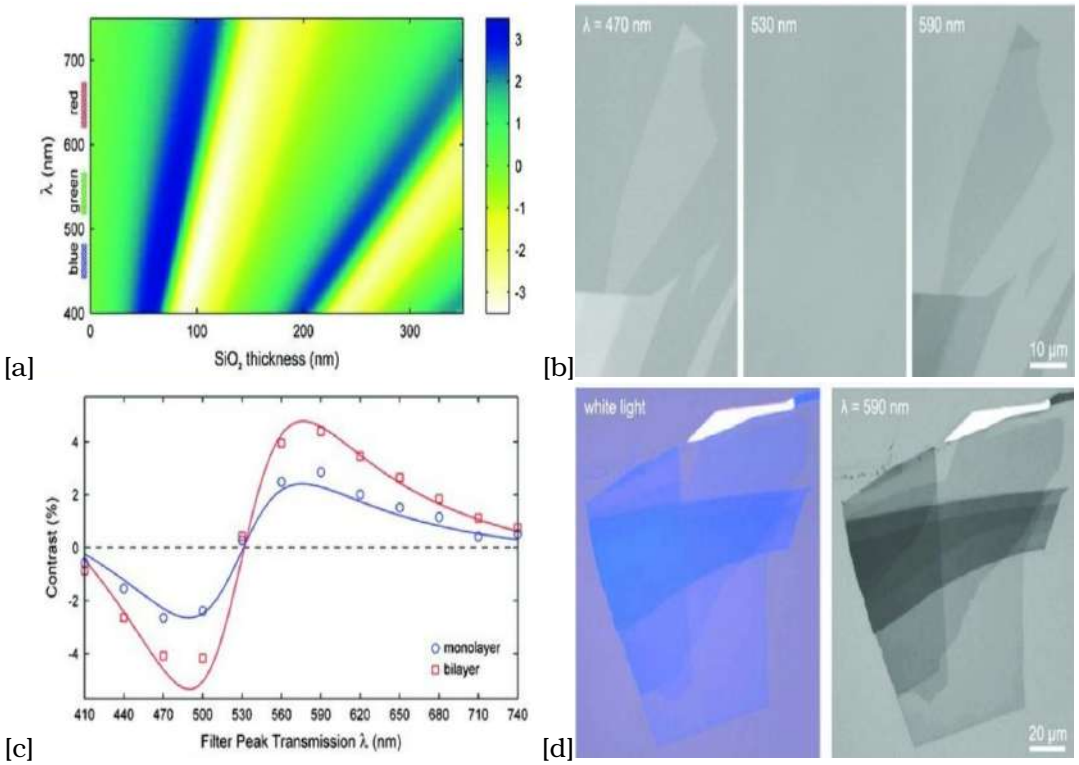

Figure 2.16: (a) Optical Contrast Colour Mapping of 2D hBN on SiO_2 substrate for Different thicknesses of SiO_2 substrates and different wavelength filter on white light used (b) Optical Micrograph of monolayer and bilayer hBN on 290 nm thick SiO_2 substrate for three wavelength filters used and green light filter at 590 nm shows the higher visibility i.e higher colour contrast out of the three (c) Optical Contrast variation in percentage with variation in the filter wavelength used on white light for monolayer and bilayer hBN on the 290 nm thick SiO_2 substrate suggest the contrast increase in steps as the number of layers of hBN increase from monolayer and shows two local maxima's in colour contrast at 490 nm (blue light) and 575 nm (green light) (d) Optical Micrograph of 2D hBN on 90 nm thick SiO_2 for white light and green wavelength filter at 590 nm used on white light clearly indicating that Green light filter has better optical contrast for mono and bilayer hBN.[4]

Practically from above colour graph it is clear that any thickness of SiO_2 can be used except 150 nm and below 30 nm combined with any wavelength of light in visible spectrum, but green light is less straining for human eyes and hence 90 nm and 280 nm thickness of SiO_2 are most suitable with green light to get the best optical contrast with less strain on the eyes so identification of the monolayers can be done under microscope for extented periods of time [1] and also the optical contrast of monolayer hBN which are much harder to find than monolayer graphene for green light filter used on white light shows maximum optical contrast upto 3 percent as shown in the figure above.[4]

In the Nano-Scale Devices Lab at IISc i.e the lab which I did my project in use an olympus optical microscope having 1.25x,5x,10x,50x and 100x magnification using white light as the light source and the typical thickness of SiO_2 on Si substrate is 250 to 300 nm and it gives sub-optimum optical contrast but is eye straining for long periods of use.Note that it is still tricky and time consuming to see separated monolayer flakes as contrast is suboptimum in this setup,but overall good contrast when there are foldings i.e mono,bi,trilayers and more in the same flake.The figure

below shows 100x images of the monolayer graphene,bilayer graphene, and hBN of some of my samples.Hence I suggest introducing various wavelength light filters to the optical microscope to get a optimum setup for various thicknesses of of SiO_2 used (the more the better).More frequently 300 nm SiO_2 is used in lab so introducing a green filter would give maximum colour contrast both for monolayer graphene and monolayer hBN concluded from the literature reference [1] and [4] studied and colour maps above. Also monolayers of other different 2D material's optimum optical contrast on different thicknesses of SiO_2 substrate study can be easily and quickly done if more wavelength light filters on white light in optical microscope are available in spare.

Note - Since White light is used the colour of the substrate when seen in optical microscope as well as colour contrast of graphene on it can change slightly but in general above information holds true.

Note - Another possibility is trying to increase the contrast by integrating the python code to increase the contrast in real time with the image generated by microscope. This has a lot potential as it can increase the contrast in real time to easily and clearly identify exfoliated mono-flakes on the sample.

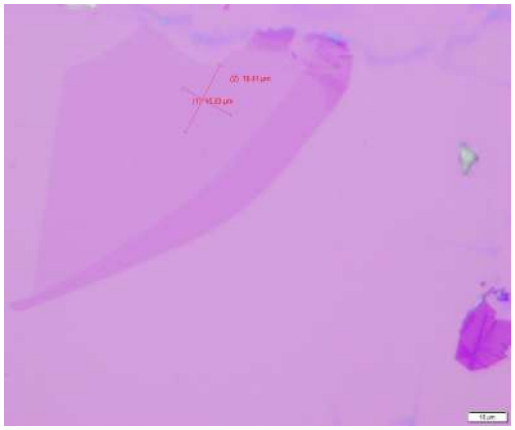

Figure 2.17: Optical Microscope image of Monolayer Graphene at 100x magnification with a foldings to bilayer at the ends

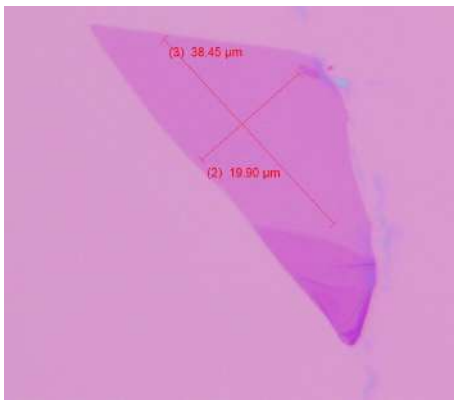

Figure 2.18: Optical Microscope image of Bi-layer Graphene at 100x magnification with a foldings to multi-layers at the ends

Figure 2.19: Optical Microscope image of Bi-layer Graphene at 100x magnification with a foldings to tri-layers and four-layers at the ends

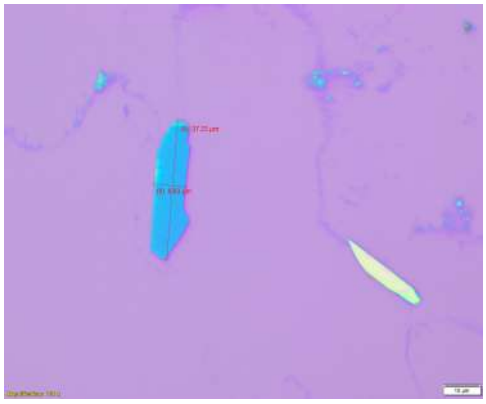

Figure 2.20: Multi-layers hBN (blue colour) and Bulk hBN - more than 10 layers (yellow colour)

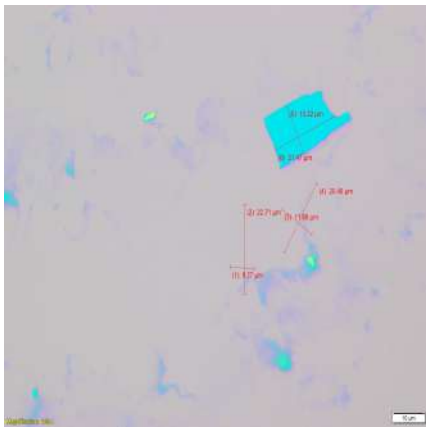

Figure 2.21: Multi-layers hBN

Figure 2.22: Multi-layers hBN with thickness inhomogeneties in hBN indicated by yellow colour

The hBN flake usually has blue shade from light to dark blue for incident white light in the optical microscope image with light blue to dark luminiscent blue transition indicating the increase in the number of layers of hBN and yellow colour indicating the bulk hBN i.e more than 10 layers of hBN as shown in the images above.

2.3 Scanning Electron Microscopy (SEM)

-

2.3.1 SEM basics

Scanning Electron Microscopy is a microscopy technique that uses electrons reflection,scattering and electron photon excitations to get a black and white image of the material at the subatomic

level at a resolution higher than the optical microscope as the electrons (wave/particle duality) has smaller wavelengths than the optical photons.

SEM uses magnetic lenses to focus the electrons in to spot on the surface of the material.Resolution of SEM is limited by the size of the spot and can have resolutions upto 10 nm. For samples to be visible under SEM it should be electrically conductive as they will be charged if they are not conductive and can cause distorted image as the incoming electrons can get attracted or repelled from the surface. If the sample is non conductive then the SEM can be performed by,

1.Increasing the pressure of the SEM chamber to reduce distortion.

2.Au coating of the sample to make it electrically conductive.

In SEM,high currents are passed through the Tungsten Filament which heats filament and it emits/ejects electrons called as thermonic emmision, the ejected electrons are then accelerated away from the filament by an accelerating voltage from 0.5 to 20 KV,these accelerated electrons are foccussed at spot by using anode,magnetic lens and scanning coils with spot focussed on the material surface then the elctrons after colloiding with the surface can,

1.Back Scatter - Primary Electrons reflected off of the surface.

2.Generate Secondary Electrons - Primary electrons beam hits the surface of the material and knocks the electron on the surface out of the material.

3.X-Ray Generation - Electrons close to nucleus gets knocked off by primary electron and electron from outer shell transitions to inner shell releasing an X ray photon, the knocked off electrons from the surface are called Auger electrons.

These Back Scattered Primary and Generated Secondary electrons are detected by detectors and then scanned to generate a black and white image having subatomic resolution with black contrast indicating less number of scattered and generated electrons and white indicating more number of scattered and generated electrons from the material surface.

Currents in the Scanning coils change the size of the area to be scanned on the material and hence can change the magnification of the image of the material.

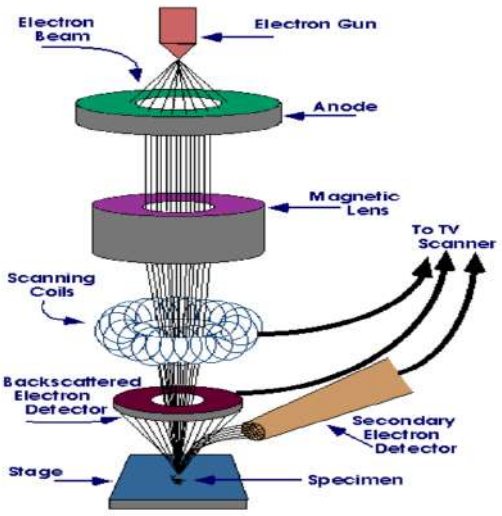

Figure 2.23: Working Principle Schematic of SEM [2]

SEM can be used to give topological information of the material ,X ray detection can give

chemical composition to identify the material,defect imaging at subatomic level,etc.

SEM resolution along with spot size typically 0.4 nm to 5nm in diameter depends on the interaction volume of the material with electron which is governed by penetration depth of the electron in the material which is higher for higher accelerating voltages and low atomic number materials and smaller for low accelerating voltages and high atomic numbers as shown in the depiction below.

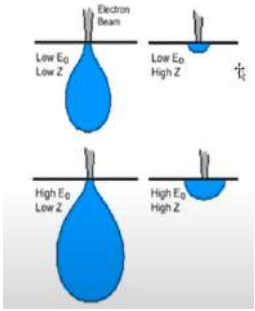

Figure 2.24: Depiction of Interaction Volume as function of atomic number and the accelerating Voltage of Electron [2]

Note => Larger the interaction volume of the material larger is its electron scattering,brighter is the image and vice versa.

2.3.2 SEM of Graphene - Mono and Multilayers

Note => SEM of hBN cannot be done as it is electrically non-conductive i.e we get distorted images due to charging issues unless we coat it with gold or create a suitable pressure in the SEM chamber for it to start electrically conducting.

SEM of graphene can be used to determine the number of graphene layers at subatomic resolutions where the Raman and Optical Spectroscopy fail. The reference "Determination of the Number of Graphene Layers: Discrete Distribution of the Secondary Electron Intensity Derived from Individual Graphene Layers " relates the discretely distributed secondary electron intensity of SEM with the number of graphene layers having a direct proportion relation at low primary electron acceleration voltages,which has advantage over conventional optical and Raman Spectroscopy as it is applicable to sub-micrometer sizes of flakes for any substrates including SiO_2 and also Raman Spectroscopy also can cause degradation of the graphene.

The number of graphene layers on the SiO_2 substrate were predetermined by reflectance measurements and then SEM images of graphene monolayer to multilayer flake were obtained by detecting the secondary electrons for accelerating voltage of 0.5 to 20 KV.Optimum contrast range as shown in the figure below was found to be at accelerating voltage for the range of 0.8 KV to 3 KV ,in particular best contrast separating the monolayer from multilayers was obtained at 1 KV having electron wavelength of = 38.76 pm.

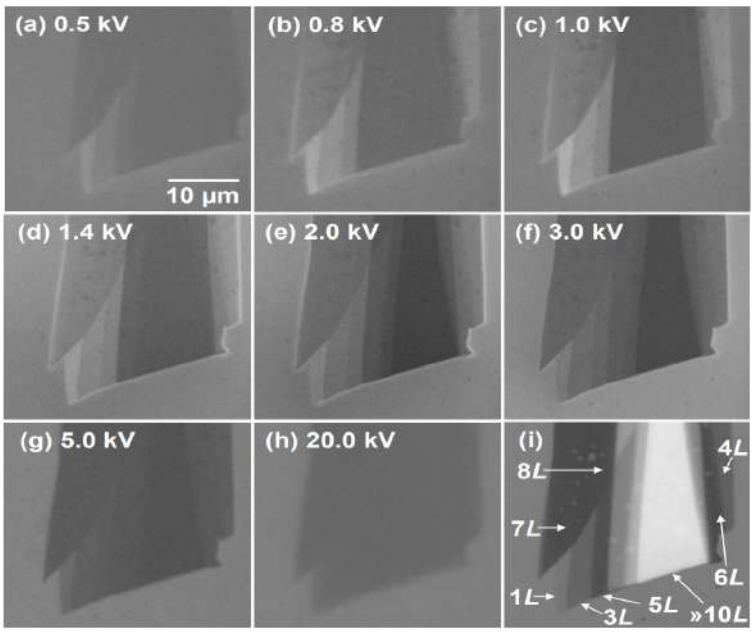

Figure 2.25: SEM Image of Monolayer and Multilayer Graphenes [3]

The Colour Contrast of monolayer and multilayer graphene at 0.8 to 3 KV accelerating voltage is higher than the remaining range of accelerating voltage as the penetration depth of the electrons is high for that accelerating voltage range and hence interaction volume is highest for mono-Layer graphene and decrease as the number of layers increase as carbon is having low atomic number hence penetration depth decrease with increase in the layers of graphene for same accelerating voltage.Hence we see increase in the darkness of the images as electron scattering decrease with increase in number of layers of graphene.

Colour Contrast image processing is done to convert the SEM dark and light colour contrast in the numerical values and that is plotted versus the acceleration voltage. The SEM contrast shows peak at 1KV for mono to 8 Layers and decrease if we deviate the accelerating voltage from 1KV, after that i.e greater than 10 layers (bulk graphite) , the number of layers by colour contrast is indistinguishable and we see continuous decrease in SEM contrast and negative SEM contrast for 10 layers or more with increasing accelerating voltage.

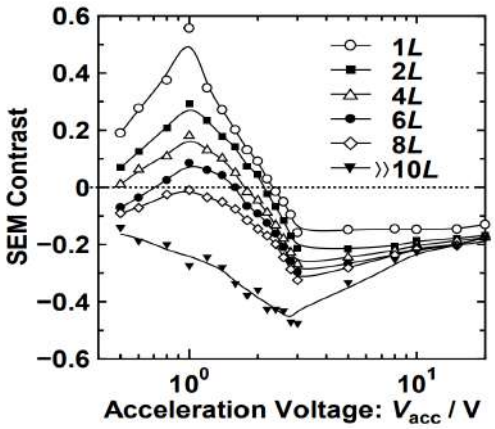

Figure 2.26: SEM contrast vs Normalized Acceleration Voltage [3]

SEM contrast vs the Number of layers follows a linear relation for any substrate except the monolayer graphene as shown in the figure below. One of the reasons could be attenuation of secondary electrons is directly proportional to number of layers it passes through. The slope of the graph shown below is dependent on the accelerating voltage but can be reproduced under similar accelerating voltage conditions and hence we can count the number of layers from the SEM contrast from the graph's slope line equation for new sample's SEM image under similar SEM experiment conditions.

Note => The monolayer graphene anyways has a high contrast and is easily distinguishable from the rest of the multilayers which is evident from the graph indicating higher penetration depth and hence more interaction area and more scattering of electrons from monolayer surface.

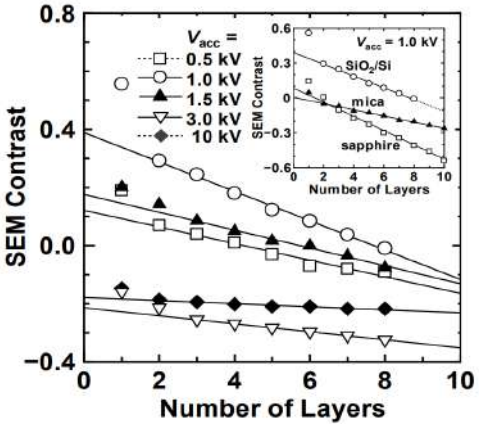

Figure 2.27: SEM contrast vs Number of Layers [3]

Finally the number of layers can be determined by plotting discrete histogram of the SEM contrast at 1KV and the discrete peaks represents the increase in the number of layers as the contrast decrease.

Number of Graphene Layers = $\frac{\text{Contrast of layer}}{\text{Contrast difference between adjacent layers}}$

Also for l KV of accelerating voltage,the number of graphene layers on SiO_2 substrate can be

mathematically calculated from figure 27 as,

SEM contrast = Slope of the line*Number of layers + y intercept of the line

S = 0.05*N + 0.4

where, S is the SEM contrast and N is the number of layers of graphene where N is greater than 1 as for monolayer graphene the linear relationship does not hold.

Number of Layers were first predetermined by optical microscopy and then SEM microscopy was done to validate SEM's results and further use it directly for any new flakes SEM image under same experimental conditions as shown in the figure below.

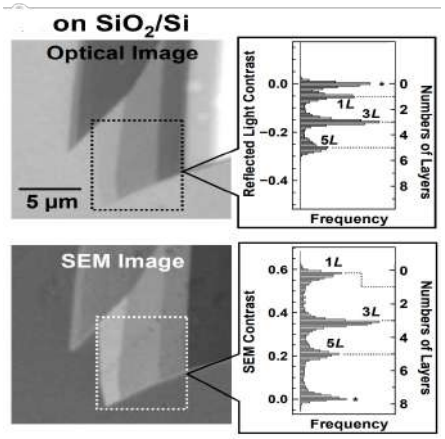

Figure 2.28: SEM contrast to determine the number of layers [3]

Hence by SEM of graphene we can identify the number of graphene layers in nano dimensions as well for fabrication of graphene nano-ribbons and other graphene nano devices where other microscopy techniques fail to identify the number of layers of graphene. But it can cause electron beam induced carbaneous contamination on the multilayer graphene surface with contamination deposition rates as high as 10nm per second but can be controlled by controlling the accelerating voltage and exposure time.

Auger Electron Spectroscopy shows a carbon peak for In-Situ formation of graphitic layers on metal surfaces and also X ray photo-emission spectroscopy can be used to identify the graphene apart from its multi-layers [1].

2.4 Transmission Electron Microscopy(TEM)

2.4.1 TEM basics

TEM is a based on the basic principle of wave particle duality of electron. TEM is a microscopy technique in which a tungsten filament is heated by passing current through it (similar to SEM) to get a thermionic emmision of the electrons,which are then accelerated by an accelerating voltage of 10^5 to 10^6 V,a higher voltage than SEM so that the electron can penetrate/transmit through a thin sample,once the electrons are accelerated it passes through condensor lens which controls electron exposed area on the sample i.e the magnification of the image generated is controlled by the condensor lens,then the transmitted electrons are foccussed through the objective lens and

then magnified further by projector lens and finally the image is generated by using a flouroscent screen or OCD camera or photographic film as shown in the schematic below.

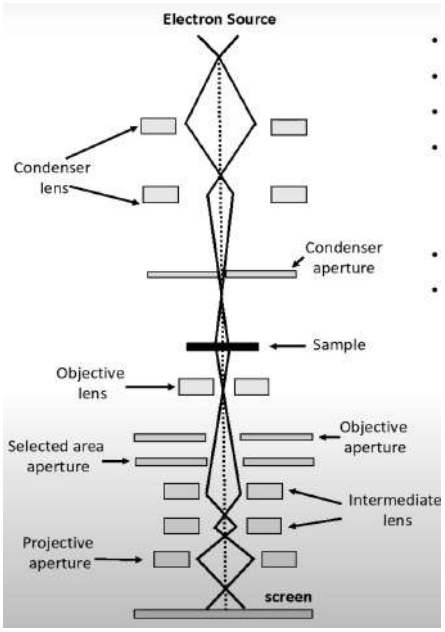

Figure 2.29: Schematic of TEM [3]

Image generated by the TEM called as micrograph can be,

1.Bright Field Image - Image generated by bombardment of transmitted electrons (the objective aperture blocks forward scattered electrons) on the fluroscent screen.

2.Dark Field Image - Image generated by bombardment of forward scattered/diffracted electrons on the flouroscent screen.

3.Electron Diffraction Pattern - Diffraction Pattern generated by the forward scattered electrons,

as shown in the figures below.

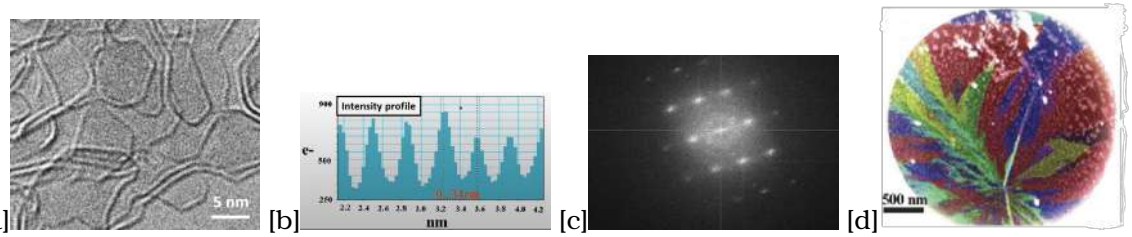

Figure 2.30: (a)Bright Field TEM micrograph of Graphene [3] (b)Transmitted Electron Intensity Peaks from Bright Field TEM micrograph [3] (c) Electron Diffraction Pattern [3] (d) False Colour Dark Field Image of Multi-grains graphene.[4]

Resolution of the TEM depends on

1.Wavelength of the electron which can be tuned by changing the accelerating voltage.

2.Numerical aperture of the system controlled by geometry location of the aperture/pinhole in TEM setup.

3.The Corrections in the defects/errors in focus of the electron beam and magnification of Electromagnetic Lenses i.e Aberrated Correction Transmission Electron Microscopy (AC-TEM)

With Recent AC-TEM a resolution of 0.05 nm can be achieved.

TEM samples are generally thinner (approx. 20 nm thin) than SEM as electrons are to be passed through the sample,hence the sample needs to be prepared by slicing it in to thin layers.Also the resolution of TEM is higher than SEM as the accelerating voltage used is higher and hence the electron wavelength governed by $\lambda = \frac{h}{\sqrt{2meV(1+\frac{eV}{2mC^2})}}$ is smaller in the range of 0.8 to 3.7 pm.

2.4.2 TEM of Graphene Mono and Multi-Layers

1. Theoretically we know the lattice structure and crystal geometry of the pristine graphene but practically in fabrication of graphene there might be defects/deviations from ideal crystal structure which can affect the electronic,chemical,mechanical and magnetic properties of the 2D-material and hence it is necessary to probe the real crystal structure of graphene by TEM which can give us information about graphene's point vacancy defects,edges,grain boundaries,dislocations,number of layers and stacking configuration as given in the reference [4] which can affect the working of graphene based nano-devices.

2. In TEM the sample should be electrically conductive and should be thin enough for electrons to penetrate through but graphene is both electrically conductive as well as atomic layer thick (0.75 nm) and hence no sample preparation of graphene is needed.

3.Graphene due to its mono-layer atomic thickness can be treated as weak phase object i.e it introduces only a local phase to the transmitted electron whose amplitude corresponds to graphene's crystal field potential.

4.Accelerating voltage used for graphene is nearly 80KV for the electrons to be able to penetrate through the graphene and also the sputtering/removal of the carbon atoms due to high kinetic energy of the electron beam incident on it can be prevented as the kinetic energy of the 80KV electron is below 22eV which is sputtering threshold for graphene.

5.But still at 80KV the chemical etching and sputtering of the dangling carbon atoms can take place and hence electron rate and area exposed to TEM of graphene should be controlled to prevent it.

6. TEM Micrograph of graphene can give us information about,

A. Point Defect by Bright Field Imaging,

1.Monovacancy - Absence of one carbon atoms at lattice site.

2.Divacancy - Absence of Two carbon atoms in the lattice.

3.Multivacancies

4.Interstitional and Substitutional Impurities/Doping

5.Stone-Wall Rotations - In plane 90 rotation of C-C bond.

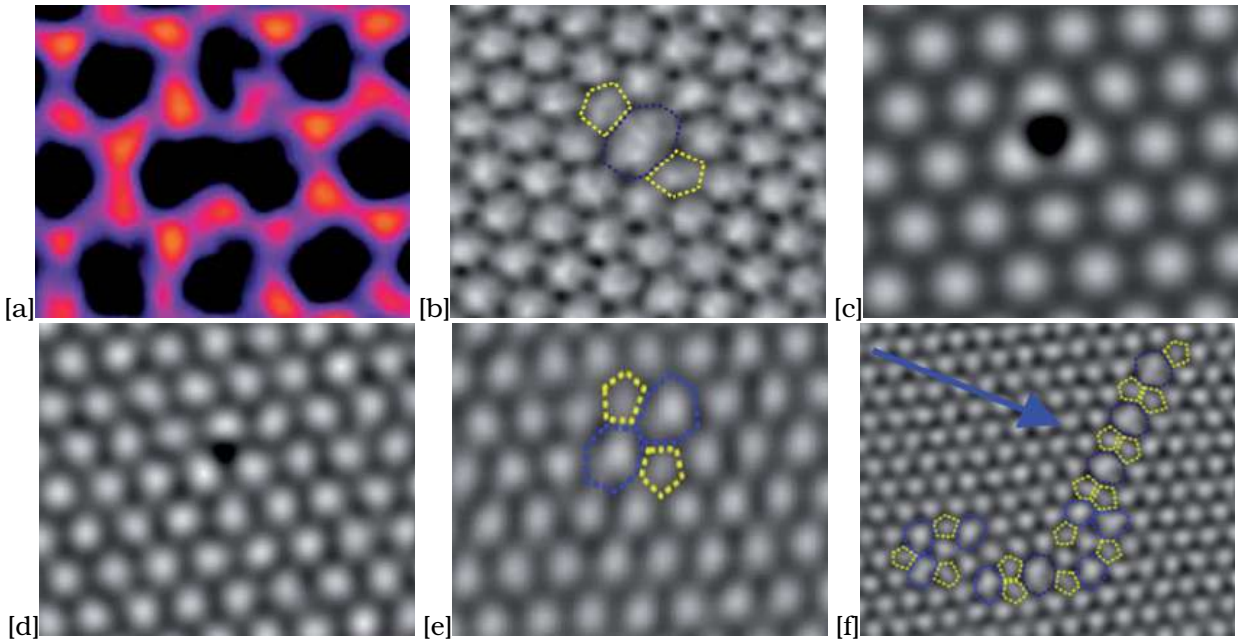

Figure 2.31: Bright Field TEM Micrograph of,(a)A 10 member Ring at the centre due to Mono-vacancy Defect in Graphene (False Colour) (b) A 5-8-5 Ring Structure due to Di-vacancy Defect in Graphene (c) Interstitional Iron Doping In Graphene (d) Substitutional Iron Doping In Graphene (e) A 5 and 7 member ring defect due to Stone wall Rotational Defect (f) Non-hexagonal lattice rings due to collection of various point defects.[4]

Note - The point defects can also be introduced by irradiation effects in the TEM i.e electron collision with atoms leading to removal of atoms.Point defects generally leads to change in the ring size from ideal 6 C-C bonds to 4,5,7,8,9 rings to reduce the ground state energy to minimum possible for the defective configuration.

Also dopants/impurity studies can help gain insights to develop graphene based electronic devices.

B.Dislocation - Climb,glide and slide studies of the carbon atoms by bright field image that governs the mechanical properties of graphene.

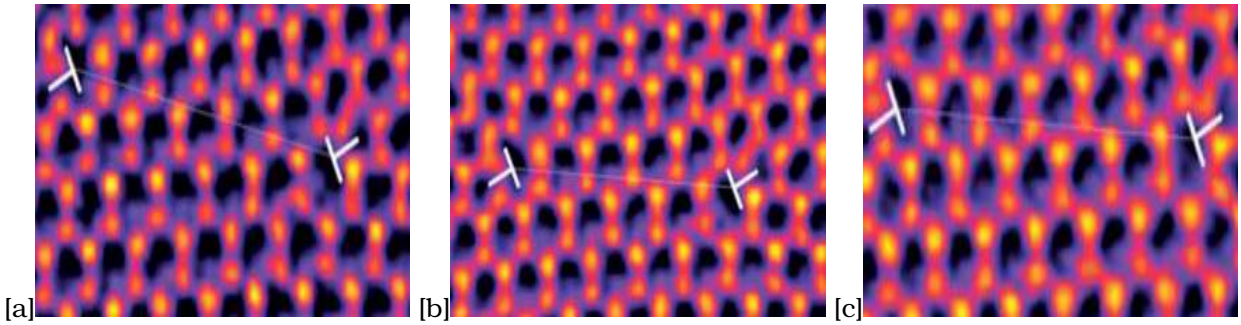

Figure 2.32: A TEM Micrograph (False Colour) showing Dislocation pairs of Carbon Atoms as shown by T's undergoing (a) glide,(b) climb,(c) slide in graphene.[4]

C.Grain Boundaries by dark field imaging as shown in Figure 31(d) which can be of inter-layer overlap or distinct atomic bonded arrangement which governs the electrical transport,optical,mechanical

and thermal properties.

D. Identification of the type of the edge by bright field imaging -

1.Zigzag

2.Armchair

3.Klien's Edge

to study the edge states topology in graphene.

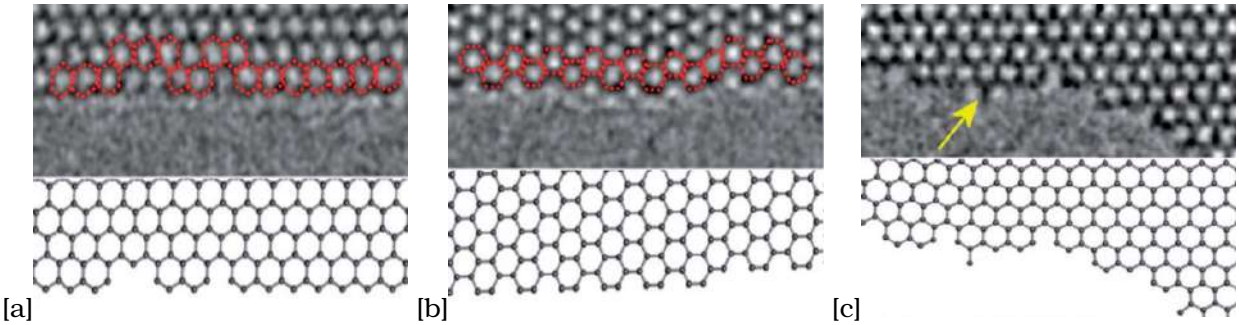

Figure 2.33: A TEM Micrograph showing (a) Zigzag (b) Armchair (c) Klien's Edge Boundaries in Graphene.[4]

E. Number of layers of Graphene by pattern identification in bright field imaging at some defocus.

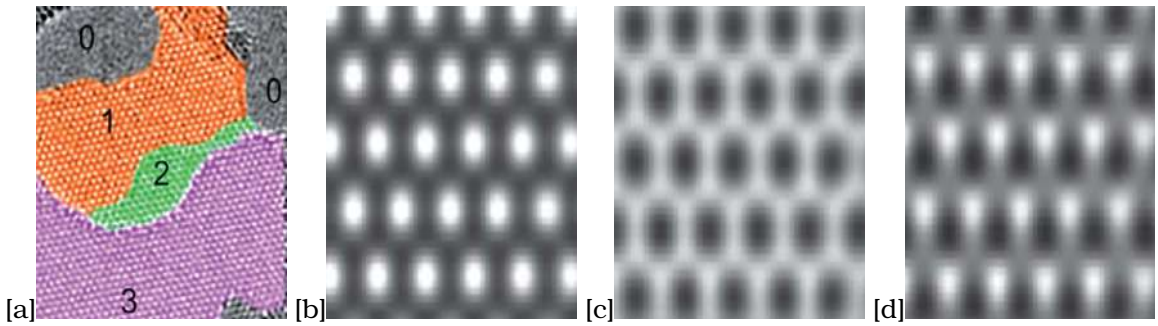

Figure 2.34: (a) False Colour TEM micrograph indicating the number of Layers of Graphene with 0 indicating hole etched in graphene due to electron beam irradiation effects (b) Zoomed TEM micrograph of Monolayer at 5nm defocus having relatively small white coloured circular pattern array (c) Zoomed TEM micrograph of Bilayer at 5nm defocus having relatively larger black coloured circular pattern array (d) Zoomed TEM micrograph of Trilayer at 5nm defocus having relatively triangular pattern array.[4]

F. Stacking Configurations by diffraction pattern imaging in the multi-layers of graphene.

[a] 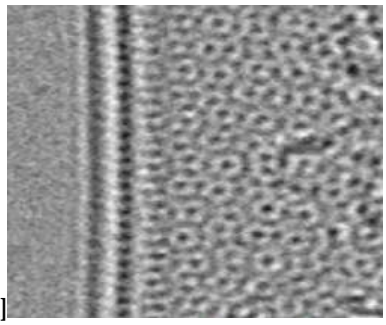 [b] 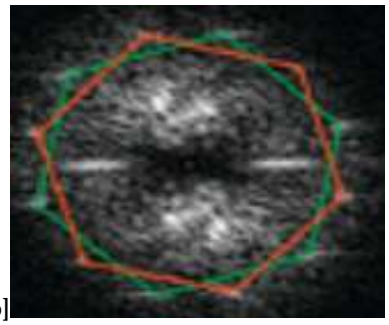

Figure 2.35: (a)TEM Micro-graph of Bilayer Graphene having Moire Pattern (b) Fast Fourier Transform Image of the (a) Indicating 30 degree twist between the two graphene layers.[4]

G. Peak distance in the Intensity profile plotted from bright field image as shown in Figure 31(b) can give us information about the defects present in graphene.

TEM micrograph in general is a 2D image and is difficult to interpret the 3D nature of the graphene,hence it needs to be combined with other microscopy/spectroscopy techniques like Raman,Optical,Scanning Tunneling Electron Microscopy (STEM),Electron Energy loss Spectroscopy (EELS),Insitu TEM (heating of the grid holding the sample to tune the properties of the sample) to get complete characterization of graphene.

2.5 Scanning Probe Microscopy

2.5.1 SPM basics

Scanning probe Microsopy is a probing technique used to characterize the electronic,magnetic,structural properties of material by using a sharp tip having lateral dimensions of orders of nm separated from the sample by a separating distance where the electron tunnelling effects, atom-atom interaction forces,collective tip material interaction dominate and by using these effects one can
,

1.Get Topographical features of the sample in vertical direction.

2.Move the Nano-Materials.

3.Get Electronic Density of States (D.O.S) with high resolution.

4.Get Landau Levels etc.

Scanning probe microscopy covers wide range of specialized microscopy and spectroscopy techniques (as shown in the figure below) used to probe specific property of the materials but is broadly classified in to two categories,

1.Scanning Tunnelling Microscopy/Spectroscopy.

2.Atomic Force Microscopy/Spectroscopy.

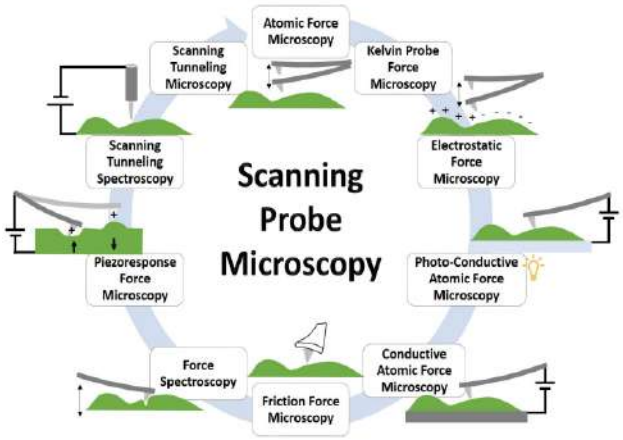

Figure 2.36: Umbrella of Scanning Probe Microscopy [2]

1.Scanning Tunelling Microscopy/Spectroscopy(STM/STS)

A potential V is applied between the sharp metallic tip and sample which causes electrons to tunnel in the spacing towards the sample from tip and enter the conducting sample ,by measuring the change in the current for the change in the sample bias voltage we can get the differential conductance (dI/dV) and from it get the D.O.S for the whole sample,3D image of the sample having atomic scale resolution by piezoelectric rastoring of the tip on the sample.Such techniques are referred to as Scanning Tunelling Spectroscopy/Microscopy.

The principle of working of STM/STS is shown in the schematic below.

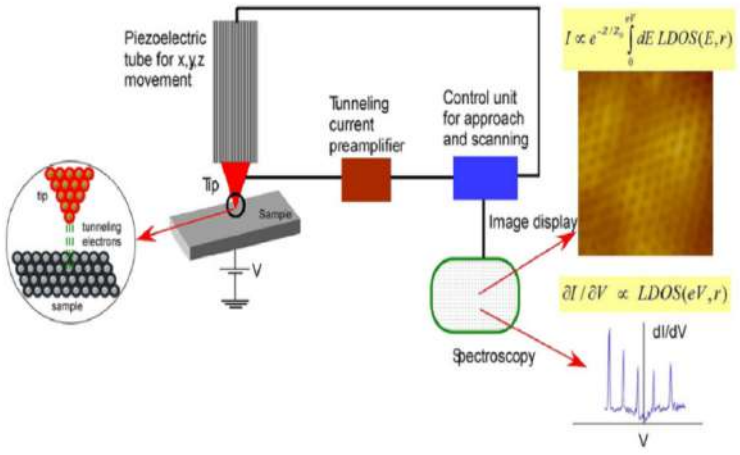

Figure 2.37: Schematic of Scanning Tunnelling Microscopy/Spectroscopy [4]

2.Atomic Force Microscopy/Spectroscopy(AFM/AFS).

AFM is a characterization technique of nano-materials in which a tip at the end of the cantilever beam is rastored/scanned over the material and whatever waviness/conformations/ripples the cantilever beam undergoes due to presence of wavy nature of the 2D material is captured by the

laser reflected from the surface of the cantilever and detected by photo-detector to produce a 3D image of the surface of the material.

The principle of working of AFM/ATS is shown in the figure below.

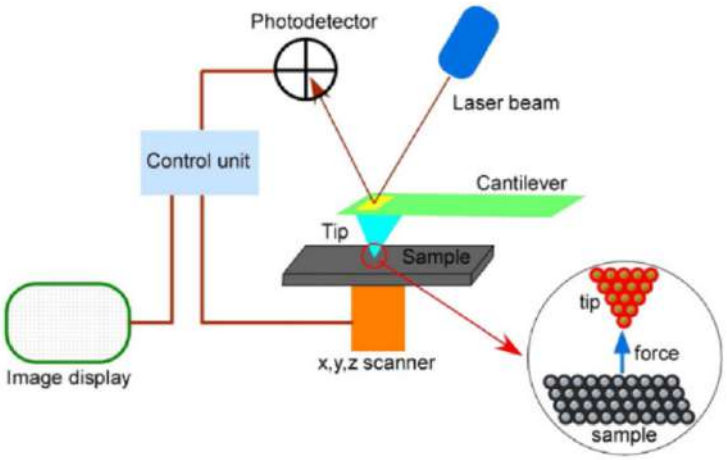

Figure 2.38: Schematic of Atomic Force Microscopy/Spectroscopy [4]

The sharp tip is brought in close contact to sample (distance approx few nm),the atom at the tip experience atom-atom attraction and repulsion as well as collective substrate tip interaction depending on the distance between the tip and sample as shown in the graph below.

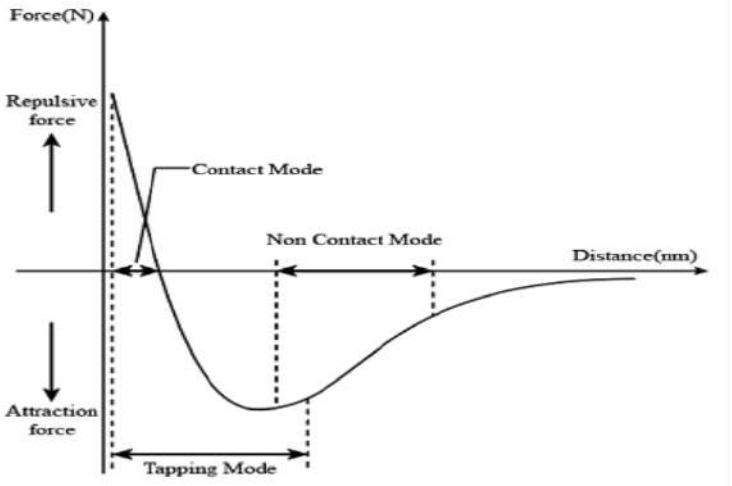

Figure 2.39: Atom-Atom Interaction Force vs Tip Sample Separating Distance [5]

A constant equilibrium force between the tip and sample is maintainted by a feedback circuit so that the distance between the tip and sample remains constant and we can get information about the topography of the sample.The feedback circuit can be driven by signal modified from tip-sample interaction,which can be in the form of,

1.Light phase and amplitude change in the optical fibres

2.Photo-detector Voltage from laser signal

3.Capacitance between tip and metal contact

4.Piezoelectric Signal etc.

giving rise to various A.F.M/A.T.S techniques as named in figure 30.

As only atom-atom interactions between tip and sample are needed to characterize the sample,the sample to be probed by AFM can be non-conductive which is main advantage of A.F.M over other techniques.

Specialized scanning probing techniques used to probe specific physical quantities of the sample can be constructed using similar principles of STM and AFM such as Scanning Single Electron Transistor (SSET) and Scanning Gate Microscopy (SGM).

Note - Vibration Isolators to isolate the SPM setup from the floor vibrations is a must in SPM measurements as the vibrations in an educational buildings are typically of the order of microns and hence should be scaled down to zero as the measurements performed by SPM techniques are of the orders of nano-meters.

2.5.2 SPM of Graphene,Bilayer Graphene and Twisted Bilayer Graphene

STM probes the roughness/conformations of the graphene on any substrate.It also probes the defects,topography,dislocation study of graphene grown on SiC,identification of number of layers,etc.

AFM can be used to characterize the mechanical,electrical properties of the nano-material.In particular AFM can be used to,

1.Measure Flake thickness of graphene (High resolution AFM image of 0.03 nm)

2.Measure Lattice Mismatch of TBG by Fourier Imaging to calculate the twist angle and hence study the lattice relaxation effects in TBG with time.

3.Cut the graphene flakes to potentially obtain graphene nanoribbons by AFM lithography.

4.Check the quality of CVD grown graphene by lateral force imaging and Kelvin Force Microscopy.

[a] 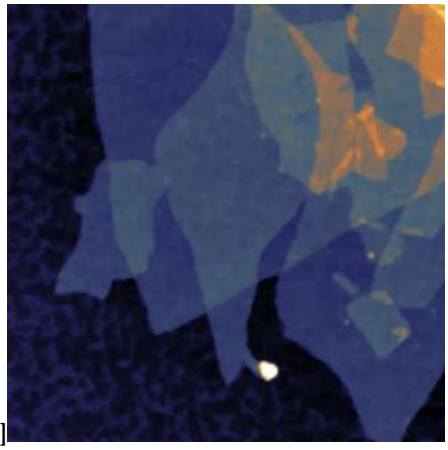 [b] 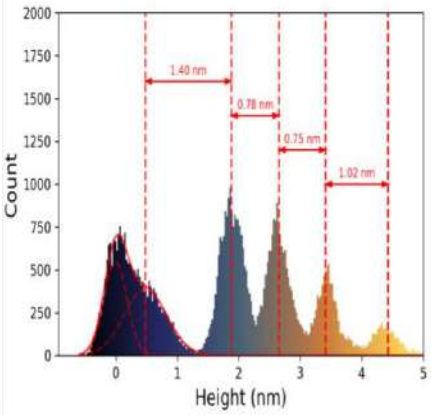

Figure 2.40: (a) AFM topographical Micrograph of Multilayer Graphene. (b) Measuring the Height of the first four layers from 3D AFM Micrograph [3]

[a]  [b] 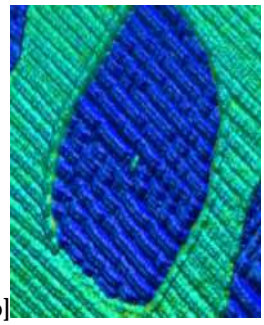 [c] 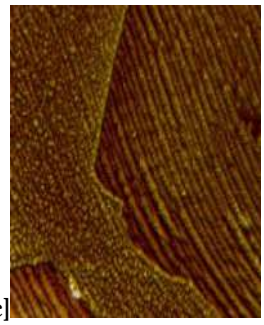 [d] 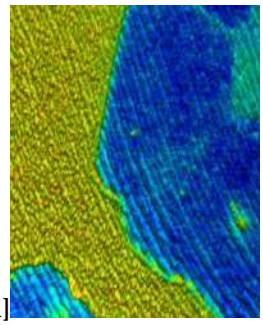

Figure 2.41: (a)AFM Topography Micrograph of graphene grown by CVD (b) Friction Force Imaging of (a) with copper substrate having green contrast and graphene having blue contrast and centre of nucleation growth is also having green contrast indicating more friction at the centre of nucleation and hence an inhomogenity in CVD grown graphene (c) Another AFM Topography Micrograph of graphene grown by CVD (d) Kelvin Probe Microscopy of Graphene grown with CVD indicating work potential inhomogenities with green colour contrast.[3]

[a] 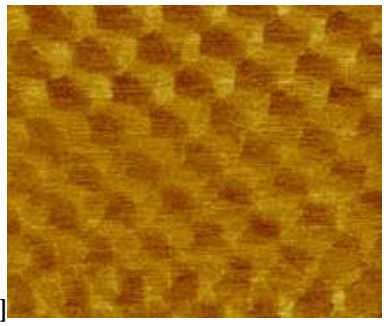 [b] 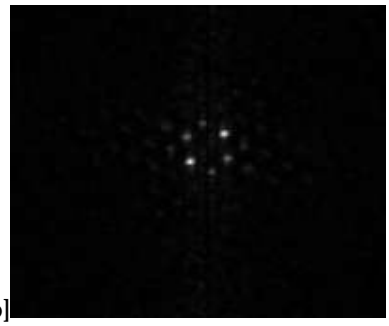 [c] 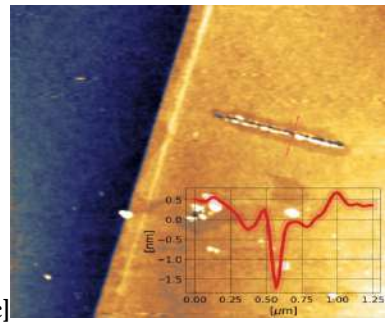

Figure 2.42: (a)AFM Micrograph of Moire Pattern in TBG (b) Fast Fourier Transform of the central part of AFM Image to calculate the twist angle and the lattice constant (c) Cut obtained on Graphene by AFM lithography.[3]

AFM showed graphene on SiO_2 is not completely flat,there are ripples on graphene which are due to its strong adhesion to SiO_2,hence there is no intrinsic rippling of graphene on substrate.Mica substrates are flatter than SiO_2,hence ripples in graphene can be minimized but gating of graphene on mica is still having issues. Ripples can also be introduced during exfoliation process or manufacturing process of graphene that influence the electric current flow in conductive AFM measurements in graphene and hence influence the local electrical properties of the material.

By Scanning Tunelling Spectroscopy we can plot the differential conductance (dI/dV) vs sample bias for different gate voltage to identify the dirac point i.e the point of minimum conductance which is dependent on gating voltage indicated by red arrow as shown in graph below.The U shaped region is independent of the gating voltage and indicates band gap as graphene on SiC break sublattice symmetry. The dI/dV is minimum but not zero hence finite conductivity is seen at dirac point due to electrons and holes puddling which leads to charge inhomogeniety which can be probed by STM measurement as shown in the figure below.

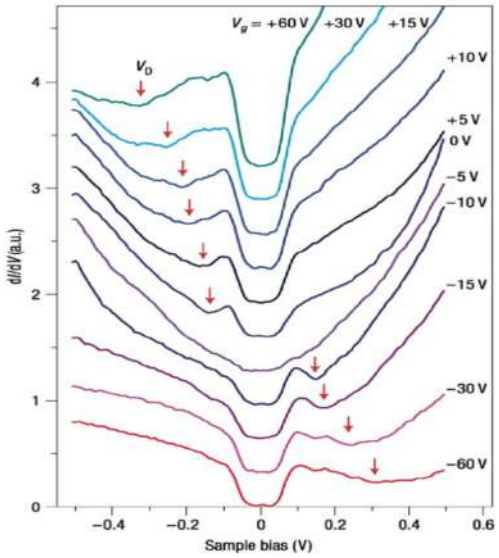

Figure 2.43: STS measurement plot of dI/dV vs sample bias V which is Gate Voltage Dependent dI/dV spectra of graphene on SiC and a Gate voltage independent U region centred at zero sample bias indicating the band gap due to sublattice symmetry breaking [4]

The shift in the dirac point is mainly due to intravalley back-scattering (electron hole puddling) which can be seen by dI/dV map.No corelation was found between ripples and charge inhomogeniety from spatially resolved STM measurement.The charge inhomogeniety was mainly found from defects,dopings and contacts.These ripples and charge inhomogenieties affect the carrier mobility and other electrical properties and can affect the graphene device performance.

Charge inhomogeniety in graphene was reduced by two orders of magnitude for graphene on hBN than compared to graphene on SiO_2,the carrier mobility of the graphene increased and also the quality of graphene on hBN was comparable to suspended graphene.

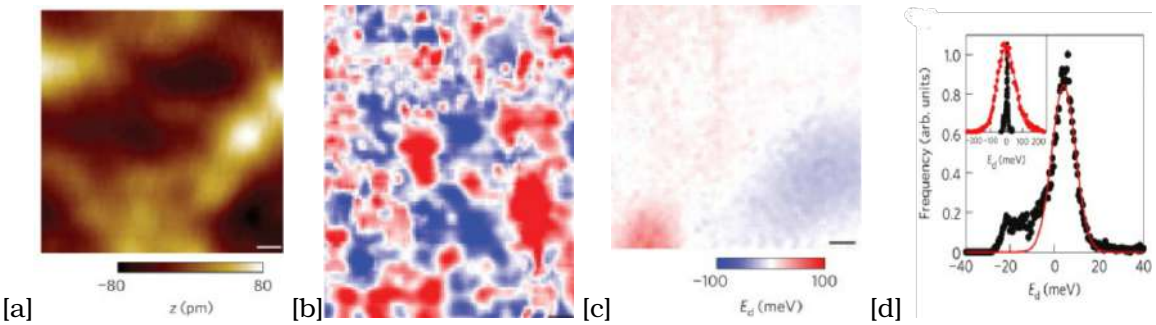

Figure 2.44: (a)STM Micrograph of Graphene on hBN (b) Tip voltage at Dirac Point of Graphene on SiO2 as a spatial mapping on the STM micrograph (c) Tip voltage at Dirac Point of Graphene on hBN as a spatial mapping on the STM micrograph (d) Comparison of Tip voltage at Dirac Point for Graphene on hBN and Graphene on SiO_2 clearly indicating lesser charge inhomogeneties in graphene on hBN (more charge neutrality at dirac point) than on SiO_2 .[4]

SGM can be used to probe the local charge inhomogeniety,localized states,universal conductance and quantum point contact in graphene device.[4]

We can identify the type of scattering from dI/dV vs n dependence which can be probed by

STS and also spatial dI/dV maps.Any structural or electronic perturbation of the honeycomb lattice of graphene can be termed as defect.Defects in graphene can be due to growth or processing of graphene which can influence its electrical,mechanical,optical and transport properties of graphene. Ripples/wrinkles/corrugations show lower conductance than non-rippled section.The dirac point minimum conductance is absent in rippled graphene i.e indicating that these ripples can give rise to finite density of states at dirac point and hence no minimum conductance at dirac point as shown in Figure 47.

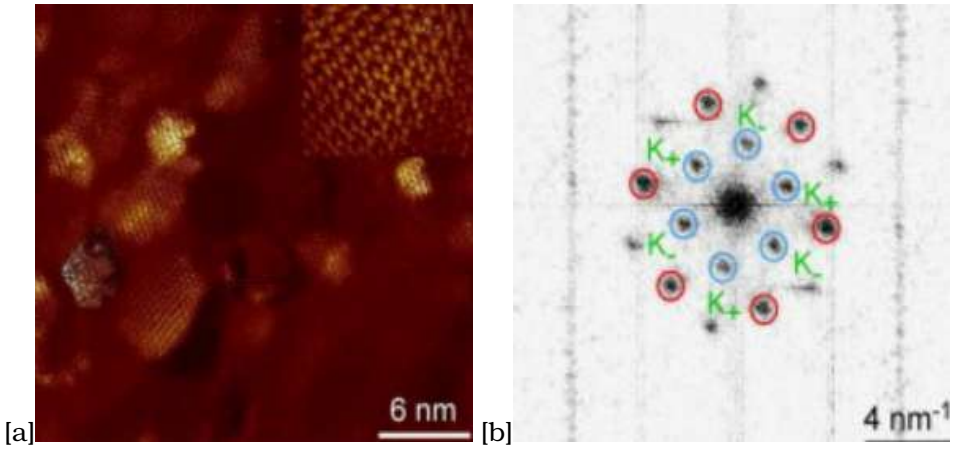

[a] [b]

Figure 2.45: (a) Intervalley Scattering (dI/dV) Spatial Maps of Exfoliated Graphene on SiO_2 with inset showing the interference pattern due to intervalley scattering from defects. (b) Fast Fourier Transform of Intervalley scattering map with central blue hexagon indicating interference pattern due to intervalley scattering.[4]

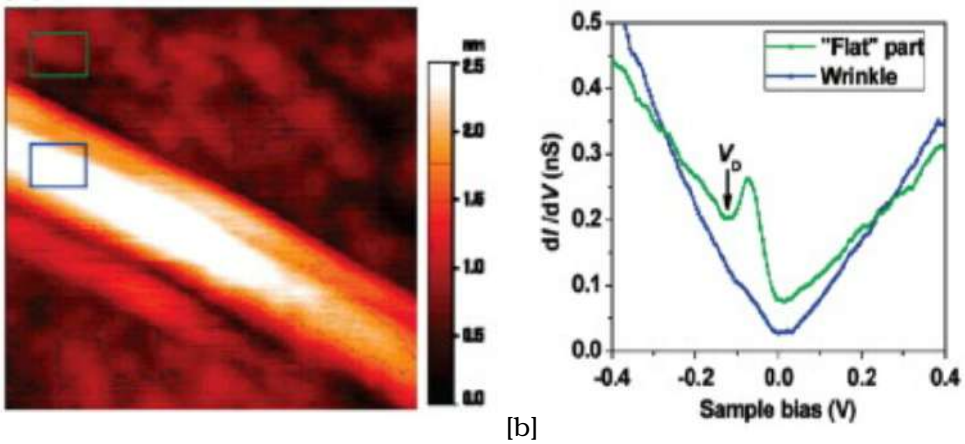

[a] [b]

Figure 2.46: (a) STM image of Exfoliated Graphene with wrinkles on SiO_2 (b) Absence of Dirac Point in STS measurements of Wrinkled Graphene on SiO_2 for the square green regions as indicated in (a).[4]

Ripples/distortion/strains on bilayer graphene can give rise to pseudo magnetic field having 300 T to 400 T intensity which can be seen by dI/dV spectral image of STM.

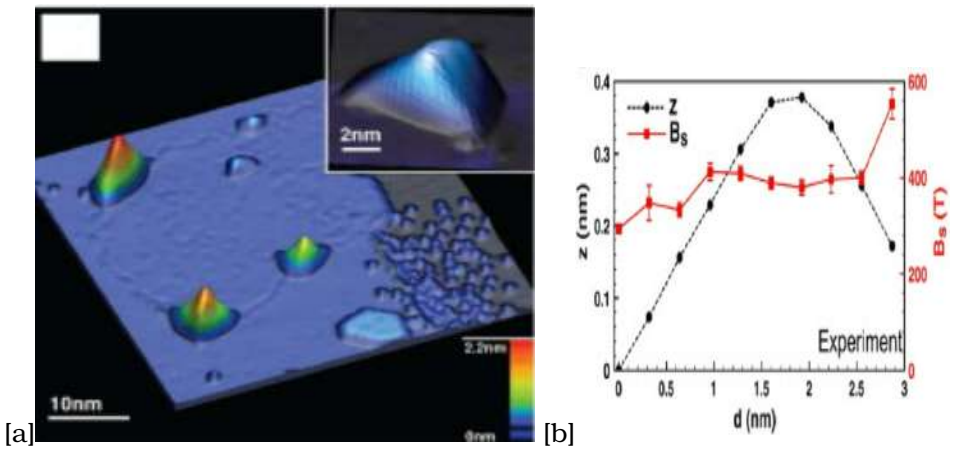

[a] [b]

Figure 2.47: (a) STM image of Induced Nanobubble on graphene with Nano-bubble in the inset (b) Pseudo Magnetic Field of 300 T to 400 T is generated over the spatial regions of Nano-bubble as probed in the STS measurement.[4]

The zero energy Landau Level state of graphene at some magnitude of transverse applied magnetic field which is the basic characteristic of graphene can be seen by STM. The difference between Landau level peaks by STM can give us the type of Dirac Fermionic behaviour i.e having massless or massive charged carriers,hence we can identify the number of layers of graphene which depends on the relation of Landau Level energy with the magnetic field and carrier density.

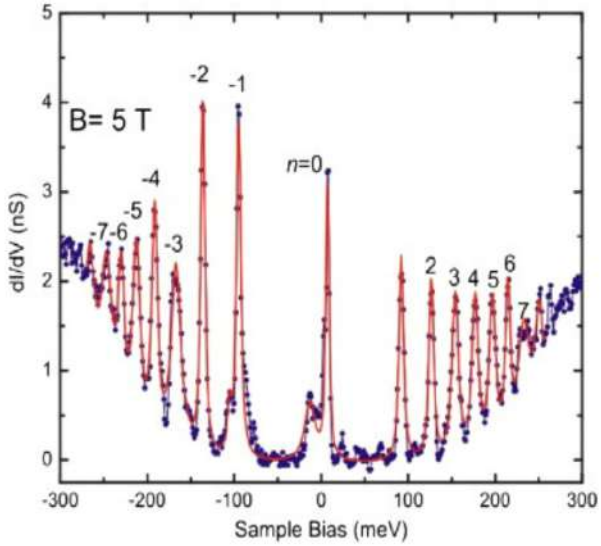

Figure 2.48: STS measurement of monolayer graphene on SiO_2 at 4.3 K for Magnetic field of 5T showing the Quantum Hall Effect phenomenon i.e the Landau Level Energy peaks at integer carrier density spacing with Landau Level Zero Energy Peak observed indicating monolayer graphene and the first L.L peak separated by 100 meV and second peak separated by 50 meV and so on from zeroth peak at 5T indicating $\sqrt{n}$ dependence of Landau Level Energy which is characteristic of massless Dirac Fermions again indicating monolayer graphene. [4]

Massless Dirac Fermions => Landau Level energy $\propto \sqrt{B}, \sqrt{n}$ => Monolayer
Massive Dirac Fermions => Landau Level energy $\propto$ B, $\sqrt{n(n+1)}$ => Bilayer and Multilayers

In Bilayer graphene the tranverse electric field can induce band gap by breaking the sublattice symmetry which can be seen by the dI/dV vs bias voltage of STM. STM image also showed band gap of bilayer and monolayer graphene on SiC substrate. The spatial variation of Dirac Point on the sample can also be plotted to get clear idea about charge inhomogenity in the sample.

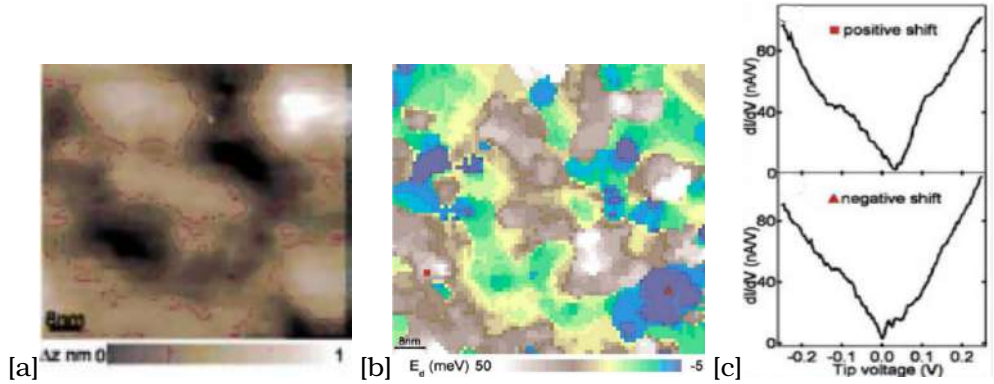

Figure 2.49: (a)SPM of bilayer graphene on SiO_2 substrate having 1 nm height fluctuations of 80 x 80 nm^2. (b) Spatial Mapping of Dirac Point Tip potential of bilayer graphene on SiO_2 substrate which varies from -5 meV (negative shift indicated by red triangle) to 50 meV (positive shift indicated by red square) (c) the dI/dV spectra of positive and negative shift spatial region .[4]

Twisted graphene layers grown by CVD show density of states divergence on either side of dirac point i.e the so called Von-Hove Singularities.TBG behave as single layer graphene i.e massless dirac behaviours for angle greater than 20 degrees which is found from STM measurements at 4K by measuring the difference between the Landau Level peaks. For low angle twist the V.H.S dominate the energy spectra and massless dirac Fermionic behaviour breaks down.

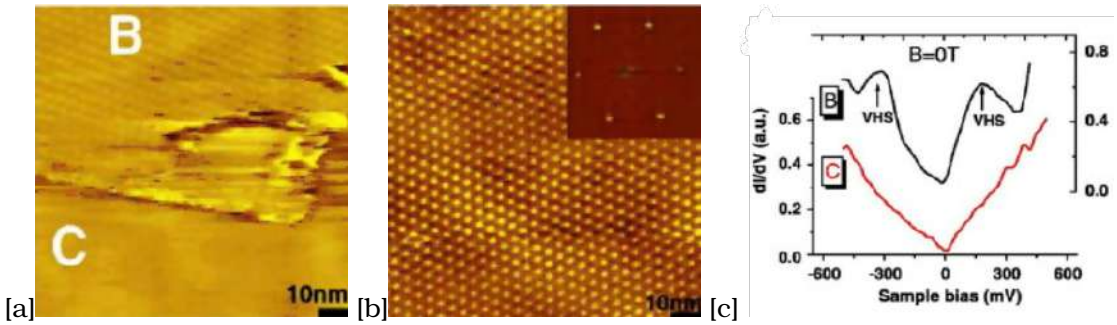

Figure 2.50: (a) STM image of Moire Pattern B and Non-Moire Pattern C of CVD grown Graphene. (b) Moire Pattern with inset showing the fast fourier transform from which we get the twist angle of B region which is 3.5 degrees with error range of 0.3 degrees (c) the dI/dV STS measurement of B region at zero magnetic field show V.H.S on either side of the dirac point .[4]

Hence AFM and STM studies on graphene can give us information about,

1.Scattering Mechanism in graphene

2.Local Dirac Point and local mobility of graphene sample.

3.Charge inhomogeneity of graphene spatially on SiO_2 and hBN ,which concludes that graphene on hBN has high mobility and lower ripples than graphene on SiO_2 and comparable to suspended graphene.

4.Quality of graphene grown from various techniques.

.

2.6 Raman Microscopy/Spectroscopy

2.6.1 Raman Microscopy/Spectroscopy Basics

Raman Spectroscopy can be explained from 3 point of views -

1.Quantum Mechanical Description in which the vibrational energy state of molecule can be considered as an analogue to the electron energy state.

2.Electrons Interactions in the lattice potential of ion i.e the band structure electron excitations

3.Classical Wave Description of photon and the polarizibility of molecule.

1.Quantum Mechanical Description

When an intense monochromatic light source typically in UV,visible or near infrared spectrum is incident on material, then the material's molecules which are vibrating at particular vibrational energy state depending on its thermal energy (i.e temperature of its surrounding),causes the electrons in the molecules to get excited to a virtual vibrational energy state by absorbing the incident photon and as the virtual vibrational energy state is unstable, the excited electrons in the molecules will again transition to real lower energy state by reradiating/scattering photon.If the reradiated/scattered photon is having an energy equal to energy of the incident photon,then such elastic scattering is called as Rayleigh Scattering i.e electrons in the molecules transition back to its original vibrational energy state after emitting photon.If the reradiated/scattered photon is having an energy greater than energy of the incident photon i.e electrons in molecules transition to a state having lower vibrational energy state than the original ground state of vibration,this inelastic scattering of photon is called Anti-Stokes Raman Scattering (which generally take place in the material having higher thermal energy i.e is at higher temperature) and if scattered photon is having energy lower than the initial incident energy then it is called as Stokes Raman Scattering.A basic Schematic of the transitions and the working schematic of Raman Spectroscopy are shown in the figure below.

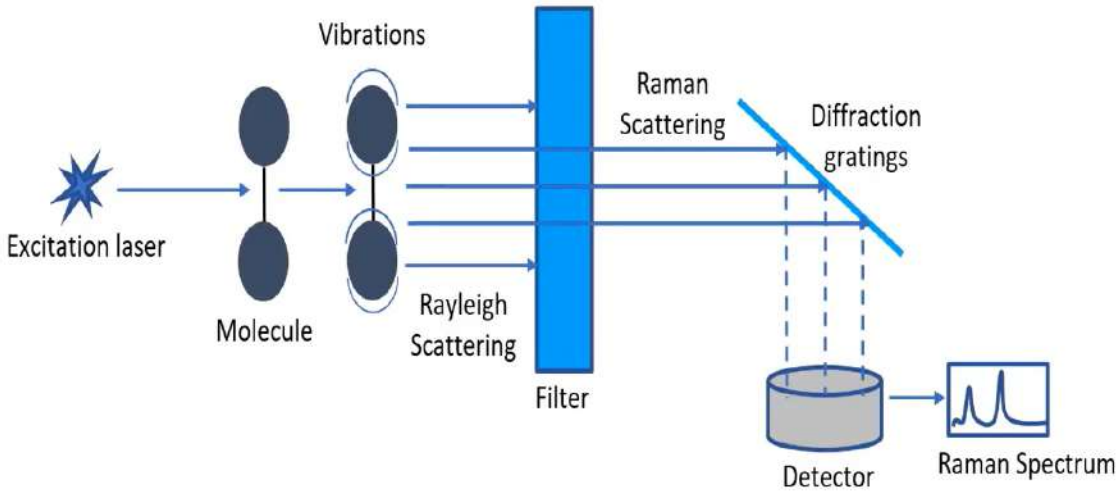

Figure 2.51: Working Schematic of Raman Spectroscopy[11]

An intense monochromatic laser source which can be in UV,visible,near IR region is incident (480 to 1064 nm Wavelength- generally higher wavelength is chosen as Raman Scattering is proportional to fourth power of incident wavelength) on the mirror to get reflected in filter which further monochromats the source and then through the lens the light beams are focussed on the sample and reflected/scattered rays are collected through collection lens which are again passed through the series of filters/Diffraction Gratings to block the Rayleigh scattering and then finally filtered Stokes and Antistokes Raman Photons are detected by Photodetector as shown in the schematic above.

Note - Flouroscence $[10^{-9}s]$ is phenomenon similar to Raman Scattering but instead of virtual intermediate state the molecules reach a higher energy state and then comes back to a level higher or lower than initial ground state but is different from Raman Scattering $[10^{-14}s]$ in terms of time scales and hence can be differentiated by using Pulsed Laser Source due to difference in time scale.[10]

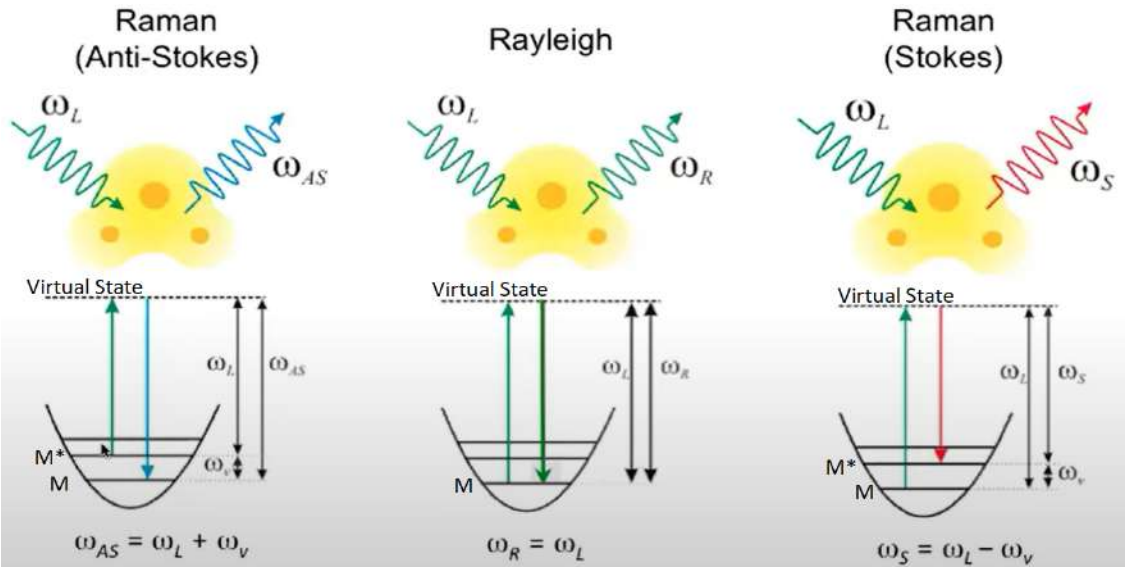

Figure 2.52: Stokes Raman Scattering,Rayleigh Scattering,Anti-Stokes Raman Scattering Ray Transitions Schematic Diagram.[9]

By energy conservation -

1. For Anti-Stokes Raman Scattering, M* + hw_L -> M + h(w_{AS} = w_L + w_v)

2.For Rayleigh Scattering, M + hw_L -> M + hw_R

3. For Stokes Raman Scattering, M + hw_L -> M* + h(w_S = w_L - w_v)

Note - The molecules remain in virtual state for nearly 10^{-14} sec and falls back to a lower vibrational state.Out of 10 lakh photons only 2-7 get Raman Scattered and hence we use an intense monochromatic laser source.[10]

2.Electron Interactions in the lattice potential of ion i.e the band structure electron excitations -

Electrons in the valence band gain energy and transition to higher virtual oe real energy state in the conduction band (unstable) ,emits phonon in the conduction band which causes the electron to lower its state to an unstable state,hence again emits photon which causes the electron to lower its state back to valence band state,if the valence band state is at higher state than initial i.e reradiated photon energy is lower than the incident then this inelastic scattering is Stokes Raman and if it is higher than the incident then it is Anti-Stokes Raman Scattering as shown in the figure for case of an insulator.This explanation of Raman Scattering is used to explain Raman Spectroscopy of graphene,TBG,hBN and Bilayer Graphene.

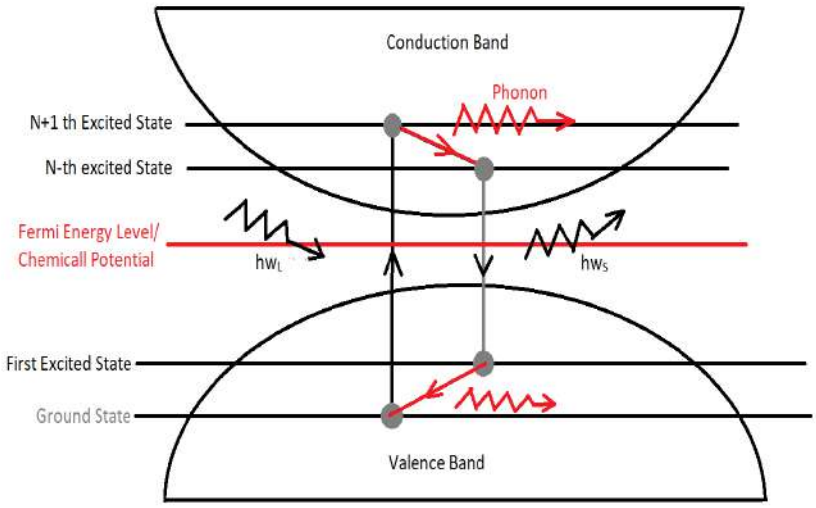

Figure 2.53: Raman Stokes Scattering Explanation Via Band Diagram of Insulator (Triple Resonance)

3.Classical Wave Description of Photon and the polarizibilty of Molecule-

1.If we consider an atom not having an intrinsic polarity (i.e having london dispersion forces) and apply an electric field on the atom,the electric field causes the atom's positively charged nuclei to shift to negative field and negatively charged electron cloud to shift to positive electric field and this cause spatial charge variation in atom giving rise to induced polarity in the atom.

2.Polarizibility (α) is property of material to induce a dipole moment (μ) under applied electric field E i.e => μ = αE.

Now,photon being electromagnetic wave/particle has both electric and magnetic field,so the electric field of incident photon causes the vibrational energy state of molecules in the material to change (dq),where q is the vibration mode of the ground energy state of the molecule i.e dα/dq = + ve => Stokes Raman Scattering and dα/dq = - ve => Anti -Stokes Raman Scattering

The vibrational energy modes of material are said to be Raman Active only when dα/dq $\neq$ 0 and vibration modes/symmetric stretch of molecules causes the ellipsoidal volume representation of the molecules to not conserve under vibrational modes.

Consider an example of CO_2 => CO_2 has 3 vibration modes as shown in figure below.

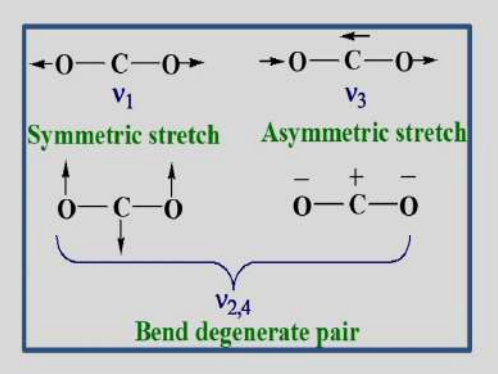

Figure 2.54: Vibration Modes of CO_2 molecule.[10]

Now,if we consider the first stretch ν_1 and consider its 3 vibration modes => +q,0,-q and represent it as an ellipsoid then +q,0,-q causes change in volume of ellipsoid which is not conserved and hence the term $d\alpha/dq$ due to change in α of the material due to incident photon is not equal to zero and hence these vibration modes are Raman Active ,where as in the remaining two stretches the volume of ellipsoid for +q and -q vibrational modes are same and hence the incident photon will cause net charge in the induced polarity of the atom at two extremes(+q and -q) and hence $d\alpha/dq$ = 0 and hence they are not Raman Active as shown in the figure below.

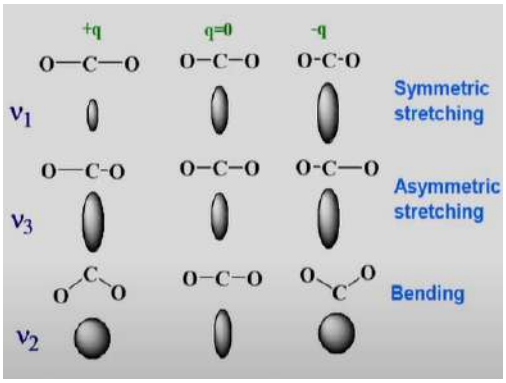

Figure 2.55: Symmetric,Assymetric and Bending Degenerate Pair Stretches of CO_2 [10]

Note - 1.Ellipsoid Changes related to vibrational modes can also be seen in the shape and orientation along with its size for the material for it to be Raman Active as these changes cause the polarizibilty of the atom to change i.e dα/dq $\neq$ 0 as observed in case of water.

Now when we detect the emitted photon with photodetector and plot the intensity of detected photon with wavenumber (v)= $\frac{1}{\lambda}$,we see peaks at $(v)_{incident}$ = $(v)_{emitted}$ => Rayleigh Scattering and $(v)_{incident} \neq (v)_{emitted}$ => Raman's Scattering.

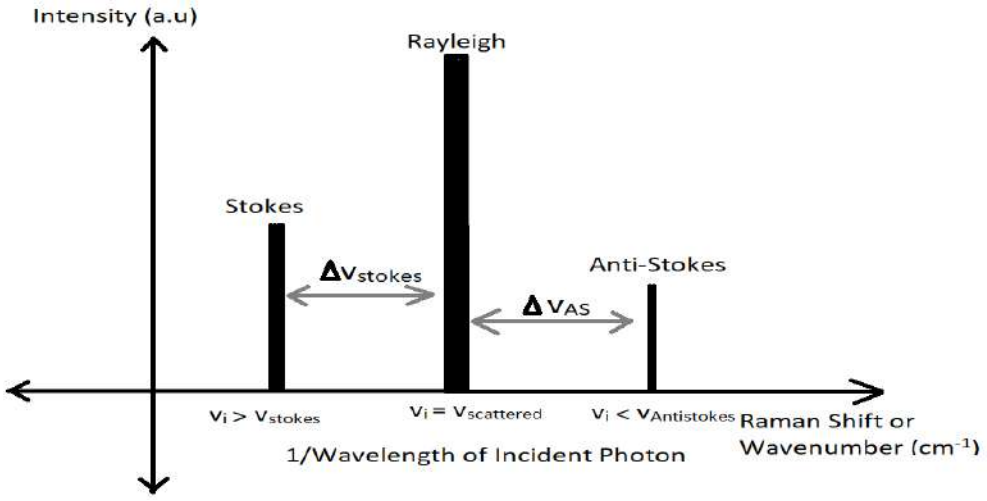

Figure 2.56: Intensity vs Raman Shift indicating Stokes,Antistokes and Rayleigh Scatterings

By using Raman Spectroscopy we can identify the material from standard material Raman Spectra graph,defects in material,Fermi Energy of the material etc.

2.6.2 Raman Spectroscopy of Graphene,Bilayer Graphene and Twisted Bilayer Graphene , hBN.

1.Raman of hBN

Raman Spectra of hBN (mono and multilayers) show characteristic peak due to E_{2g} phonon mode which is analogous to the G peak of graphene. In hBN single crystals the Raman Peak occurs for a 514.5 nm laser source at $1366cm^{-1}$ and generally downshifts (Red shifts) as number of layers increase and the intensity also increase proportional to N (Number of hBN Layers) for first few layers as shown in figure below.[7]

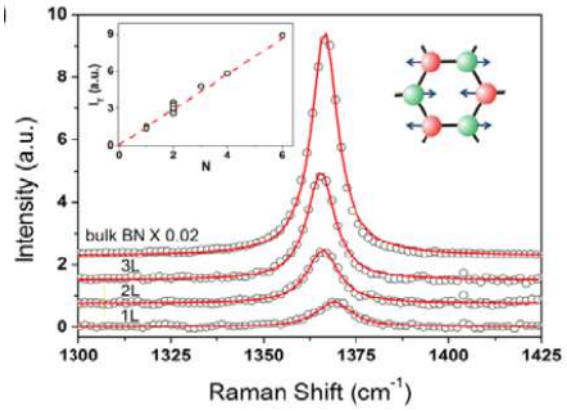

Figure 2.57: Raman Spectra for mono-multilayer hBN mono blue shift with left inset showing proportional increase in intensity with number of layers and right inset showing E2G phonon mode of vibration in hBN and the blue shift is evident as there is transition from bulk hBN to monolayer [7]

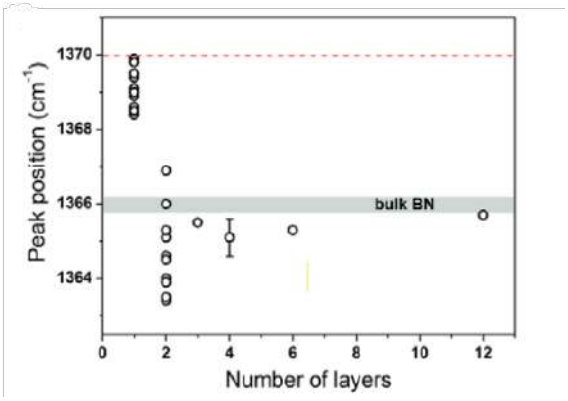

Figure 2.58: Raman G Peak Position vs Number of Layers with error bar indicating the error of instrument used in the Raman Spectroscopy and also the monolayer hBN are clearly identifiable due to blue shift of nearly 4cm [7]

In ideal hBN with no defects the equivalent G mode peak will be observed due to excitation of electron from ground state to a excited state followed by a phonon scattering and then followed by de-excitation of electron from the excited state again to ground state by scattering of photon which is the main reason for Raman's equivalent G Peak observed in Raman Spectra of hBN as shown in the figure below.

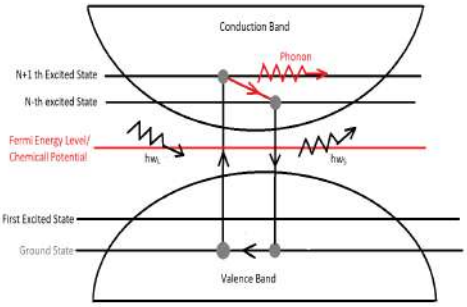

Figure 2.59: Stokes Raman Scattering Explanation Via Band Diagram for hBN insulator showing Equivalent Single Resonant G peak Stokes transition in band diagram.(Double Resonance)

The Raman Spectra for hBN used in this thesis's heterostructure for capacitance measurement was performed by LabRAM spectrometer at 532 nm laser with 100 mW incident power at room temperature with 10 percent notch filtering $(50cm^{-1})$.A Double Lorentzian curve fit was used to fit the Raman Spectra of hBN showing peak at 1366.93 cm^{-1} and FWHM of $7.86cm^{-1}$ as shown in the figure below.(Credits to Suvronil Dutta for performing Raman)

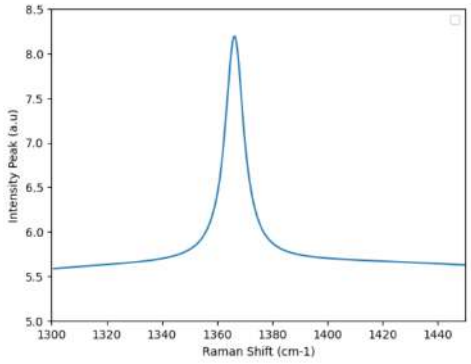

Figure 2.60: Double Lorrentzian Curve Fit of Raman Spectra of hBN showing a peak at 1366.93 cm-1 .

But if we consider the actual plot of hBN there are small intensity peaks in the Raman Spectra other than the equivalent G peak which are due to defects which can,

1.Obstruct the path of electron jump to excitation state and hence scatter a phonon and emit an photon at frequency lesser than the G peak frequency i.e observed on the left side shift (Red shift peaks as visible on the left side of G peak in figure below.)

2.Intermediate phonon scattering can lead to photon emission at higher frequencies than the equivalent G peak (Blue Shift peaks as visible on the right side of G peak in figure below.)

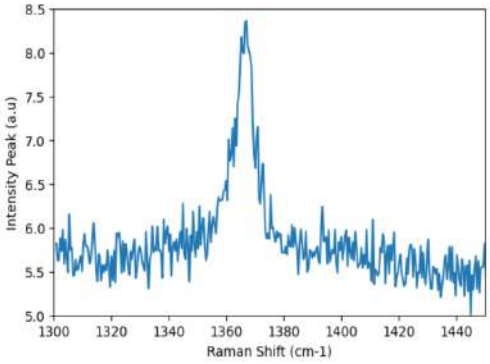

Figure 2.61: Actual Stokes Raman Line Spectra of hBN

It is difficult to investigate the number of layers of hBN from Raman Shift alone once the number reaches greater than 4-5 layers as evident from figure 57 .Hence Raman is usually performed with AFM or optical microscopy to give a conclusive result on the number of layers.[7] Based on the images and spectra obtained in optical microscopy contrast (blue bright contrast -section 3.2) and Raman Spectroscopy (Raman Peak at 1366 cm^{-1}), the determination of number of layers of hBN for the heterostructure was inconclusive but it definitely has more than 5 layers and less than or equal to 12 layers.

2.Raman of Graphene and Bilayer Graphene

1.Raman Spectroscopy of Graphene based materials can give us information about band structures,many body interactions,nature of defects,edges,number of layers,Doping,Fermi Level,strain and stress effects,temperatures effects,stacking order,growth mechanics etc.[4]

2.Let us consider the case of graphene and Bilayer graphene.

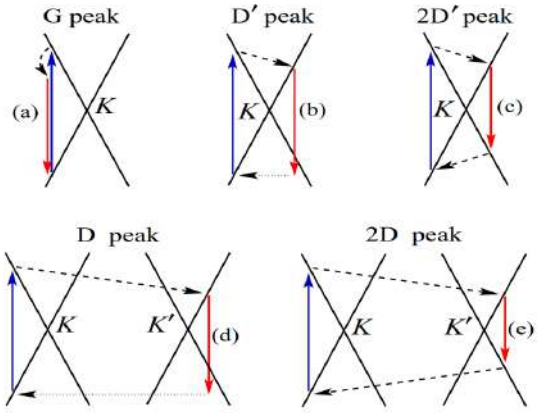

Figure 2.62: Stokes Raman Explaination via Dirac Cone in Graphene with (a).The intra-valley one phonon Single Resonance G peak(b).Defect Assisted Intravalley one phonon D' peak. (c).Intra-valley two phonon 2D' Peak. (d).Intervalley two phonon D peak (e).Intervalley two phonon Triple Resonance 2D peak.[5]

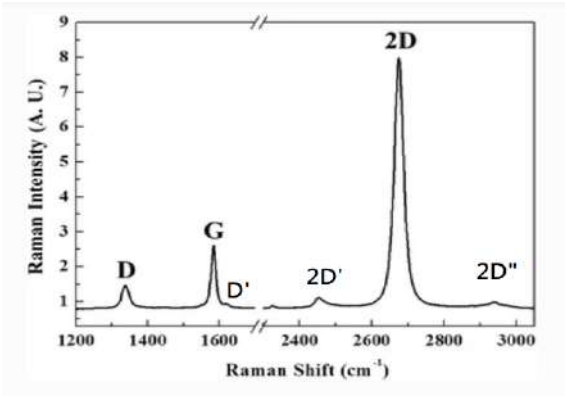

Figure 2.63: Raman Spectra of Monolayer Graphene with 532 nm excitation laser [11].

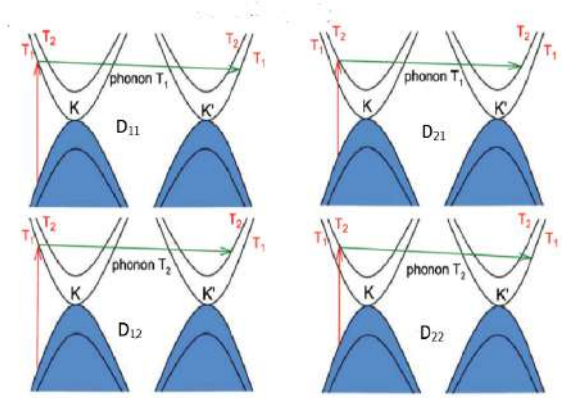

Figure 2.64: 2D peak Band Transition in Bilayer Graphene [4].

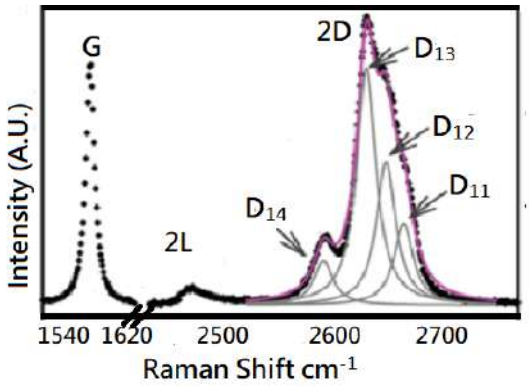

Figure 2.65: Raman Spectra of Bilayer Graphene with 633 nm excitation laser [4].

Raman Spectra of Graphene from above figure shows G peak in graphene observed around 1580 cm^{-1} and is due to E_{2g} phonon modes at Brilluoin Zone centre (γ point). D peak is observed around 1350 cm^{-1} and is due to breathing modes of six atom rings and require defect for its activation and comes out from Tranverse optical (TO) phonon around k point of the Brillouin Zone and is active by Double Resonance as shown in fig. 61.The D peak activation is intervalley having, 1. Electron Excitation By Laser (Blue Arrow). 2.Electron Phonon Scattering with exchanged momentum q equal to k.(Line Dotted arrow) 3.Defect Scattering.(Point Dotted arrow)

4.Electron-Hole Recombination.(Red Arrow)

D' peak is similar to D peak but due to intra-valley process around 1620 cm^{-1}. 2D and 2D' peaks are second orders of D and D' peaks respectively. Since 2D' and 2D originate from a process where momentum conservation is satisfied by two phonons with opposite wave vectors (q and -q) they do not require the presence of defects for their activation and are always inherently present.[5]. D and D' however require defects for their activation hence not observed in pristine graphene. 2D peak in graphene is roughly 4 times more intense than G peak and its frequency is twice the frequency of scattering photon.

All the Stokes spectra Raman peaks observed in bilayer graphene are similar to monolayer graphene with similar explaination as shown in fig. 64 but with the exception of 2D peak.The 2D peak of Bilayer graphene has 4 components D_{11},D_{12},D_{21} and D_{22} which are due to possible combinations of inter-valley scattering of phonon in two conduction band as shown in fig 63.

Now consider the Raman Spectra of the Monolayer sample (Double Lorrentzian Fit) used in the van der Waal Heterostructure for its compressibility measurement in this thesis as shown in figure below which shows D peak at 1356 cm^{-1},G peak at 1585 cm^{-1} , 2D peak at 2680 cm^{-1} ,2D' peak at 2450 cm^{-1}. An hBN peak is observed at 1366 cm^{-1} as noted previously in Raman of hBN and can be easily confused with D_2 subpeak of D peak.

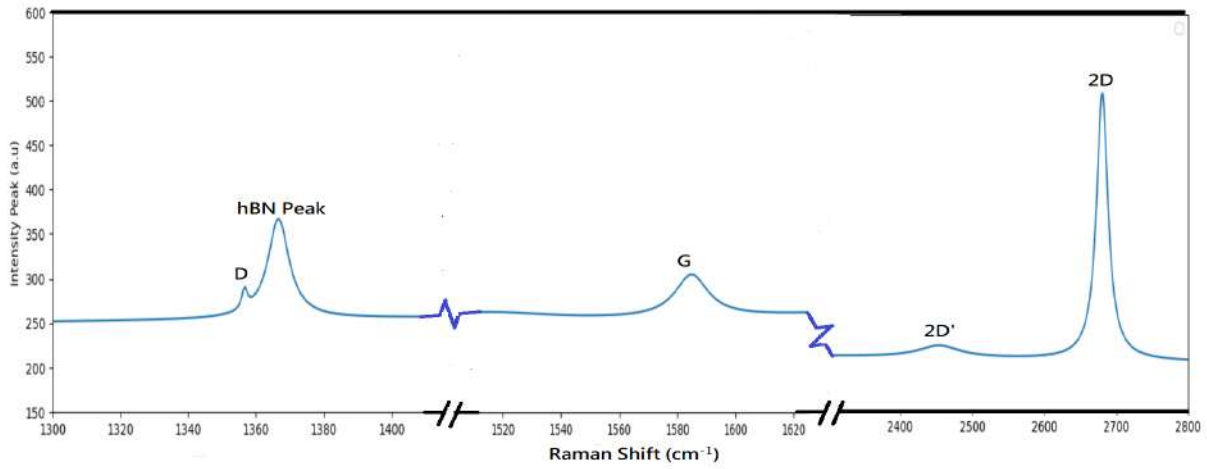

Figure 2.66: Raman Spectra for Monolayer Sample showing D,G,2D' and 2D peak for this thesis's Monolayer sample

Note - The intensity of the D peak is small compared to intensity of G peak and also the intensity of 2D peak is almost 6 times that of G peak indicating the graphene monolayer sample has relatively lower concentration of defects and is comparable to pristine graphene sample.An analogous study of ionizing graphene with plasma of Ar^+ ions indicates that for this sample the defects are equivalent of 10^{11} Ar^+ ions per cm^2 i.e equivalent of performing plasma with Ar^+ ions for 3 to 5 seconds.For more details of the equivalent study one can refer Figure 14(a) of reference [4]. Such analogous studies can help us characterize defects equivalently for any other monolayer sample from its Raman Spectra comparison.

Raman Spectroscopy of the Bilayer Graphene (2D peak) of this thesis's Bilayer Sample is shown

in figure below having 4 sub 2D peaks which confirms the bilayer nature of the sample.

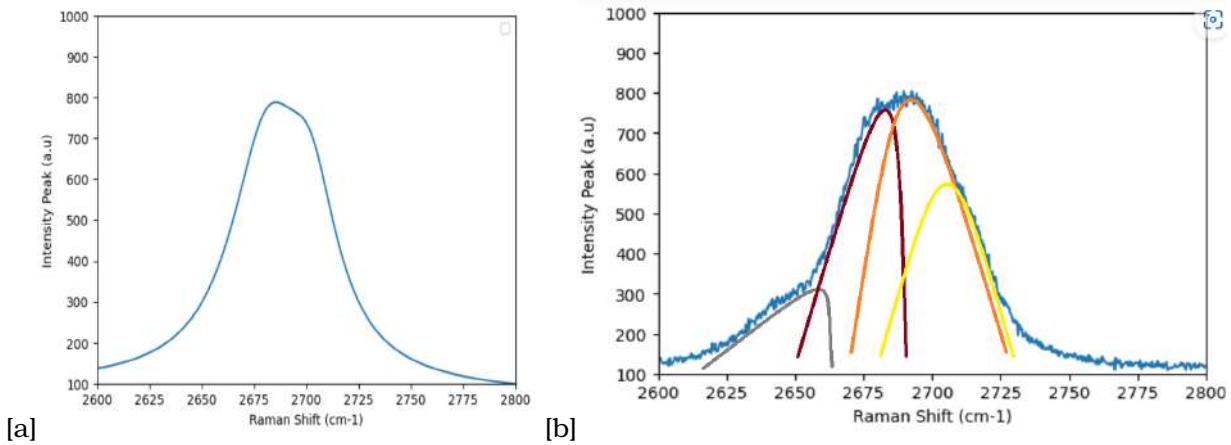

[a] [b]

Figure 2.67: (a) Double Lorentzian Curve Fit of 2D peak of Bilayer Graphene Sample (b) 4 Sub 2D peaks drawn approximately on actual Raman Spectra (without fit)

Raman Spectroscopy of graphene for this thesis's heterostructure was done by excitation energy of 2.33 eV i.e 532 nm.Here Raman Shift for 532 nm will be extrapolated from previous experimental data of Raman Shift for different excitation.Then the group velocity of the phonon dispersion is obtained by the relation between E_{ex} and $\triangle$ w,then the number of layers of graphene flakes from the 2D peak changes in shape,width and position is obtained confirming the bilayer nature of the sample,then finally the Fermi Energy and electron concentration of the monolayer sample is extracted by extrapolating previous experimental data which shows that the monolayer sample has intrinsic doping level.Similar analysis of extraction of Raman Shift,group velocity of phonon, the Fermi Energy and Doping level can be extented to bilayers and multilayers.

Let's find the quantities for this thesis's monolayer sample one by one.

1.Extrapolation of Raman Shift of 2D peak from Previous Experimental Raman Spectra Data for different Excitation Lasers -

The position of Raman Shift of G peak in the Raman Spectra is independent of laser Excitation used as observed from the experimental data shown in the figure below.The postion of the 2D peak however depends on the Energy of the Excitation laser. The Excitation of the laser used for the Raman Spectroscopy of this sample is 2.33 eV.So let's extrapolate the Raman Shift from experimental data by linear fit for excitation laser of 2.33 eV and verify whether it matches with Raman Shift of 2D peak of the mono-layer sample.

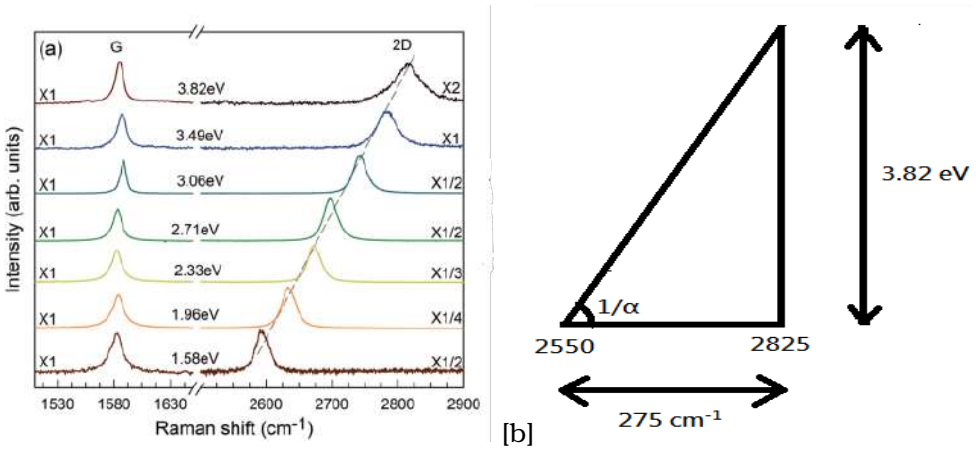

Figure 2.68: (a) Raman Spectroscopy of monolayer sample for various excitations of lasers [2] (b) Extraction of slope from the Visual Experimental Raman Spectra Data.

The linear fit equation is, Excitation Energy of Laser = Slope x Raman Shift(2D) + Constant

From above figure , 3.82 = tan($1/\alpha$) x 2825 + Constant

3.82 = 0.013890 x 2825 + Constant

Constant = -35.42

For a 2.33 eV excitation laser, Raman Shift(2D) = 2717.78 cm^{-1} indicating an overfit of the data as the 2D peak is observed at 2680 cm^{-1} for the monolayer as confirmed from another reference [4] (Figure 5(a) of reference [4]) .Experimental Raman Spectra Data as shown in Figure 5(a) of reference [4] indicating that the sample is monolayer graphene and the dependence of the Raman Shift of 2D peak is linear with the excitation energy having a slope of nearly 0.01.

Phonon Velocity Extraction,Fermi Energy Extraction and Raman Of TBG. Now let's extract the phonon velocity for our monolayer sample. The phonon velocity by using the change in 2D peak frequency for Raman Stokes and Antistokes and the Energy of Excitation slope with Raman Shift of stokes 2D peak it is found that [2],

$v_{ph} = \frac{\alpha_s/2}{1-\alpha_s/2} v_f$

where, $1/\alpha_s = \frac{1}{tan(1/\alpha)} = 100\ \frac{cm^{-1}}{eV}$ (ideal linear fit)

Now the Fermi Velocity for monolayer graphene can be related to Fermi Energy E_F and the carrier concentration n by,

$E_F = hv_f\sqrt{\pi n}$.

So before extracting the phonon dispersion velocity of the Raman Process in the monolayer sample ,the Fermi Energy and the carrier concentration should be extracted. So we will come back to the phonon velocity extraction after extracting the Fermi Energy and the carrier concentration for our sample.

There are two possible ways (more ways will be discussed in chapter 4) to extract the Fermi Energy and carrier concentration of our monolayer sample,

1. Extracting the Fermi Energy and carrier concentration from the previous experimental Raman Spectra plots plotted by varying the doping level in the sample by varying the gate voltage.The reference [12] has used 514.5 nm excitation laser as opposed to 532 nm laser used in Raman Spectra of our sample.The plots of variation of G peak position versus Fermi Energy and electron concentration are particularly useful (as the position of G peak of graphene is inde-

pendent of the Excitation Laser Frequency used in Raman so the scaling of Raman Shift with excitation frequency does not matter for G peak) as plotted in reference [12] as shown in the figure below. One can also extrapolate the value of Raman Shift for 2D peak by using linear fit for 514.5 nm to get Fermi Energy and carrier concentration from position of 2D peak.

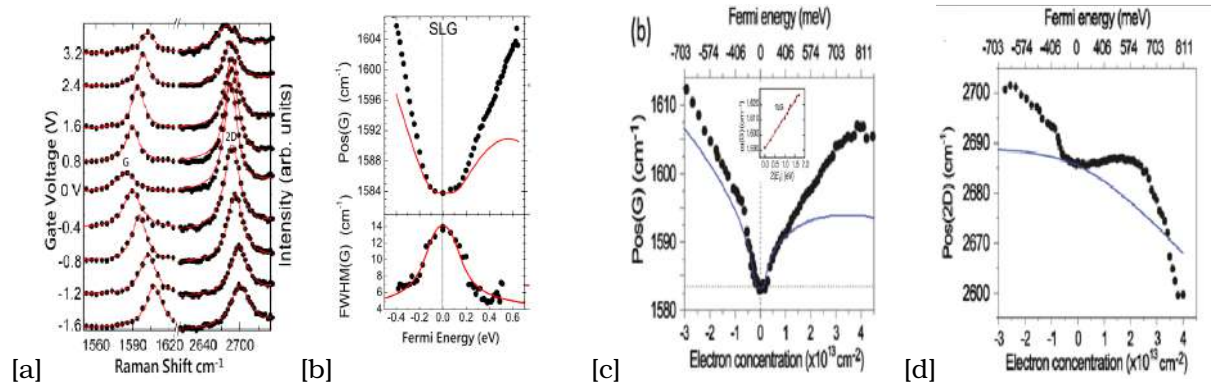

[a] [b] [c] [d]

Figure 2.69: (a) Raman Spectra of G and 2D peak variation with Gating Voltage (b) Position and FWHM of G peak with respect to Fermi Energy variation [12] (c),(d) Variation of Position of G and 2D peak with Carrier Concentration and Fermi Energy for monolayer sample [4,12].

The Position of the G and 2D peak of the Raman Spectra for our sample is at 1585 cm^{-1} and 2680 cm^{-1} respectively.The FWHM of the G peak is around 11 cm^{-1}.Hence extrapolating the Fermi Energy for our single layer graphene sample we get E_F = 0.15 eV ,which can be also found by using the linear fit equation from the inset of figure 68 [c],

w (G) = Slope x $2E_F$ + constant (Valid only if Fermi Level shift is larger than 0.1 eV)

From inset of figure 68 [c] the constant and the slope of the linear fit comes out to be 1591.79 cm^{-1} and 20.51 approx. and the E_F comes out to be 0.1655 eV. The corresponding electron carrier concentration comes out to be 0.25 x 10^{13} cm^{-2} indicating that the monolayer sample's doping level is nearly same as pristine graphene. One can also use the location of 2D peak to determine the Fermi Energy and carrier concentration but since the plot is available for excitation laser of 514.5 nm (2.4097 eV) , and our sample's Raman Spectra was performed by 532 nm, a linear fit can be used to find the equivalent Raman Shift of 514.5 nm laser excitation.

2.33 = 0.01 x 2680 + Constant

Constant = -24.47

Now, 2.4097 = 0.01 x Raman Shift (2D) - 24.47

Raman Shift (2D) = 2687.97 cm^{-1}, hence the values of E_F and electron carrier concentration are nearly same as the pristine graphene as visually seen from the Figure 68[d].

2. Another way to find the Fermi Energy is from the relation between ratio of the peak area intensity of the G and the 2D peak with the Fermi Energy by considering electron electron interactions,

$\sqrt{\frac{A(G)}{A(2D)}}$ = C' [γ_{e-ph} + $|E_F|f(e^2/\epsilon v_f)$] [5]

The electron phonon scattering Rate γ_{e-ph} as well as C' constant can be obtained by curve of $\sqrt{\frac{A(G)}{A(2D)}}$ vs E_F which is dependent on the frequency of the excitation laser used.Previous experimental data is for 514 nm and hence one needs to either extrapolate the A(2D) and A(G) for 532 nm laser or perform Raman Probing of the monolayer sample by varying the doping level

(gate voltage) and get the data.As we have already extracted the Fermi Energy and the electron concentration let's leave this method at that point.

Now the Fermi Velocity becomes,

v_f = $\frac{E_F}{h\sqrt{\pi n}}$ = 0.8116 x 10^6

Hence the phonon velocity of scattering is ,

v_{ph} = $\frac{0.01/2}{1-0.01/2} v_f$ = $\frac{0.005}{0.995} v_f$ = 4078.39 m/s

Note - The value of the α_s (best linear fit slope) varies by $\pm$ 7 from 100 $\frac{cm^{-1}}{eV}$ for the range of frequencies of excitation lasers and hence the phonon velocity can vary in small range because of it.[2]

Note - Using this approach of Raman Spectroscopy one can get the Fermi Energy and carrier concentration variation directly for varying gate voltage and hence it is an alternative to probe the quantum capacitance of any 2D material as measuring the Quantum Capacitance of any 2D material is the main goal of this thesis ,which in this thesis is done by constructing a hetero-structure as explained in chapter 4.

Finally we extract the number of layers of graphene from the previous experimental data plot of $\frac{I(G)_{NLG}}{I(G)_{SLG}}$ vs Number of layers for a excitation of 532 nm which is plotted after confirming the number of layers by optical microscopy [4]. But since we don't have the G peak data of the Bilayer Graphene of our sample we will leave it at this process of extraction.

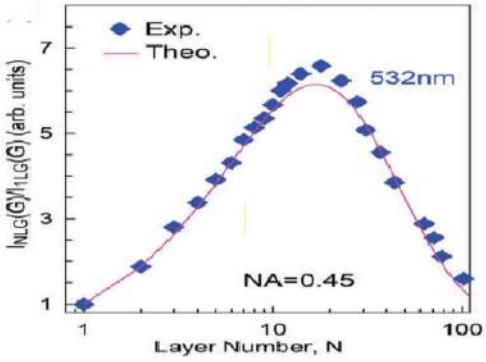

Figure 2.70: Intensity Ratio of G peaks of N layered Graphene to single layer graphene vs the number of layers of Graphene [4]

Note - One can also identify the number of layers of Graphene beyond 10 layers upto 100 layers by plotting ratio of Intensity of G peak of the Si substrate having N layered graphene on it to Intensity of bare Si Substrate to Number of layers.[4].

3.Raman of Twisted Bilayer Graphene.

Raman of TBG can be done at nano level and micro-level(one which is usually done in any Nanoscience lab).The FWHM of the G peak at the nano level Raman spectra of TBG varies with local location as shown in figure 70[f].This is mainly due to two reasons - 1.The Local Density of States which differs for the type of Stacking (AA,AB,BA,SP) 2.The Fermi Energy Level of the TBG as shown in the Figure 71 (h).

The G peak intensity and FWHM which we observe in micro-level Raman Spectra is due to overall percentage contribution of the AA stacking region,AB-BA stacking Region and SP stacking

region and also Fermi Energy level of the sample an example of which is shown in Figure 71 (a),71 (b).

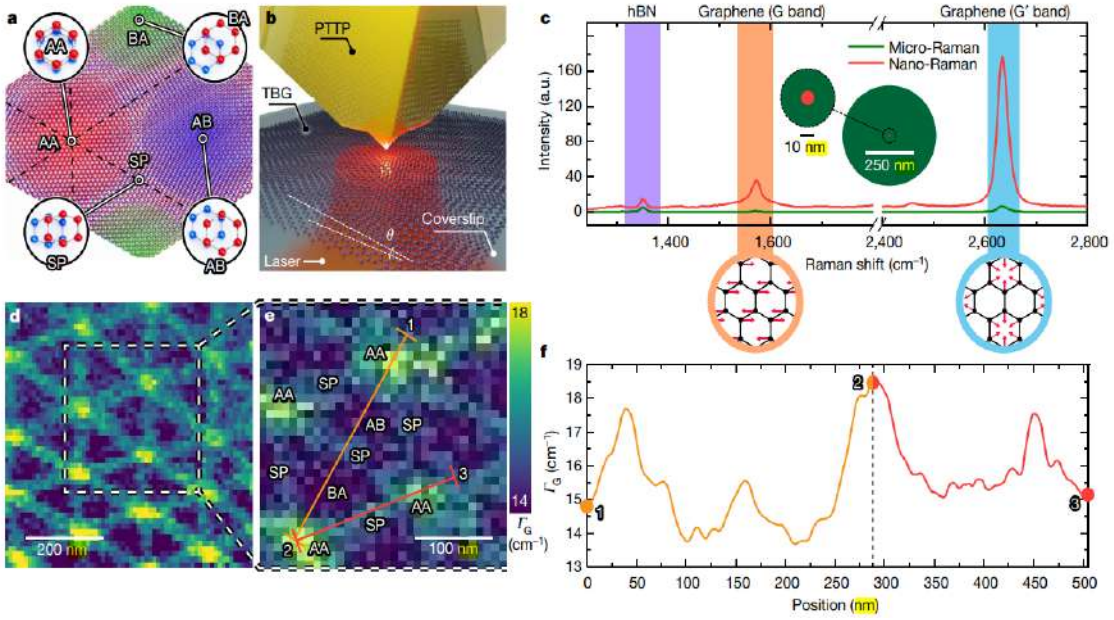

Figure 2.71: [a] AA,BA,SP and AB stacking orders for twist of 0.09 $\pm$ 0.02 degrees. [b] Nano Raman Setup [c] Micro-Raman (Green Line) and Nano-Raman (Red Line) Spectra of Twisted Bilayer Graphene [d] Full Width at Half Maximum Mapping in the real space crystallographic image of TBG [e] Movement of Raman Nano-Tip in 1-2-3 order along straight line in real crystallographic image mapping with linewidth of G Peak of TBG. [f] The Full Width at Half Maximum Variation with position of the Nano-Raman Tip due to variation of Local Density of states as indicated in 71(h) which is due to variation in the order of stacking (AA,AB,BA and SP), for example a peak in the Linewidth is observed at AA stacking point in zero Fermi Energy TBG sample as the Local density of states at zero energy for AA stacking diverges as shown in figure 71(h).[13]

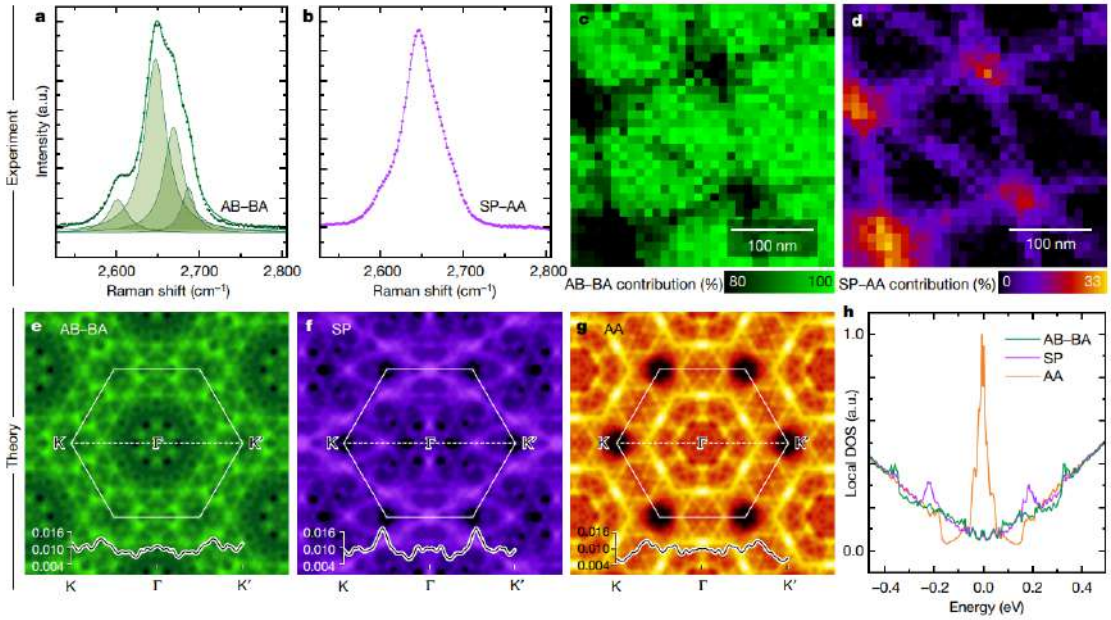

Figure 2.72: [a]Raman Spectra Due to contribution of AB-BA stacking order (as the TBG sample in Ref [13] is at -0.98 eV so the local DOS is more for AB-BA than AA-SP as indicated in fig [h] and hence the contribution of AB-BA(80-100 percent) is more than the contribution of SP-AA (0 to 33 percent) as shown in [c] and [d],[e] DOS plotted in momentum space for AB-BA,SP and AA regions for the regions in real space indicated by green-black in [c] and orange-red-black in [d].[13]

Hence it is experimentally very difficult to get a clear idea of the variation of FWHM of the G peak with respect to Fermi Energy Level as various twist angles of different samples might have different percentage contributions arising from the stacking order and also the main governing factor for the local D.O.S (on which the FWHM of the G peak depends) is the Fermi Energy of the samples and hence extreme care has to be taken for maintaining the Fermi Energy to same level in all samples which is dependent on the manufacturing process of graphene and also the twist precision to get same Raman Spectra contributions from stacking order for every sample (very difficult). But if the above precision is achieved experimentally then we can observe that around the magic angle i.e 1.08 ,as there is flattening of bands,there is an increase in density of states at zero Fermi Energy,hence the Raman Shift of the scattered photon can be in a range (with this range increasing to maximum as we approach magic angle) near to G peak and hence there is broadening of the G peak i.e FWHM of the G peak increases near magic angle and is max at 1.08 twist angle as shown in figure below.

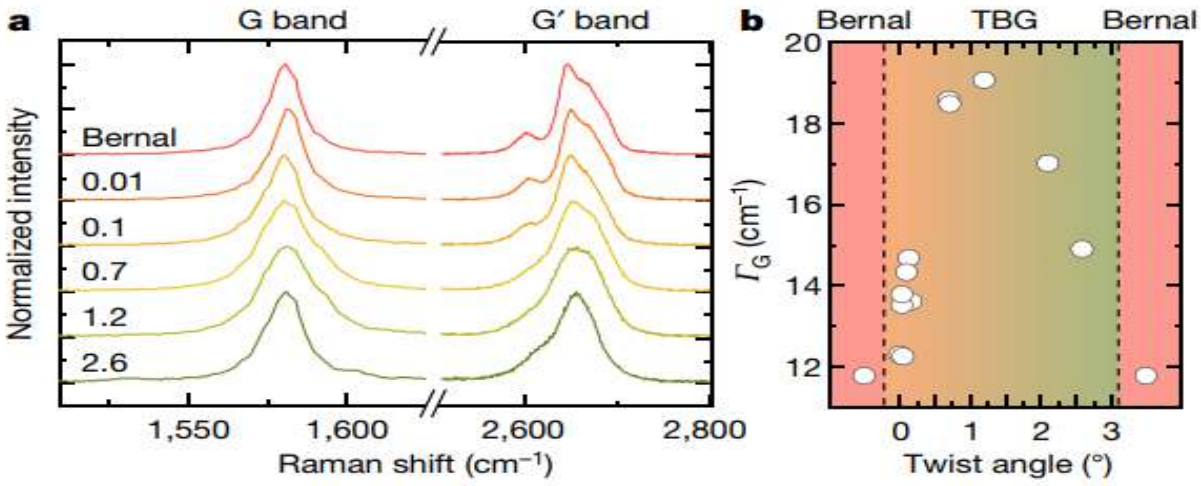

Figure 2.73: [a] Raman Spectra of Twisted Bilayer Graphene sample for various twist angle starting from zero (Bernal Stack) to 2.6 degree twists [b] Ideal Variation of FWHM of TBG samples with Twist Angles with maximum line width at 1.08 degrees i.e the magic angle which can be curve fitted with Lorentzian Fit.[13]

Now experimentally if we perform Raman Spectroscopy of TBG samples at different twist angles and plot the FWHM dependence of the G peak with the twist angle there will be discrepencies observed as indicated in the near zero twist angle region which is due to sample having either different contributions from stacking order or having different Fermi Energies or contribution of both.These discrepencies if ignored we can observe a general trend of increase in the FWHM of the G peak upto magic angle and then decrease.

Note - The FWHM of G peak generally increases with decrease in wavelength and at higher wavelength micro-Raman spectra of TBG we observe lesser discrepencies as indicated from experimental data for different laser excitations in reference [14] and hence higher wavelength Raman Spectra can help us quantitatively characterize the twist angle dependence with the FWHM of G peak with care taken that at least the Fermi Energies of the sample on which the Raman Spectra is to be performned should be same (as stacking order control will be very difficult to obtain). One can also look at the variation of FWHM of 2D peak with twist angle as it also broadens to max at magic angle but its Raman Shift again varies with the Excitation wavelength of the laser so we have to worry about one more parameter to analyze and it is given in extented data figure 4 of reference [13].

Coming back to our TBG sample,its Raman Spectroscopy is performed at 532 nm Laser Excitation and shows very small D peak at 1315 cm^{-1},hBN peak at 1366 cm^{-1}, G peak at 1585cm^{-1},2D peak at 2695 cm^{-1} as shown in the figure below.

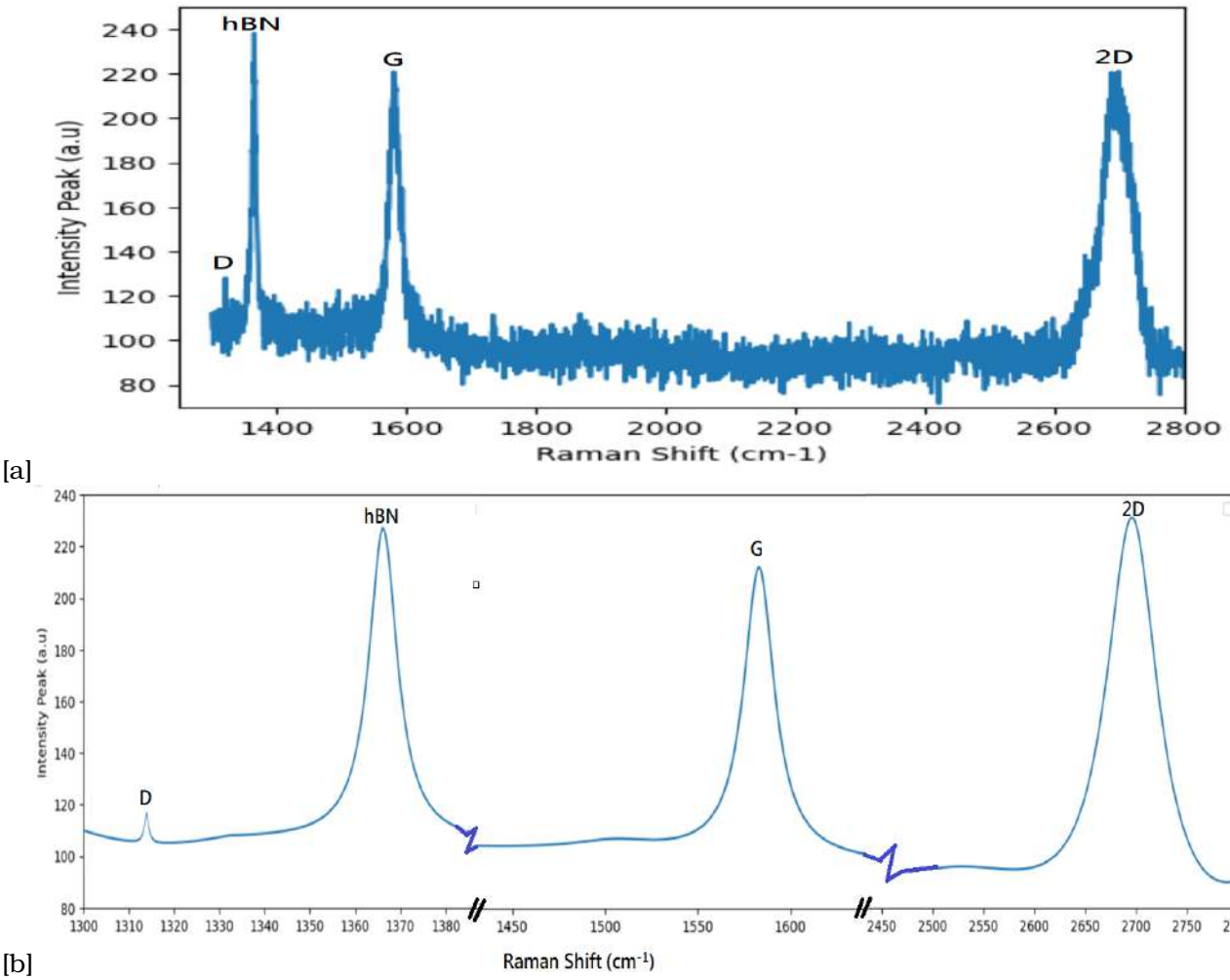

Figure 2.74: (a) Raman Spectroscopy of TBG of our sample with 532 nm laser Excitation without fit (b) Raman Spectra of TBG of our sample with 532 nm laser excitation Double Lorentzian Curve Fit.

An experimental data of the variation of the FWHM of the G peak with a 532 nm laser is available so we can try to quantify the twist angle of our TBG sample from the data available in [14] ignoring the discrepencies.The FWHM of G peak of our TBG sample is in range of 20.25 cm^{-1} to 21.2 cm^{-1}. Now if we try to hand wavy fit (linear fit gives an error range of 1 cm^{-1} but if we still do it the maximum of FWHM occurs at 21 to 22 cm^{-1} and is at 1.08 degree magic angle,also Lorrentzian fit is same as linear fit as previous experimental data has only 4 relevant data points so hand wavy fit is preferred) the previous experimental data such that the maximum is observed at 1.08 degrees and ignore the near zero twist angle discrepencies of the FWHM of the G peak then at twist angle of 1.08 degrees (magic angle) for 532 nm laser excitation we observe a FWHM of 24 cm^{-1} indicating that our TBG sample is near magic angle (in the range of 0.8 to 1.15 degrees) as shown in the figure below. But if linear fit is considered then our sample is already at magic angle.

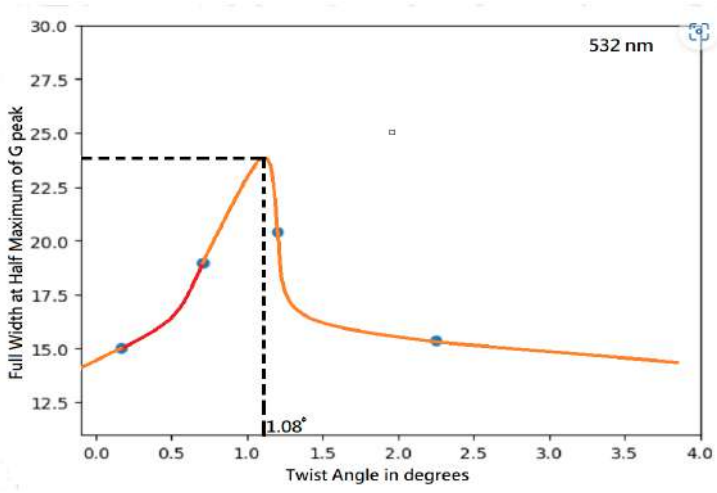

Figure 2.75: Hand Wavy Fit of the Experimental Data Points collected from Reference [14] indicating the variation of FWHM with Twist Angle in degrees.

The Nano Raman technique can be used as a tool to study the twistronics,Ferromagnetism,Anamolous Quantum Hall Effect and large linearity in temperature resistivity etc.[13].

Micro-Raman Specroscopy can be used to quantify the twist angle of the Twisted Bilayer Graphene sample from the line width of the G peak ,with extreme care taken in Fabrication of graphene and making the TBG stack and can be also used to characterize the relaxation effects to twist angle with time.

Chapter 3

Capacitance Measurements of Any 2D Material

There are two ways to measure Quantum capacitance of 2D materials as far as I know -

1.Capacitance Measurement by constructing a Van Der Waal hetero-structure sandwich.

2.Capacitance Measurement by Direct Capacitance Measurement Scheme.

Note - One Another way to measure Quantum Capacitance of 2D material is to relate the position of G peak and 2D peak shift's with gate voltage modulation to the Fermi Energy and electron concentration through which we will be able to find the quantum capacitance of the 2D material,provided the vibrational modes of the 2D material are Raman Active as briefly discussed in 2.6.2.

3.1 Quantum Capacitance Measurement by Direct Capacitance Measurement

The part 2 of this scheme is a direct Measurement Scheme in which a gate voltage is applied on the Si-SiO_2-Dielectric-2D material-Dielectric sandwich of van der waal Hetero-structure and we are measuring the out of plane tunnelling current from the 2D material. The basis of this scheme is the equivalent circuit analogue to out of plane layer resistance in terms of capacitance by applying an AC voltage as shown in the figure below.

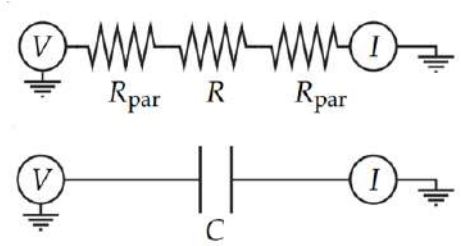

Figure 3.1: Tunnelling Capacitance Analogue Schematic Lumped Model of Tunnelling Resistance for the sample Heterostructure[2]

The issue with this type of direct capacitance measurement scheme is,that most current amplifiers show large input impedance for above 10 KHz limiting the tunnelling current to about 1 pico-amperes for a sample on the order of 1 pf or less for 1 mV gate voltage.[2]

An alternative way would be to construct a capacitance bridge circuit followed by a lock in amplifier as shown in the figure. So we are balancing out the tunnelling capacitance of our heterostructure and its applied gate voltage (Dielectric-2D material-Dielectric) with standard capacitor and a standard voltage applied in parallel 180 degree out of phase and finding a balance point with the use of lock in amplifier.Again there are two issues with this type of measurement,

1.The input noise of the lock in amplifier is around 2 nV/$\sqrt{Hz}$ dominated by $\frac{1}{Hz}$ below 100 Hz of input gate voltage,due to which the measured capacitance signal sensitivity is limited to $\frac{0.5fF}{\sqrt{Hz}}$ for input gate voltage of 1mV.But our total capacitance measurement of hetero-structure is in the range of 50 fF and the changes are in the range of 50 attofarad which can barely be detected as at 10000 Hz input frequency signal our capacitance sensitivity becomes $0.5 * 10^{-2}$ fF. So the sensitivity is one orders higher than changes,but for it to be a reliable measurement scheme it should at least be two or more orders higher as the floor noise in the cryogenic bridge circuits is around $\frac{5fF}{\sqrt{Hz}}$.

2.The capacitance of the coaxial cable that connects the bread board with the input of lock in amplifier which depends on the length of the cable and is around 30 pF/feet,which magnitudes the parasitic parallel capacitor to 300 pF to 600 pF for a length of 10 to 20 ft.This shunt capacitor dominates the changes in the balance point at the lock in amplifier and hence can give a false circuit balance reading of circuit being balanced deviated from the original value.

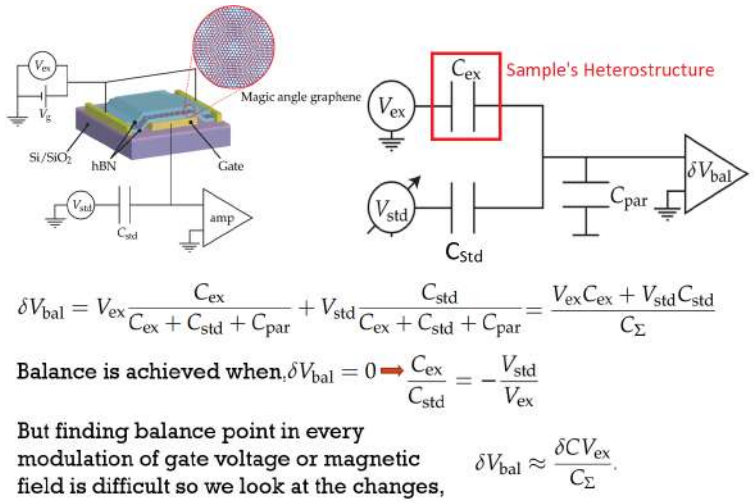

Figure 3.2: Capacitance Bridge Lumped Model for balancing followed by a lock in amplifier for tunnelling capacitance Measurement of sample with expression for the Voltage balance.[2]

Hence our main goal now in the next measurement scheme will be to reduce this parasitic capacitance so as to reduce the sensitivity of capacitance measurement further.One way can be to average out the noise over longer periods of measurements but DC drifts and low frequency noise will be difficult to average away.

Second Way is introduce an amplifier to amplify the measurement signal and shift the balance point away from the input of the Lock In Amplifier near the sample capacitance so as to reduce

the parasitic capacitance to lesser value.This can be done with the use of HEMT (High electron Mobility Transistor) which is set to unity or sub-unity voltage gain and its input resistance and input voltage is set to its DC operating point and output/drain resistance and output voltage governs its drain characteristics.So it shifts the voltage balance point across the HEMT and hence the parasitic capacitance can be reduced to 1 pF.Hence sensitivity of the measurement signal by Lock amplifier can be reduced can be $\frac{1aF}{\sqrt{Hz}}$.Further circuit design modifications may be done to reduce this capacitance sensitivity further by two stage amplification design i.e using two HEMTs ,a bias tee and two amplifiers at near zero kelvin and room temperature before Lock in Amplifier.

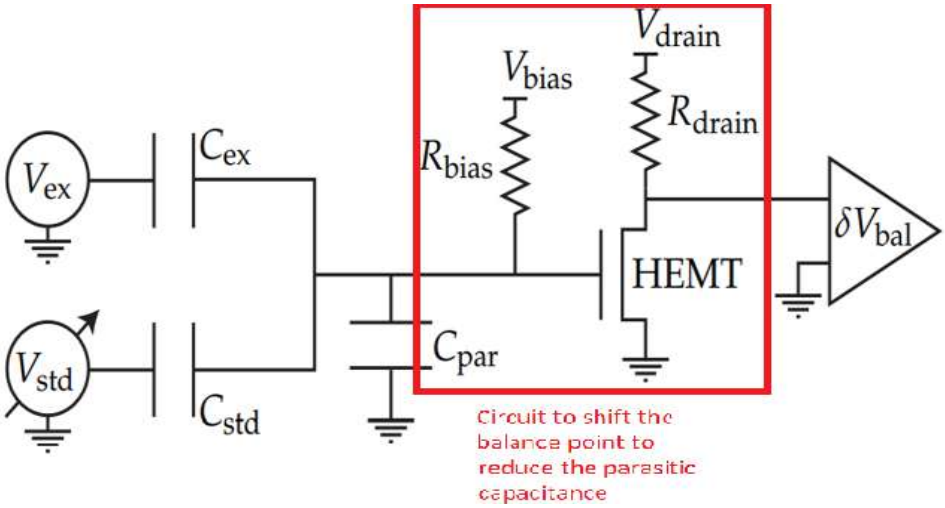

Figure 3.3: Balancing Point shifted to near the bread board to reduce the Parasitic Capacitance with the use of HEMT[2]

Further complications may be introduced in this lumped model by, adding in background capacitance which can be due to wire bonds,bond pands,cabling etc. which can be substracted from the circuit by finding the balance point,adding out of plane resistance of the hetero-structure in which case our standard voltage will not be 180 degree out of phase with the gate voltage, but will be at some angle lesser than it as shown in the figure below.

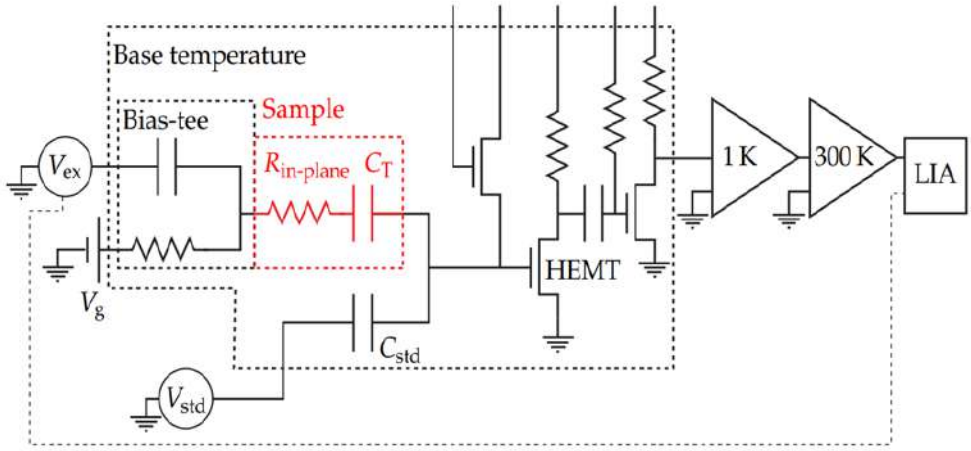

Figure 3.4: Two HEMT's coupled by a parallel capacitor ,amplification by two amplifiers at cryostat temperature and room temperature,bias tee with additional components in the model to improve the accuracy of model and amplify the measurement signal[2]

Now Let's look at the mathematical circuit calculations involved to get the total capacitance of the hetero-structure for the Lumped model with out of plane tunnelling resistance of hetero-structure shown in the figure below.

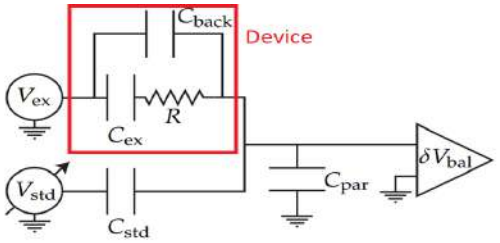

By Voltage Divider Balance in the circuit,

$$V_{bal} = \frac{GZ_{par}(V_{ex}Z_{std} + V_{std}Z_{ex})}{Z_{par}(Z_{ex} + Z_{std}) + Z_{ex}Z_{std}}$$

Now the impedances in the circuit can b calculated as,

$$Z_{ex} = \frac{1 + i\omega RC_T}{i\omega(C_{back} + C_T) - \omega^2 C_{back}C_T R}$$

$$Z_{std} = \frac{1}{i\omega C_{std}} \quad Z_{par} = \frac{1}{i\omega C_{par}}$$

At Voltage Balance Point,

$$0 = V_{bal} \Rightarrow \frac{Z_{std}}{Z_{ex}} = -\frac{V_{std}}{V_{ex}}$$, Now the Impedance ratio will contain both the real and the imaginary terms.

Real Term, $X = -\frac{(C_T + C_{back})/C_{std}}{1 + (\omega RC_T)^2} - \frac{C_{back}(\omega C_T R)^2/C_{std}}{1 + (\omega RC_T)^2}$

Imaginary Term, $Y = \frac{C_T^2 R\omega/C_{std}}{1 + (\omega RC_T)^2}$.

In Low frequency limit, $\omega RC_T \ll 1$

$$X = -\frac{C_T + C_{back}}{C_{std}}\left(1 - (\omega\tau)^2\right) + \mathcal{O}(\omega\tau)^3$$

$$Y = \frac{C_T\omega\tau}{C_{std}}\left(1 - (\omega\tau)^2\right) + \mathcal{O}(\omega\tau)^4$$

In High Frequency Limit, $\omega RC_T \gg 1$

$$X \approx -\frac{C_{back}}{C_{std}} - \frac{(C_T + C_{back})/C_{std}}{(\omega RC_T)^2}$$

$$Y \approx \frac{1}{C_{std}R\omega}.$$

In the low Frequency limit we can get total capactance from the real term of the impedance ratio and substract out the background/stray capacitance by taking X at two different applied frequency values and substracting it.

Figure 3.5: Equivalent Capacitance Model Calculations involved to get the total capacitance from which we will get the quantum capacitance [2]

With the tunnelling Resistance (out of plane resistance of heterostructure) (R) magnitude cal-

culated from the model we are able to predict where is the Fermi Energy Level in the 2D material,if Resistance is lower we are in band gap regime,if resistance is higher we are at the edge of band gap or in the band gap regime. For more details one can refer [2] but the explanation given here forms the basis of this measurement scheme as it was not used in our thesis.We used technique 1 to determine the Quantum Capacitance of 2D material for our thesis.

3.2 Quantum Capacitance Measurement of 2D material by constructing a Van Der Waal hetero-structure sandwich

Now considering the first part of the measurement scheme i.e Capacitance Measurement by constructing a Van der Hetero-structure Sandwich. So let's discuss this model of tunnelling/Quantum Capacitance Measurement in Detail.

Let's first look at what is quantum capacitance/tunnelling capacitance of 2D material. Before that let's look at what is electronic compressibility of states.

To understand what a electronic compressibility ($dn/d\mu$) is,we can consider an analogous mechanical term i.e mechanical compressibility in which we apply stress on the material and calculate its strain from the deformation observed. If the material undergoes relatively higher deformation i.e change in volume under applied stress then we can conclude it as highly compressible material mechanically and vice versa,at constant temperature and number of carriers in the material. Now in the electronic compressibilty we are keeping the temperature constant,the stress on the material to be atmosphere pressure but we are changing its number of carriers and we are observing the electronic deformation in the material i.e the number of occupied states by charge carries deforms i,e the chemical potential level in the material changes, this electronic deformation with introduction of charge carriers in material at constant temperature and volume of material is called electronic compressibilty of the material.It can be also thought of how much charge enters the system when we change its chemical potential level slightly.

So the Quantum Capacitance is the charge stored in the 2D material for voltage drop across 2D material due to transverse electric field at the gates.What is a Quantum/Tunnelling Capacitance and how it relates to electronic bulk modulus is explained in detail in the figure below.Why the name Quantum ,because the capacitance of 2D material changes with number of charge carriers in the 2D material i.e a addition/removal of single charge carrier in 2D material by gate voltage modulation can change the 2D material's capacitance and hence the name quantum capacitance.

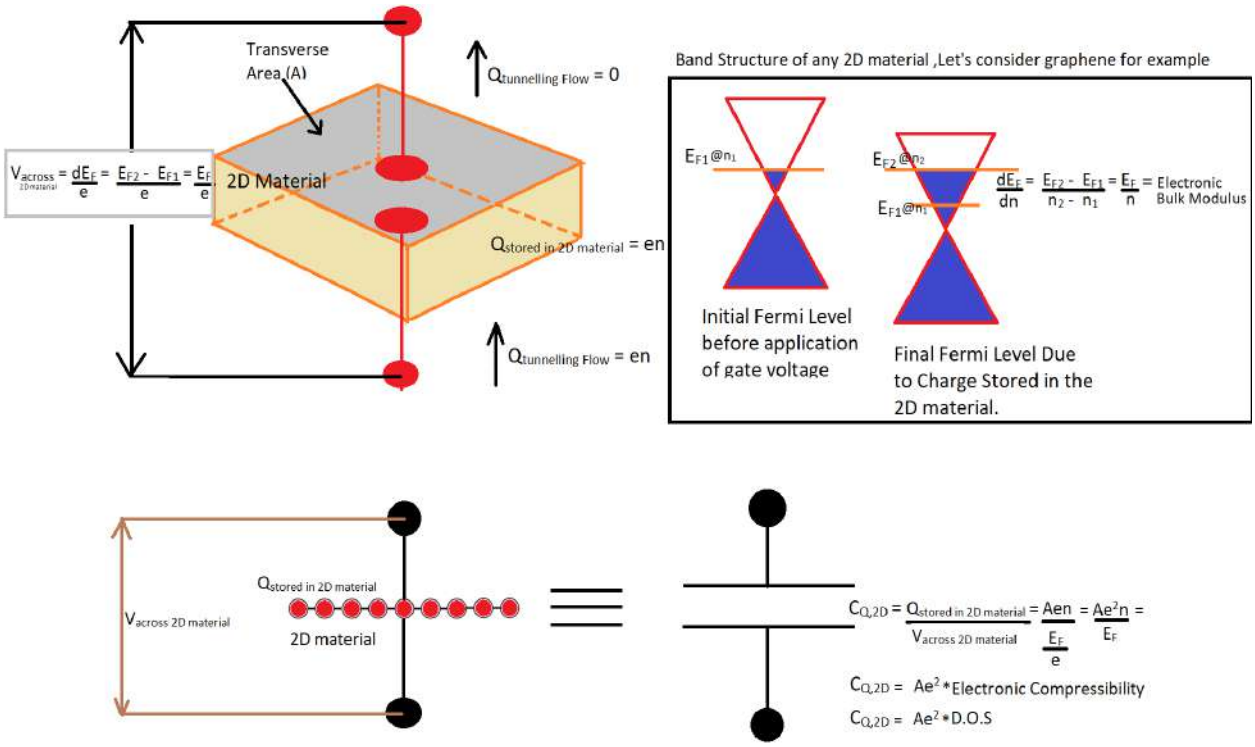

Figure 3.6: Concept of Quantum Capacitance of 2D material in Detail.

So we are stating here that the potential difference applied at the gate across the heterostructure makes a charge flow through the dielectric 2D materials of our heterostructure and gets stored in our 2D material whose quantum capacitance we want to measure causing the potential drop across our 2D material which is equal to Fermi Energy change per electron charge.

Once we know the concept of quantum capacitance we will proceed with the principle required for quantum capacitance measurement of our 2D material i.e Kelvin Probe Microscopy.

Kelvin Probe Microscopy is introduced in brief in section 2.5 of this thesis,but I would like to briefly review it here again.So consider two materials having different work function ϕ_1 and ϕ_2 are brought close to each other such that the charged field particles of both materials affect each other such that the charged field particles of both material affect each other i.e positively charged and negative charged from the respective two materials attract each other and shifts the Fermi Energy level of one material such that the work function difference between two material system will now magnitude to ϕ_1 - ϕ_2.So when we apply across plane i.e transverse voltage then the current flow through the two materials system separated by air acting as dielectric material due to difference in the Fermi Energy Level between the two materials as shown in the figure below.

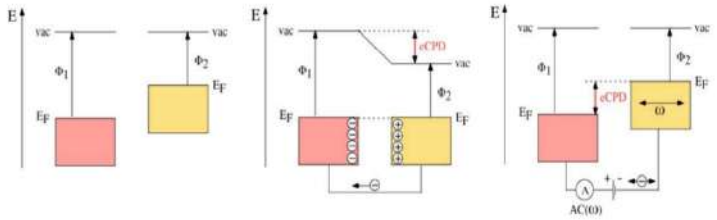

Figure 3.7: Kelvin Probe Microscopy Principle [1]

A Kelvin Probe Microscopy involves a metallic cantilever beam that probes the surface work potential fluctuations of the material at atomic scale separated from the material by air as a dielectric between the two as shown in the schematic below.

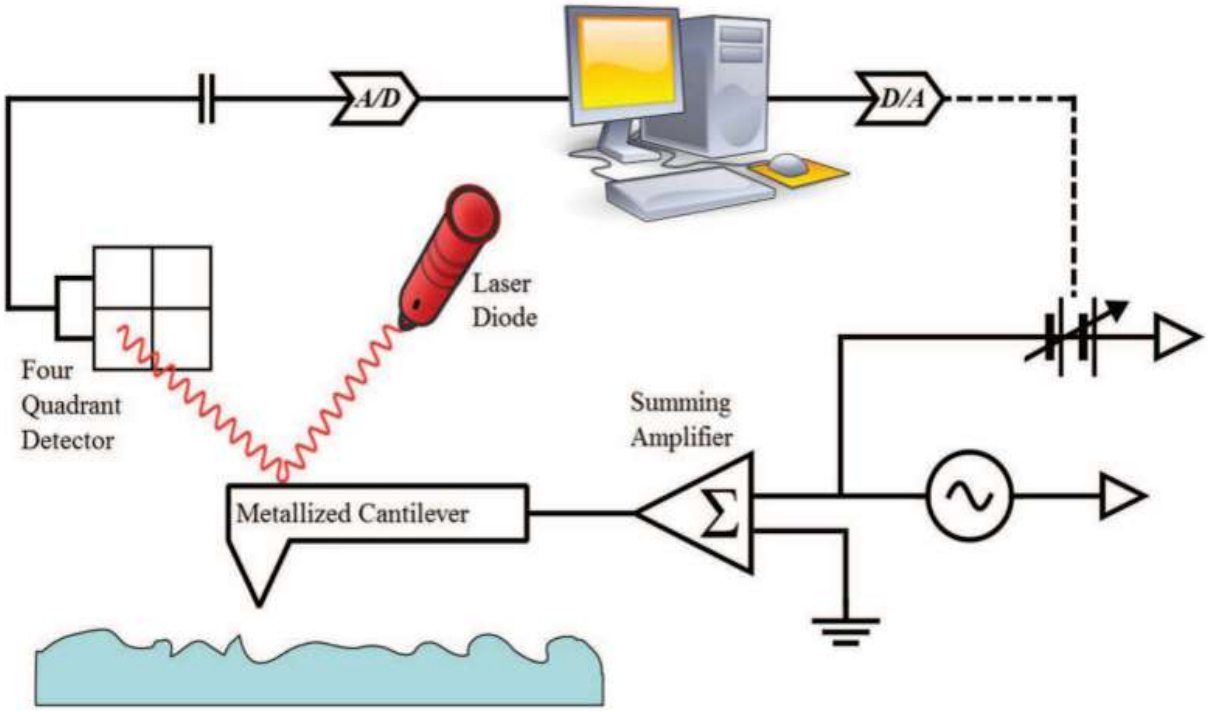

Figure 3.8: Working Schematic of Kelvin Probe Microscopy [1]

What we are doing for Quantum Capacitance measurement of our 2D material is based on similar principle of working of Kelvin Probe Microscopy.So we are separating two 2D materials by dielectric ,one 2D material acting as an equivalent metallic cantilever which probes the other 2D material's work potential separated by a dielectric. So in our case we are varying the carrier density of the 2D material and by modulating the gate potential and finding the charge neutrality point of the one 2D material (let's say bottom) i.e n_B = 0 i.e it will have a maximum in plane resistivity at that point (point as in values of top and bottom gate potential) i.e its Fermi Energy will be nearly zero and due to the charge carriers introduced in the top 2D material owing to applied gate potentials n_T ,its Fermi Energy Level will shift to higher value and as they are separated

by a dielectric,a tunnelling current will flow transverse to the 2D material owing to the charge carriers flow across the hetero-structure sandwich which is due to difference in the respective Fermi Energy Levels due to charge stored in the 2D materials in the 2D materials as shown in the figure below.

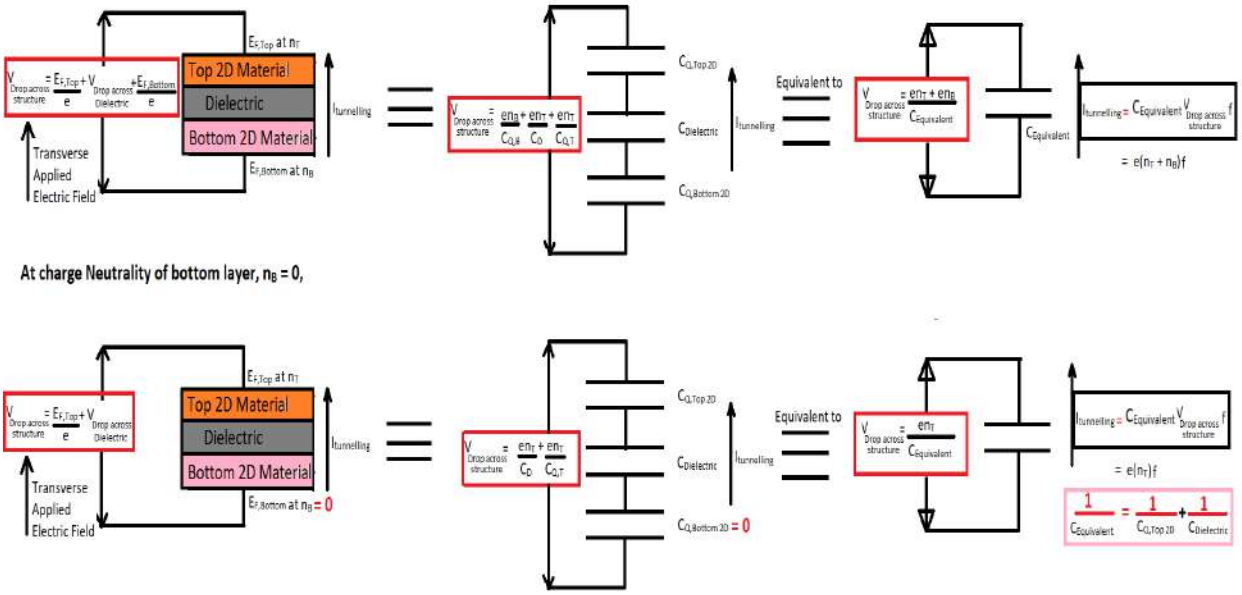

Figure 3.9: Tunnelling Out of Plane Current Calculations in 2D material Hetero-structure not including the top dielectric and bottom Si-SiO_2 for simplicity as this figure is just for schematic demonstration of how to relate the measured tunnelling current to quantum capacitance of 2D material.

The out of plane tunnelling current across 2D materials requires device fabrication in between transfers to take out the contacts from the top and the bottom surfaces of the 2D materials which is time consuming and complicated in terms of fabrications as careful device handling would be needed and also not every device fabrications are successful ,also not every transfer processes are successful,so proper transfer and device Fabrication of one sample will require lots of trial and errored samples and that one proper sample can also have transfer defects,cracks etc in it.

So instead of measuring $I_{\text{tunnelling out of plane}}$,we can relate it to $I_{\text{in plane}}$ which is much easier to estimate and pass in to the 2D material in terms of fabrication as the fabrication process can be done in one go after the whole transfer process is over.

So $I_{\text{tunnelling out of plane across 2D material}} = \frac{Q}{t} = \frac{en}{t} = Q*f = C_{Q,2D}V_{\text{across the 2D material}}f = C_{Q,2D}\frac{E_{F,2D}}{e}f$, which is 10^{-5} orders of magnitude for 100 Hz AC gate modulation and can be easily measured by conventional ammeters.

where f = $\frac{1}{t}$ is the frequency of the applied gate potential,zero in case of DC voltage.

Now the in plane conductivity ($\sigma_{inplane}$) of the 2D material can be written as,

$\sigma_{inplane} = \mu en = \frac{L_{\text{2D material}}}{R*A_{\text{Cross Section of 2D material}}}$,where μ = carrier mobility

Therefore,$I_{\text{tunnelling out of plane across 2D material}} = \frac{\sigma_{inplane}}{\mu t} = \frac{LI_{inplane}}{V_{inplane}A\mu t} = \frac{C_{Q,2D}V_{\text{across the 2D material}}}{t}$

Hence $I_{\text{tunnelling out of plane across 2D material}} \propto I_{\text{in plane}}$, and is zero for DC applied gate voltage as f =

0 in that case.

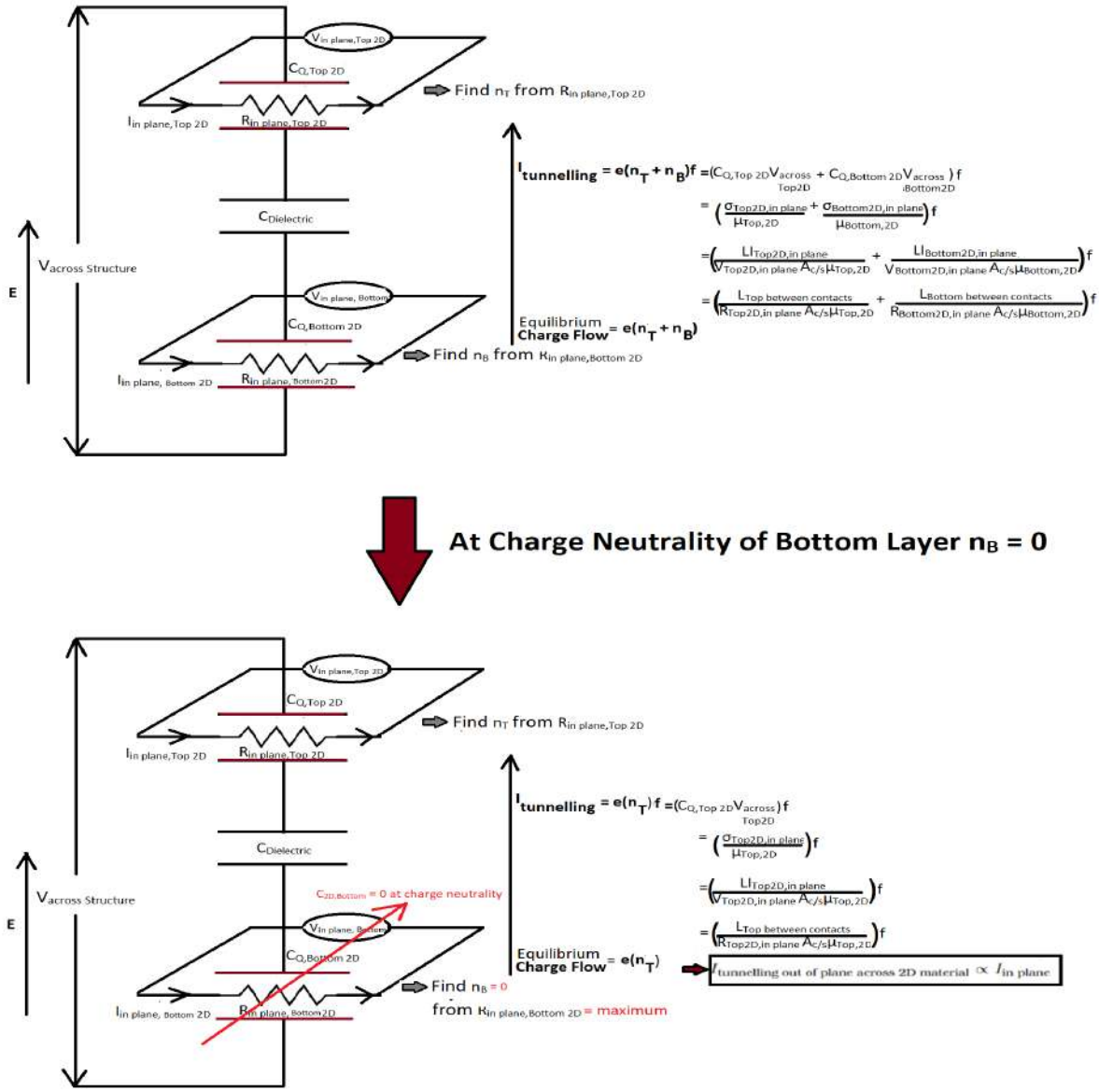

Figure 3.10: Finding Tunnelling Current Mathematically from measuring In plane Longitudinal Voltage by passing In plane current in the top and bottom 2D materials.

Note - Here we have already taken in to consideration,the tunnelling probability of charge carriers across the hetero-structure as those charge carriers that tunnel through the dielectrics and the reach the 2D material are n_T and n_B respectively.So before the carrier tunnelling that is happening in the dielectrics,we are considering the equilibrium charge flow across the hetero-structure at which we apply our mathematical expressions that will happen only after tunnelling across the hetero-structure.

So we are passing $I_{\text{in plane}}$,measuring $V_{\text{in plane}}$ in Hall Bar Geometry of our Van Der waal Heterostructure as explained in section [5.1.1] and then we are finding $R_{\text{in plane}}$ from which we will get the $\sigma_{inplane}$ and then the $I_{\text{tunnelling out of plane}}$ and then the Quantum Capacitance of top 2D material.

Alternative way is to skip calculation of the $I_{\text{tunnelling out of plane}}$ and directly find the Quantum Capacitance by in plane resistivity measurement of the bottom 2D material to make n_B = 0 and then measuring resistivity of the top 2D material to find the n_T values for all gate voltage modulations of n_B = 0. Once we have all the n_T values for all the gate modulations of V_{BG} vs V_{TL} sweeping then we can use our below shown capacitance model to extract out the Quantum Capacitance of the top 2D material.

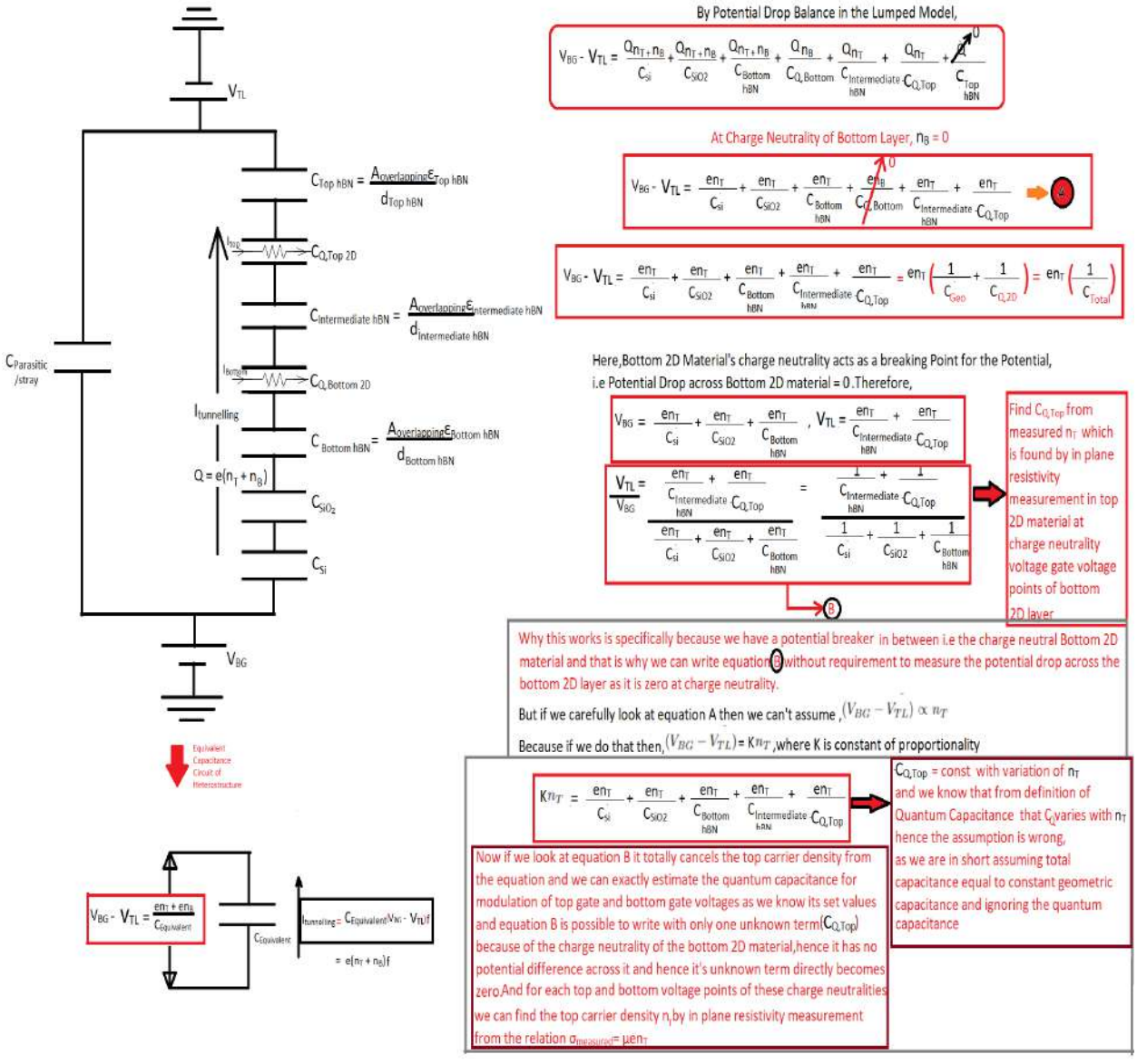

Figure 3.11: Schematic of Capacitance Model of Van Der Heterostructure and why it works

Other than the model described here ,a more accurate model will be including the wire bond resistance ,equipments which are used for measurement's accuracy and its resistance,the coaxial cable resistance,the gold pads,[gold contacts resistance is accounted for in the Resistance model of measurement as described in section 5.1.2],temperature change of the measured signal from Liquid Nitrogen (70 K) of sample to room temperature of equipments can incur thermal noise in coaxial cable which will additionally incur some resistance,some loss (negligible as hBN will offer high in plane resistance compared to other conducting 2D material) of in plane current signal through the hBN as the gold contacts are common of hBN with 2D material.So what in plane resistance of 2D material we are measuring is series combination of all these resistance which we are safely ignoring in our model as it will only scale up the magnitude (considering all these resistances as constant series background resistance) of the measured voltage but profile of the measured resistance vs gate voltage applied will remain the same.Also what sample/device we are considering is defect free i.e there are no air bubble gaps in the heterostructure ,no defects in the 2D materials in the overlapping area of the heterostructure etc,if they are considered then they will vary for each samples and the readings that we measure vary from the sample to sample consisting of same set of 2D materials and dielectrics in heterostructure.Also we have not included the losses of the electric signal to the environment in the form of heat disscipation.

3.3 Quantum Capacitance Extraction by using in plane Resistivity Measurements of 2D material in just Dielectric-2D material-Dielwctric on $Si - SiO_2$ substrate by a Novel Way

The Quantum Capacitance can also be extracted for just Bottom Gate,Silicon Dioxide,Bottom Dielectric,2D material,Top Dielectric using a novel way as described below,

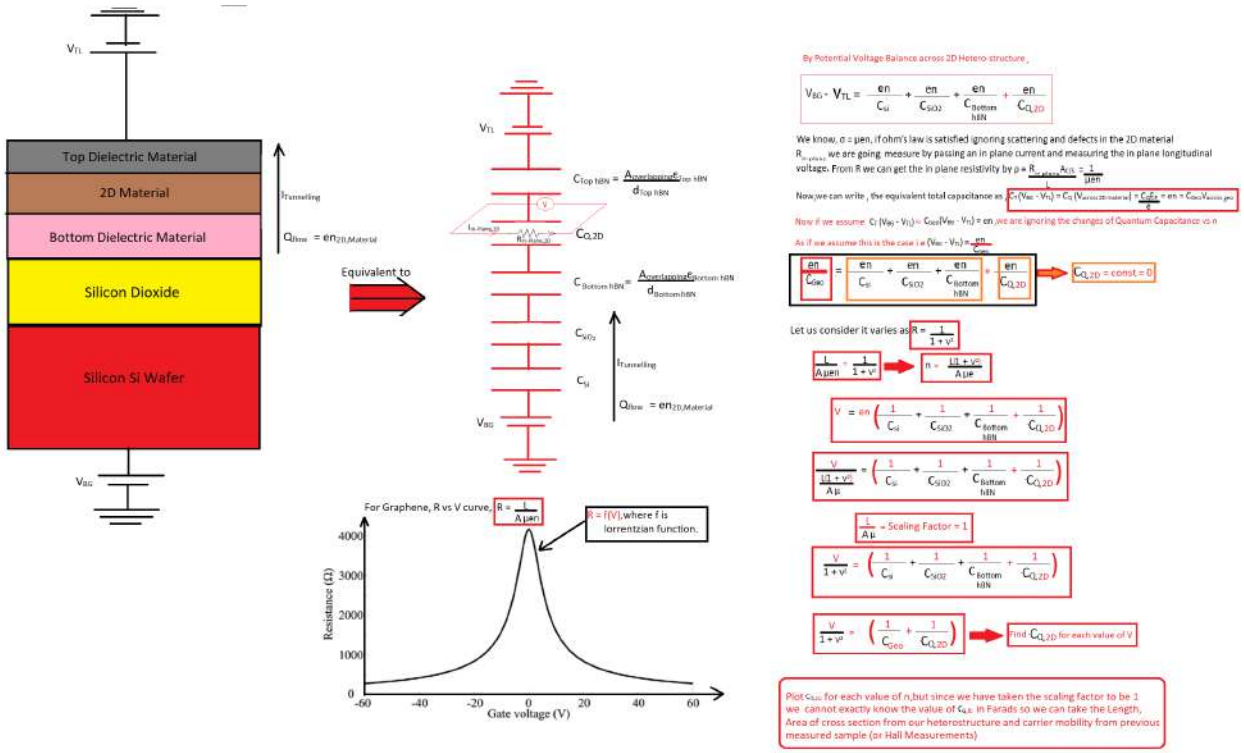

Figure 3.12: Novel Way of Extracting the Quantum Capacitance from the Dielectric,2D material,Dielectric,Si,SiO_2 Van Der Waal Hetero-structure

But to measure carrier density (n) and carrier mobility (μ) accurately we will have to look at Hall Bar Measurements in some applied transverse magnetic field and also the scattering effects should be considered for model to be accurate which can be found from conductivity vs n plot and hence changes in the model should be made in accordance to it.

Let us consider,Novel Extraction of Quantum Capacitance for Graphene using its in-plane resistivity measurement.

As shown in the figure above let us Lorentzian curve fit the Resistance vs Gate voltage data to obtain a relation,

R = $\frac{4000}{1+V^2}$ = $\frac{L}{A_{c/s}\mu en}$

n = $\frac{L(1+V^2)}{4000A_{c/s}\mu e}$,this n is number of charge carriers per unit volume of the 2D material as we are considering the thickness of 2D material in the cross section area term.

Now if we consider our sample has $L_{contact}$ = $8\mu m$

The Area of cross section = 8x0.375x10^{-15} m^2

Assume Mobility of the carriers in graphene at low temperature = 20 m^2/Vs = constant as observed in most of experimental data for long range scattering (charge impurity scattering).But mobility changes with n for short range scattering as observed experimentally as conductivity varies with $\sqrt{n}$ and combination of the two in a non-pristine sample of graphene.

Accurate Estimation of Quantum Capacitance without the need for assuming any model except the intrinsic Quantum Capacitance one !!!

=> We will require the transverse voltage measurement data i.e V_{xy},longitudinal Voltage mea-

surement data i.e V_{xx} for passed in plane longitudinal current I_{xx} under applied transverse magnetic field of magnitude B to accurately estimate the carrier density as discussed in section [5.1],so once we get the carrier density then we can plot n vs gate potential (V) and curve fit it to get an accurate relation between n and V and then plot the In plane Longitudinal Resistance (R) vs V to get the mathematical relation by curve fitting between the two,then we can plot R vs n and then in plane longitudinal conductivity (σ) vs n to accurately determine the mathematical relation between (σ) and n.Well actually curve fitting is required only twice, once to determine the relation between the R and V and once to determine the relation between R and n,that too to accurately extract the quantum capacitance without having the need to assume ρ = $\frac{1}{\mu * e * n}$

The conductivity vs n relation can be mathematically described as superposition of the conductivities due to various known and unknown types of scattering with weightage constants assigned as a,b,c,d and j which are normalized and can be found by curve fitted mathematical relation between σ and n.Depending on the weightage parameters assigned we can exactly quantify, which scattering is the electron transport in sample is dominated by, which can give us tremendous insight on resistance of the 2D material as scattering of electrons during transport is why the resistance occurs in the materials in the first place.Also one can realize/think in the direction of how to synthesize a no resistance material at room temperature and pressure by using this insight studies for various material.

Therefore the conductivity can be defined as,

σ_{Total} = m*$\sigma_{\text{Ballistic regime Transport}}$ + n*$\sigma_{\text{Diffusive regime Transport}}$

σ_{Total} = m*o$\sigma_{\text{Ballistic regime Transport}}$ + n$\sigma_{\text{Ballistic regime Transport}}$

i.e σ_{Total} = (m*o+n)*$\sigma_{\text{Ballistic regime Transport}}$

where m = b and n are normalization constants and (m*o+n) is the diffusion transport fraction.

σ_{Total} = a*$\sigma_{\text{long range or charged impurity scattering}}$ + b*$\sigma_{\text{Ballistic regime}}$ + c*$\sigma_{\text{Optical Phonons}}$ + d*$\sigma_{\text{Acoustic Phonons or short range scatterin}}$ + j*$\sigma_{\text{other defects or reasons}}$

where a,b,c,d,j are numerical real constants that follow normalization.

We know that in the Ballistic Regime the conductivity varies as $\sqrt{n}$.

By basic definition of conductivity , σ = carrier mobility*Charge stored in the material.

We know that Charge stored in material Q = e*n i.e Q is always directly proportional to n irrespective of the type of scattering by it's basic definition.

So for above relation to be valid, carrier mobility should be varying with n ,which also can be understood physically by basic definition of carrier mobility as the velocity (drift velocity) of the charge carriers under applied in plane electric field,i.e the velocity of charge carriers varies with n (which varies with out of plane electric field) for a constant applied in plane electric field.

So for Ballistic limit, σ = constant*($\sqrt{n}$) = μ en ,

hence $\mu_{\text{Ballistic Limit}}$ = $\frac{constant*(\sqrt{n})}{en}$ = $\frac{constant}{e\sqrt{n}}$ => $\mu \propto \frac{1}{\sqrt{n}}$.

Now for long range scattering,σ = constant*(n)

σ = $\mu_{\text{long range scattering or charged impurity scattering}}$ en which implies mobility is constant for long range scattering.

Now for short range scattering or acoustic phonons scattering,σ = constant. => $\mu = constant$

So in general,

σ_{Total} = (en)*(a*$\mu_{\text{long range or charged impurity scattering}}$ + b*$\mu_{\text{Ballistic regime}}$ + c*$\mu_{\text{Optical Phonons}}$ + d*$\mu_{\text{Acoustic Phonons or short range s}}$ + j*$\mu_{\text{other defects or reasons}}$)

This will be the most accurate model of quantifying the relation between σ and n as opposed to our's basic assumption of long range scattering or charge impurity scattering of $\sigma = \mu * en$ i.e $\frac{1}{\rho} = \mu * en$

Note => If we compared the experimentally obtained mathematical relation between the σ and n to the one mathematically modelled above we can get exact values of a,b,c,d, and j to exactly quantify which type of scattering dominates in that particular sample of 2D material. Also carrier density can be negative so consider |n| in the equations.

Now,Coming back to the calculations for graphene,

Therefore, n = 2.08 x $10^{23}(1+V^2)$ $/m^3$ volume of sample.

n = 0.78 x $10^{14}(1+V^2)$ $/m^2$ overlapping area of sample

Total Number of charge carriers in the sample (N) = n*(volume of sample)

N = 2.08 x $10^{23}(1+V^2)$ x 8 x 8 x 0.375 x 10^{-21}

N = 49.92 x $10^{2}(1+V^2)$

By Potential Balance,

$V_{BG} - V_{TL}$ = $\frac{eN}{C_{Si}}$ + $\frac{eN}{C_{SiO_2}}$ + $\frac{eN}{C_{BottomhBN}}$ + $\frac{eN}{C_{Q,2D}}$

$V_{BG} - V_{TL}$ = V = Gate Potential

C_{Si} = $A\epsilon_{Si}$/d_{Si} = 3.7376 mF (has been calculated in section 4.1.3)

C_{SiO_2} = 0.832 mF

$C_{BottomhBN}$ = 24.064 mF

Now the Potential Balance equation becomes,

V = 49.92 x $10^{2}(1+V^2)$ e ($\frac{1}{3.7376}$ + $\frac{1}{0.832}$ + $\frac{1}{24.064}$ + $\frac{1}{C_{Q,2D}}$)

$\frac{V}{1+V^2}$ = 79.872 x 10^{-16}($\frac{1}{3.7376}$ + $\frac{1}{0.832}$ + $\frac{1}{24.064}$ + $\frac{1}{C_{Q,2D}}$)

$\frac{V}{1+V^2}$ = 79.872 x 10^{-16}((1.5110x10^3) + $\frac{1}{C_{Q,2D}}$)

$C_{Q,2D}$ = $\frac{1}{1.2520*10^{14}(\frac{V}{1+V^2})-1.5110*10^3}$ => [A]

Note - This technique is universal and can be used for any Hetero-structure provided we should perform Hall Bar Measurements with applied transverse magnetic field to extract out the carrier density and the carrier mobility i.e we will require the $I_{xx}, V_{xy}, V_{xx}, B$ data to plot Resistance vs Gate potential to curve fit it to get the mathematical relation between V and R, conductivity vs n to get the mathematical relation between resistance and n and then write the potential balance for the hetero-structure and find the relation between the Quantum Capacitance of our 2D material and the gate potential(V) and Quantum Capacitance and the carrier density(n). A plot of Quantum capacitance vs n and Quantum Capacitance vs Gate Potential V is shown below for above sample calculation.So basically we are integrating physics i.e constructing such hetero-structure with known process of exfoliation and transfer,characterizing the structure under microscopy,device fabrication to get the gold contacts out from the heterostructure,then modelling the hetero-structure in to capacitance structure by making appropriate balances that satisfy thermodynamics first law (Either energy balance or potential balance),making in plane resistivity measurements on the device by physical equip-ments such as source meter and the Lock-in Amplifier,**and** Data Science i.e curve fitting the measured data to obtain the mathematical relation between the resistance and the gate potential and further resistance and carrier density and extracting out quantum capacitance from the modelled structure.And then from the mathematical expressions of the solid state physics as discussed in section [5.1.2] ,we are extracting the Density Of States,Electronic Compressibility,Energy Band-

width,Energy Band-Gap,carrier Density,Fermi-Energy/chemical Potential,Fermi Velocity,Ground State and its properties of the 2D material,Number of Modes,Conductance in the Ballistic and Diffusive Limit,Transmission Function,Mean Free Path,Electron Scattering Mechanisms and Landau Levels and its spacing.These quantities can help us to actually realize the fascinating outlook applications in real life in the coming future.A simple way but a novel one which has not been ideated and implemented anywhere in the literatures as far as I know.

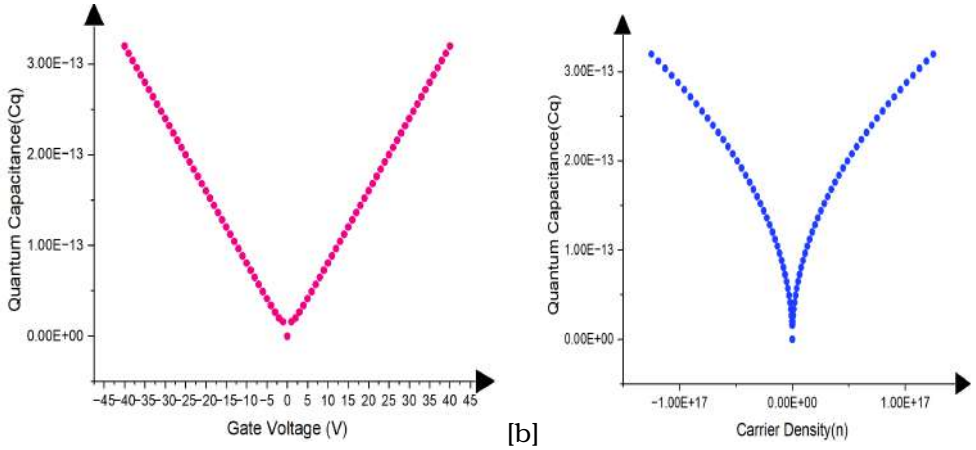

Figure 3.13: (a) Quantum Capacitance vs Gate Potential (b) Quantum Capacitance vs Carrier Density of monolayer Graphene at low temperature near zero Kelvin

Below figure shows the Fermi Energy variation vs carrier density,Quantum Capacitance variation with Graphene Potential (Fermi Energy of graphene/e),Compressibility vs Carrier Density,Density of states vs carrier density to completely know the transport of charge carriers in the material.All these physical quantities are extracted from the Quantum Capacitance Data.

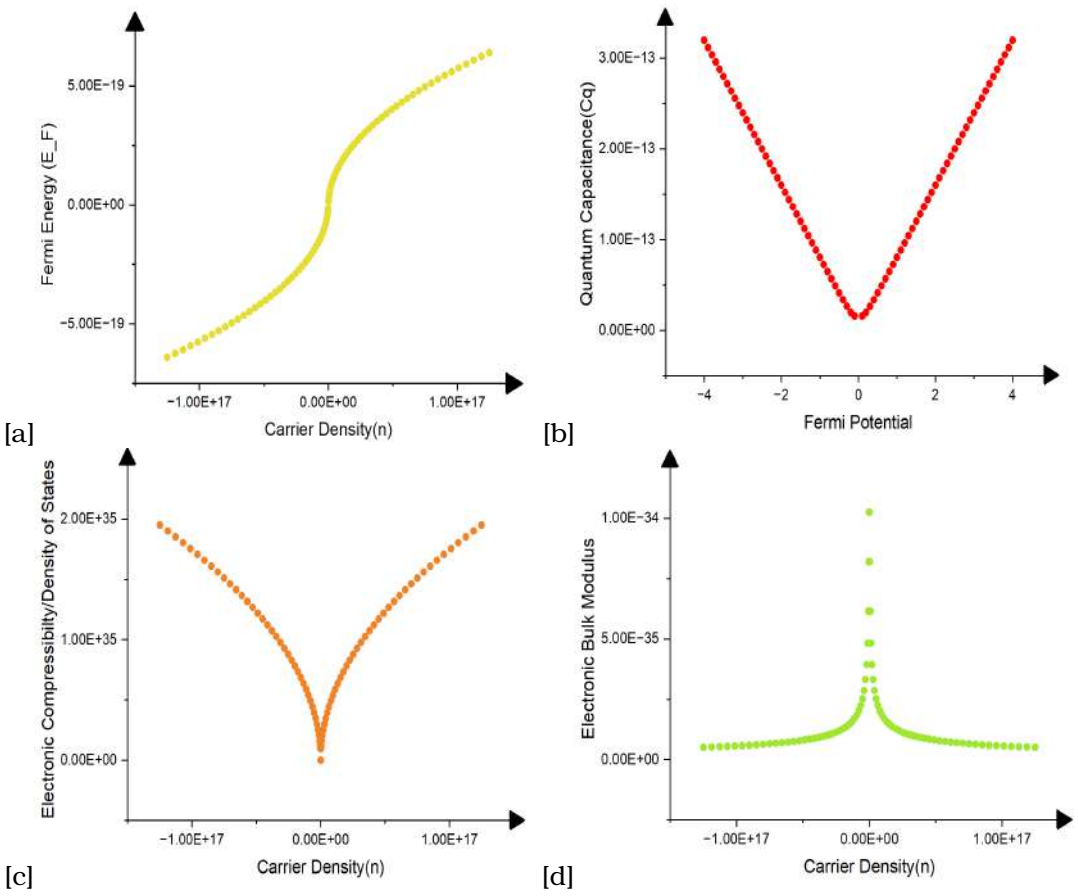

Figure 3.14: (a) Fermi Energy vs Carrier Density (b)Quantum Capacitance vs Fermi Potential (c)Electronic Compressibility or D.O.S vs Carrier Density (d) Electronic Bulk Modulus vs Carrier Density of monolayer Graphene at low temperature near zero Kelvin.

Let's start extracting the physical quantities one by one with reference from section [5.1.2] from Estimated Quantum Capacitance.

1.**Density of States (D.O.S)** -

D.O.S = $\frac{C_Q}{A_{overlap}e^2}$ = $\frac{\frac{1}{1.2520*10^{14}(\frac{V}{1+V^2})-1.5110*10^3}}{A_{overlap}e^2}$ => This equation gives the relation between D.O.S and V and we know from earlier calculations n = 0.78 x $10^{14}(1+V^2)$ /m^2 and hence we get relation of D.O.S with n which is plotted in the above graph.

2.**Fermi Energy** (E_F) -

We know C_Q = $Ae^2\frac{dn}{dE_F}$

Therefore E_F = $\int_{-n}^{n}\frac{Ae^2}{C_Q}dn$ => [B]

So we know equation C_Q as function of V and also n as function of V ,so we can get C_Q as function of n by putting V = $\sqrt{\frac{n}{0.78*10^{14}}-1}$ in equation A and put that in equation B and solving we get E_F as function of n and E_F as function of V as plotted in graph 3.14[a]

E_F = $\int_{-n}^{n}Ae^2(1.2520*10^{14}(\frac{\sqrt{\frac{n}{0.78*10^{14}}-1}}{(\frac{n}{0.78*10^{14}})})-1.5110*10^3)dn$ => we can get the E_F vs n relation. Alternative way instead of integration we can consider the discrete data of V as was plotted in above graph.

3.**Electronic Compressibility** -

As discussed in section [5.1.2] D.O.S is directly proportional to Electronic Compressibility i.e D.O.S = K*(Electronic Compressibility) where K is constant of proportionality. By definition Electronic Compressibility is $\frac{dn}{dE_F}$.So we want the relation of Fermi Energy with carrier density which we already have from above calculation.So just by taking the derivative of the obtained function we can get the Electronic Compressibility.Also we can use discrete data of V to plot Electronic Compressibility vs n as plotted above.

Also by using the fitting function y = $a * (b * x)^c$ on origin pro for the Fermi Energy vs n plot we can get a crude relation between Fermi Energy and n as y = $2.81156\text{x}10^{-29}(6\text{x}10^{-7}x)^{0.50245}$ i.e E_F = $4.48\text{x}10^{-14}(1.8229\text{x}10^{-27}n)^{0.50247}$. We can get the electronic compressibility as function of n by taking its derivative and separating out the $\frac{dn}{dE_F}$ term.

Also we can plot the electronic compressibility vs n curve by considering discrete values of V and then discrete values of n to find Fermi Energy and then the electronic Compressibility as plotted above.

4.**Electronic Bulk Modulus** -

Again just the inverse of the Electronic Compressibility gives us the Electronic Bulk Modulus or we can take the derivative of the Fermi Energy vs n relation to get the Electronic Bulk Modulus or consider discrete data of voltage as plotted above.

5.**Energy Band-Width between the two extreme points of the Gate Potential** -

Energy band-Width between two extreme points of the carrier density = Area under the curve of the Electronic bulk Modulus vs n plot.

= $\int_{-n}^{n} \frac{dE_F}{dn}$ dn = $\int_{-n}^{n}$ d(Electronic Bulk Modulus) dn

We know the E_F vs n relation from above and hence we can find the Energy BandWidth from above.

6.**Energy Band Gap** -

Graphene has no energy band gap which is evident from the plot of Electronic Compressibility vs carrier density as it has only one value near zero.For Band Gap to exist by definition as discussed in section [5.1.2] the electronic compressibility should have two values near zero at different n's .

7.**Carrier Density** -

For Gate potential V,

We know that , n = $\int_0^V \frac{C_T}{Ae} dV$ = $\int_0^{E_F/e} \frac{C_Q}{Ae^2} dE_F$,where C_T is the total capacitance which can be found by, $\frac{1}{C_T}$ = $\frac{1}{C_Q}$ + $\frac{1}{C_{Geo}}$ = $1.2520 * 10^9(\frac{V}{1+V^2})$ as we already know C_{Geo} = constant and C_Q as function of V. This is just to verify the function of n vs V as it has already been obtained previously by considering the relation ρ = $\frac{1}{\mu en}$ for long range (charged impurity scattering).

8.**Ground State and its Properties**

Identification of Ground State can be done at zero quantum capacitance value. think in the direction of how can one relate the quantum capacitance with electron wave function in graphene and hence we can obtain ground state of graphene from quantum capacitance which can be generalized to any material for extracting it's ground state experimentally (novel way) and add later on.

9.**Number of Modes and Transmission Function,Ballistic Conductance,Diffusive Conductance,Mean Free Path,Fermi Wave Vector,Fermi Velocity,Type of Electron Scattering,Mean Scattering time,Scattering Density.**

The total resistance of the 2D material is contribution of the ballistic transport regime i.e short range scattering (actually the resistance of material is zero in ballistic regime but this resistance is due to contacts taken out from the 2D material) and the long range scattering or the diffusive transport regime as expressed by,

R_{total} = R_{contacts} + $R_{\text{actual conductor}}$

= $\frac{1}{G_{\text{Ballistic conductor}}}$ + $\frac{1-T}{G_{\text{Diffusive conductor}}}$

R_{total} = $(h/2e^2M)$ + $(h/2e^2M)(\frac{1-T}{T})$ = $(\frac{h}{2e^2MT})$

Now Measured resistance is ,R = $\frac{4000}{1+V^2}$ = $\frac{L}{A_{c/s}\mu en}$

$\frac{L}{A_{c/s}\mu en}$ = $(\frac{h}{2e^2MT})$ = Resistance of contacts in the ballistic regime of 2D material * $(\frac{1}{T})$

Now we assumed that the transport is diffusive hence $\sigma = \mu en$ but this equation can be written as $\sigma = \mu e\sqrt{n} * \sqrt{n}$.

Consider a constant C that we can multiply and divide equation of R_{total} with.

Hence the resistance of contacts in the Ballistic Regime is,

R_{contact} = $\frac{h}{2e^2M}$ = $\frac{L}{A_{c/s}\mu e\sqrt{n}C}$

Define , $R_{\text{Diffusion}}$ = $\frac{1}{T}$ = $\frac{C}{\sqrt{n}}$ as the Diffusion Resistance fraction.

We know that Transmission function range from 0 to 1 hence C is constant introduced to satisfy this condition.

Now the maximum value of carrier density for our case is n = $2 * 10^{17}$ for which the Resistance nears zero for graphene and hence we can safely assume T = 1 in that case. i.e T = $\frac{\sqrt{n}}{C}$ therefore C = $\sqrt{2 * 10^{17}}$ = $4.472 * 10^8$,

Now considering the geometric factor $(L/A_{c/s})$ to be 1 i.e neglecting the thickness of the 2D material.

hence M = 185.588 * $10^{-7} * \sqrt{n}$

and T = $2.236 * 10^{-9} * \sqrt{n}$

The above two functions can be plotted to visually see how the number of modes in 2D material with which the electric current flow in the material and how many number of electrons that started from input contacts reached the output contact with or without scattering i.e the transmission function changes with the carrier density.

Now let's extract the Fermi Wave Vector K_F from M and Mean Free Path Length from T as discussed in section [5.1.2]

M = 2*$Int(\frac{K_F W}{\pi})$ (Factor 2 accounts for spin degeneracy)

For the sample considered $W = 8 * 10^{-6}$ m,

then K_F essentially becomes,

K_F = $3.6422\sqrt{n}$

From K_F relation with n and E_F relation with n we can extract out the Fermi Velocity of the charge carriers by,

V_F = $\frac{1}{h}\frac{dE_F}{dK_F}$ = $\frac{2\pi}{6.64*10^{-34}} * \frac{4.48*10^{-14}(1.8229*10^{-27}n)^{0.50247}}{3.6422}$ = $4.9669 * 10^6$ m/s ,a slight variation from the actual Fermi Velocity because the Lorentzian Function curve-fit is approximate function that I came up with by observing the Resistivity vs gate potential plot,so if accurate curve fitting is done for the data then the Fermi Velocity will be exact for any 2D material as in this case graphene.

Now let's calculate the mean free path (L_0) of the electron in graphene from the Transmission function.

T = $\frac{2L_0}{L+L_0}$ = $2.236 * 10^{-9} * \sqrt{n}$

Hence L_0 = $\frac{0.5*L}{\frac{4.472*10^8}{\sqrt{n}}-0.5}$

L_0 = $\frac{0.5*L}{\frac{4.472*10^8}{\sqrt{n}}-0.5}$

for a Length of sample as $8*10^{-6}$,

L_0 = $\frac{4*10^{-6}}{\frac{4.472*10^8}{\sqrt{n}}-0.5}$

It is clear that L_0 varies proportional to $\sqrt{n}$ i.e L_0 varies directly proportional to Fermi Energy and hence the type of scattering that the graphene sample undergoes is long range scattering as discussed in section [5.1.2] and thus we have successfully identified the type of scattering for the graphene sample.

Now we can extract the Ballistic Conductance in graphene by $G_{\text{Ballistic Limit}}$ = $1/R_{contact}$

Also we can extract the mean scattering time (τ) from the mean free path and also the scattering density present in the 2D material i.e the number of scatters per unit length/area/volume for sample to completely characterize the resistance of the material.

The Diffusive Conductance Fraction in Graphene by $G_{\text{Diffusion Limit}}$ = $1/R_{\text{Diffusion}}$ i.e this factor tells us what percent of Ballistic conductance transport is our sample's transport operating on.

Hence the Diffusion Conductance $G_{\text{Diffusion Conductance}}$ = $G_{\text{Diffusion Limit}}$*$G_{\text{Ballistic Conductance}}$ = T*$G_{\text{Ballistic Conductance}}$

Below shows the plots for all of the above calculated quantities vs its carrier density.

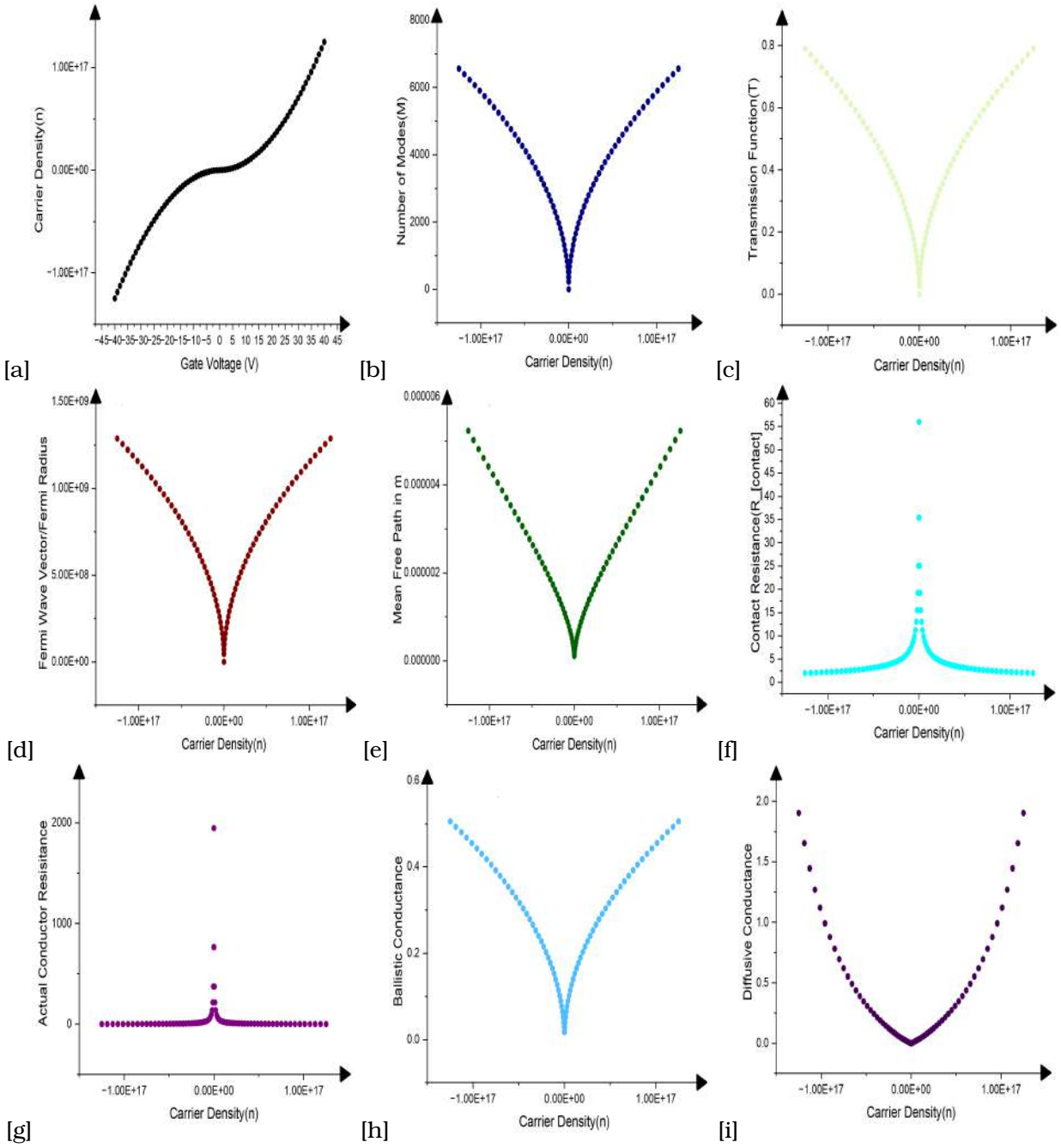

Figure 3.15: (a) Fermi Energy vs Carrier Density (b)Number of Modes vs Carrier Density (c)Transmission Function vs Carrier Density (d) Fermi Wave Vector vs Carrier Density.(e) Mean Free Path vs Carrier Density (f) Contact Resistance vs Carrier Density (g) Actual Conductor Resistance vs Carrier Density(h) Ballistic Conductance vs Carrier Density (i) Diffusive Conductance vs Carrier Density of monolayer Graphene at low temperature near zero Kelvin

Note - This calculations are purely done from the experimental data and hence all these quantities can help update the theoretical Hamiltonian for the transport as discussed in detail in section [5.1.2]

Chapter 4

Van der Waal Hetero-structure Stack Making,It's Analogue Capacitance Mathematical Modelling and Device Fabrication

4.1 Van der Waal Hetero-structure Stack Making

4.1.1 Exfoliation of Graphene on Plasma O_2 Etched and Acetone ultra-sonicated SiO_2-Si Substrate

Graphene can be manufactured by various processes such as Layer Engineered large area exfoliated graphene,Micro-mechanical exfoliation,Liquid Phase Exfoliation,Chemical Vapour Deposition (many sub-types),Flame Synthesis,Pulsed Laser Deposition,Electrochemical Exfoliation,Organic Modified Hummers Method,Epitaxial Growth,Ethanol Assisted Reduction Treatment,Freeze Drying gas phase synthesized graphene,Electrophoretic Deposition,Micro-fluidized Technique flash Joule Heating,Green Synthesis,Organic Materials such as Mango Leaves dipping in ethanol [1,3] etc.Out of these techniques CVD is leading in terms of providing industrial scalabilty options but has lower carrier mobilities compared to mechanical exfoliation.Layer Engineering Large Area Exfoliated Graphene can provide large flakes of graphene of the order of centimeters and if we follow it by transfering these exfoliated graphene flakes (having same type of edges,can have different edges but again the carrier transport will vary proportional to the extent of inhomogeneity) such that they create lap joint which are then joint by current assisted CO_2 laser irradiation then they can be scaled to whatever size we want,but the joint's stacking order as well as the CO_2 laser joining can cause the carrier transport to vary in the lap jointed region and hence extreme experimental care and control should be taken at the time of stacking and joining so that the carrier transport at the joint/junction can be nearly same as pristine graphene and also the production rates can be increased by optimizing the process parameters exactly (as they do not vary arbitarily with each new execution of process) and this whole process can be automated for

industrial use [2,4,5], but we manufactured graphene by exfoliation technique using scotch tape as it very easy,fast,low defected and reliable process with downside that no guarantee of seeing (under microscope) monolayer graphene flake in every substrate as it is trial and error process as the parameters governing the process vary arbitarily even if same user is performing it and also size of the flake is limited to few (at max tens of micrometers) micrometers. But since our main goal is to only probe the capacitance of 2D material the size of 2D material can be in the range of micrometers.The Parameters governing the mechanical exfoliation of graphene using a scotch tape is 1.$Si-SiO_2$ substrate surface roughness. 2.The Timing of Acetone Ultra-sonication of $Si-SiO_2$ substrate 3.The Uniformity ,Density and thickness of Graphene/Graphite material on the scotch tape 4.Plasma O_2 Exposed time of the $Si-SiO_2$ substrate. 5.Pressure and uniformity (arbitary and varies even if performed by same user) of pressing the scotch tape on the $Si-SiO_2$ substrate. 6.The Heating time of the Scotch taped $Si-SiO_2$ substrate on hot plate. 7.The Waxing Process of the scotch tape from the $Si-SiO_2$ substrate.

We can't exactly quantify mathematically the process parameters of points 3,5 and 7 but we can perform computer processed simulations of the exfoliation of graphene to get a quantitative picture of 3,5, and 7 points written above and optimize these 7 parameters and if possible automate it to get a sure shot large area monolayer flakes of graphene for every $Si-SiO_2$ substrate but again there are other minute factors such as environmental conditions such as moisture content,temperature of the experimental room,etc (can be controlled by using AC's),the size of the graphite flake taken for exfoliation on the scotch tape (so a automated process of getting the same amount of graphite content for each exfoliation on scotch tape needs to be done).

Process of Mechanical Exfoliation of Graphene-

1.Take $Si-SiO_2$ wafer out of the vaccumized dessicator.

2.Cut the $Si-SiO_2$ wafer with pencil shaped diamond cutter in 1 to 1.5 cm arbitary square shaped wafer.

3.Put the $Si-SiO_2$ wafer's cut squares in acetone,then ultrasonicate it for 5 minutes either full wave or half wave for cleaning,roughning,removing organic adsorbates and removing moisture from the substrate.

4.Clean the $Si-SiO_2$ wafer using Iso-propyl Alcohol then blow dry using N_2 .

5.Then plasma O_2 treat $Si-SiO_2$ wafer for 1-2 min for removing the contaminants and roughning the surface,increasing the hydrophilicity of $Si-SiO_2$ wafer.

6.Now take a piece of scotch tape sufficiently larger than square wafer length then fold its edges.

7.Take few graphite flakes using cleaned Teflon end covered tweezer and then put it on the sticky side of the tape.

8.Fold and unfold the tape to spread the flakes uniformly throughout the tape.

9.Now place the sticky side of the tape on the $Si-SiO_2$ substrate and apply a uniform pressure using a back side of the plastic dropper.

10.Now place the $Si-SiO_2$ substrate on a hot plate at 100 $\deg$ C for 2-5 minutes.

11.Then air cool it for 10 to 15 minutes and gently remove the scotch tape from the substrate.

12.Finally visually magnify the image of $Si-SiO_2$ substrate by seeing it under optical microscope and identify the number of layers based on the colour contrast difference between graphene (mono and multi-layers) on the $Si-SiO_2$ substrate as discussed in section 3.2.

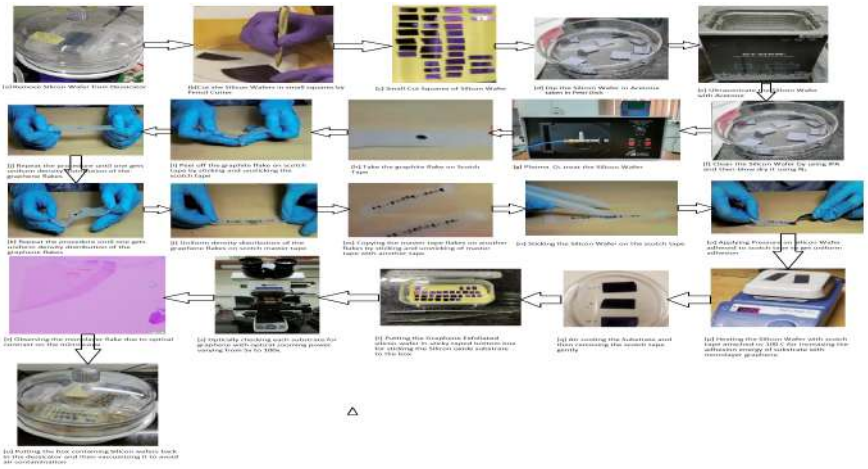

Figure 4.1: Step by Step Procedure of Mechanical Exfoliation of Graphene with few diagrams taken from Reference [7],[9] and few from Our Nanoscale Lab.

Generally we perform exfoliation of graphene by 3 types of Forces - 1.Normal Force 2.Shear Force 3.Fragmentation and then Normal Force/Shear Force but size of the flakes is limited to smaller areas.[10]

The Mechanical Exfoliation of Graphene which is performed in Nano-Scale Device and Fabrication Lab at IISc is of the 3rd type i.e Fragmentation and then Normal Force.

If we consider the binding energy between two materials that is energy that binds the two surfaces owing to its surface energies ,it can be divided in to 3 types -

1.Cohesion Energy - The Binding Energy between the graphene monolayer and graphite flakes.

2.Cleaving Energy - The Binding Energy between the graphite and graphite flakes.

3.Adhesion Energy - The Binding Energy between the graphene and any other material/substrate. [13]

Note - The Exfoliation Energy i.e the energy required to separate monolayer graphene material from graphite is generally slightly less than the binding energy.

Now if we consider the adhesion energy of monolayer graphene with the $Si - SiO_2$,it is 0.096 J/m^2 [value taken from [18]] at room temperature.The adhesion energy of any material with scotch tape is nearly 113 J/m^2 [value taken from [17]] and the cohesion energy between monolayer graphene and monolayer graphene is nearly 0.15 J/m^2 [value taken from [4]]. If we consider a uniform smooth $Si - SiO_2$ substrate,then it cannot separate monolayer graphene from its neighbouring van der waal forced monoloayer graphene as,

$\Gamma_{Graphene-Si-SiO_2}$ < $\Gamma_{monolayerGraphene-monolayerGraphene}$ and if we try to exfoliate graphene on this $Si - SiO_2$ substrate directly then due to larger adhesion energy of the tape with graphene and larger cohesion energy between graphene-graphene layers no graphene will be exfoliated on $Si - SiO_2$ substrate.If we want an exact monolayer then the relation that should be followed is,

2 x $\Gamma_{monolayerGraphene-monolayerGraphene}$ > $\Gamma_{Graphene-Si-SiO_2}$ > $\Gamma_{monolayerGraphene-monolayerGraphene}$.

Hence we want the adhesion energy between monolayer and $Si - SiO_2$ between 0.15 J/m^2 to 0.30 J/m^2.If it is greater than 0.30 J/m^2 then more than 1 layer will be adhered to the $Si - SiO_2$ substrate.There are two ways to increase the adhesion energy suitable for $Si - SiO_2$ substrate i.e first removing the contaminants and increasing the surface roughness of $Si - SiO_2$ substrate by

plasma cleaning for 1-2 min and second is annealing i.e heating the $Si-SiO_2$ substrate with scotch tape attached to 100 degree C for 2-3 minutes and then cooling it down to room temperature by air exposure.Doing this two steps optimally will increase the adhesion energy ideally to a value in between 0.15 J/m^2 to 0.30 J/m^2.In ideal case for a uniform $Si-SiO_2$ having uniform adhesion binding energy between graphene and $Si-SiO_2$ of in between 0.15 J/m^2 to 0.30 J/m^2 we will by exfoliation only get single layer of graphene exfoliated i.e we will only get monolayer graphene exfoliated throughout $Si-SiO_2$ substrate.But practically due to surface uneven roughness distribution of $Si-SiO_2$ the binding adhesion energy can vary a lot (also pressure of pressing the scotch tape and also uniformity,density,thickness of flakes on scotch tape can play a role in changing the adhesion energies of graphene-graphene interface and graphene - $Si-SiO_2$ interface) and hence we see different number of layers of exfoliation of graphene/graphite (more than 10 layers) on $Si-SiO_2$ when we see in the optical microscope.It may also so happen that if heating time or temperature and plasma O_2 time is increased beyond certain range then graphene-$Si-SiO_2$ interface energy is greater than 0.30 J/m^2 in which we see increasing number of layers exfoliated on substrate with no monolayer graphene anywhere on the substrate. Hence the seven parameters that governs the mechanical exfoliation of graphene all boils down to one main governing parameter, the adhesion energy between the substrate and graphene.This theory can be verified experimentally by measuring the adhesion energy of $Si-SiO_2$ substrate locally at nanoscale by AFM measurements [15] and colour mapping the surface adhesion energy location wise on the $Si-SiO_2$ substrate and then performing exfoliation of graphene on $Si-SiO_2$ substrate and finding the relation between the number of layers we see locally on the $Si-SiO_2$ substrate on optical microscope with adhesion energy.

This theory also promotes the study to get an exact increasing relation by curve fit between the adhesion energy between monolayer graphene and different surface treated $Si-SiO_2$ substrate with the annealing time and temperature as the annealing time and temperature can govern the conformal contacts of monolayer graphene with corrugated SiO_2 surfaces which can be seen by AFM measurements.[11]

Note - The adhesion energy measurements of $Si-SiO_2$ substrate with monolayer graphene varies greatly in the literature available till date from 0.096 to as high as 0.45 J/m^2 (nearly equal to trilayers cohesion energy of graphene),which can arise due to surface properties of SiO_2, such as surface roughness and chemical reactivity [18].The values taken in this thesis from literature are such that it is consistent with the theory proposed above.

4.1.2 Exfoliation of Hexagonal Boron Nitride (hBN)

Mechanical Exfoliation of hBN on $Si-SiO_2$ substrate using scotch tape is similar process as described above with main difference that there is no need for plasma O_2 treatment and annealing treatment of $Si-SiO_2$ substrate as the adhesion energy of hBN with $Si-SiO_2$ substrate is nearly equal to cohesion energy of hBN with hBN approximately 0.26 J/m^2 [approximate average value taken from [15] by ignoring the error range at room temperature],hence just acetone ultrasonication is sufficient for increasing the substrate-hBN adhesion energy to be greater than hBN-hBN cohesion energy by removing the contaminants and increasing hydrophilicity (also increasing surface energy) of substrate. Three hBN's are present in our vanderwaal heterostructure i.e 1.Top hBN 2.Intermediate hBN 3.Bottom hBN. The in-plane dielectric constant of the hBN varies from

6.82 (monolayer hBN) to 6.93 (bulk hBN) and out of plane dielectric constant varies from 3.29 (monolayer hBN) to 3.76 (bulk hBN)[19].Hence the variation in the dielectric constant can be considered as negligible with the increase in number of layers i.e the electric screening due to dielectric constant by the hBN is nearly independent of its number of layers.Hence we can use any number of hBN layers for creation of our heterostructure but,if we consider a simple model of capacitance then C = Aϵ/d,i.e the electric screening increases with the number of layers as capacitance decrease with increasing thickness and hence we have limited hBN thickness to maximum 12 layers as found from the Raman Spectroscopy and Optical Microscopy.

Note - Reference [19] ab initio calculations showed that dielectric constant of hBN is nearly independent with number of layers has discrepancy with reference [20] where dielectric constant is directly proportional to number of layers of hBN,this discrepancy is due to different definition of thickness of hBN but the definition of thickness in reference [19] is more relevant for 2D material stack [19] and hence relevent for this thesis.

4.1.3 Design of the Van der waal Geometry/Identification of the Right hBN and Graphene Flakes for creating plus shaped Heterostructure under microscope

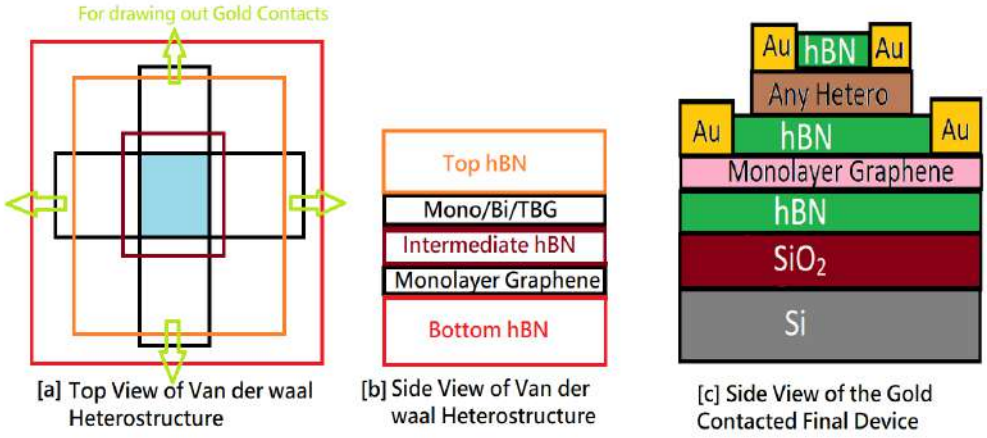

Figure 4.2: Top and side views of the required Ideal Van der waal Heterostructure with Monolayer graphene and Mono/Bilayer/TBG making a plus shape essential for drawing out gold contacts for probing its in plane layer resistivity measurements to finally measure the quantum capacitance.

We want to measure the quantum capacitance/Fermi Energy of the top 2D material by measuring the out of plane layer resistivity at charge neutrality point of the bottom monolayer graphene as function of V_{TL} and V_{BG}. So essentially we are applying potential at the top hBN, V_{TL} and at the bottom Si/SiO_2, V_{BG} and then modulating V_{BG} from V_{maxBG} to -V_{maxBG} for zero applied V_{TL} and then measuring the tunnelling current through the bottom monolayer graphene which is due to applied potential V_{BG} which is screened by the Si/SiO_2 substrate and then by the bottom hBN and then getting the out of plane layer resistivity from the measured tunnelling current by $\rho_{outofplane}$

= $\frac{RA_{overlap}}{L_{monolayer}}$ = $\frac{\triangle V A_{overlap}}{I_{tunnelling} L_{monolayer}}$ (where $\triangle$ V is the difference between the potential between the top and bottom surfaces of bottom monolayer graphene,$L_{monolayer}$ is thickness of the monolayer graphene = 0.345 nm) and then noting the point of highest resisitivity i.e minimum current,this is the charge neutrality point for near zero potential applied at V_{TL}.Now repeating this procedure for changing values of V_{TL} from a V_{maxTL} to -V_{maxTL} and noting the charge neutrality point for each value of V_{TL}.The V_{TL} is only screened by the top hBN,2D material (whose quantum capacitance we want to measure) and the intermediate hBN . Now if we plot the V_{TL} vs V_{BG} curve we observe a kink in the charge neutrality line at near zero V_{BG} and zero V_{TL} value (provided the intrinsic fermi energy of bottom monolayer graphene is near zero V_{BG} and zero V_{TL} value).This kink i.e change in the slope of the charge neutrality line indicates that the electric screening of the V_{TL} from the top hBN,2D material and intermediate hBN is not 100 percent and there is some leakage that modulates the tunnelling current in bottom monolayer graphene. This change in slope of charge neutrality line observed for all V_{BG} from V_{maxBG} to -V_{maxBG} and zero V_{TL} range can be modelled as simple capacitance model as shown in the figure below.

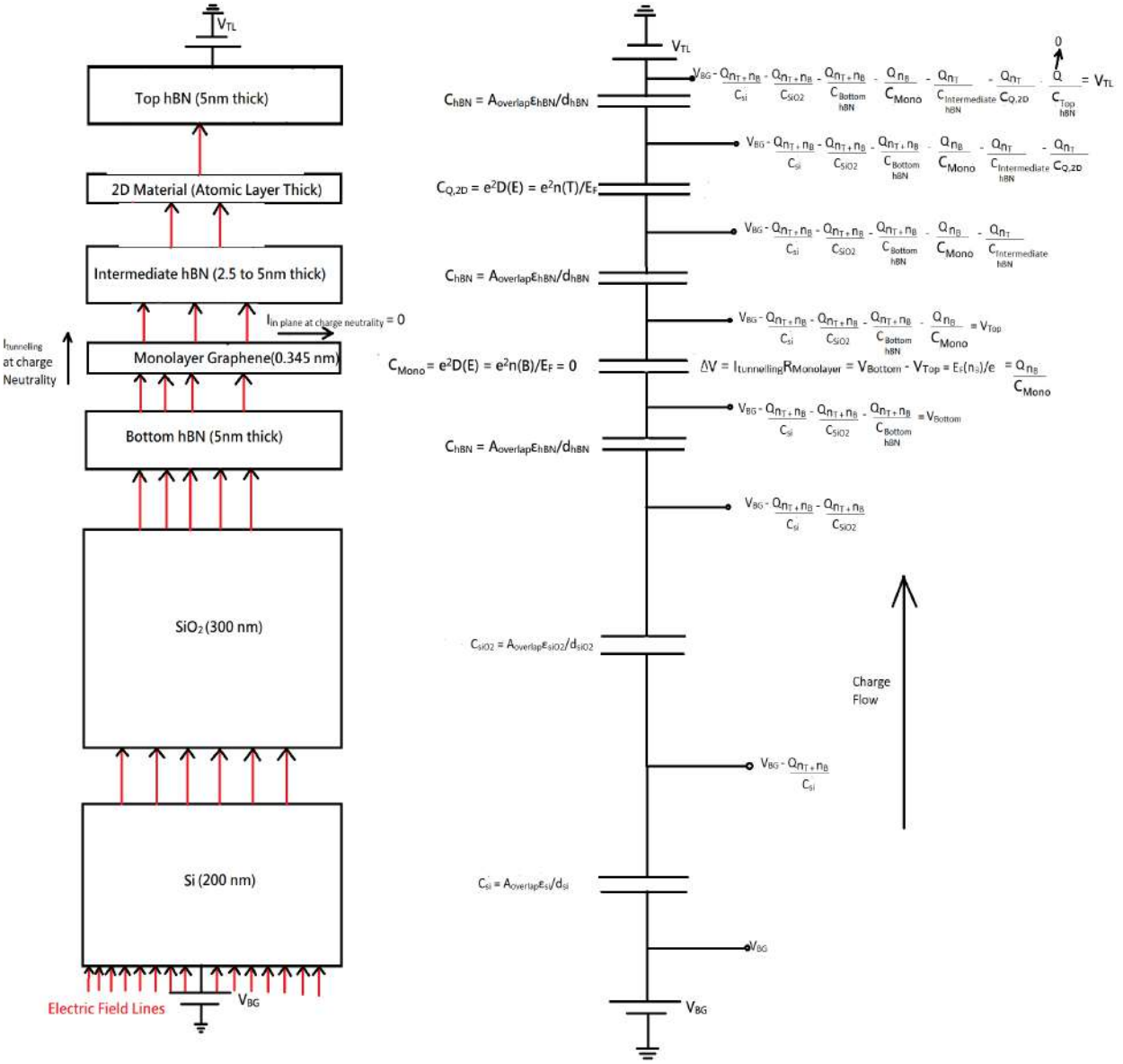

Figure 4.3: Capacitance Model of Van der waal Heterostructure for Quantum Capacitance Measurements with monolayer graphene at charge neutrality.

Important Note - The out of plane tunnelling current in graphene is due to the potential difference between the top surface and the bottom surface of the monolayer graphene.This potential difference is also responsible for introducing charge carriers in the conduction band of the monolayer graphene n_B which is the driving factor for the in plane electrical transport in graphene .Hence we can draw out a direct proportion relation between the in plane electrical transport in monolayer graphene and the out of plane tunneling in monolayer graphene i.e there is direct proportion relation between the out of plane tunnelling resistivity and the in plane transport resistivity in monolayer graphene.This statement is relevant here because for measuring the out

of plane tunnelling current in graphene we will require gold contacts at the top and bottom of the monolayer graphene i.e after transfering the first hBN on the Si-SiO_2 substrate,the gold deposition and lithography should be done to get the contacts from from top surface of hBN and then monolayer graphene should be transfered on top of hBN i.e essentially getting contacts from bottom surface of the monolayer graphene and then the gold deposition and lithography should be done to get contacts from the top surface of the monolayer graphene to measure the out of plane potential difference and the out of plane tunnelling current in graphene due to the applied gate potentials at the top and the bottom gates.But here in this thesis we have constructed the van der waal heterostructure such that we are taking in plane gold contacts from top surface of the monolayer graphene and the top surface of 2D material and then measuring the in plane current in monolayer graphene for applied in plane potential difference by four probe measurement and then finding the in plane resistivity by using the relation $\rho_{inplane} = \frac{R_{inplane}A_{crosssection}}{L_{betweenthetwocontacts}} = \frac{V_{inplane}A_{crosssection}}{I_{inplane}L_{betweenthecontacts}}$ by modulating the V_{BG} and V_{TL} potentials.

Note - The Silicon is n doped for our heterostructure and is acting as a bottom/back gate along with the bottom gold contact on plastic chip (which here is indicated as bottom gate),so its capacitance may be neglected but it still screens some electric field lines so it still shows some capacitance and hence our model includes that effect of capacitance of n doped Si.

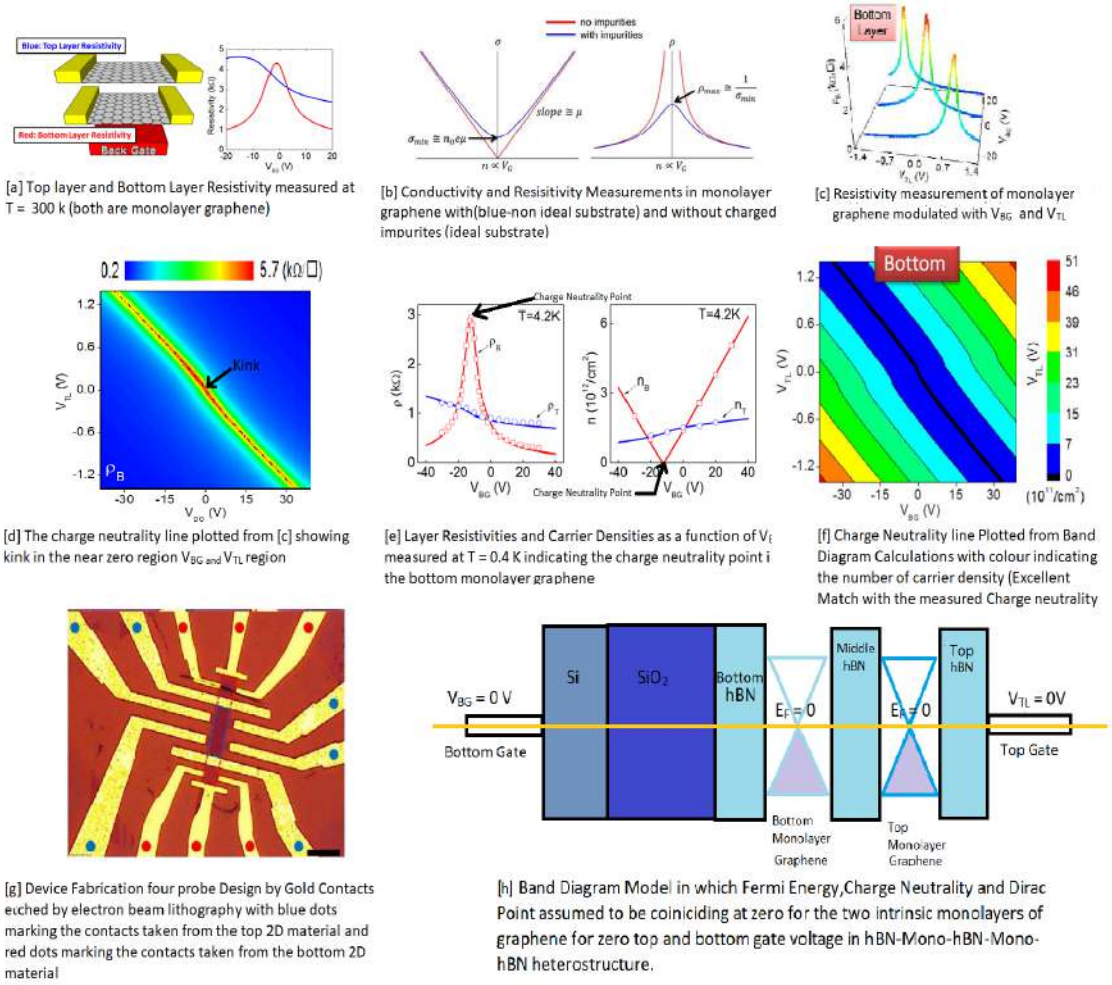

[a] Top layer and Bottom Layer Resistivity measured at T = 300 k (both are monolayer graphene)

[b] Conductivity and Resisitivity Measurements in monolayer graphene with(blue-non ideal substrate) and without charged impurites (ideal substrate)

[c] Resistivity measurement of monolayer graphene modulated with V_{BG} and V_{TL}

[d] The charge neutrality line plotted from [c] showing kink in the near zero region V_{BG} and V_{TL} region

[e] Layer Resistivities and Carrier Densities as a function of V_t measured at T = 0.4 K indicating the charge neutrality point i the bottom monolayer graphene

[f] Charge Neutrality line Plotted from Band Diagram Calculations with colour indicating the number of carrier density (Excellent Match with the measured Charge neutrality

[g] Device Fabrication four probe Design by Gold Contacts euched by electron beam lithography with blue dots marking the contacts taken from the top 2D material and red dots marking the contacts taken from the bottom 2D material

[h] Band Diagram Model in which Fermi Energy,Charge Neutrality and Dirac Point assumed to be coiniciding at zero for the two intrinsic monolayers of graphene for zero top and bottom gate voltage in hBN-Mono-hBN-Mono-hBN heterostructure.

Figure 4.4: The Measurements Required,Device Fabrication Design,Analysis,The Band Diagram model,all that is required for Quantum Capacitance Measurement of any 2D material with varying carrier concentration via gate voltage by method of Monolayer Graphene acting as a probe to measure the Fermi Energy/Quantum Capacitance of Any 2D material.[a] to [g] figures adapted from reference [21]

As the monolayer graphene is at charge neutrality point we get two equations, from simple capacitance Model,(Considering V_{BG} being the higher potential i.e the flow of the charge is from Bottom gate to top gate (hence n_T will be screened by the intermediate hBN and not n_B and top gate will not screen any charge(might lead to confusion))

$V_{TL} - Q_{TophBN}/C_{TophBN} - Q_{n_T}/C_{Q,2D} - Q_{n_T}/C_{IntermediatehBN} = Q_{n_B}/C_{Q,Monolayer} = 0$

Q_{TophBN} = 0 as there is no charge screening in top hBN if we consider the charge flow from bottom gate to top gate

- $V_{BG} - Q_{n_B+n_T}/C_{Si} - Q_{n_B+n_T}/C_{SiO_2} - Q_{n_B+n_T}/C_{BottomhBN} = Q_{n_B}/C_{Q,Monolayer} = 0$

(Negative sign is given to V_{BG} as we are taking potential equation opposite to current flow)

Here $Q_{monolayer} = Q_{n_B} = en_B = 0$ at charge neutrality point for monolayer graphene,

$Q_{2D} = en_T$

Manipulating above 2 equations,

$\frac{V_{TL}}{V_{BG}}$ = - $\frac{\frac{1}{C_{Q,2D}}+\frac{1}{C_{IntermediatehBN}}}{\frac{1}{C_{Si}}+\frac{1}{C_{SiO_2}}+\frac{1}{C_{BottomhBN}}}$

Hence the slope of the kink in $V_{TL}vsV_{BG}$ charge neutrality line is given by,

$\frac{dV_{TL}}{dV_{BG}}$ = - $\frac{\frac{1}{C_{Q,2D}}+\frac{1}{C_{IntermediatehBN}}}{\frac{1}{C_{Si}}+\frac{1}{C_{SiO_2}}+\frac{1}{C_{BottomhBN}}}$

The value of the R.H.S can be found by taking the slope of the kink in V_{TL} vs V_{BG} charge neutrality plot.In L.H.S all the capacitance values can be calculated by C = A$\epsilon_r\epsilon_o$/d.The values of d are mentioned in the above figure, overlapping area can be taken as 8 by 8 micrometer for sample calculation and the values of ϵ can be directly taken from data sheets as ϵ_{Si} = 11.68,ϵ_{SiO_2} = 3.9,ϵ_{hBN} (out of plane) = 3.76. Hence solving we get,

C_{Si} = 3.7376 mF , C_{SiO_2} = 0.832 mF, $C_{Top,bottomhBN}$ = 24.064 mF , $C_{IntermediatehBN}$ (for thickness of 2 nm) = 120.32 mF, if the thickness of hBN is 50 nm then the $C_{thickhBN}$ has capacitance of 4.8128 mF and decrease with increase in number of layers i.e the electric screening increase.

Note - hBN flakes thickness in this thesis was characterized by Raman and Optical Microscope hence we do not have a exact thickness of hBN for which AFM needs to be performed.

Note - Above equation of slope holds for the whole charge neutrality line variation from -max V_{TL} to +max V_{TL} but at higher $\pm$ V_{TL} values away from zero i.e at high n_T values the value of Quantum Capacitance increases and $C_{Q,2D}$ > $C_{\text{other terms from dielectric}}$ and hence the slope equation is dominated by $1/C_{\text{other terms from dielectric}}$ and the effect of 1/quantum capacitance term is negligible and hence the slope equation reduces approximately to,

$\frac{dV_{TL}}{dV_{BG}}$ = $\frac{\frac{1}{C_{IntermediatehBN}}}{\frac{1}{C_{Si}}+\frac{1}{C_{SiO_2}}+\frac{1}{C_{BottomhBN}}}$,

hence the kink is not observed at higher $n_T$values i.e at higher V_{TL} potentials and its length is limited to near zero V_{TL} values for V_{BG} variation from V_{maxBG} to -V_{maxBG}.

but still we can try finding the quantum capacitance at higher n_T values at charge neutrality line by analyzing the slope equation,

$\frac{dV_{TL}}{dV_{BG}}$ = - $\frac{\frac{1}{C_{Q,2D}}+\frac{1}{C_{IntermediatehBN}}}{\frac{1}{C_{Si}}+\frac{1}{C_{SiO_2}}+\frac{1}{C_{BottomhBN}}}$

for 0.41 nm thick hBN i.e 1 monolayer hBN the capacitance for an area of 8 by 8 $\mu - m^2$ is 585.52 mF. Hence capacitance as function of number of layers (N) of hBN can be written as, C_{hBN} = 585.52/N.

$\frac{dV_{TL}}{dV_{BG}}$ = - $\frac{\frac{1}{C_{Q,2D}}+\frac{N_{IntermediatehBN}}{585.52}}{\frac{1}{3.7376}+\frac{1}{0.832}+\frac{N_{BottomhBN}}{585.52}}$

As the $\frac{dV_{TL}}{dV_{BG}}$ term is negative for charge neutrality line as it is having negative slope, so removing the minus sign,

$\frac{1}{C_{Q,2D}}$ = $\frac{dV_{TL}}{dV_{BG}}$ (1.4694 + $\frac{N_{BottomhBN}}{585.52}$) - $\frac{N_{IntermediatehBN}}{585.52}$

Hence from above equation it is clear that by increasing the slope of charge neutrality line,increasing the Number of layers of bottom hBN,decreasing the number of layers of intermediate hBN,reducing the overlapping area we can reduce the value of Quantum Capacitance and increase the value of the term $\frac{1}{C_{Q,2D}}$,to increase the size length of the kink at higher V_{TL} region.

Hence we can find the quantum capacitance/fermi Energy of 2D material from above equation of slope.Also it can be seen from the equation that in R.H.S all the capacitances are constant for given heterostructure except the Quantum capacitance of 2D material which confirms that it is the cause of the kink in the charge neutrality line of V_{TL} vs V_{BG} plot.

Note - Here in thesis I have consistently used the term Fermi Energy instead of chemical potential,as Fermi Energy is the chemical potential at zero or near zero kelvin temperature,so

depending on the temperature of measurement the wording changes.

Note - In the above figure the top potential V_{TL} is applied directly to top monolayer graphene but we in this thesis apply it to top hBN gate.

Note - Here we have considered the charge flow from bottom gate to top gate i.e the $V_{BG} > V_{TL}$, one can also write equation in opposite direction for charge flow in case when $V_{TL} > V_{BG}$ i.e total charge will be screened by top hBN and no charge will be screened by bottom hBN,Si and SiO_2.

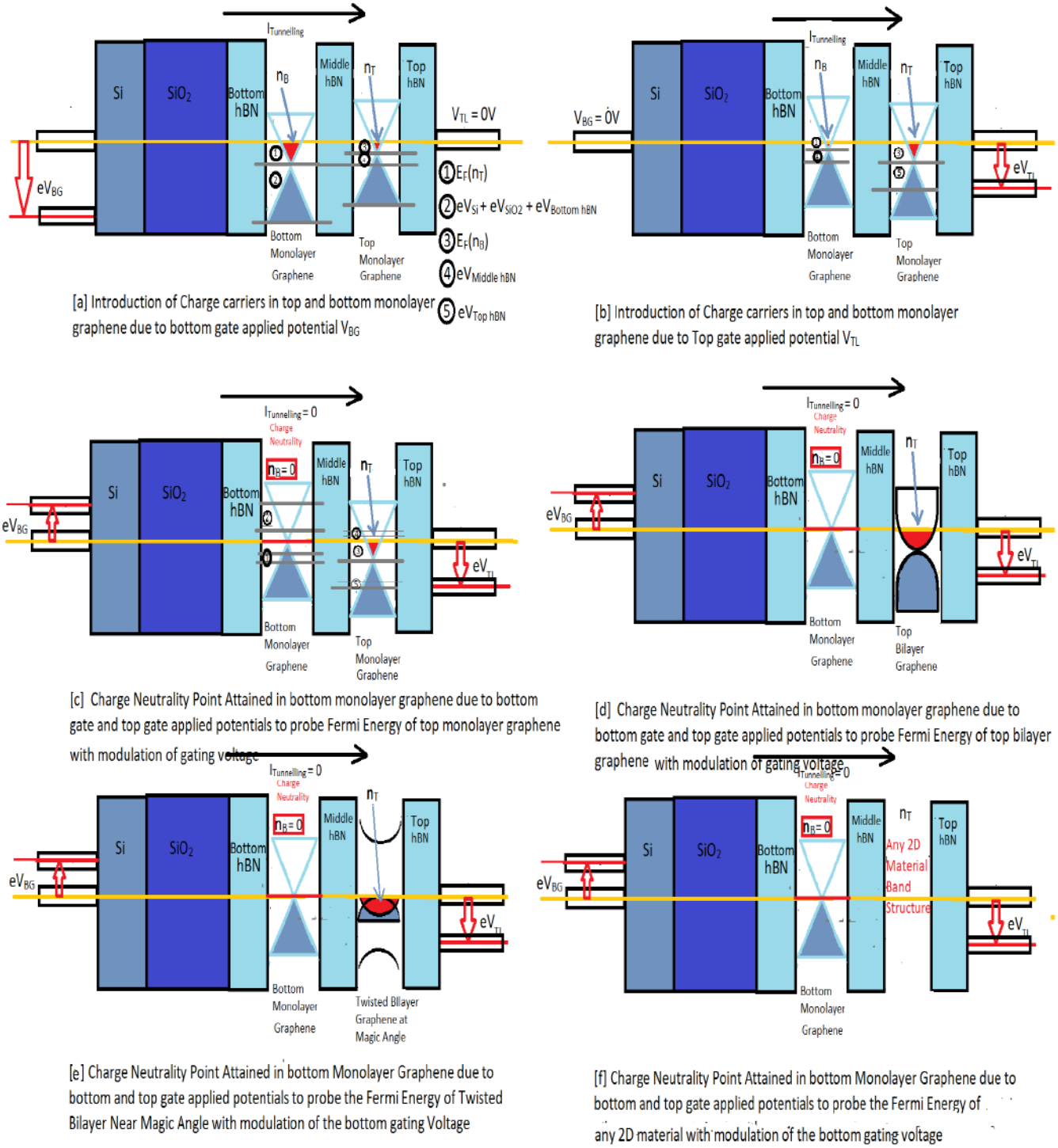

Figure 4.5: Band Diagram Model of Fermi Energy Variation with top gating and bottom gating and identification of charge neutrality point of the bottom monolayer graphene to get Quantum Capacitance/Fermi Energy of the Top Monolayer,Top Bilayer,Top Twisted Bilayer Graphene at Magic Angle and Any 2D material.

Here we will show that Band Diagram Model and Capacitance Model are analogous by mathematical expressions analysis and comparison. Considering the Band Diagram Model as depicted in figure above,

By simple energy balance equation, (Assuming the Energy Flow from Left to Right i.e V_{BG} being the higher potential)

1.Applied between bottom Si-SiO_2 gate and Monolayer Graphene - Equation [A]

2.Applied between top hBN gate and Monolayer Graphene - Equation [B]

Energy difference between the Back/Bottom Gate where potential V_{BG} is applied and the Monolayer Layer Graphene Fermi Energy = Energy lost due to screening of electric field lines by the Si,SiO_2 and Bottom hBN + Energy lost in the environment (generally neglected).

eV_{BG} - $E_F(n_B)$ = eV_{Si} + eV_{SiO_2} + e$V_{BottomhBN}$

eV_{BG} = eV_{Si} + eV_{SiO_2} + e$V_{BottomhBN}$ + $E_F(n_B)$ - [A]

Now,Energy difference between the Top Gate where potential V_{TL} is applied and the Monolayer Layer Graphene Fermi Energy = Energy lost due to screening of electric field lines by the Top hBN,Introducing charge carriers (n_T) to increase the Fermi Energy of middle hBN as function of charge carriers and Middle hBN + Energy lost in the environment (generally neglected).

$E_F(n_B)$ - eV_{TL} = eV_{TophBN} + $E_F(n_T)$ + e$V_{MiddlehBN}$

- eV_{TL} = - $E_F(n_B)$ + eV_{TophBN} + $E_F(n_T)$ + e$V_{MiddlehBN}$ - [B]

Taking Ratio [B]/[A],

$\frac{V_{TL}}{V_{BG}}$ = - $\frac{-E_F(n_B)+eV_{TophBN}+E_F(n_T)+eV_{MiddlehBN}}{eV_{Si}+eV_{SiO_2}+eV_{BottomhBN}+E_F(n_B)}$ - [C]

Above equation is general equation which can be applied to any resistivity point of the V_{TL} and V_{BG} plot and not just along the charge neutrality line.

Considering the charge neutrality point of the monolayer Graphene,

$E_F(n_B)$ = 0 eV, assuming the charge neutrality point and dirac point (the zero Fermi Energy point) coincide as n_B = 0,

$\frac{V_{TL}}{V_{BG}}$ = - $\frac{eV_{TophBN}+E_F(n_T)+eV_{MiddlehBN}}{eV_{Si}+eV_{SiO_2}+eV_{BottomhBN}}$ - [D]

Now here we introduce our analogy of capacitance model, following a relation Q = CV,

V_{Si} = $\frac{\text{Charge that passes through Si wafer from Bottom Gate is responsible for introducing charge carries in monolayer graphene and 2D material}}{\text{Capacitance of Si wafer which can be modelled as A}\epsilon_{Si}/d_{Si}}$

V_{Si} = $\frac{Q_{Si}(n_B+n_T)}{C_{Si}}$

Now, Q(n_B + n_T) = Electron charge(e) x No of carriers introduced in monolayer graphene and 2D material(n_B + n_T)

Q_{Si} = e(n_B + n_T)

V_{Si} = $\frac{e(n_B+n_T)}{C_{Si}}$

Similarly,V_{SiO_2} = $\frac{e(n_B+n_T)}{C_{SiO_2}}$

$V_{BottomhBN}$ = $\frac{e(n_B+n_T)}{C_{BottomhBN}}$

Similarly,

V_{TophBN} = $\frac{\text{Charge passing through Top hBN from top gate is responsible for introducing charge carries in 2D material and Monolayer Graphene = 0}}{\text{Capacitance of Si wafer which can be modelled as A}\epsilon_{TophBN}/d_{TophBN}}$

(as the Current/Energy flow is from Bottom Gate to Top gate no charge carriers will be screened by top hBN)

V_{TophBN} = $\frac{e(0)}{C_{TophBN}}$ = 0

$V_{MiddlehBN}$ = $\frac{e(n_T)}{C_{MiddlehBN}}$

Now the Fermi Energy of the bottom Monolayer graphene can be modelled as,

Potential Due to Fermi Energy of bottom Monolayer V_{FB}= $E_F(n_B)$/e = Electron charge (e) * Number of charge carriers introduced above or below the dirac point of Monolayer Graphene (n_B)/Quantum Capacitance of Monolayer Graphene.

$E_F(n_B) = \frac{e^2 n_B}{C_{Q,Mono}}$

$V_{FB} = E_F(n_B)/e = \frac{e^2 * 0}{C_{Q,Mono}}$ = 0 for Charge Neutrality Point.

Similarly,$V_{FT} = E_F(n_T)/e = \frac{e n_T}{C_{Q,2D}}$

$E_F(n_T) = \frac{e^2 n_T}{C_{Q,2D}}$

Putting the above values of Voltages (Putting n_B = 0 for Charge Neutrality of Monolayer Layer) and Fermi Energies in equation [D],

$\frac{V_{TL}}{V_{BG}} = - \frac{\frac{e^2 n_T}{C_{Q,2D}} + \frac{e^2 n_T}{C_{IntermediatehBN}}}{\frac{e^2 n_T}{C_{Si}} + \frac{e^2 n_T}{C_{SiO_2}} + \frac{e^2 n_T}{C_{BottomhBN}}}$

$\frac{V_{TL}}{V_{BG}} = - \frac{\frac{1}{C_{Q,2D}} + \frac{1}{C_{IntermediatehBN}}}{\frac{1}{C_{Si}} + \frac{1}{C_{SiO_2}} + \frac{1}{C_{BottomhBN}}}$,

which is exact same equation obtained from Capacitance Model and hence both the models are deep down fundamentally the same with same end result,having same mathematical and but different physical interpretation language of expressing.

Important Note - **Since both the capacitance Model and Band Diagram Model do not in any step specifically substitute in the mathematical relation between Fermi Energy of the 2D material with the number of carrier concentration,hence the Quantum Capacitance/Fermi Energy Probing Heterostructure by charge neutrality point plot can be constructed for any combination of the 2D materials ,for example TBG with WSe_2,Bilayer with Bilayer Graphene, Transition Dichalcogenides with Monolayer etc. (any 2D combination is possible) provided we can access the charge neutrality point of one of the 2D materials by varying V_{TL} and V_{BG} in combination used to probe the Quantum Capacitance of the other 2D material.**

At charge neutrality point of the bottom monolayer graphene the tunnelling current is limited to minimum (approx zero) and no charge carriers are introduced in the bottom monolayer i.e n_B = 0 and the monolayer graphene acts as a near perfect electric screener that is no electric field lines due to potential V_{BG} is permitted upwards and no electric field lines due to potential V_{TL} is permitted downwards from monolayer graphene .Whatever difference in the electric field lines comes perpendicular to bottom monolayer graphene are responsible only for the tunneling current flow which is minimum at charge neutrality point and can be assumed as near to zero value.i.e the monolayer is nearly perfect electric screener at charge neutrality.

By a similar argument one can also measure the quantum capacitance of the bottom monolayer graphene from the charge neutrality kink observed in the resistivity of the top 2D material in near zero V_{BG} and V_{TL} range.

More details of principle and measurement of quantum capacitance of any 2D material is discussed in chapter 4 and 6.

Hence from above it can be understood that at least two gold contacts for measuring the tunneling current need to be provided at the monolayer graphene and the top 2D material each and hence the size of the monolayer graphene and 2D material should be enough for the contacts to be made independently .Hence we opt for plus shaped geometry between 2D material and monolayer graphene to ensure sufficient independent space for making the gold contacts for probing the tunnelling current measurement.

The main cross section area in our Van der Waal heterostructure is the overlapping cross

sectional area of the top hBN,2D material,intermediate hBN,monolayer graphene and bottom hBN marked by light blue colour in figure 77 as this area is responsible for the electric screening and is responsible for quantum capacitance measurement of 2D material. For measurement data to be viable and independent of the local defects in the overlapping area of heterostructure , the overlapping area should be as large as possible ,at least should be 8 x 8 micrometers.

Intermediate hBN should be selected to have lower thickness,to have lesser electric screening than the top and the bottom hBN.This is because if the intermediate hBN thickness is high and if we increase the V_{TL} beyond certain voltage the 2D material can get damaged before the electric field lines screened by the intermediate hBN reach the monolayer. Certain number of electric field lines should reach the monolayer from V_{TL} to observe the kink and to measure the quantum capacitance of 2D material. Also the cross sectional size of the hBN should be selected such that there is no physical contact between the 2D material and monolayer i.e it should at least cover the overlapping area, and if there is physical contact same electric current will flow in both 2D material and monolayer and no electric screening effect responsible for quantum capacitance measurement from intermediate hBN will be observed.

Cross Sectional Size of the bottom hBN flake should be as large as possible as the entire remaining van der waal structure is to be transfered on it ,hence we can transfer the remaining structure without worrying about the governing of overlapping screened cross section area by bottom hBN.

The Top hBN only acts as a electric screener (only in the case when top gate potential is greater than the bottom gate potential) and a protective cover to protect the top 2D material from contaminants and it can be only of the size to cover the 2D material completely (naturally covering the overlapping area completely).

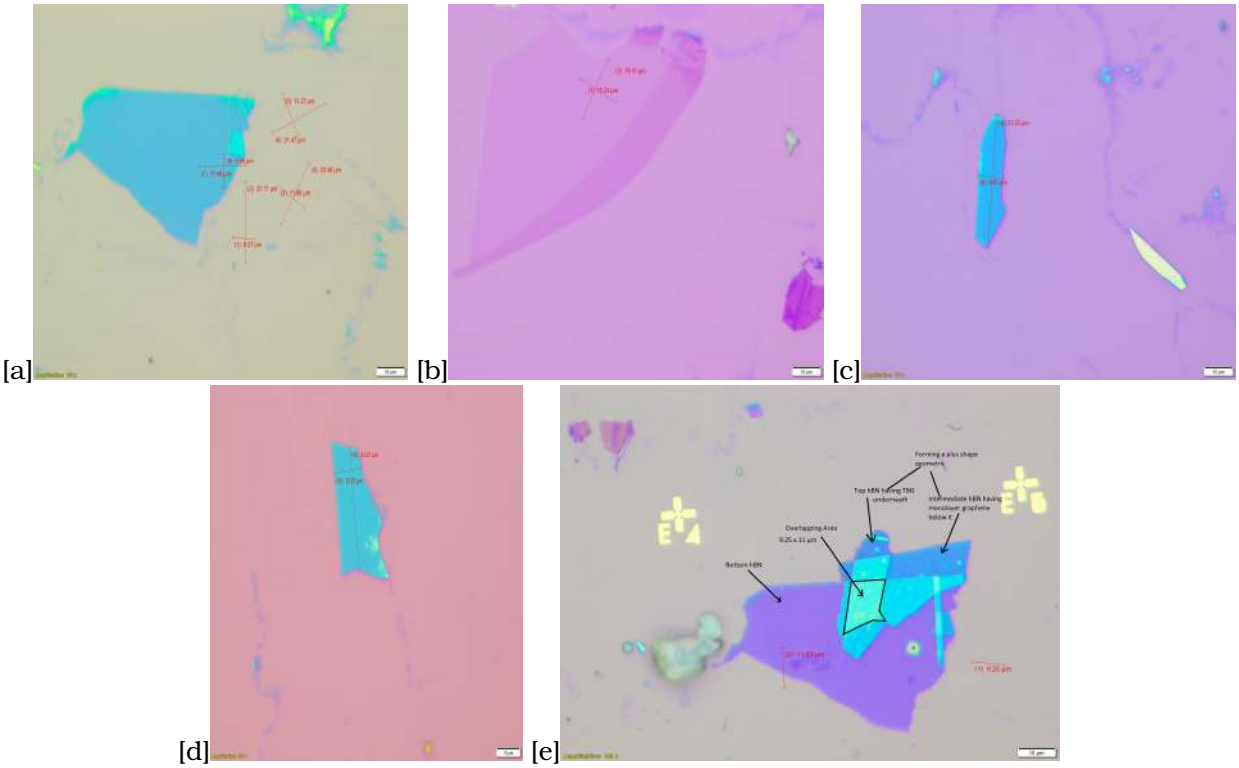

Figure 4.6: (a) Bottom hBN flake of the Van Der Waal Heterostructure Stack (large size) (b) Monolayer Graphene flake same is used for T.B.G tear and stack as well as bottom monolayer as the size of the flake obtained was large(100 x 45 μm) (c)Top hBN having a sharp edge to facilitate the tear and stack of monolayer graphene to get TBG (d) Intermediate hBN separates the monolayer from TBG and also forms a plus shape with top hBN (e) Top hBN-TBG-Intermediate hBN-Mono-Bottom hBN Van Der Waal Heterostructure Stack on Alignment Marked $Si - SiO_2$ substrate.

4.1.4 Pre-Transfer Process - PPC Making,Stamp Creation

A.PPC Solution Making (Poly - Propylene Carbonate) Procedure -

1.Take a graduated cylinder (a container to measure the volume of liquid) and a teflon tweezer and wash it using acetone/IPA (to remove any contaminants and clean it thoroughly),then blow dry it using N_2.

2.Heat the graduated cylinder to some temperature above room temperature (60 C) for 5 min and check for any eye visible signs of contaminants in graduated cylinder.If there are repeat steps 1 and 2.

3.Now take the PPC crystals out from the refrigerator (storing temperature should be at -25 C to not degrade its properties which can later affect its adhesion energy with hBN during pickup) and allow it to cool down to room temperature.

4.Now the PPC is completely soluble in anisole to form a liquid solution in the ratio of 15 $\%$ PPC to 85 $\%$ anisole by weight.(So depending on the amount of PPC solution one wants one can take the volume of the anisole in that proportion but it is advised to make the PPC solution in lesser amounts around 10 ml or depending on the frequency of one's dry transfer processes as after 1 month the adhesion property of the PPC solution start to degrade).

5.The density of anisole at room temperature is 995 kg/m^3.Now if we want to make x grams of PPC solution. x grams of PPC solution = 0.85x grams of anisole + 0.15x grams of PPC crystals.

For 20 grams creation of PPC solution one will require 17 grams of anisole and 3 grams of PPC crystals.

1 ml of anisole = 0.995 gram of anisole

Hence 20 grams of PPC solution creation will require 19.9 ml of Anisole and 3 grams of PPC crystals.

6.Now take a small glass bottle and repeat steps 1 and 2 to get it contamination free and then put the required ml of anisole measured from graduated cylinder in the glass bottle.

7.Now weigh the required PPC crystals on the weighing machine and with a tweezer put the PPC crystals in the anisole filled glass bottle.

8.Shake the glass bottle vigourously and check after 12 hours ,if the PPC crystals are fully dissolved in the anisole ,if it is,its available directly for transfer use.

Images of the Procedure.

B. Visco-elastic Stamp Creation (Generally PDMS)

There are two types of stamps creation in dry transfer technique of 2D materials -

1.Flat Viscoelastic Stamp Creation

2.Hemispherical Viscoelastic Stamp Creation.

The Flat Stamp consists of glass slide (cover slip),Flat PDMS and PPC spin coated on top of it.But here in this thesis we use hemispherical PDMS stamp as it introduces contact angle between the target flakes which is responsible for a bubble free and contamination free transfer process of 2D materials as during the transfer it paves a way for bubbles and contamination to be driven out of the flakes when PPC/hBN makes angular contact with hBN/graphene.[22]

Hemisperical Viscoeleatic Stamp Creation Procedure [14 and Suvronil Dutta]

1. Sonicate the coverslips in acetone,wash with IPA and blowdry it using N_2.

2.Heat/bake the coverslips for 5 minutes at 150 C to remove moisture.

3.Mix the PDMS solution with curing agent in 10:1 ratio on a clean glass slide using a clean toothpick.

4.Put the PDMS on to the coverslips using a toothpick picking up some PDMS mixture by holding the toothpick vertically.

5.It will take one minute to spread the mixture and take hemispherical shape.

6.Bake at 150 degree Celsius for 30 minutes.

Once we create a visco-elastic stamp,next step is to spin coat the PPC on top of the hemispherical PDMS surface.

1.Put the PDMS hemispherical shape stamped cover glass slip in the sample holder either connected to vaccumized pump or stick the cover slip manually by using a two sided sticky tape in the spin coater's centre sample holder if its open to atmosphere.

2.Pour 1-2 drops of PPC at the centre of the PDMS stamp and close the lid of the spin coater.

3.Spin coat the PPC on the PDMS hemispherical shape stamped cover glass slip with 3000 RPM and for 30 seconds.

4.Remove the cover slip from the spin coater with teflon-tweezer or gloved hands and bake cover slip on the hot plate for 10 min at 70 degree celsius to form a uniform thin film coating of

PPC adhered to hemispherical PDMS stamped cover glass slip with final schematic of the stamp and the real image shown below.

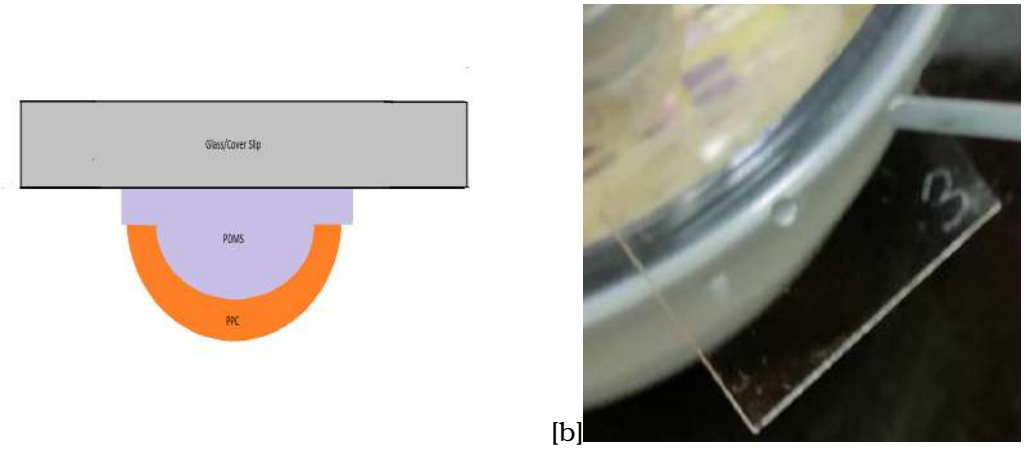

[a] [b]

Figure 4.7: (a) A schematic of Hemispherical Stamp of PDMS-PPC on glass slide or cover Slip (b) Hemispherical Stamp of PDMS-PPC on glass slide or cover Slip as observed in our Nano-scale lab.[14]

Once the PDMS-PPC stamp creation on glass slide is ready, the glass slide is scotch taped/adhesive glued using industrial adhesive like araldite on the aluminium plate and the plate is scotch taped to the transfer setup.

Note - PDMS can be air or O_2 plasma treated to avoid PPC falling off of it or PDMS falling off of glass slide during transfer but it is secondary process,not once in my transfer process did PPC fall off of PDMS or PDMS fall off of the glass slide even without plasma treatment.

4.1.5 Dry Transfer Process for 3 Stacks on Alignment Marked SiO_2-Si Substrate and then the post transfer process on glass slide,the anisole dipping of substrate to dissolve the PPC - 1.hBN - Monolayer Graphene - hBN - Monolayer Graphene - hBN Van der waal Heterostructure Stack 2.hBN - Monolayer Graphene - hBN - Bilayer Graphene - hBN Van der waal Heterostructure Stack 3.hBN - Monolayer Graphene - hBN - Twisted Bilayer Graphene - hBN Van der waal Heterostructure Stack

Conventional Heterostructure consists of three 2D materials stacked on top of each other by dry transfer and stack technique.Dry transfer and stack technique is extremely clean,does not require use of any organic solvents in the process but it quite slow process compared to other transfer techniques [24].But here we are creating a heterostructure that consists of 5 2D materials stacked on top of each other,so there are various ways one can think of to create this heterostructure by transfer technique such as,

1.Transfering the whole hetero-structure of 5 2D materials in one go on the Alignment Marked $Si - SiO_2$ substrate.

2.Transfering the hetero-structure in two steps -

A. Intermediate hBN- 2D material - Intermediate hBN

B. Top hBN- mono-layer graphene,

on the alignment marked $Si - SiO_2$ substrate.

3.Transfering the heterostructure in 3 steps -

A. Bottom hBN

B. Intermediate hBN - 2D material

C. Top hBN - Monolayer Graphene.

Depending on one's familarity and experience with the transfer setup one can follow any one of the above suggested ways.For our two samples,hBN - Monolayer Graphene - hBN - Monolayer Graphene - hBN Van der waal Heterostructure Stack and hBN - Monolayer Graphene - hBN - Bilayer Graphene - hBN Van der waal Heterostructure Stack were created using way 2 and hBN - Monolayer Graphene - hBN - Twisted Bilayer Graphene - hBN Van der waal Heterostructure Stack was created with way 3.

Dry Transfer Procedure -

1.Put Kaplon Tape on the microscope stage and then put the double sticky sided tape at the centre of microscope stage and with Teflon Tweezers put the $Si - SiO_2$ substrate containing the required hBN flake on it such that we can at access the location of the hBN flake on the microscope that we want to transfer under the permitted microscope stage movement in x and y direction.

2.Once the location of the hBN flake is identified on the microscope, hand move the transfer component containing the aluminium plate with cover slip attached and peizo-controller in between the objective lens of the microscope and microscope stage such that stamp section of the cover slip is visually under the objective lens.

3.Now the objective lens of the microscope is already focussed previously in step 1 on the hBN flake so it's better to just move the aluminium plate downwards i.e negative z direction towards the $Si-SiO_2$ substrate until we can see the glass slide with some offset of focus from the $Si-SiO_2$ substrate.

4.Once the objective lens is focussed on the glass slide,move the piezo-controller in x-y direction until we see the optical contrast difference between PDMS-PPC stamp and the glass slide,marking the position of the edge-ring of the hemispherical PDMS-PPC stamp.Move the peizo-controller in x and y direction to get that edge ring at the centre of the computer screen connected to microscope.

5.Now move the piezo-controller in x direction and measure manually and arbitarily the number of hand rotations you perform for tracing the edge ring to edge ring distance in x direction and then come to the centre of x direction and repeat the same procedure in y direction and once it is done you will arbitarily be at the centre of the hemispherical stamp. This is relevant because you want the location of pickup of hBN away from the centre of Stamp by at least 100 micro-meters to ensure a contact angle of PPC with hBN in the range of 15 to 19 degrees [22] again to ensure a bubble free and contamination free pickup of hBN on PPC.

6.Now move the peizo-controller down by using the micro-motion software to ensure slow,steady and unidirectional movement of the aluminium plate towards the $Si - SiO_2$ substrate until the PPC touches the $Si-SiO_2$ substrate. Now touching of the PPC to substrate is indicated by rippling and change in the contrast visually identifiable,but the tricky part is that the touching starts at the centre of the stamp and if we are away from centre far enough then it may happen that hBN flake will not contact PPC and before that only the glass slide will break due to downward force

exceeding the breaking tensile point of the glass slide. So it is necessary to ensure the contact angle of 15 to 19 degrees between the PPC and hBN and still be within the permitted range of the contact area of PPC without breaking the glass slide or one can break many glass slides and measure the diameter of the contact area or how many mm of movement (can be checked on computer screen in the micro-imaging software) from point of centre touch of the aluminium plate downward is permitted before the glass slide breaks and note that diameter/ring size for future use.

7.Once the PPC touches the hBN flake that we want to pick up at room temperature ,increase the temperature of the micro-stage to 60 to 64 degree C by PID temperature controller (not more than 70 C as PPC liftoff from the $Si-SiO_2$ substrate will not be smooth) for 5 min so that the PPC will reach a temperature above 40 degree celsius i.e its glass transition temperature and soften on to hBN flake i.e its storage modulus (hardness) will decrease and when we reduce it back to below 40 degree C it will form a strong adhesion with the hBN flake.Experimentally owing to its thermoplastic nature PPC is known to form strong adhesion with 2D material in the temperature range near its glass transition temperature and the adhesion decrease as we increase the temperature and is minimum at 70 degree celsius.[23]

8.After heating the stage to 70 degree celsius for 5 min ,reduce the temperature knob to 40 C and wait for the micro-stage temperature to air cool up-to 40 degree Celsius and lift off the aluminium plate with micro-motion software to form sufficient distance between the $Si-SiO_2$ substrate and the glass slide.

9.During Pickup it self on the computer screen connected to microscope you will see if the required hBN flake is lifted off or not. The adhesion energy of hBN with $Si-SiO_2$ substrate at 40 degree C is on average 0.26 J/m^2 (can be more if the $Si-SiO_2$ substrate is plasma treated) ,the adhesion energy of a typical polymer is at least 100 times the surface energy of polymer [25] and is modulated by its glass transition temperature generally maximum at glass transition temperature.The lowest measured surface energy of PPC film is 47 mJ/m^2 [value taken from 26],hence the typical adhesion energy of PPC is 4.7 J/m^2 and hence it is able to lift off the hBN from the $Si-SiO_2$ substrate by mechanical adhesion as PPC at 70 C flows into the voids / pores of the hBN flake and thus interlocks with the porosity of the hBN and when the PPC hardens at 40 C a strong bond is formed between hBN and PPC (this reasoning is given in the reference for macro-scale and similar analogical reasoning can be given at nano-scale) [25].

10.Now move the aluminium plate upwards in positive z direction with piezo-controller without changing its x and y direction.Now move the micro-stage downwards again without disturbing its x and y direction and remove the $Si-SiO_2$ substrate gently with teflon tweezer. (not disturbing x and y positions of the micro-stage and transfer component helps in the 2D materials flakes vertical alignment faster as we just have to control the z movement of the transfer component and search for next 2D flake on the $Si-SiO_2$ substrate by changing the x and y position of the microstage once it is focussed on the microscope ,hence it is advised but not compulsory)

11.Now place the next $Si-SiO_2$ substrate with teflon tweezer on the micro-stage containing the required graphene flake such that the location of the graphene flake is accessible in the permitted movement of the micro-stage under microscope.

12.Again move the aluminium plate of transfer component downwards and the micro-stage upwards so that both are visually accessible on the computer screen in permitted z change of the

focus of the microscope.

13.Now align the position of hBN flake on the stamp to the graphene flake on the $Si - SiO_2$ substrate by seeing it on the computer screen through micro-imaging software.This step must be repeated at finite intervals as we move down the aluminium plate of transfer component as there might be dis-alignment between hBN and graphene due to external factors that might disturb the transfer stage (even by micrometer) or error range in the downward movement of piezo-controller until the hBN flake is just about to touch the graphene flake.

14.Once they are aligned to desired position move the transfer component downwards until the hBN touches the monolayer graphene flake and ripple ring in the PPC as observed on computer screen due to touch is some distance away from hBN-graphene flakes stack.

15.Now repeat the step 7 with same temperatures and lift-off the graphene with hBN at contact angle. The energy of adhesion of hBN with graphene is typically 0.3 J/m^2 and the adhesion energy between the graphene and $Si - SiO_2$ substrate is 0.096 J/m^2 and increase with annealing temperature.Now the micro-stage is heated to 60 to 64 degree celcius causing the PPC to soften and reducing its adhesion with the hBN,hBN on the other hand will strongly adhere to graphene as its adhesion energy increase with temperature and when micro-stage is again air cooled to 40 degree celsius the PPC will again strongly adhere to hBN causing hBN-graphene to be picked off from the $Si - SiO_2$ substrate.

16. Repeat this procedure for lifting off the remaining heterostructure i.e hBN-graphene-hBN in one go as here we have considered the way 1 of the Pickup ,with care should be taken while transfer aligning to form a plus shape of the two graphene layers in the heterostructure and remaining details as discussed in 5.1.3.

17.Now transfer the hetero-structure on alignment marked substrate. The alignment marks typically range from A1 to G10.It is advised to select the central square area in between the marks (D_5, D_6, E_6, E_5) where you want your hetero-structure transfered ,and the surface of this central square area should be deformities free,uniform,etch free to avoid the local surface properties of the $Si - SiO_2$ substrate govern the charge flow from the bottom gate in to the bottom hBN. So first place the alignment marked $Si - SiO_2$ substrate on the micro-stage and align the heterostructure on the glass cover slip attached to aluminium plate of transfer component with the central square of the alignment marks visually using the micro-motion software and the micro imaging software.

18.Once the alignment is done move the aluminium plate down to make contact with central alignment marked square area of the $Si - SiO_2$ substrate and increase the temperature of the PID controller to 100 degree celsius for 5 mins as at this temperature PPC film softens enough to be detached from the PDMS and fall off of PDMS with van der waal hetero-structure ,and then move the aluminium plate upwards.Remove the substrate with teflon tweezer ,it will have bubble kind of region visible to naked eye in the area on transfer that is the PPC film on top of the hetero-structure.

19.To remove the PPC film from the top of hetero-structure on Alignment marked $Si - SiO_2$ substrate there are various ways ,but we in our lab dissolve it in anisole,by taking anisole in petri dish and putting the $Si - SiO_2$ substrate in it and leaving it for 25 to 30 minutes and then N_2 blow drying it and checking the quality of transfer (bubbles and contamination) by optically imaging the van der waal heterostructure under microscope. The glass/cover slip is untaped from the aluminium plate.

Note - If in any step the transfer fails it is advised to remove the PPC thin film by hand/tweezer from the PDMS stamp or one can also use anisole to dissolve it,but do not use IPA/acetone to clean the cover slip after using anisole ,before PPC spin coating for next transfer as it can make the cover slip's PDMS hydrophobic and PPC film during transfer setup can form convex wedge shape due to weak adhesion with PDMS and fall off of PDMS only after 1 to 2 pickups.

Note - For creating a twisted Bilayer Graphene sample one can use the tear and pickup method.

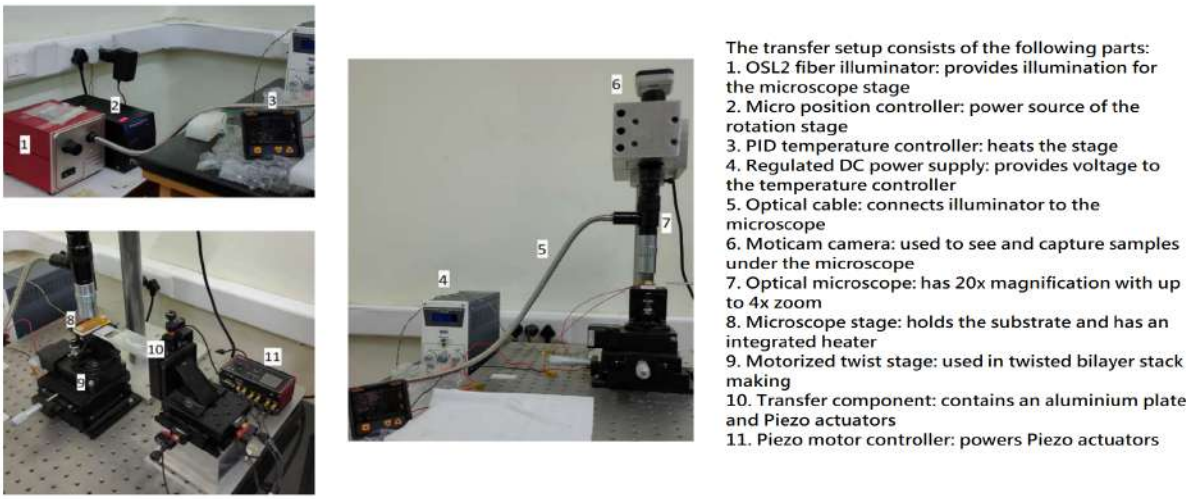

Figure 4.8: Transfer Setup with the name of the equipments used at Our Nanoscale Lab.[14]

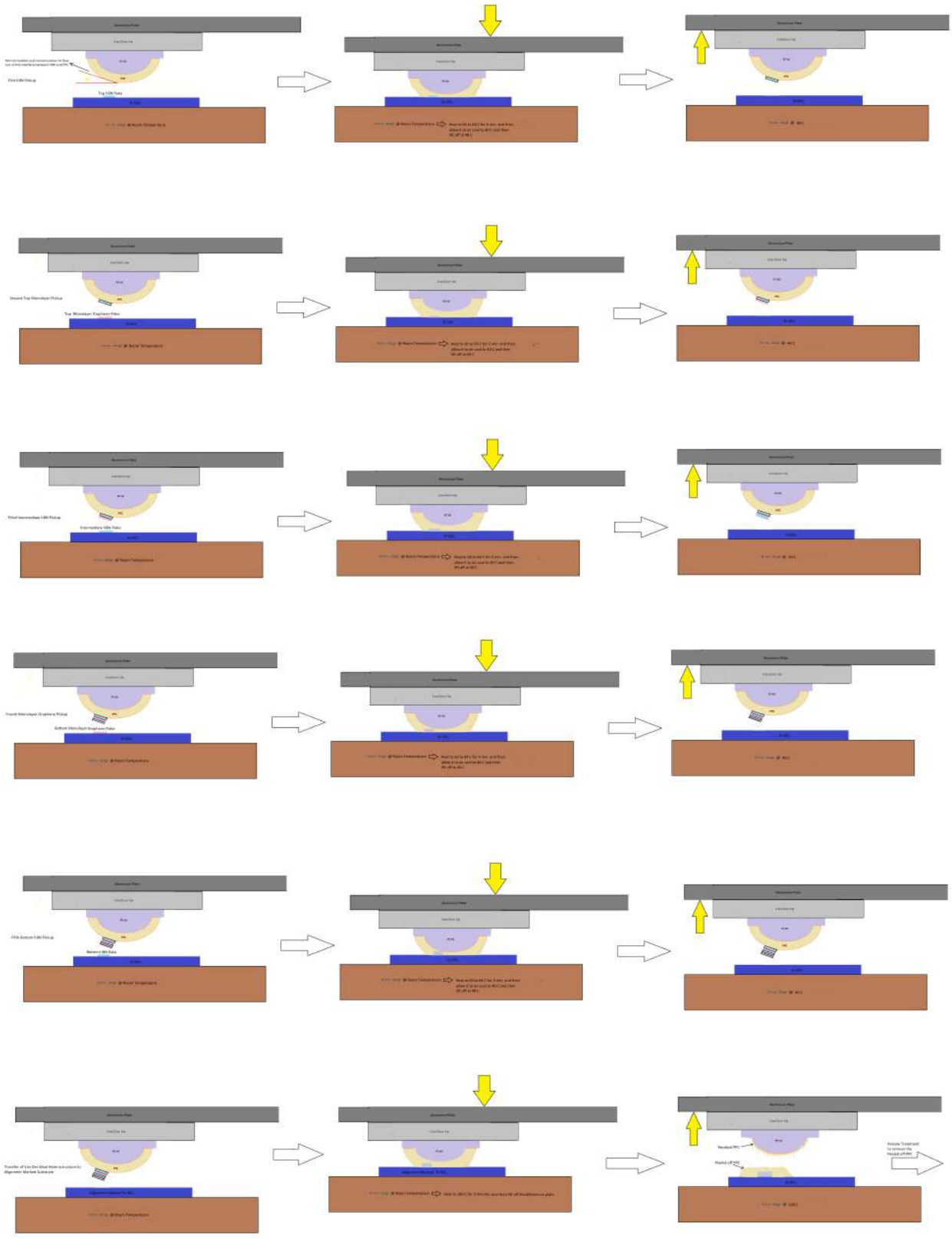

Figure 4.9: Vdw Pickup and Transfer Work Flow to create a hetero-structure stack of 5 2D materials

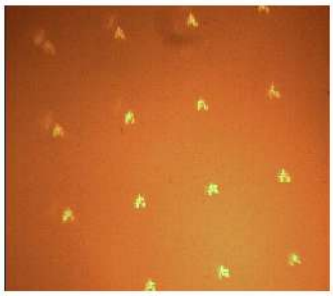

[a] Location of the central alignment mark on the substrate

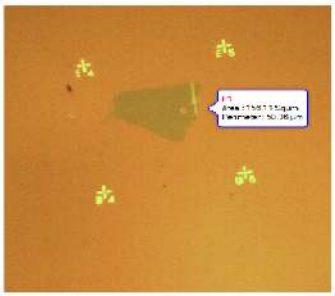

[b] Bottom hBN first transfer on central alignment mark

[c] Second Transfer of hBN -TBG stack in which the pickup of graphene was teared up by sharp edge of hBN and then in second pickup the graphene from same previous flake was twisted to 1.08 degrees by rotating the microstage and picked up to get a hBN-TBG stack

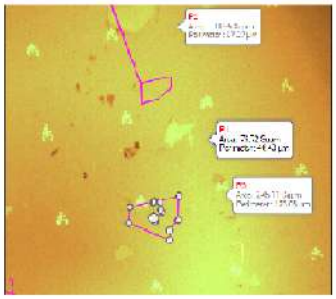

[d] Final Transfer of hBN-graphene flake on the previous hBN-TBG-hBN stack on substrate

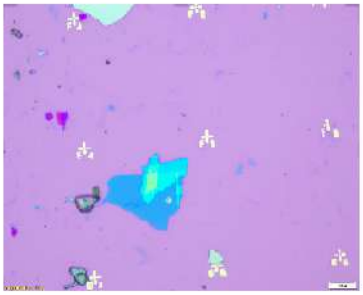

[e] Optical Microscope Image of the Final stack at 50x

Figure 4.10: Microscope Images of the hBN-TBG-hBN-Monolayer Graphene-hBN van der waal stack

4.2 Device Fabrication

4.2.1 Pre-Device Fabrication

Pre-Device Fabrication process involves Alignment Marking of the SiO_2-Si Substrate,Big Gold Pads Creating on Substrate which can be later used for soldering gold wiring connection between gold line bar contacts connection drawn out from van der waal heterostructure contacts and the carrier chip and Transfering the Van Der Waal Heterostructure on it.

Alignment Marks can be generated on the SiO_2-Si Substrate by using,

A.Photo-lithography. B.Electron Beam Lithography (EBL). (More lithography techniques are there but we in this thesis limit our explaination to two.)

Generally photo-lithography is prefered option as the area of the rastor scan for EBL is more (generally (0.3 to 0.4) by (0.3 to 0.4 cm)) in which the alignment marks are spaced at equi-distance ranging from A1 to G10 generally,but again the mask with total alignment pattern is required in photo-lithography so depends on one's choice and machine and equipments availability. So the general process of lithography is to first clean the SiO_2-Si Substrate with IPA,acetone,Distilled De-ionized water rinse followed by N_2 blow drying. The substrate is then spin coated with resist upto

few hundred nano-meters and baked for uniform thin film coating of resist on the substrate.The substrate is then loaded in the lithography tool machine equipped with alignment patterned mask in case of photo-lithography or cad file containing the alignment pattern and after optimizing the lithography parameters such as exposure time,distance alignment of the substrate etc in case of EBL, the resist on the substrate is exposed to photons/electrons as per the type of lithography and then the substrate is removed from the machine and chemically developed to remove the exposed area in case of positive resist or unexposed area in case of negative resist depending on the type of resist used. Then gold is deposited (few nm thick) by using a thermal evaporator tool on the substrate and then substrate is again chemically developed to perform the so called resist liftoff and get the final alignment marks on the substrate ,one can also perform reactive ion etching/plasma etching to etch out the pattern on the substrate itself after getting the pattern on the resist on substrate by using a carbon tetraflouride or sulfur Hexa-flouride gas and then perform gold deposition and resist liftoff to achieve better mechanical bonding of gold alignment marks on the SiO_2-Si Substrate than just gold deposition and resist liftoff.Then the Big Gold Pads in square shapes are created by similar process described above or both alignment marking and the Big Gold Padding of substrate can be done in one same lithography process to save time.The final hetero-structure is then transfered on the alignment marked substrate as explained above in section 5.1.5 for further device fabrication.(More details on EBL will be discussed in 5.2.2)

Alignment Marks are gold symbol marks of form $_{alphabet}+_{number}$ arrayed on SiO_2-Si Substrate in square form used for,

1.Alignment of the mask and the substrate prior to light exposure of the photo-resist nano-spin coated SiO_2-Si Substrate (only in photo-lithography).

2.Used for focussing the SEM image on the SiO_2-Si Substrate and knowing prior hand before the electron beam lithography where the sample heterostructure on substrate is ,as we can't take an SEM image of it as the EBL resist is sensitive to electron beam and if we take SEM image of it,it becomes exposed to EBL and the final pattern shape of resist on substrate after developing is affected.Also once the focus of SEM is adjusted the distance between the SiO_2-Si Substrate and the EBL electron gun can be taken (generally in mm) from the beam control software for each corner of the sample transfered alignment mark to know the flatness of the SiO_2-Si Substrate and then an average value of the 4 values is taken as the distance between the electron gun and the substrate for performing EBL on the hetero-structure.

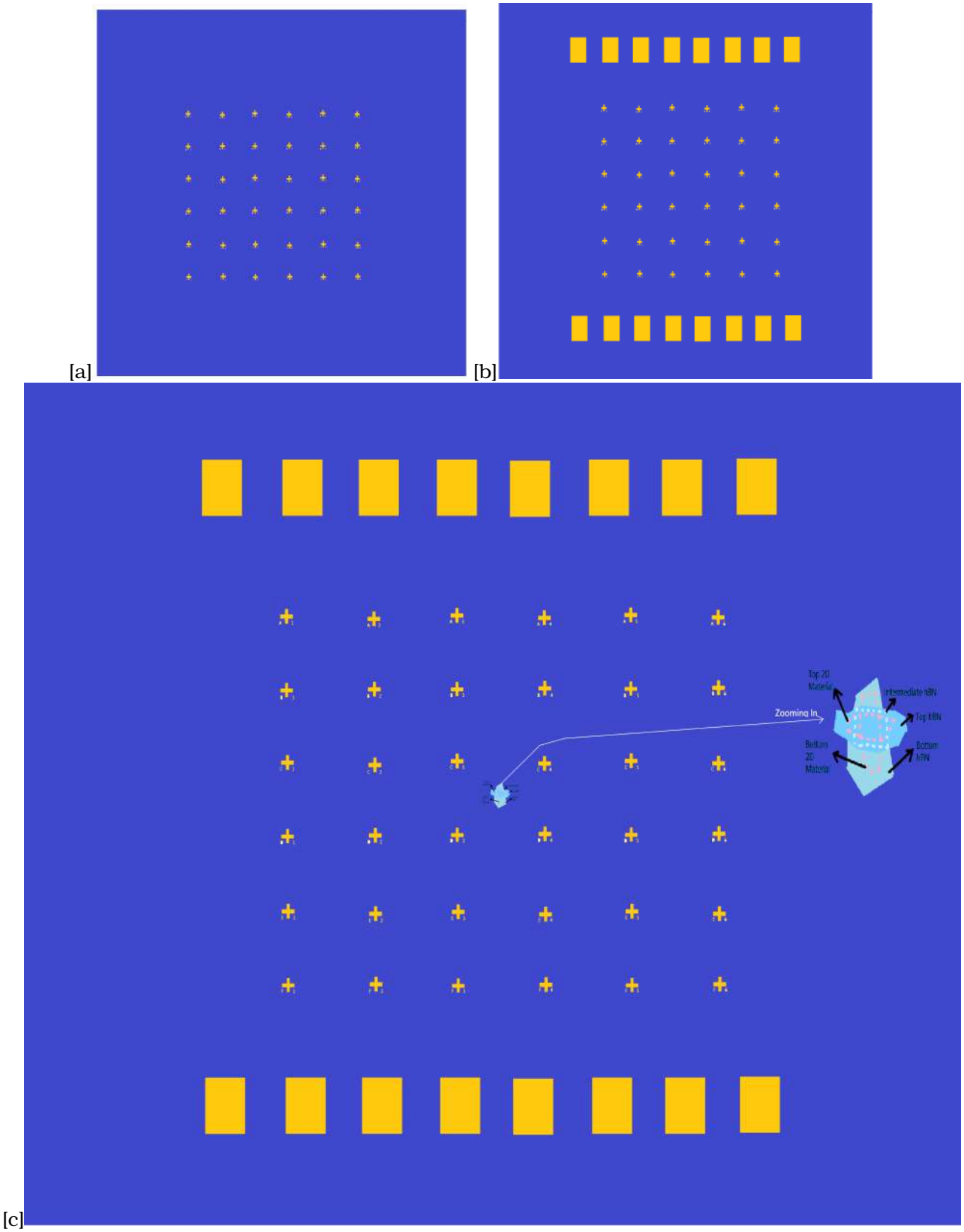

Figure 4.11: Work Flow of Pre-Device Fabrication Process showing Schematic of (a) Alignment Marking Via Lithography of the SiO_2-Si Wafer (b) Big Gold Padding Via Lithography of the Alignment SiO_2-Si Wafer. (c) Final Transfered Van Der Waal Hetero-structure Stack of three hBN's and two 2D materials on Big Gold Padded Alignment Marked SiO_2-Si Substrate.

4.2.2 Device Fabrication

Note - Here we are taking gold contacts from one 2D material at a time sandwiched between the hBN's assuming that the hBN layers will not contribute in any way to the inplane voltage measurements for the input source current as no current can flow in plane through the hBN as it is insulating in nature,but at low temperature measurements particularly below 12 k there is transition of the insulating state of hBN into metallic state with 12 K having 4387 KΩ as the peak resistance and then decreases to the lowest value to 193 KΩ at 500 mK[23].The pristine graphene is in insulating state below 250 K and has maximum resistance of 1.3 KΩ[23] near zero kelvin and at least for graphene as 2D material we can use this type of common gold contacts as the contribution to voltage measurements via hBN is negligible compared to graphene,but for other 2D materials care should taken to first find resistance and the state (insulating or conducting) at temperature of measurement and then select an alternative dielectric if resistance of the 2D material is near to resistance of hBN as current in this case will have parallel paths to flow and the measurement out of voltage will not be solely due to charge carriers in the 2D material and we cannot exactly find the charge neutrality point of the 2D material due to this interference from hBN below 12K measurements.

Note - The Number of EBL processes may be reduced from 3 to 2 or 1 by performing one or more patterns (of gold contacts,Top gate,gold contact lines) on the resist in single EBL process rather than three times as shown in the figure.

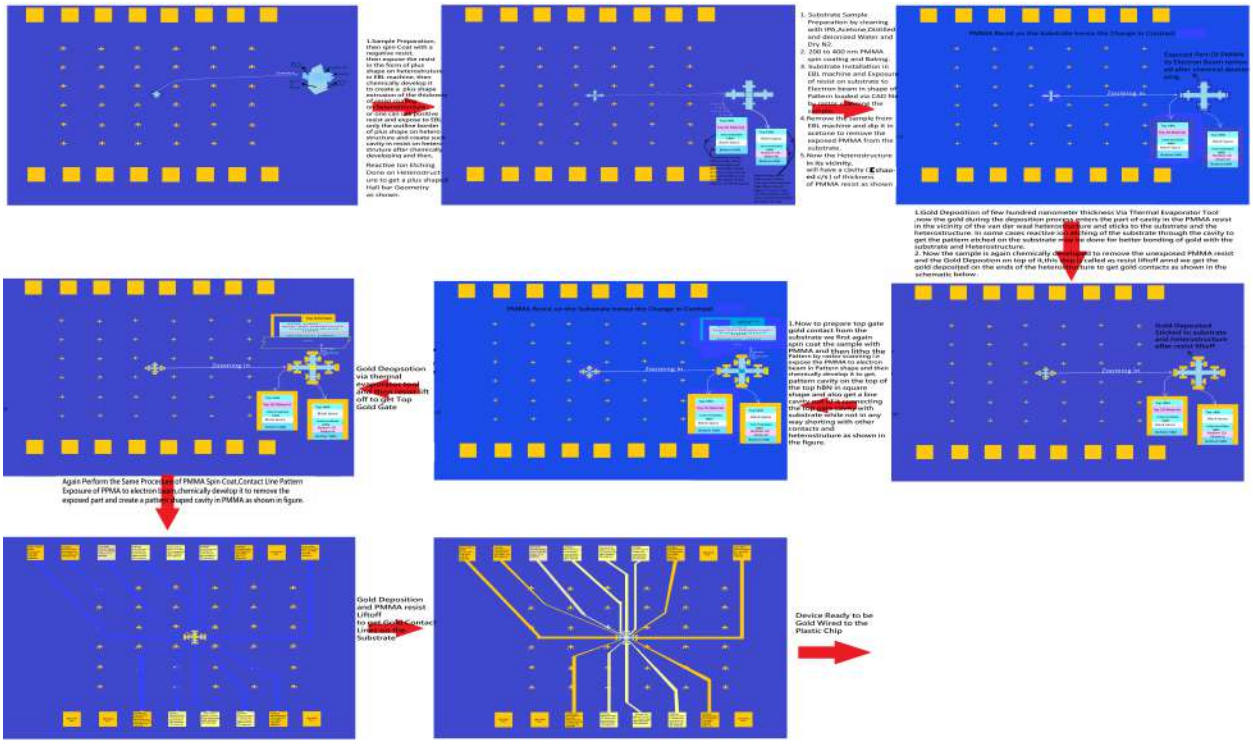

Figure 4.12: Detailed Work Flow of the Device Fabrication

General Procedure of Electron Beam Lithography-

1.The Alignment Marked Si-$SiO2$ substrate containing the van der waal Hetero-structure is first cleaned by using IPA,acetone,Deionized and Distilled Water and then blow dried using N_2.

2.Then the sample is spin coated with PMMA resist (positive Resist) with thickness of 200 nm to 400 nm depending on the thickness of the heterostructure and the size of gold contacts one wants.(the thickness of spin coating can be controlled via time of spin coat,viscosity of the PMMA in the PMMA-acetone solution,speed of the spin coat and the baking temp. (to some extent)).

3.Bake the Sample to 150 C for few minutes to get a uniform coating of PMMA on the substrate and to get rid of the excess PMMA solution from the substrate.

4.Now load the sample in the EBL machine and also the CAD file of the Pattern you want in the interface software that controls the path direction of the Electron beam via lens movement to get the pattern shape rastor scanned and exposed on the PMMA substrate.

5.Now adjust the focus of the SEM image on the substrate with the use of the alignment marks with taking care that the alignment square area in which the heterostucture is transfered is not exposed to the electron beam of the SEM to avoid the exposure of PMMA in that area to electron beam of SEM.

6.Now optimize the parameters of the EBL based on user's experience such as the exposure time,the average distance between electron gun and the substrate based on the SEM focus,intensity of the electron beam,wavelength of the electrons,diameter spot size of the electron beam etc depending on the accuracy of the pattern one wants which can be written in form of python file or directly adjusted via software interface.

Note - One can optimize the parameters by using a dummy substrate and check the quality of the pattern we get on the substrate,if it satisfies the required quality we can proceed with our original sample otherwise repeat the optimizing process with dummy substrate to avoid damaging our precious sample.

7.Now start the Electron Beam Lithography process ,as per the pattern CAD file ,the electron beam rastor scans the substrate and only the pattern shape is electron beam exposed and then once the complete rastor scanning is done,remove the sample and chemically develop it in acetone to remove the electron beam exposed part of the PMMA and create a pattern shaped cavity in the PMMA on the substrate.

8.Now deposit the Gold few hundred nanometers thick depending on the thickness of the cavity in the PMMA resist and the size of the gold contacts we want which further depends on the maximum magnitude of the current/voltage of the measurements as it should not electrically breakdown/damage/liquidify due to excess current/voltage than the deposited thickness of the gold contacts can sustain.

9.Now again chemically develop the sample in higher concentration of acetone to remove the unexposed PMMA along with gold deposited on top of it and the gold that entered in the cavity adheres to the substrate and hence not affected by this process.This process is also called resist liftoff.Before performing resist liftoff one can perform reactive ion etching of pattern on the substrate to increase the adhering of the deposited gold to the substrate.

10. Once the process of making gold contacts from the ends of the hetero-structure,the top gate gold contact and the gold contact lines is done, the device is ready to be wire bonded on the plastic chip i.e the post device fabrication.

4.2.3 Post - Device Fabrication

The SiO_2-Si substrate is either adhesive glued (the glue may be conducting or non-conducting depending on the type of application , conducting sliver epoxy in our case) or hole can be drilled in the substrate and PCB/ceramic/plastic chip to exactly position the substrate on the gold pad of the device chip and then screwed mechanically to fix its position on the plastic chip. Gold Wiring of the Big Pads to the plastic chip is done via a wire bonder machine.

There are 3 types of wire bonding processes -

1.Ultra-Sonic/Thermo-Sonic Wedge Bonder - Basics Will be discussed in Detail Here from Reference [15,17,18,19,20] as we use this bonder in Nano-Scale Devices Lab at IISc.

2.Ribbon Bonding - Used for Radio-Frequency Applications due to its higher intermetallic bonding strength and more current carrying capacities of the wire owing to its larger widths.

3.Ball Bonding - Faster Industrially Automated Process and better bonding strength than wedge Bonding.For Basic details one can refer [16].

Ultrasonic and Thermo-Sonic Wedge Bonding processes are similar with only difference that in the thermo-sonic wedge bonding the heat is provided to the stage holder holding the plastic chip via a power source to increase the temperature upto about 150 C which acts as an extra source of energy for bonding between wire and pad to occur other than ultrasonic power vibrations of the tool in ultrasonic wedge bonding which creates the rubbing/sputtering/smearing action of wire on the metal pad forming a inter-metallic bond between the pad and the wire.The first step in the wire bonding process is needling.So the Gold/Aluminium/Silver/Copper wire is needled into the needle which the main tool performing the wire bonding process.Once the wire is needled in, the SiO_2-Si substrate glued plastic chip is mounted on the sample stage holder of the wire bonder.Then the bonding of wire from gold pads of plastic chip to SiO_2-Si substrate's gold pads take place in 3 steps (First Bond Creation,Looping of the wire,Second Bond Creation) to complete on bonding cycle. Prior to bonding cycle one can optimize the parameters of 1.Ultrasonic Power 2.Contact Force 3.Temperature of the Stage 4.Time of the Contact 5.Needle Height by trail and error on a sample plastic/ceramic chip or PCB and sample substrate different than our device to protect our device's pads and substrate against wrong parameters.

Note - Both the bond pads on the SiO_2-Si Substrate and the bond pads on the Plastic Chip can be cleaned by using plasma cleaning as part of material preparation to remove any contamination.

1.First Bond Creation -

Once the Parameters are optimized and the device with plastic chip is mounted on the stage of the wire bonder , bring the needle to the location of the gold pad of the plastic carrier chip observing via microscope and mouse controlling the needle movement and force contact the needle on the gold pad of the substrate and then the ultrasonic power generated via horn holding the tool/needle creates a heat and forms an inter-metallic bond between the wire and the metal pad.Here the clamp is the kept open for continuous flow of wire in the needle/tool from the spool for looping and next bond creation. Generally the first bond is created on the plastic chip gold pads rather than substrate's gold pads as the parameters of wire bonding as described above needs to be optimized for sufficient strength first bond formation and if it is done first on the plastic chip's gold pad than our substrate's gold pads are preserved for bonding if the first bond fails on the plastic chip's gold pads as the plastic chip if damaged can be replaced but it will be difficult to replace the gold pad on your substrate if damaged.

2.Wire Looping After First Bond -

To avoid shorting of the wire after first bond to substrate a loop of wire is created i.e the needle/tool is lifted up vertically and given a side kink by reverse motion knob to some height depending on the height you want of the loop to be after first bond with clamp open to allow free movement of wire in through the needle (generally depends on the package size of the chip one wants) followed by horizontal movement to create a loop of the wire then we proceed on next bond creation on the gold pad of the SiO_2-Si substrate.

3.Second Bond Creation -

After First Bond Creation and Wire looping bring the Needle to gold pads of the substrate where one wants the gold wire second connection and then move the needle downward and force touch needle on the gold pad of the substrate and then ultrasonic vibrational power of the needle/tool again create an inter-metallic bond between the gold pad of the substrate and the gold wire.Now if one wants to further continue the same connections on the next gold pad then keep the clamp open and repeat the first bond the wire looping process.For creation of the final bond the clamp after intermetallic bond formation is closed restricting the free flow movement of wire through the clamp into the needle and now the needle is moved horizontally a little to create a table tear of the wire or the needle is moved upwards to tear the wire and the wire bonding process between gold pads of the SiO_2-Si substrate and the gold pads/soldered contacts of the plastic chip is complete.

For Wedge Bond Defects and Parameters Optimization one can refer more advanced literatures and reference [15,17,18,19,20] as it is out of scope of this thesis but just to understand a basic flavour of its complexity one can refer below paragraph.

Gold Pads on the substrate or the plastic chip may come off if the gold pads are not properly adhered during pre-device fabrication and device fabrication process.Also during bonding care should be taken that the gold pads are contamination free so substrate and plastic chip can be first prepared by plasma cleaning. A wegde bond can be considered a good one if in general the bond wedge size is 1.5 to 2 times the wire diameter and in between the pad size lift.To achieve this optimization of the parameters 1.Ultrasonic Power 2.Contact Force 3.Temperature of the Stage 4.Time of the Contact 5.Needle Height can be done one at a time. i.e vary only power keeping other parameters to a standard value to limit the number of parameters to be optimized to single quantity on a sample substrate and plastic chip combo.Too high value of power can damage the gold pads and substrate as well during bonding and too little value of power can lead to non bonding of the wire to the pads.The bonding parameters varies with machine,substrate,type of wires,each separate usage,gold pad contamination leve,gold pad thickness,bond pad opening,bond pad pitch,sample stage design and quality,substrate preparation,hence there is no universal set of magic values of these parameters but needs to be optimized for each different bonding by following a power varying stratergy from a low value to a optimize value i.e the value of ultrasonic power for which we get a bond size of 1.5 times to 2 times the wire diameter,which can be measured by a deformation sensor which measures the bond size width ,also SEM images of the bond can help characterize the adhesion strength.

The bond strength of the wire can be tested by 1.Wire bond shear test. 2.Wire bond Pull test.[16]

At IISc we use Ultra-Sonic Wire bonder as shown in figure below,as the sample is only used for measurement for a week's duration at maximum,there is no need to go for ball bonding (which

has higher bonding strength and durability that is why used industrially),all in all a proper gold wired wedge bond can have a shell life of upto 1 year which is more than enough for research labs usage.

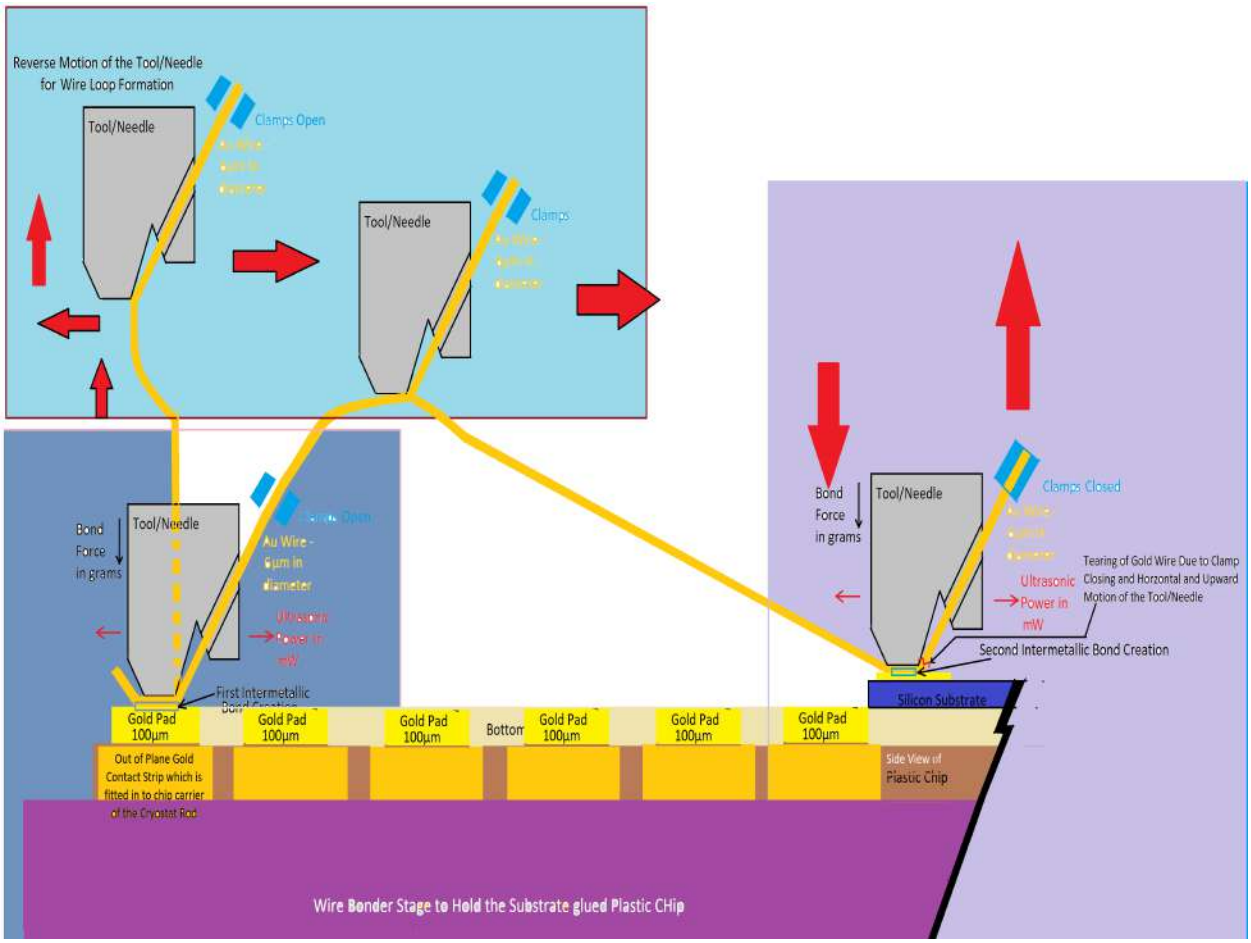

Figure 4.13: Schematic of Bonding Cycle of the Wedge Wire Bonding Process

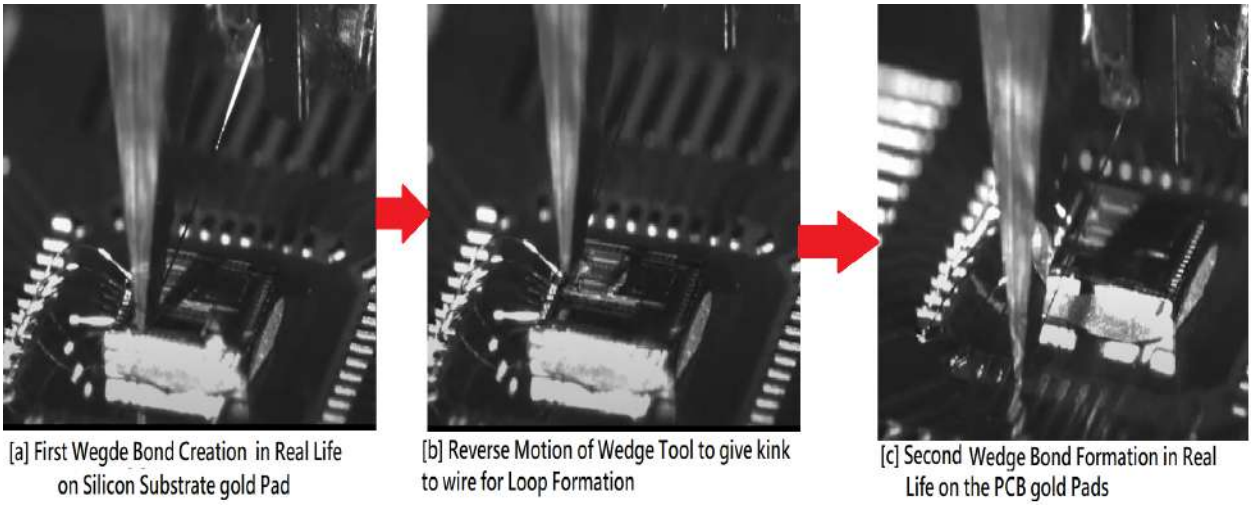

Figure 4.14: Wedge Bonding Cycle on Real Wedge Wire Bonder Machine [20].

Figure 4.15: Ultra or Thermo-sonic Wire Bonder At Our Nano-Scale and Device Fabrication Lab at IISc

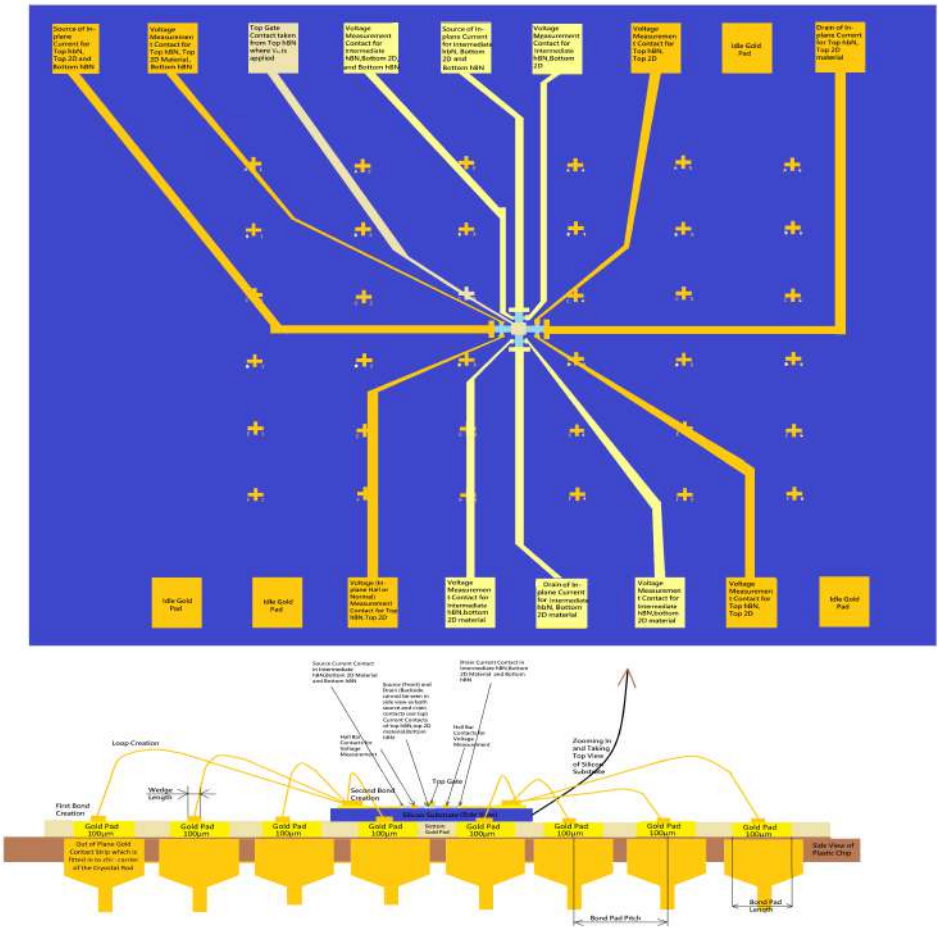

Figure 4.16: Schematic of Side View of Final Device Glued on Plastic Chip with gold pads between them wedge wire bonded

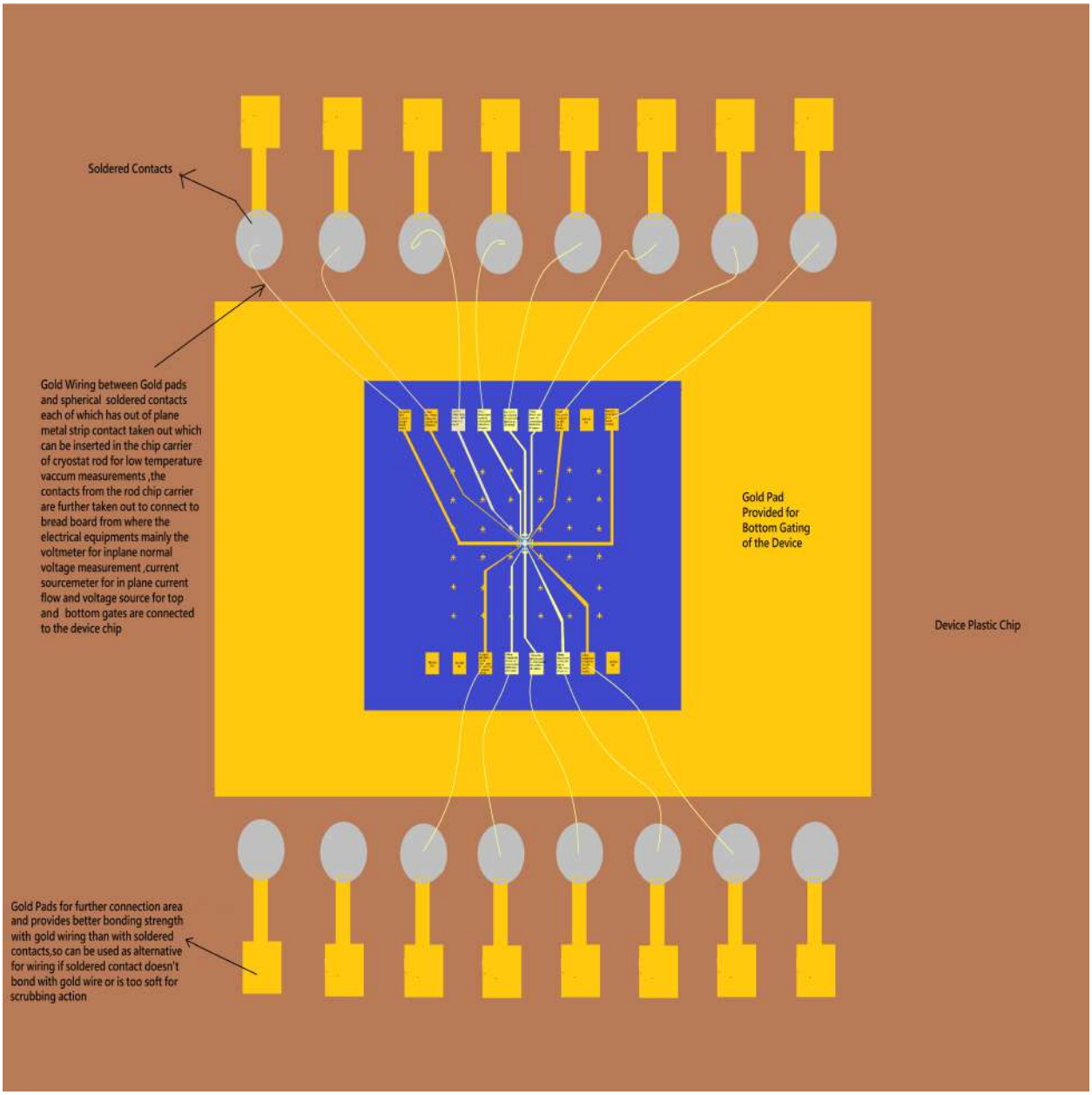

Figure 4.17: Schematic of the Top View Final Device on Plastic Chip ready to be installed in the chip carrier of the Cryostat Dipper for Measurement.

Device Fabrication of Our Devices was done by Suvronil Dutta in Cleaning Room at Cense IISc and Physics Department,IISc.

Chapter 5

Analysis,Measurements and Interpretation of the Results Observed

5.1 Analysis

5.1.1 Two possible types of Contacts/Methods/Geometries for Measurements

Van Der Pauw Geometry - Please Refer online content for its basic Explaination as this was not used for our measurement setup.

Hall Bar Geometry - Explained in Detail Here as this is used for our Quantum Capacitance of 2D material Measurement.

There are two ways to measure in plane values in hall bar geometry i.e with or without application of out of plane i.e perpendicular magnetic field.

Consider first case i.e with application of out of plane magnetic field,so when we pass an in plane longitudinal current in material, the electrons flowing longitudinally under the influence of out of plane magnetic field shift to one side due to lorentz force experienced by electron i.e left or right thus creating negative charge on that side and naturally positive charge in the other side,so now if measure this transverse voltage then it will be due this shifted charges under influence of out of plane magnetic field due to longitudinal current flow,this transverse voltage that we measure is called Hall Voltage. After measuring we basically know three values,the Hall Voltage (V_H),the in plane longitudinal current ($I_{inplane}$) that we pass,the out of plane magnetic field that we apply.

By using the below mathematical expressions we can extract in plane longitudinal resisitance (R_{xx}) the carrier density (n),the hall coefficient (V_H)and the hall carrier mobility (μ_H).

$R_{xx} = \frac{V_{xx}}{I_{xx}} = \frac{\rho_{xx} L}{A} = \frac{L}{\sigma_{xx} A}$,where σ_{xx} is the longitudinal conductivity of the sample.

$V_{xy} = V_H = \frac{I_{xx} B_{zz}}{nte}$, where t is the thickness of the sample.

R_H = $\frac{V_H t}{I_{xx}}$ = - $\frac{1}{ne}$,sign of R_H denotes sign of the charge carriers.

μ_H = $\frac{R_H L}{R_{xx} A_{c/s}}$ = $\frac{R_H}{R_{xx}} g$ = σR_H ,where g = $\frac{A_{c/s}}{L}$ is the geometric factor of our 2D material.

The second way is without application of out of plane magnetic field as shown in figure below as just for in plane longitudinal resistivity measurement we don't require to apply out of plane magnetic field,we require out of plane magnetic field only when we want hall voltage,hall coefficient measurement and carrier mobility.It's fairly straight forward when we use first expression given above,

R_{xx} = $\frac{V_{xx}}{I_{xx}}$ = $\frac{\rho_{xx} L}{A}$ = $\frac{L}{\sigma_{xx} A}$,where σ_{xx} is the longitudinal conductivity of the sample,L is the length between the contacts where we are measuring the voltage and A is the area of cross section of sample.

σ_{xx} = μen = $constant * n$ i.e n is scaled down version of in plane longitudinal conductivity. (only if the 2D material follows the ohms law of conduction)

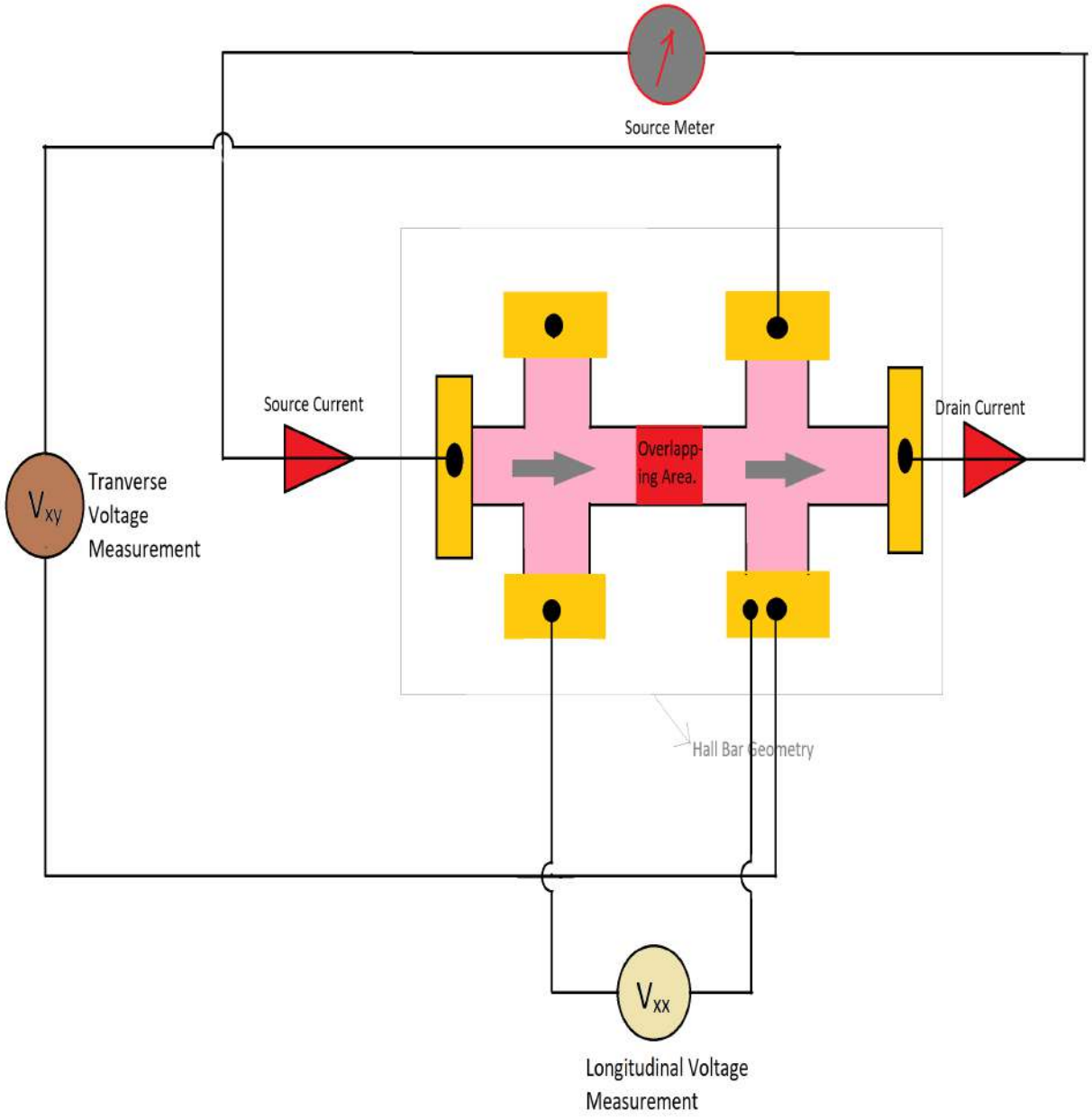

Figure 5.1: Hall Bar Geometry Longitudinal and Transverse Voltage Measurement By Passing In Plane Current Through it.

5.1.2 Mathematical Expression/Derivation of the Physical Quantities from Quantum Capacitance of 2D materials.

Here we will derive/extract mathematical Quantities from the Quantum Capacitance i.e **Density Of States,Electronic Compressibility,Energy Bandwidth,Energy BandGap,carrier Density,Fermi-Energy/chemical Potential,Fermi Velocity,Ground State and its properties of the 2D material,Number of Modes,Conductance in the Ballistic and Diffusive Limit,Tranmission Function,Mean Free Path,Electron Scattering Mechanisms and Landau Levels and its spacing.**

The Capacitance in general is mathematically expressed as,

C = $\frac{\text{Charge Stored by Material}}{\text{Potential Difference Across Material}}$

C = $\frac{\text{en}}{\text{V}}$ = e$\frac{\text{dn}}{\text{dV}}$

for case of 2D material, the material is at Fermi Energy potential (E_F) or chemical potential (μ), i.e V in this case becomes E_F/e or μ/e , in which case our equation becomes,

C_Q = A$e^2 \frac{dn}{dE_F}$ at near zero temperature or

C_Q = A$e^2 \frac{dn}{d\mu}$ at above zero temperatures

where A is the overlapping area as taken previous calculations.

so depending on the 2D material, the relation between the Fermi Energy(chemical potential) and carrier concentration changes and hence the explicit expression for quantum capacitance changes as per 2D material.

The term $\frac{dn}{d\mu}$ denotes the change in the Fermi Energy or chemical Potential level with change in the carrier concentration in the 2D material,this term hence is called as electronic compressibility of the material.

To understand what a electronic compressibility is,we can consider an analogous mechanical term i.e mechanical compressibility in which we apply stress on the material and calculate its strain from the deformation observed. If the material undergoes relatively higher deformation i.e change in volume under applied stress then we can conclude it as highly compressible material mechanically and vice versa,at constant temperature and number of carriers in the material. Now in the electronic compressibilty we are keeping the temperature constant,the stress on the material to be atmosphere pressure but we are changing its number of carriers and we are observing the electronic deformation in the material i.e the number of occupied states by charge carries deforms i,e the chemical potential level in the material changes, this electronic deformation with introduction of charge carriers in material at constant temperature and volume of material is called electronic compressibilty of the material.It can be also thought of how much charge enters the system when we change its chemical potential level slightly.

To get a physical picture if we consider the band structure of material i.e the electron interactions with the ions in the material and consider change in the energy level of the highest occupied states with the carrier concentration change ,this quantity is nothing but the electronic compressibility in the material.

This concept of electronic compressibility is explained here in detail because by knowing its value we can understand in which region of the band structure is the Fermi Energy level or chemical potential is, i.e consider two cases,

A.The electronic compressibility is having a continuous relatively higher values regime (peaks) ,i.e the 2D material is electronically compressible indicating that Fermi Energy Level is in energy band regime of band structure as the charge carriers that are introduced in the system has electronic states to occupy and hence change in the Fermi Energy Level shift is relatively much lower than the number of charge carriers added in the system and hence the material can be considered as electronically incompressible indicating that we are in the energy band regime of the band structure. By using this data we can accurately calculate the band-width of the conduction and valence band of the material as the energy difference between two regimes where the electronic compressibility has continuous relatively higher values region provided the entire band width of the material is within the carrier density regime of the 2D material (i.e its filling

factor).

Energy Band Width = $((\frac{d\mu}{dn})_{\text{first near zero value}} - (\frac{d\mu}{dn})_{\text{second near zero value}})$*(Number density of carriers introduced in the material for causing the Fermi Level sweep of the Entire Band Width of Energy Band)

= Area under the curve between two points having near zero values of the plot of $(\frac{d\mu}{dn})$ vs n

= Distance between the two points where the Quantum Capacitance value has continuous region of relatively higher values as Quantum Capacitance has direct relation with the electronic compressibility and then scaling it to get the distance in Energy scale to get the energy band width.

Note - The term $\frac{1}{\text{Electronic Compressibility}}$ can be called as **the electronic bulk modulus term.**

This concept can also be explained from capacitance point of view,the capacitance indicate the ability of the material to store charge with respect to potential difference between its two terminals , so when the Fermi Level is in the band,for the charge carriers introduced in the 2D material the Fermi Energy level shift is relatively small i.e the change in the potential difference value between the two surfaces of the 2D material is smaller than compared to charge stored and hence has continuous regime of high values of quantum capacitance.

B.The electronic compressibility is having near zero values indicating that the charge carriers introduced in the system has no electronic states to occupy and hence the Fermi Level Shifts continuously with little to no charge carriers added in the system i.e the 2D material is electronically incompressible indicating that the Fermi Level of the material is in Band Gap Regime.

Energy Band Gap = $\frac{\text{Number Density of carriers introduced in the material for causing the Fermi Level Shift so that it can cross the Band Gap}}{(\frac{dn}{d\mu})_{\text{first near zero value}} - (\frac{dn}{d\mu})_{\text{second near zero value}}}$

= Area under the curve between two points having relatively continuous higher values of the plot of $(\frac{d\mu}{dn})$ vs n

Again the same concept can be explained via the Quantum Capacitance point of view i.e the relatively very small charge carriers introduced in the 2D material causes the Fermi Energy Level shifted by higher value i.e the 2D material stores no charge for higher value of change in the potential difference across the top and bottom surfaces of the 2D material.

The Density of states can be defined as the change in the number of charge carriers occupying the electronic states per unit volume of the 2D material per change in the energy of the electronic states of the 2D material.

i.e D.O.S = $\frac{\text{Number of electronic states between energy E and E + dE}}{\text{The difference in between the Energy of the electronic states considered i.e dE}}$

In our case of 2D material this ratio reduces to electronic compressibility,because whatever charge carriers per unit volume of the material we are introducing in the 2D material cause Fermi Level Shift,hence this itself is the definition of the Density of States of the 2D Material.

D.O.S = D(E) = $\frac{dn}{d\mu} = \frac{C_Q}{Ae^2}$

Depending on the relation between the Fermi Energy/Chemical Potential and the number density of charge carriers we can extract the Fermi Energy or Chemical Potential from the Quantum Capacitance Data. Let's assume a case where the Dependence is linear then $\triangle E_F = \frac{Ae^2 \triangle n}{C_Q}$,

if we assume the initial Fermi Level at zero Energy Level and then adding the charge carriers and now the Fermi Level is in conduction band , then $E_F = \frac{Ae^2 n}{C_Q}$

But now the Quantum Capacitance will also be dependent on the doping concentration n and hence we can explicitly calculate the net dependence of Fermi Energy on n and identify their relation by curve fitting for any 2D material.

Also we can extract the chemical potential by,

$\mu = \int_{n_C}^{n_F} \frac{1}{f}\frac{d\mu}{dn}dn$

Now the carrier density (n) can be measured by measuring the in plane resistivity of our 2D material by using $\rho = \frac{1}{\mu en}$ i.e ρ = constant/n . We can also calculate it mathematically by,

n = $\int_{E_C}^{E_F} fD(E)dE = \int_{E_C}^{E_F} f\frac{dn}{d\mu}dE = \int_0^{(V_{topgate}-V_{bottomgate})_{\text{charge neutrality at the other 2D layer}}} \frac{C_T}{(Ae)}dV$, where f is the Fermi Dirac Distribution at energy E ,E_C is the conduction band energy ,D(E) is the density of states of 2D material, C_T is the total capacitance of our Van der Waal heterostructure.(concept of total capacitance is explained at the end of this sub-section). So to get the profile of n vs V $((V_{topgate} - V_{bottomgate)_{\text{charge neutrality at the other 2D layer}}})$ we can plot the measured n value of the 2D material in the hetero-structure with the difference in the gate potential applied at the gate of the charge neutrality point of our other 2D material.

Typically in experiments n is assumed as directly proportional to V for 90 nm to 300 nm Silicon Oxide thickness in graphene heterostructures.[6]

V = $(V_{topgate} - V_{bottomgate)} \propto (n_T + n_B) \propto (n_T)$@ Charge Neutrality of Bottom Layer as we can neglect the variation of Quantum Capacitance w.r.to n that can change total capacitance vs n ,as this quantity will be small compared to total Capacitance of our heterostructure and hence we can assume it constant. But for different 2D material we have to verify if this is the case, if not then we have to consider total capacitance as function of n,in which case V will follow some nonlinear relationship with n.

Hence we can assume V = $((V_{topgate} - V_{bottomgate)_{\text{charge neutrality at the other 2D layer}}})$

To extract the Fermi Velocity first way is to plot E_F vs n as we know C_Q and n already,we can calculate Fermi Energy from from E_F = $\frac{Ae^2n}{C_Q}$ and then the constant term in it i.e the curve will follow some model depending on the 2D material i.e E_F = c*$(n)^{\text{some exponential Constant}}$ where c contains the Fermi Velocity term in it along with some other constants,depending on the 2D material these constants will vary and the exponential constant of n will also vary.So comparing this equation with already known model for monolayer graphene we can calculate the reduction in the Fermi Velocity when compared to monolayer graphene which follows the equation, E_F = h$v_F\sqrt{\pi n}$.

The Fermi Velocity in general is calculated as v_F = $\frac{1}{h}\frac{dE_F}{dk_F}$, where k_F is Fermi Wave Vector and dependent on n i.e k_F = constant*$n^{\text{exponential constant}}$ so essentially Fermi Velocity is the constant velocity with which the charge carriers flow/hop in the nearest neighbour lattice site of the material when the material conducts and it can be extracted only from E_F vs n plot with scaling up by some constants,but can be exactly extracted if we know the constant values in the model for the 2D material as in the case of monolayer graphene.We can extract the Fermi Wave Vector dependence on n from the number of modes dependence on n which is discussed later in this subsection.So what we have now is K_F as a function of n and E_F as function of n can be extracted out from C_Q vs n data as discussed in the next paragraph,so we have both K_F and E_F as function of n and hence we can exactly extract the Fermi Velocity for any 2D material.

So similarly from the Quantum Capacitance of the 2D material we can extract the Fermi Velocity by C_Q = $\frac{ne^2}{E_F}$ = $\frac{ne^2}{jn^c}$ = $\frac{n^{1-c}e^2}{j}$ where j and c are some constants depending on the 2D material of the heterostructure which can be extracted by curve fitting the plot of C_Q vs n.

So C_Q = $n^{1-c}const$,the Fermi Velocity term is present in the constant scaled with other constants and when we plot C_Q vs n we get this constant value by curve fitting, now for the 2D

material if the model is known we can get the exact value of the Fermi Velocity otherwise we can compare it with the pristine graphene model and calculate the reduction or increase in 2D material's Fermi Velocity when compared to pristine graphene model.

Before moving on to ground state of other 2D materials let's consider the ground state case of monolayer graphene.

To get the Hamiltonian of the electrical transport in graphene we can follow three approaches (there are many other approximations but we limit ourselves to three.)

1.Quantum Mechanical Schrodinger Equation by Approximating that electrons follow quantum relativistic mechanics at low energy regime near dirac point.

2.Tight Binding Approximation in which we assume that the electron hop to nearest neighbour lattice site for electrical conduction to occur,a approximation by which we construct the hamiltonian in momentum space.

3.Hatree Fock Method in which the ground state for graphene is assumed as the linear combination of the spin orbitals (slater Determinant) and then this ansatz is used to solve the time independent Schrodinger equation to get the hamitonian and later the energy eigen values from it.

Part 1 is discussed briefly in my term paper [1],Part 2 is discussed in the chapter 1,and Part 3 will be briefly discussed here.

The Carbon has six electrons in total in its orbitals and has ground state electronic configuration of $1s^2$,$2s^2$,$2p_x^1$,$2p_y^1$. The excited state of carbon is $1s^2$,$2s^1$,$2p_x^1$,$2p_y^1$,$2p_z^1$. Now if we want to write slater determinant for the ground state of the carbon atom then the number of electrons forms the number of rows and the number of spins i.e two (spin up and spin down for a particular spatial wave-function form the number of columns),

The slator determinant (ϕ) for carbon atom in an excited state can be written as,

$$\phi = \frac{1}{\sqrt{6!}} \begin{vmatrix} \psi_{1s_1}|\uparrow\rangle_1 & \psi_{1s_1}|\downarrow\rangle_1 & \psi_{2s_1}|\uparrow\rangle_1 & \psi_{2p_{x1}}|\uparrow\rangle_1 & \psi_{2p_{y1}}|\uparrow\rangle_1 & \psi_{2p_{z1}}|\uparrow\rangle_1 \\ \psi_{1s_2}|\uparrow\rangle_2 & \psi_{1s_2}|\downarrow\rangle_2 & \psi_{2s_2}|\uparrow\rangle_2 & \psi_{2p_{x2}}|\uparrow\rangle_2 & \psi_{2p_{y2}}|\uparrow\rangle_2 & \psi_{2p_{z2}}|\uparrow\rangle_2 \\ \psi_{1s_3}|\uparrow\rangle_3 & \psi_{1s_3}|\downarrow\rangle_3 & \psi_{2s_3}|\uparrow\rangle_3 & \psi_{2p_{x3}}|\uparrow\rangle_3 & \psi_{2p_{y3}}|\uparrow\rangle_3 & \psi_{2p_{z3}}|\uparrow\rangle_3 \\ \psi_{1s_4}|\uparrow\rangle_4 & \psi_{1s_4}|\downarrow\rangle_4 & \psi_{2s_4}|\uparrow\rangle_4 & \psi_{2p_{x4}}|\uparrow\rangle_4 & \psi_{2p_{y4}}|\uparrow\rangle_4 & \psi_{2p_{z4}}|\uparrow\rangle_4 \\ \psi_{1s_5}|\uparrow\rangle_5 & \psi_{1s_5}|\downarrow\rangle_5 & \psi_{2s_5}|\uparrow\rangle_5 & \psi_{2p_{x5}}|\uparrow\rangle_5 & \psi_{2p_{y5}}|\uparrow\rangle_5 & \psi_{2p_{z5}}|\uparrow\rangle_5 \\ \psi_{1s_6}|\uparrow\rangle_6 & \psi_{1s_6}|\downarrow\rangle_6 & \psi_{2s_6}|\uparrow\rangle_6 & \psi_{2p_{x6}}|\uparrow\rangle_6 & \psi_{2p_{y6}}|\uparrow\rangle_6 & \psi_{2p_{z6}}|\uparrow\rangle_6 \end{vmatrix}_{6\times 6}$$

where ψ is the spatial wave-function and its suffix denotes the electron number and $|\uparrow\rangle$ and $|\downarrow\rangle$ denotes the spin states of the electron.

Now, In graphene the carbon atom undergoes sp_2 hybridization i.e it's 2s orbital wave function and $2p_x$ and $2p_y$ orbital wave-functions undergo intermixing to form a sp_2 hybridization and leaving the $2p_z$ orbital wave-function unhybridized. Now the 2s shell in ground state of carbon atom's sp_2 hybridization contains 2 electrons in spin up and spin down state as per the Pauli-Exclusion principle and then p_x and p_y as per Hund's Rule of filling after sp_2 hybridization should both contain one spin up electron each i.e the electronic configuration of the carbon atom after sp_2 hybridization is $1s^2|\uparrow\downarrow\rangle$,$2sp_2^2|\uparrow\downarrow\rangle$,$2sp_2^1|\uparrow\rangle$,$2sp_2^1|\uparrow\rangle$,$2p_z^0$. But for sp_2 hybridization of carbon atom to form 3 sigma in plane bonds to form graphene mono-layer ,all the three sp_2 hybridizations should have only one electron each so that it can form sigma bond with neighbouring carbon by sharing one electron each to fill the sp_2 orbital and hence this bonding is only possible when the carbon atom's sp_2 hybridization is in excited state,so one can conclude that the carbon's sp_2

hybridization's excited state's in plane sigma bonds is the ground state of the graphene carbon atom. Therefore the graphene carbon atom's ground state is, $1s^2\,|\uparrow\downarrow\rangle$,$2sp_2^1\,|\uparrow\rangle$,$2sp_2^1\,|\uparrow\rangle$,$2sp_2^1\,|\uparrow\rangle$,$2p_z^1\,|\uparrow\rangle$ and hence the slater determinant of single carbon atom of the graphene is,

$$\phi = \frac{1}{\sqrt{6!}}\begin{vmatrix} \psi_{1s_1}|\uparrow\rangle_1 & \psi_{1s_1}|\downarrow\rangle_1 & \psi_{2sp_{2,1}}|\uparrow\rangle_1 & \psi_{2sp_{2,1}}|\uparrow\rangle_1 & \psi_{2sp_{2,1}}|\uparrow\rangle_1 & \psi_{2p_{z1}}|\uparrow\rangle_1 \\ \psi_{1s_2}|\uparrow\rangle_2 & \psi_{1s_2}|\downarrow\rangle_2 & \psi_{2sp_{2,2}}|\uparrow\rangle_2 & \psi_{2sp_{2,2}}|\uparrow\rangle_2 & \psi_{2sp_{2,2}}|\uparrow\rangle_2 & \psi_{2p_{z2}}|\uparrow\rangle_2 \\ \psi_{1s_3}|\uparrow\rangle_3 & \psi_{1s_3}|\downarrow\rangle_3 & \psi_{2sp_{2,3}}|\uparrow\rangle_3 & \psi_{2sp_{2,3}}|\uparrow\rangle_3 & \psi_{2sp_{2,3}}|\uparrow\rangle_3 & \psi_{2p_{z3}}|\uparrow\rangle_3 \\ \psi_{1s_4}|\uparrow\rangle_4 & \psi_{1s_4}|\downarrow\rangle_4 & \psi_{2sp_{2,4}}|\uparrow\rangle_4 & \psi_{2sp_{2,4}}|\uparrow\rangle_4 & \psi_{2sp_{2,4}}|\uparrow\rangle_4 & \psi_{2p_{z4}}|\uparrow\rangle_4 \\ \psi_{1s_5}|\uparrow\rangle_5 & \psi_{1s_5}|\downarrow\rangle_5 & \psi_{2sp_{2,5}}|\uparrow\rangle_5 & \psi_{2sp_{2,5}}|\uparrow\rangle_5 & \psi_{2sp_{2,5}}|\uparrow\rangle_5 & \psi_{2p_{z5}}|\uparrow\rangle_5 \\ \psi_{1s_6}|\uparrow\rangle_6 & \psi_{1s_6}|\downarrow\rangle_6 & \psi_{2sp_{2,6}}|\uparrow\rangle_6 & \psi_{2sp_{2,6}}|\uparrow\rangle_6 & \psi_{2sp_{2,6}}|\uparrow\rangle_6 & \psi_{2p_{z6}}|\uparrow\rangle_6 \end{vmatrix}_{6\times 6}$$

But now when we consider the graphene's unit cell ,then it consists of two atoms having distinct valleys K,K' because the reciprocal lattice vector in the graphene's hexagonal lattice cannot trace K and K' valleys simultaneously.So we can write the ground state electronic configuration of the graphene's unit cell as, for one carbon atom having K valley forming three sigma bonds with neighbouring carbon atoms as,

$1s^2_{2,K}\,|\uparrow\downarrow\rangle$,$2sp^1_{2,K}\,|\uparrow\downarrow\rangle$,$2sp^1_{2,K}\,|\uparrow\downarrow\rangle$,$2sp^1_{2,K}\,|\uparrow\downarrow\rangle$,$2p^1_{z,K}\,|\uparrow\rangle$.

and for one carbon atom having K' valley forming three sigma bonds with the neighbouring carbon atoms as,

$1s^2_{2,K'}\,|\uparrow\downarrow\rangle$,$2sp^1_{2,K'}\,|\uparrow\downarrow\rangle$,$2sp^1_{2,K'}\,|\uparrow\downarrow\rangle$,$2sp^1_{2,K'}\,|\uparrow\downarrow\rangle$,$2p^1_{z,K'}\,|\uparrow\rangle$.

and hence the number of electrons are 17 (one electron shared in the sigma bond of this C-C unit cell) in graphene's one unit cell and hence,the slater determinant will contain 17 rows and 17 columns and it's solving terms linear combination will form a approximated ground state in Hatree Fock approximation of the graphene's unit cell.

$$\phi = \frac{1}{\sqrt{17!}}\begin{vmatrix} \psi_{1s_{1,K}}|\uparrow\rangle_1 & \psi_{1s_{1,K}}|\downarrow\rangle_1 & \psi_{2sp_{2,1,K}}|\uparrow\rangle_1 & \cdots & \psi_{2sp_{2,1,K'}}|\downarrow\rangle_1 & \psi_{2p_{z1,K'}}|\uparrow\rangle_1 \\ \psi_{1s_{2,K}}|\uparrow\rangle_2 & \psi_{1s_{2,K}}|\downarrow\rangle_2 & \psi_{2sp_{2,2,K}}|\uparrow\rangle_2 & \cdots & \psi_{2sp_{2,2,K'}}|\downarrow\rangle_2 & \psi_{2p_{z2,K'}}|\uparrow\rangle_2 \\ \vdots & \vdots & \vdots & \ddots & \vdots & \vdots \\ \psi_{1s_{16}}|\uparrow\rangle_{16} & \psi_{1s_{16,K}}|\downarrow\rangle_{16} & \psi_{2sp_{2,16,K}}|\uparrow\rangle_{16} & \cdots & \psi_{2sp_{2,16,K'}}|\downarrow\rangle_{16} & \psi_{2p_{z16,K'}}|\uparrow\rangle_{16} \\ \psi_{1s_{17}}|\uparrow\rangle_{17} & \psi_{1s_{17,K}}|\downarrow\rangle_{17} & \psi_{2sp_{2,17,K}}|\uparrow\rangle_{17} & \cdots & \psi_{2sp_{2,17,K'}}|\downarrow\rangle_{17} & \psi_{2p_{z17,K'}}|\uparrow\rangle_{17} \end{vmatrix}_{17\times 17}.$$

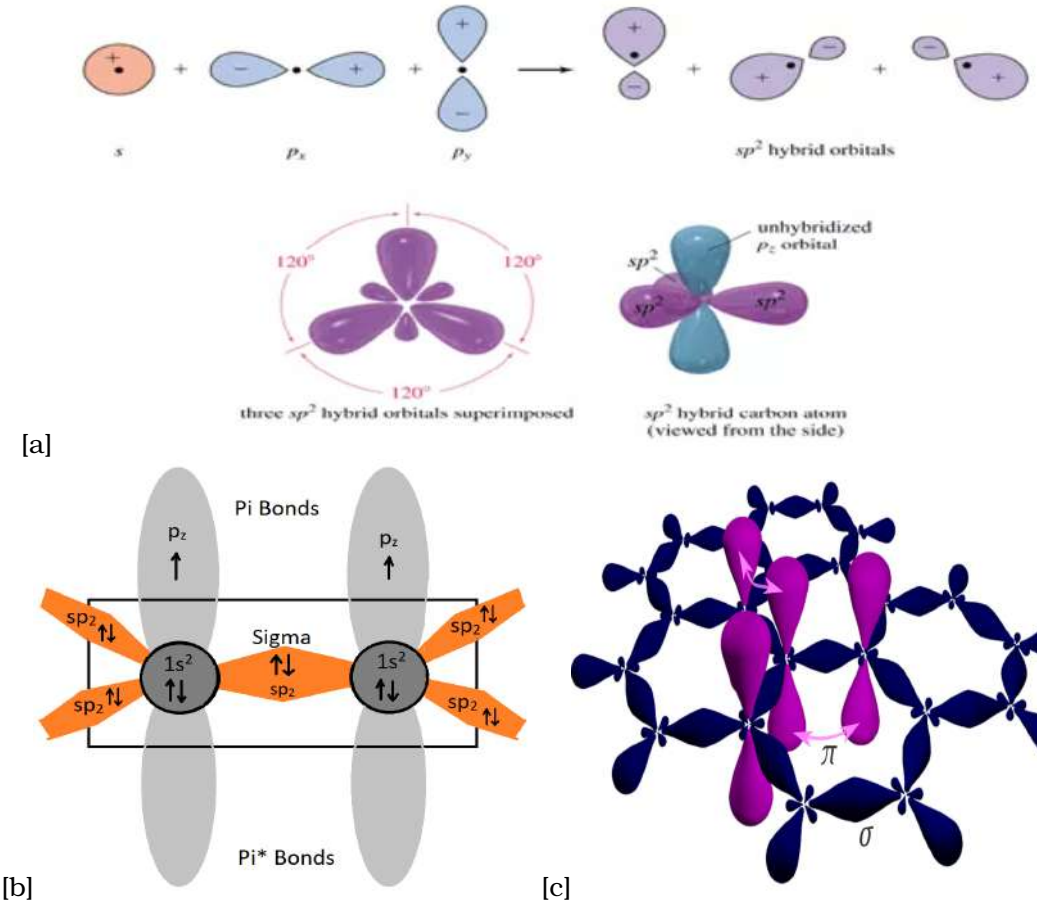

Figure 5.2: (a) sp^2 hybridization in carbon atom [3](b) Graphene Unit Cell (c) Graphene Sigma and Pi Bonds.[4]

From ground state electronic configuration we can get idea about 2D material's properties mainly,[2]

1.Electronic Energy, One point on Potential Energy Surface and hence the equilibrium geometry,reaction pathways etc.

2.Electrostatic Wave-function can give idea about dipole moment,polarizibility,electrostatic potential and other properties.

3.Orbitals (Chemistry of Bonding) and Orbital Energies.

4.Occupied and Unoccupied Orbital Energies.(Energies required to put an electron in and out of the orbitals).

How it relates to the Quantum Capacitance vs n plot is that the value of quantum capacitance ideally reduces to zero or to lowest value at the ground state electronic configuration of any 2D material as there are no charge carriers to conduct at n=0 in the graphene or any 2D material i.e we are at charge neutrality point. Therefore the lowest value of Quantum Capacitance in the Quantum Capacitance vs n plot is an indicator to identify whether the 2D material is in ground state electronic configuration or not and can hence used as a characterization tool to improve the ansatz for the ground state electronic configuration of any 2D material by reverse feedback

mathematics updating the ansatz.

Because we can get the energy eigen values from the Hamiltonian in the model for particular 2D material and from which we can explicitly get all the quantities including quantum capacitance mentioned here,hence quantum capacitance measurement itself can act as a tool to improve ansatz and give us the exact mathematical expression of Hamiltonian for any 2D material and understand the transport physics further. Once we get the exact transport Hamiltonian for any 2D material,then we can again exactly predict the ground state of any 2D material from Hatree Fock Approximation method by taking an ansatz as slater determinant's linear combination.

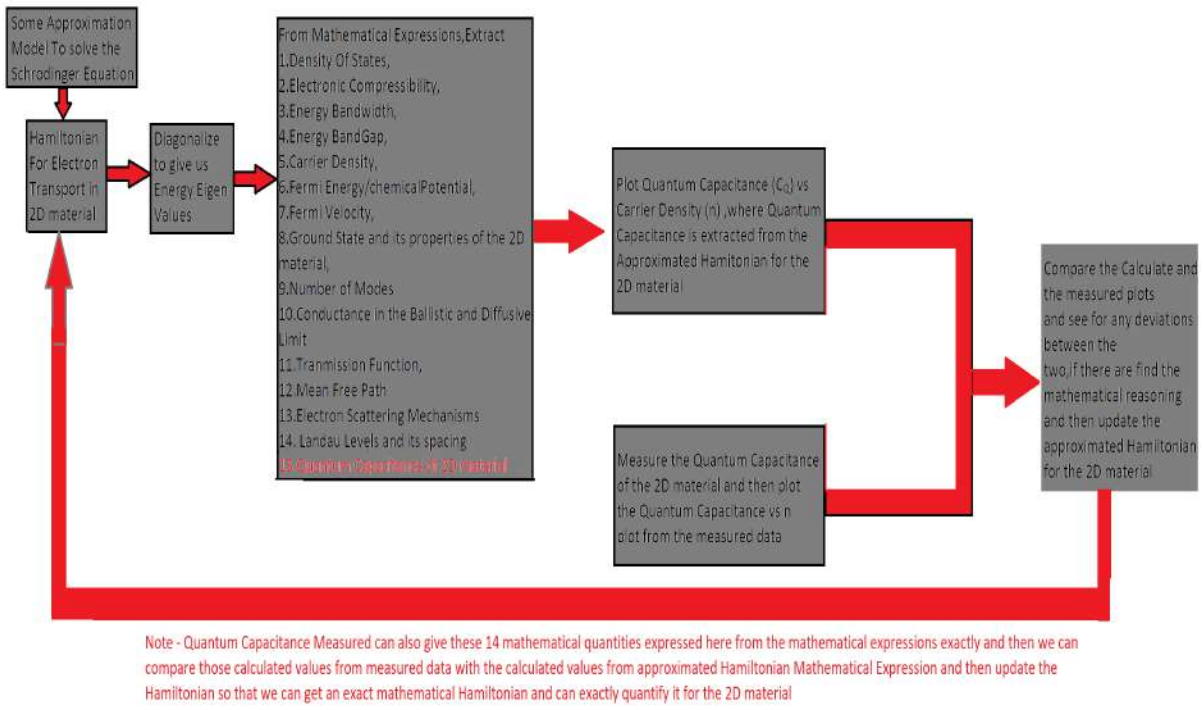

Figure 5.3: Quantum Capacitance Measured Data Process flow Schematic to exactly quantify the Hamiltonian of the 2D material and hence exactly understand the electronic transport in 2D material

Now,if we consider the electrical transport in 2D material at microscopic level, i.e for electric current to flow in 2D material there should be difference in the chemical potential spatially between these two points (i.e the quasi-Fermi Level is different for these two points) and the energy states of the flowing charge carriers is in between the two chemical potentials and the wave vector/k states allowed for the current to propogate in the form of modes is in the range of the extreme wave vectors allowed in between the two chemical potentials.To change the chemical potential of the 2D material spatially a potential difference in between the two contacts taken out from the conductor may be applied as shown in the figure below.Now we have to find the number of the modes in which the charge carriers can propogate in 2D material.

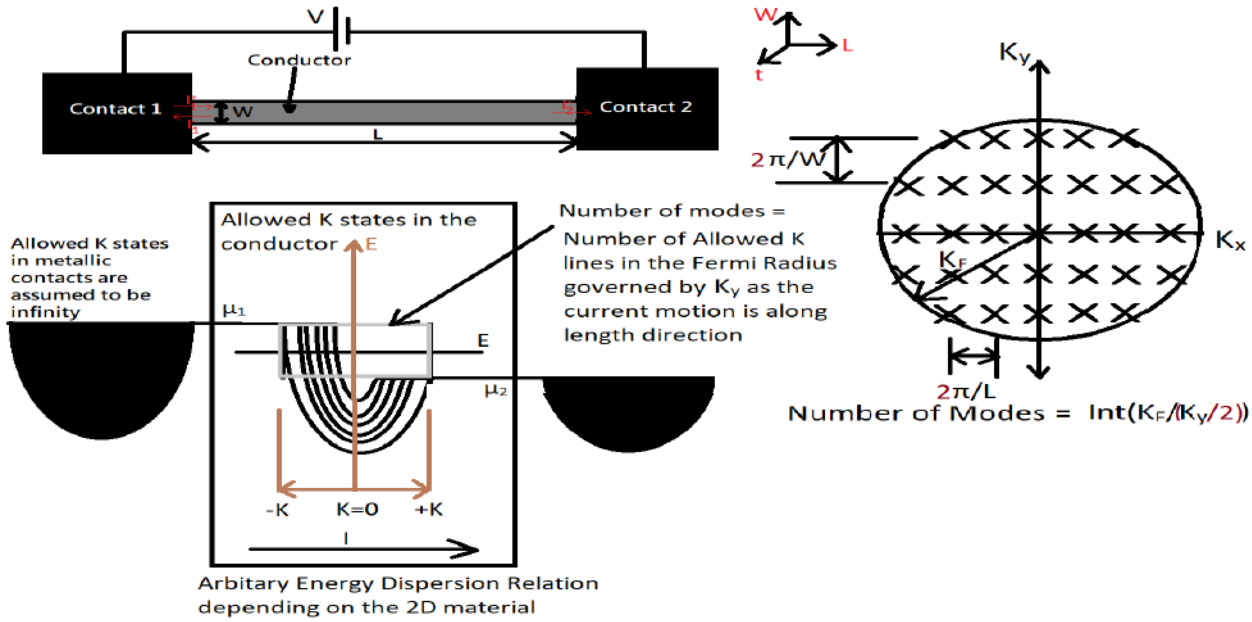

Figure 5.4: Number of Modes Pictorial Representation

Number of Modes in Transverse Direction for propogation of electrons in x direction by assuming a periodic boundary condition, M = Int($\frac{2K_F}{K_Y}$) = Int($\frac{K_F W}{\pi}$) , Now K_F is dependent on Fermi Energy which is further dependent on n i.e K_F = c*$(n)^{\text{some exponential Constant}}$.

Where Int represents the smaller Integer Value of the mode.

For graphene ,K_F = $\frac{E_F}{\hbar v_f}$ = $\frac{\sqrt{|n|}}{\sqrt{\pi}}$ = f(n)

Now, M = Int($\frac{K_F W}{\pi}$) = Int($\frac{f(n)W}{\pi}$)

Taking into account the spin degeneracy, M = 2Int($\frac{f(n)W}{\pi}$) for any 2D material in general.

More Formally total transverse modes can be expressed as summation of number of modes in k space in y direction above a certain minimum allowed threshold energy μ_2 in our case which again boils down to above equation when we apply the boundary condition. Refer [6] for more details.

Now,the Transmission function, can be simply defined as the probability that the electron when inserted in the metallic contact 1 will reach the metallic contact 2 i.e it will be 1 when the material do not undergo any electron scattering and reach the end and 0 when it back-scatters in between. In between the transport it may or may not forward scatter and hence it is probability and not a definite function.

T = $\frac{L_0}{L+L_0}$,

where L is the Length of the conductor and L_0 is the mean free path of the conductor. The mean free path of the conductor can then be further written as the product of the Fermi velocity and scattering time, and also in terms of linear density of scattering (ν) as,

L_0 = $\frac{T}{\nu(1-T)}$,where ν = N/L , where N is the number of scatterers.

Now we look at how to find the Transmission function from the experimental in plane resistance.From above we already have the neccessary data to find M.

Now the forward current if passed through contact 1 i.e ,

I_1^+ = (2e/h)M[$\mu_1 - \mu_2$] (assuming the number of modes are constant in the range μ_1 to μ_2 and ignoring the fermi function for simplicity i.e we are at zero Kelvin).

Now the forward current reached at contact 2 from contact 1 i.e the current measured,

I_2^- = (2e/h)MT($\mu_1 - \mu_2$)

Now the reflected current at contact 1 due to back-scattered electrons

I_1^- = (2e/h)M(1-T)($\mu_1 - \mu_2$)

Now the Conductance G of the 2D material in Diffusive limit i.e T is less than 1 i.e the length of the conductor is very much greater than mean free path of the conductor

$G_{\text{Diffusive conductor}} = \frac{I_2^-}{V} = \frac{I_2^-}{\triangle E_F/e} = (2e^2/h)MT$

The conductance of the 2D material in Ballistic Limit i.e length of the conductor is in orders of the mean free path i.e T = 1,

$G_{\text{Ballistic conductor}} = \frac{I_1^+}{V} = (2e^2/h)M$

Ideally the Resistance of the Ballistic Conductor would be zero i.e the conductance would be infinity as there is no scattering in the conductor,but this resistance is finite due to contact resistance which finally is inversely related to number of modes in the conductor.

Hence we can write the total resistance measured of the conductor between two contacts by passing a current and measuring the potential difference between the two contacts as,

$R_{total} = R_{\text{contacts}} + R_{\text{actual conductor}}$

$= \frac{1}{G_{\text{Ballistic conductor}}} + \frac{1-T}{G_{\text{Diffusive conductor}}}$

$R_{total} = (h/2e^2M) + (h/2e^2M)(\frac{1-T}{T})$

From the measured longitudinal resistance of the top 2D material we can get R_{top} vs $(V_{\text{top gate}} - V_{\text{Bottom gate}})$ plot and from that we can get R_{top} vs n_{top} and by curve fitting we can get exact values of number of modes and the transmission function and then from number of modes we can get the Fermi Wave Vector and from the transmission function we can get the mean free path of the top 2D material.

Also we are anyways measuring $R_{\text{bottom 2D}}$vs$n_{\text{bottom 2D}}$ of bottom 2D material to finally calculate the Quantum Capacitance of the top 2D material so we can also get M and T values of bottom 2D material.

Note - M is function of n but depending on type of scattering T (i.e L_0) may or may not be function of n.

Now to identify the type of scattering in 2D materials with graphene as reference material,[6]

1.Short Range Scattering => If the mean free path L_0 is inversely proportional to Fermi Energy E_F then the type of scattering is short range scattering.As if we increase the carrier density, the scatterer present in 2D material at some length x will cause electrons to scatter and the scattered electrons will again collide with the forward moving electrons and thus reduce the mean free path of the electrons.

2.Charged Impurity Scattering => If the mean free path is directly proportional to Fermi Energy E_F then the type of scattering is charged impurity scattering. As we increase the Fermi Potential i.e the carrier density ,the charge impurities will decrease in number as the charge carriers will repel/attract them and drive them out of the 2D material and hence mean free path will increase with Fermi Energy.

3.Electron Scattering by Phonons => Acoustic and Optical Phonon scattering independent of the Fermi Energy can occur in the 2D material which might be responsible for reduced conduc-

tivity of graphene above 300 K.

Now let's look at quantum Interference effect in 2D materials.The reflected electrons can interfere with the forward moving electrons,for example if the forward moving electrons wave-function where the probe is taken out is in the range of the reflected electrons then interference can cause the readings of the probing to deviate from the actual.These concepts of quantum interference and large mean free paths and phase relaxation lengths in graphene makes electron transport in graphene nano-ribbons as one of the platforms for realizing quantum gates and circuit and eventually quantum computation in graphene which is briefly discussed in chapter 1 Outlook.

For all the mathematical quantities derivation from eigen energy values in momentum space related to graphene as 2D material one can refer [6].And for more in detail discussions on conductance via transmissions in semiconductor refer [5].

Now coming to Landau Levels, when our heterostructure is subjected to a Transverse Magnetic Field,the charge neutrality point of the let's say bottom 2D material (the material that probes the Quantum Capacitance of the top 2D material) shifts from the original position as the magnetic field causes the Fermi Energy of the top 2D material to shift and hence the screening voltage potential across the top 2D material changes which causes values of the top gate potential and the bottom gate potential at which the charge neutrality occurs in the bottom 2D material to change and hence the slope of the charge neutrality line to change and finally the quantum capacitance of the top 2D material to change. So what does this transverse applied magnetic field do? In general as what we know from monolayer graphene ,it will cause the Energy levels to increase at constant n with some relation to applied transverse applied magnetic field (i.e theoritically ,E $\propto \sqrt{B}$ in case of graphene for constant n).This energy level that varies with applied transverse magnetic field is the Landau Level and the quantization of these energy levels in this phenomenon as we change n is called Landau Level Quantization and the spacing between two Landau Level is characterized by an integer number called as Filling Factor which is dependent on the number of degeneracies in top 2D material (for monolayer graphene that value is 4 due to spin and valley degeneracy).So experimentally to recognize this effect apply a transverse magnetic field of some magnitude and keep it constant and calculate the quantum capacitance of the top 2D material by measuring the local slope of the charge neutrality of the bottom 2D material and also measure the top 2D material's n value by Longitudinal Measurement for each charge neutrality point of bottom 2D material,now repeat the procedure for different B values and we will get C_Q vs n_T data of the top 2D material for different B values and then we can plot it for different B values and analyze the results of Quantum Capacitance variation of the top 2D material with transverse applied magnetic field for the top 2D material.

Now, also from above we can get the B vs n_T data and also B vs Net Gate Potential Data i.e B vs $(V_{BG} - V_{TL})_{\text{charge neutrality of the bottom layer}}$ data ,which we can plot to visualize the Landau Level Quantizations at integer filling factors spaced by number of degeneracies in top 2D material,the so called Landau Fan Diagrams.

Let's begin by calculating the filling factor (y) of our top 2D material,

y = $\frac{\text{Number of Charge Carriers in Total}}{\text{Number of Flux Quanta}}$

y = $\frac{(n_T+n_B)(A_{overlap})}{(\frac{BA_{overlap}}{\phi_0})}$

y = $\phi_0 \frac{(n_T+n_B)}{B}$

But we are at charge neutrality of the Bottom layer i.e n_B = 0

therefore, y = $\phi_0 \frac{(n_T)}{B}$

Now let's recall our capacitance model,the charge flow in the model is constant i.e Q = $e(n_T+n_B)$ = $e(n_T)$ at charge neutrality of the bottom layer.

Q = $e(n_T + n_B)$ = $(C_{\text{Q,top 2D}} V_{\text{across top 2D}})$ + $(C_{\text{Q,Bottom 2D}} V_{\text{across bottom 2D}})$ = $C_{total}(V_{BG} - V_{TL})$

Now let's review briefly what is total capacitance of our van der waal heterostructure.

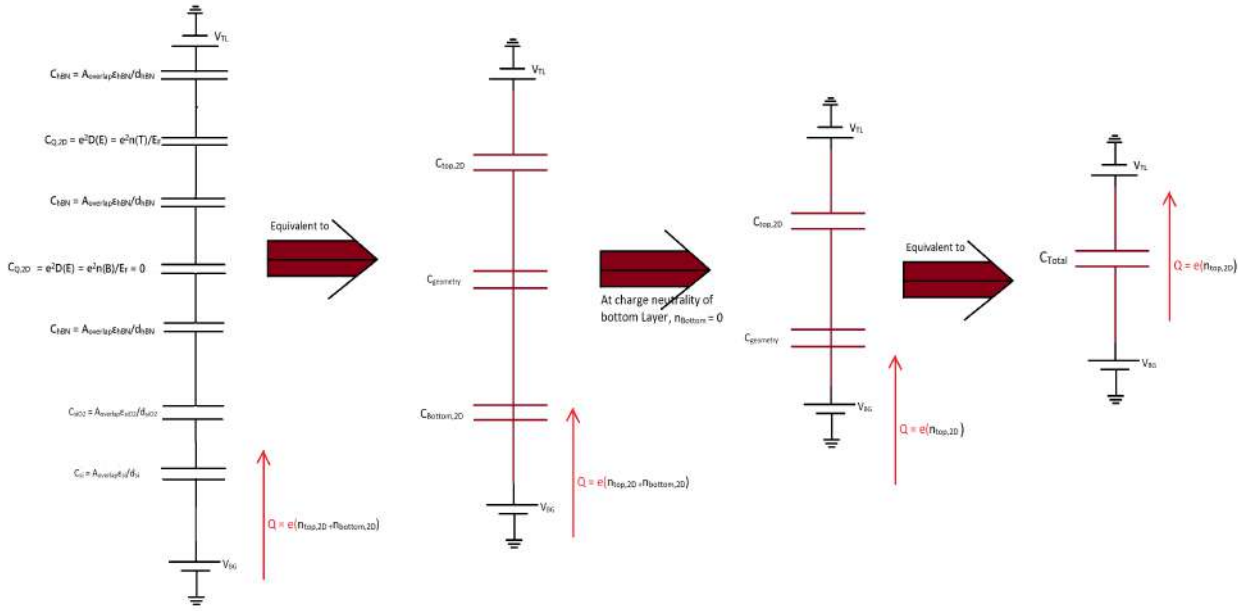

Figure 5.5: Equivalent Total and Geometric Capacitance Model of Van der waal Heterostructure

Now by simple Potential balance across our Van Der Waal Hetero-structure,

$V_{TL}-V_{BG}$ = $\triangle V_{\text{across Top hBN}}$ + $\triangle V_{\text{across Top 2D material}}$ + $\triangle V_{\text{across Intermediate hBN}}$ + $\triangle V_{\text{across Bottom 2D material}}$ + $\triangle V_{\text{Bottom Silicon Oxide}}$ + $\triangle V_{\text{Bottom n doped Silicon}}$

$\frac{e(n_T+n_B)}{C_{Total}}$ = $\frac{e(n_T+n_B)}{C_{\text{Top hBN}}}$ + $\frac{e(n_T)}{C_{\text{Top 2D material}}}$ + $\frac{e(n_T+n_B)}{C_{\text{Intermediate hBN}}}$ + $\frac{e(n_B)}{C_{\text{Bottom 2D material}}}$ + $\frac{e(n_T+n_B)}{C_{\text{Bottom hBN}}}$ + $\frac{e(n_T+n_B)}{C_{\text{Silicon Oxide}}}$ + $\frac{e(n_T+n_B)}{C_{\text{n doped Silicon}}}$

$\frac{e(n_T+n_B)}{C_{Total}}$ = $\frac{e(n_T)}{C_{\text{Top 2D material}}}$ + $\frac{e(n_T+n_B)}{C_{\text{Geometry}}}$ + $\frac{en_B}{C_{\text{Bottom 2D material}}}$

At charge neutrality point $Q_{\text{Bottom 2D material}} = 0$ as $n_B = 0$, hence its Quantum Capacitance effect is neglected in C_{Total} and cancelling the common en_T term of charge.

$\frac{1}{C_{Total}}$ = $\frac{1}{C_{\text{Top 2D material}}}$ + $\frac{1}{C_{\text{Geometry}}}$ => $C_{Total} \approx C_{Geometry}$ as Quantum Capacitance of 2D material is small compared to Geometry Capacitance of our Heterostructure.

Now coming back to our expression of filling factor,

y = $\phi_0 \frac{(n_T)}{B}$

y = $\phi_0 \frac{(\int_0^{(V_{TL}-V_{BG})_{\text{@ CNP of Bottom 2D}}} \frac{C_T}{(Ae)} dV)}{B}$

= $\phi_0 \frac{(\int_0^{(V_{\text{across top 2D material@ CNP of Bottom 2D}}} \frac{C_{Q,top2D}}{(Ae)} dV)}{B}$

Assuming a linear relation of top 2D material charge carrier density with Gating Potential,

y = $\phi_0 \frac{C_T}{(BAe)}(V_{TL} - V_{BG\text{@ CNP of Bottom 2D}})$ = $\phi_0 \frac{C_{Q,top2D}}{(BAe)}(V_{\text{across top 2D material}})$

Now we know all the quantities on the R.H.S i.e B (applied),ϕ_0 (constant),A (overlapping area from overlapping geometry of our heterostructure), $C_{Q,top2D}$ (mathematically calculated from measured data),$(V_{\text{across top 2D material}})$ is a difficult quantity to measure as we will require to probe

two contacts across our 2D material so it involves fabrication in between transfering our heterostrucutre,but we can calculate it mathematically by our model,as we know the Quantum Capacitance of our top 2D material and it's carrier density and hence we can get it by $\frac{e(n_T)}{C_{Q,top2D}}$ and hence get the filling factor from it.

Alternative to above equation is,we know the geometric capacitance of our van der waal Heterostructure by mathematically calculating it from $A\epsilon/d$ relation.Hence we can get the total capacitance value from it and then use y = $\phi_0 \frac{C_T}{(BAe)}(V_{TL} - V_{BG\text{@ CNP of Bottom 2D}})$ relation to find the filling factor and hence the number of degeneracies in our 2D material and the Landau Level Spacing from it. or alternative is to approximate C_T nearly equal to $C_{Geometry}$ and then find filling's factor's integer value.

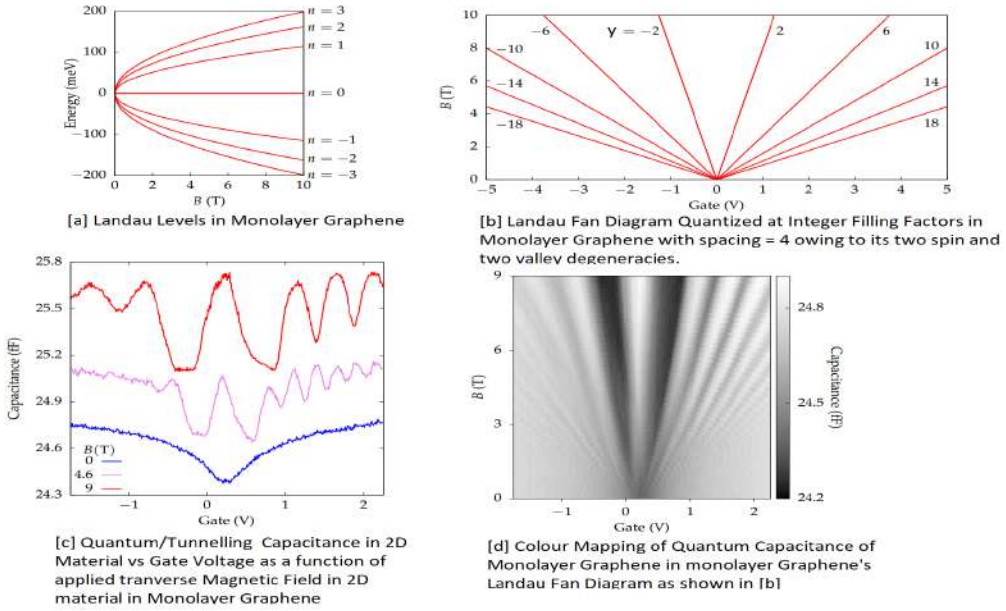

Figure 5.6: Landau Levels,Spacings,Quantum Capacitance as function of n by varying applied transverse magnetic field,Fan Diagrams of monolayer graphene [10].

5.2 Measurement

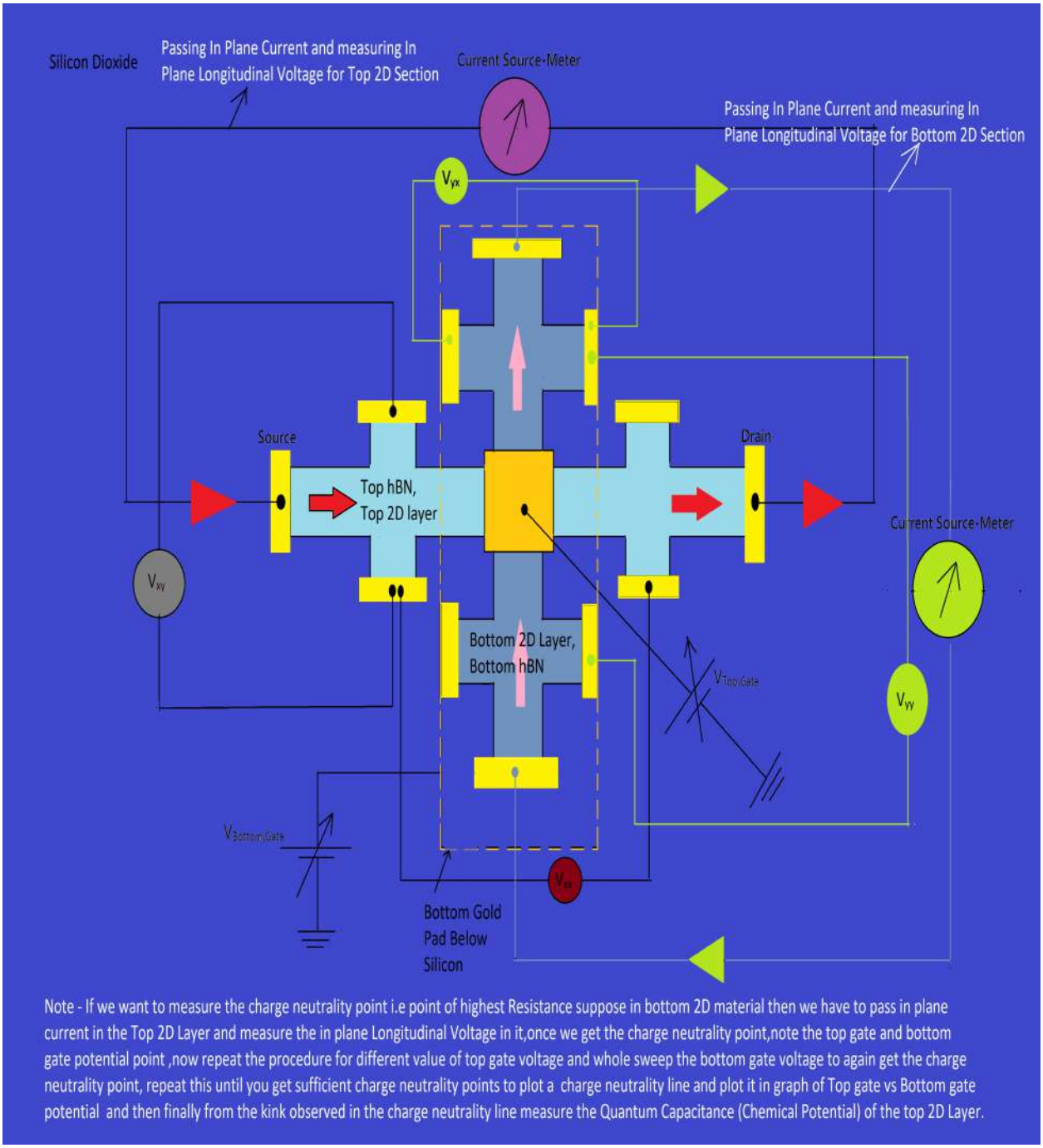

Figure 5.7: In Detail Hall Bar Geometry Schematic of In Plane Resistivity/Resistance Measurement Setup of top/bottom 2D material by keeping top potential constant and sweeping the bottom potential from - max to + max and again repeating the same process for different top gate potential to get a charge neutrality line and then Quantum Capacitance of bottom/top 2D material

Note - For in plane Resistivity measurement of our 2D material we use source meter that is responsible for introducing top and bottom gate voltages in our hetero-structure and in plane current which is passed in the 2D material layer and the Longitudinal Voltage measurement because of it is done by Lock In Amplifier as the magnitudes of longitudinal voltages ($10^{-7}V$) cannot be measured by conventional voltmeter and ammeter measurers.

Important Note - Also for particular charge neutrality point of let's say bottom 2D material we will require the value of the number of charge carriers introduced in the top layer so again we will have to perform the same in plane resistivity measurement of the top 2D material and note its resistivity at which the bottom layer is charge neutral and then from resistivity of top 2D material find the number of charge carriers (n) introduced in the top 2D material for each charge neutrality point or **we can calculate it mathematically from our model as** $(V_{BG} - V_{TL})$ **=** en_T/C_T **,assuming** C_T **=** C_{geo} **= constant i.e neglecting changes in the** C_T **because of quantum capacitance,so** $(V_{BG} - V_{TL}) \propto n_T$ **at charge neutrality point of the bottom 2D material.** This can be assumed so only when we have a hetero-structure of dielectric - 2D material - Dielectric - 2D material - Dielectric - SiO_2 - Si i.e we have one 2D material acting as a probe.For normal hetero-structure of Dielectric-2D material-Dielectric-Si-SiO_2 we cannot use this proportionality as we are neglecting the Quantum Capacitance of the 2D material we want to find.

5.3 General Basic Procedure and Work-Flow of Measurement

The first step about starting a measurement is to ground yourself to avoid your static potential interfering with the measurement setup in any way by rubbing the ground potential ribbon taken out from the ground terminal of any equipment on your body.Now after grounding yourself,for doing the measurement in the lab what we require first is checking resistance of the dipper connection of chip carrier on the dipper with the bread board.So first we will take the multi-meter ,set it to ohm range with sound selection on the multimeter and connect the one probe of the multi-meter to bread board and second end to the chip carrier on the dipper.So there will be 16 or 20 lines connected internally of the bread board to the chip carrier,now from multi-meter we are measuring the resistance of this internal connection by opening the contact on the bread board,so its resistance should be nearly equal to zero for all the 20 connections of the bread board on the dipper,if on multi-meter the connection shows high resistance then the internal connection of that particular port on bread board is damaged and we cannot use that as contact while inserting/mounting the chip carrier which contains the sample on the chip carrier of the dipper.Once we identify that all the connections are working,next step is mapping the connections of the chip carrier containing the sample to chip carrier containing the dipper rod.So what we can do is take an optical micro-graph of the sample and name the connections (number varies as per requirement of measurement but typically can be 20) of the gold contacts taken out from the sample and map it to the connection/contact of the bread board's 20 connections.This is because we are inserting the one end of coaxial cable in the bread board and second end in the equipments such as source meter,Lock In Amplifier etc. as per the mapping of the device and the type of measurement we want to do.Once the contact connection checking between the bread board and the chip carrier of the dipper is done,next step is to insert the chip carrier containing the sample in the chip carrier of the dipper as per the mapping.Also a dummy chip

carrier containing a dummy sample may be used to check the connections.So for our dipper in the nano-scale lab we had four contacts on bread board that were pre-utilized for temperature sensor,pressure sensor,etc ,so avoiding these four connections we have to insert the chip carrier containing the sample on the chip carrier of the dipper in accordance with the working connections of the dipper.Once the chip carrier containing the sample is inserted on the chip carrier on the dipper,next step to insert this dipper in the jacket of the cryo-stat rod carefully without hitting the walls of the jacket which might damage the sample and it's chip carrier.Next step is to vaccumize the dipper and the jacket to a pressure of some hecto-pascal (10^{-4} hPa to be exact below room pressure) .This is done to avoid air impurities affecting the measurements data and also at low temperature measurement there is chance of the air freezing and damaging the sample.Once that is done the probes i.e the coaxial cable are inserted from the equipments to the bread board as per the mapping and the type of measurement we want.So then the room temperature checking of the sample is done i.e for in-plane resistivity measurement we require six mapped working connections on the bread board,two for the top and bottom gate modulation from the source meter,two for in-plane voltage measurement,one for passing an in-plane current from Lock in amplifier and one for grounding.These equip-ments are connected to computer and the signal read on the equipments can directly be visualized by real time plotting of the data with the help of Lab View Application software that directly modulates the total bottom gate voltage sweep without us requiring to manually modulate it by changing the knob on the source meter.So once we look at the room temperature plot of the Resistance and the gate Potential which should peak to maximum at charge neutrality i.e near zero top and bottom gate potential we can verify where our 2D material in the hetero-structure is, is behaving correctly i.e all the procedures of characterization,transfer and device fabrication and measurement process went well. Now to reduce the thermal noise of the environment and explore the discrete electronic states of the 2D material and get a sound plot i.e without noise fluctuations,we will dip the dipper in the cryo-can containing liquid helium (near zero to 4K measurements) or liquid nitrogen (near 70 K) or we can have a separate thermodynamic cryogenic cycle (Vapour Compression Cycle) system consisting of compressor,condensor,Expansion valve and Evaporator which in our case is cryo-stat to achieve near zero Kelvin temperatures with Helium 4 and Helium 3 as the refrigerent for this cycle,then get the plot for the resistance vs gate voltage modulation and extract the quantum capacitance from it by the mathematical model as discussed earlier.

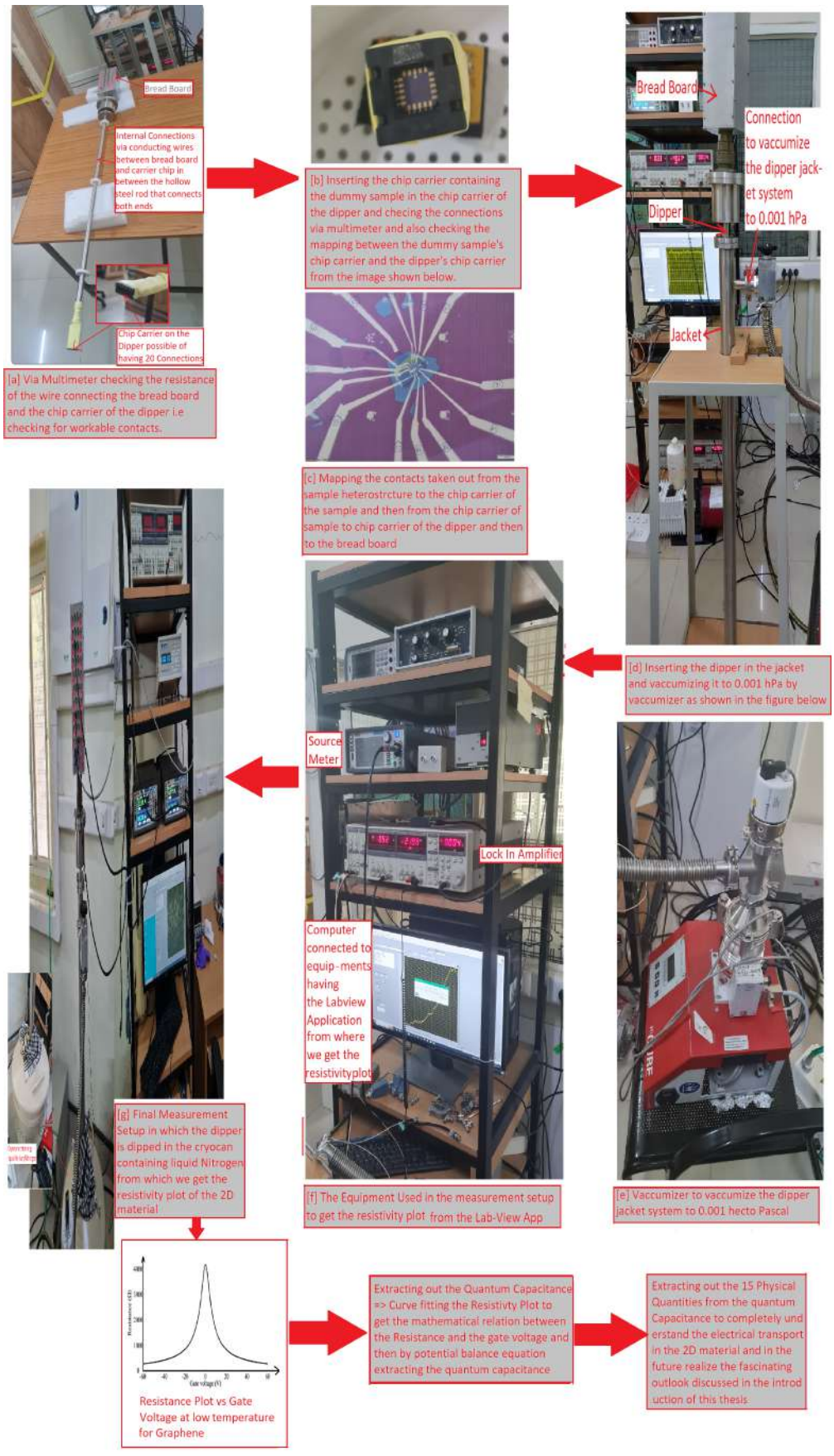

Figure 5.8: Measurement Work Flow for In plane resistivity measurement done in the IISc Nanoscale Device Fabrication Lab

Explanation of the Equip-ments Used (Review Cryogenics and its Operation Cycle later).

5.4 Interpretation of the Compressibility,Quantum Capacitance Data Plots.

[Future Scope of Work]

1.Many Body Interpretations.

2.Realizing and Interpreting the 1.Superconductivity 2.Magnetism (orbital and Spin) and Anti-Magnetism 3.Spin Orbit Coupling 4.Quantum Hall Effect A.Quantum Anamolous Hall Effect B.Quantum Spin Hall Effect 5.Corelated,Mott Insulators,Topological Insulators,Fractional Chern Insulators 6.Charge Density Wave Fluctuations 7.Nemacity 8.Pomeranchuk Effect 9.Many Body Interactions and Interpretations from the Quantum Capacitance vs n and quantum capacitance vs Fermi Energy or 2D material Potential plot,Compressibility vs n plot etc.

Chapter 6

Mathematical Models and Experiments on Correlated Phenomenons in 2D materials

(Future Scope of Work)

1.Superconductivity
2.Magnetism (orbital and Spin)
3.Spin Orbit Coupling and Quantum Hall Effect
A.Quantum Anamolous Hall Effect
B.Quantum Spin Hall Effect
4.Corelated,Mott Insulators,Topological Insulators,Fractional Chern Insulators
5.Charge Density Wave Fluctuations
6.Nemacity
7.Pomeranchuk Effect
8.Many Body Interactions and Interpretations

Conclusion

We have successfully discussed the Probing of the 2D materials using various microscopy techniques and extracted out some dope quantities like Fermi Velocity,Fermi Energy,Phonon Velocity,Twist Angle,Thickness,Defect Characterization,etc. from Raman Spectroscopy and thickness of graphene and hBN from its optical contrast in Microscopy technique for our transfered heterostructure.Moving on we have successfully extracted out Quantum Capacitance for our Dielectric-2D material-Dielectric hetero-structure on $Si - SiO_2$ substrate by novel way and for graphene as 2D material's inplane resistivity measurement and from extracted quantum capacitance calculated close to 15 physical quantities and all of them successfully match the already available data for graphene both extracted theoretically from energy eigen values and experimentally via various in plane measurement technique suggesting that this novel technique of extracting quantum capacitance is 100 percent accurate and a majority improvement over the already available complex techniques of 1.constructing dielectric-2D material (whose quantum capacitance we want to measure)-dielectric-2D material (probes the top 2D material via its charge neutrality point)-dielectric using transfer technique and then carrying out in plane resistivity measurement of two Hall bar 2D material layers and 2.Making hardware changes in the capacitance measurement circuit using HEMT's to reduce its parasitic capacitance.This novel technique of extracting quantum capacitance can be applied for any 2D material and also the expressions discussed are general and not in any way specific to graphene and hence one can extract and completely characterize the electron transport of any 2D material using this technique and can move one step closer to observing more interesting phenomenons in 2D materials and finally find more suitable 2D material candidates for realizing the fascinating outlook's discussed in Introduction,for example TBG's magic angle graphene's superconductivity phenomenon can be one of the material to characterize and realize a room temperature room pressure superconductivity,Negative compressibilities in graphene can be one of the candidates in realizing Negative capacitances which will be tremendously beneficial for CMOS industry,Quantum Memory Devices realization in TBG's,Quantum Computing Scaling up by using the Ballistic transport in graphene etc.

Reference Citations

6.1 Introduction

1.D. Dragoman, "Quantum computing with graphene devices," 2016 International Semiconductor Conference (CAS), Sinaia, Romania, 2016, pp. 3-9, doi: 10.1109/SMICND.2016.7783024.

2.M. Dragoman, A. Dinescu and D. Dragoman, "Wafer-Scale Fabrication and Room-Temperature Experiments on Graphene-Based Gates for Quantum Computation," in IEEE Transactions on Nanotechnology, vol. 17, no. 2, pp. 362-367, March 2018, doi: 10.1109/TNANO.2018.2803079.

3.Akshay Patil (2022)."Moire Superlattice-Twisted Bilayer Graphene". IAP,IISc Bengaluru,India.

4.Akshay Patil (2022)."Ferro-Electric Negative Capacitances". IAP,IISc Bengaluru,India.

6.2 Probing/Characterization of 2D materials using Microscopy and Spectroscopy Techniques.

6.2.1 ARPES

-

1.Park, Cheol-Hwan Giustino, Feliciano Spataru, Catalin Cohen, Marvin Louie, Steven. (2009). Angle-Resolved Photoemission Spectra of Graphene from First-Principles Calculations. Nano letters. 9. 4234-9. 10.1021/nl902448v.

2.Topological quantum matter - Weizmann online,"ANGULAR RESOLVED PHOTO-EMISSION SPECTROSCOPY (ARPES)." Youtube Video, 11:39. April 12,2022. $https://www.youtube.com/watch?v = zZul8Y036qAt = 440s.$

3.Department of Theoretical Physics, TIFR,"Study of Dirac Electrons in BiPd and Graphene using Angle-Resolved Photoemission Spectroscopy." Youtube Video, 1:12:07. December 18,2020. $https://www.youtube.com/watch?v = YRVLV0Ar0SMt = 3541s.$

4.Vishik Lab,"Lecture 4 introduction to ARPES." Youtube Video, 1:08:59 . June 19,2021. $https://www.youtube.com/watch?v = RC7L3v4FET8t = 3671s.$

5.Center for Integrated Quantum Materials,"Jyoti Katoch: Probing 2D materials using focused angle-resolved photoemission spectroscopy." Youtube Video, 53:48 . February 18,2021. $https://www.youtube.com/watch?v = o6Y6naPnve0.$

6.Ohta T, Bostwick A, Seyller T, Horn K, Rotenberg E. Controlling the electronic structure of bilayer graphene. Science. 2006 Aug 18;313(5789):951-4. doi: 10.1126/science.1130681.

PMID: 16917057.

7.Eli Rotenberg,Dr. Aaron Bostwick, Dr. Taisuke Ohta "Bandstructure and Spectral Function of Single and Bilayer Graphene Measured by ARPES." $https://www.pks.mpg.de/\ coqusy06/SLIDES$ /rotenberg.pdf.

8.Andrei, Eva Li, Guohong Du, Xu. (2012). Electronic properties of graphene: A perspective from scanning tunneling microscopy and magnetotransport. Reports on progress in physics. Physical Society (Great Britain). 75. 056501. 10.1088/0034-4885/75/5/056501.

9.Bostwick, Aaron Ohta, Taisuke Seyller, Thomas Horn, Karsten Rotenberg, Eli. (2006). Experimental Determination of the Spectral Function of Graphene.

6.2.2 Optical Microscopy (OM)

1.Blake, P. Novoselov, K. Castro Neto, Antonio Jiang, Dingde Yang, Rongduan Booth, Timothy Geim, A. Hill, Ernie. (2007). Making graphene visible. Applied Physics Letters. 91. 10.1063/1.2768624.

2.Duhee Yoon, Hyerim Moon, Young-Woo Son, Jin Sik Choi, Bae Ho Park, Young Hun Cha, Young Dong Kim, and Hyeonsik Cheong. (2009).Interference effect on Raman spectrum of graphene on SiO_2/Si. Phys. Rev. B 80, 125422.

3.Andrei, Eva Li, Guohong Du, Xu. (2012). Electronic properties of graphene: A perspective from scanning tunneling microscopy and magnetotransport. Reports on progress in physics. Physical Society (Great Britain). 75. 056501. 10.1088/0034-4885/75/5/056501.

4.Gorbachev, Roman Riaz, Ibtsam Raveendran-Nair, Rahul Jalil, Rashid Britnell, Liam Belle, B. Hill, Ernie Novoselov, K. Watanabe, K Taniguchi, Takashi Geim, A. Blake, P.. (2010). Hunting for Monolayer Boron Nitride: Optical and Raman Signatures.

6.2.3 Scanning Electron Microscopy (SEM)

1.Andrei, Eva Li, Guohong Du, Xu. (2012). Electronic properties of graphene: A perspective from scanning tunneling microscopy and magnetotransport. Reports on progress in physics. Physical Society (Great Britain). 75. 056501. 10.1088/0034-4885/75/5/056501.

2.Tonya Coffey, "Scanning Electron Microscopy (SEM) Basics." Youtube Video, 30:39 . June 16,2017. $https://www.youtube.com/watch?v=d7ch1XSmOgI$.

3.Hiura, Hidefumi Miyazaki, Hisao Tsukagoshi, Kazuhito. (2010). Determination of the Number of Graphene Layers: Discrete Distribution of the Secondary Electron Intensity Derived from Individual Graphene Layers. Apex. 3. 095101. 10.1143/APEX.3.095101.

6.2.4 Transmission Electron Microscopy (TEM)

1.Tonya Coffey, "Transmission Electron Microscopy (TEM) Basics." Youtube Video, 29:07 . June 16,2017. $https://www.youtube.com/watch?v=d7ch1XSmOgI$.

2.Andrei, Eva Li, Guohong Du, Xu. (2012). Electronic properties of graphene: A perspective from scanning tunneling microscopy and magnetotransport. Reports on progress in physics. Physical Society (Great Britain). 75. 056501. 10.1088/0034-4885/75/5/056501.

3.NPTEL-NOC IITM,"Transmission Electron Microscopy of Carbon Materials." Youtube Video, 56:59 . April 13,2021. $https://www.youtube.com/watch?v=pXxL7F-MNpY$.

4.Robertson, Alex Warner, Jamie. (2013). Atomic resolution imaging of graphene by transmission electron microscopy. Nanoscale. 5. 10.1039/c3nr00934c.

5.Bachmatiuk, Alicja Zhao, Jiong Gorantla, Sandeep Gonzalez Martinez, Ignacio Wiedermann, Jerzy Lee, Changgu Eckert, Jürgen Rümmeli, Mark. (2014). Low Voltage Transmission Electron Microscopy of Graphene. Small. 11. 10.1002/smll.201401804.

6.2.5 Scanning Probe Microscopy (SPM)

1.Andrei, Eva Li, Guohong Du, Xu. (2012). Electronic properties of graphene: A perspective from scanning tunneling microscopy and magnetotransport. Reports on progress in physics. Physical Society (Great Britain). 75. 056501. 10.1088/0034-4885/75/5/056501.

2.Musumeci, Chiara. (2017). Advanced Scanning Probe Microscopy of Graphene and Other 2D Materials. Crystals. 7. 216. 10.3390/cryst7070216.

3.Nanosurf AG. "Evaluating AFM as an analysis tool for graphene".
$https://www.nanosurf.com/images/applications/Evaluation$

4.Tautz, Pamela. (2011). Scanning Probe Microscopy of Graphene. 1044-.

5.nanohubtechtalks,"Overview of Scanning Probe Microscopy (SPM)." Youtube Video, 1:08:47 . April 13,2016. $https://www.youtube.com/watch?v=hnhv40Q0fCQ$

6.2.6 Raman Microscopy (RM)

1.Ferrari, AC Meyer, Jannik Scardaci, Vittorio Casiraghi, C Lazzeri, Michele Mauri, Francesco Piscanec, S Jiang, Dingde Novoselov, K Roth, Siegmar Geim, AK. (2006). Raman Spectrum of Graphene and Graphene Layers. Physical review letters. 97. 187401. 10.1103/PhysRevLett.97.187401.

2.Xin, Cong Wu, Jiangbin Lin, Miao-Ling Xuelu, Liu Shi, Wei Venezuela, Pedro Tan, Ping-Heng. (2018). Anti-Stokes Raman scattering in mono- and bilayer graphenes. Nanoscale. 10. 10.1039/C8NR04554B.

3.Moutinho, Marcus Venezuela, Pedro Pimenta, Marcos. (2021). Raman Spectroscopy of Twisted Bilayer Graphene. C. 7. 10. 10.3390/c7010010.

4.Wu, Jiangbin Lin, Miao-Ling Xin, Cong Liu, Henan Tan, Ping-Heng. (2018). Raman spectroscopy of graphene-based materials and its applications in related devices. Chemical Society Reviews. 47. 10.1039/C6CS00915H.

5.Basko, D. Piscanec, S. Ferrari, A.. (2009). Electron-electron interactions and doping dependence of the two-phonon Raman intensity in graphene. Physical Review B. 80. 10.1103/PhysRevB.80.165413.

6.Duhee Yoon, Hyerim Moon, Young-Woo Son, Jin Sik Choi, Bae Ho Park, Young Hun Cha, Young Dong Kim, and Hyeonsik Cheong. (2009).Interference effect on Raman spectrum of graphene on SiO_2/Si. Phys. Rev. B 80, 125422.

7.Gorbachev, Roman Riaz, Ibtsam Raveendran-Nair, Rahul Jalil, Rashid Britnell, Liam Belle, B. Hill, Ernie Novoselov, K. Watanabe, K Taniguchi, Takashi Geim, A. Blake, P.. (2010). Hunting for Monolayer Boron Nitride: Optical and Raman Signatures.

8.The Graphene Council,"RAMAN SPECTROSCOPY MASTER CLASS." Youtube Video, 1:35:18 . Sept 14,2022. $https://www.youtube.com/watch?v=6NbO4U41SkA$

9.NPTEL IIT Guwahati,"Lec 6: Raman Spectroscopy." Youtube Video, 1:18:14 . December 29,2021. $https://www.youtube.com/watch?v=6NbO4U41SkA$

10.NPTEL-NOC IITM,"Raman Spectroscopy of Carbon Materials." Youtube Video, 35:35 . April 13,2021. $https://www.youtube.com/watch?v=6NbO4U41SkA$

11.Heo, Gaeun Kim, Yong Chun, Seung-Hyun Seong, Maeng-Je. (2015). Polarized Raman spectroscopy with differing angles of laser incidence on single-layer graphene. Nanoscale Research Letters. 10. 10.1186/s11671-015-0743-4.

12.Das, A Chakraborty, Biswanath Piscanec, S. Pisana, S. Sood, A. Ferrari, A.. (2008). Phonon renormalisation in doped bilayer graphene. Phys Rev B. 79

13.Gadelha, Andreij Ohlberg, Douglas Rabelo, Cassiano Silva, Eliel Vasconcelos, Thiago Campos, Joao Luiz Lemos, Jéssica Ornelas, Vinícius Miranda, Daniel Nadas, Rafael Santana, Fabiano Watanabe, Kenji Taniguchi, Takashi Van Troeye, Benoit Lamparski, Michael Meunier, Vincent Nguyen, Viet-Hung Paszko, Dawid Charlier, Jean-Christophe Jorio, Ado. (2021). Localization of lattice dynamics in low-angle twisted bilayer graphene. Nature. 590. 405-409. 10.1038/s41586-021-03252-5.

14.Campolina, Tiago Gadelha, Andreij Ohlberg, Douglas Watanabe, Kenji Taniguchi, Takashi Medeiros-Ribeiro, Gilberto Jorio, Ado Campos, Leonardo. (2022). Raman spectra of twisted bilayer graphene close to the magic angle.

6.3 Capacitance Measurement Of Any 2D Material

1.Seyoung Kim (2012). Electron Transport in Graphene Transistors and Heterostructures: Towards Graphene-based Nanoelectronics, The University of Texas,Austin.

Retrieved from,https://repositories.lib.utexas.edu/bitstream/handle/2152/ETD-UT-2012-05-5420/KIM-DISSERTATION.pdf?sequence=1.

2.Tomarken, Spencer. (2019). Thermodynamic and tunneling measurements of van der Waals heterostructures.

6.4 Van der Waal Heterostructure Stack Making and Device Fabrication

6.4.1 Van der Waal Heterostructure Stack Making

1.Rudrapati, Ramesh. (2020). Graphene: Fabrication Methods, Properties, and Applications in Modern Industries. 10.5772/intechopen.83309.

2.Kamta, Yannick. (2022). Graphene Exfoliation from HOPG Using the Difference in Binding Energy between Graphite, Graphene and a Substrate. 10.5772/intechopen.107142.

3.Urade, Akanksha Lahiri, Indranil Suresh, K.. (2022). Graphene Properties, Synthesis and Applications: A Review. JOM. 10.1007/s11837-022-05505-8.

4.Moon, Ji-Yun Kim, Minsoo Kim, Seung-Il Xu, Shuigang Choi, Jun-Hui Whang, Dongmok Watanabe, Kenji Taniguchi, Takashi Park, Dong Seo, Juyeon Cho, Sung Son, Seok-Kyun Lee, Jae Hyun. (2020). Layer-engineered large-area exfoliation of graphene. Science Advances. 6. eabc6601. 10.1126/sciadv.abc6601.

5.Ye, Xiaohui Huang, Ting Lin, Zhe Zhong, Minlin Li, Lin Yan, Yinzhou Zhu, Hongwei. (2013). Lap joining of graphene flakes by current-assisted CO2 laser irradiation. Carbon. 61. 329-335. 10.1016/j.carbon.2013.05.012.

6.Nagashio, Kosuke Yamashita, T. Nishimura, T. Kita, K. Toriumi, A.. (2011). Electrical transport properties of graphene on SiO2 with specific surface structures. Journal of Applied Physics - J APPL PHYS. 110. 10.1063/1.3611394.

7.Song, Jianguo Wang, Xinzhi Chang, Chang-Tang. (2014). Preparation and Characterization of Graphene Oxide. Journal of Nanomaterials. 2014. 1-6. 10.1155/2014/276143.

8.Fan, Sidi Vu, Quoc Tran, Minh Adhikari, Subash Lee, Young Hee. (2020). Transfer assembly for two-dimensional van der Waals Heterostructures. 2D Materials. 7. 10.1088/2053-1583/ab7629.

9.Bhuyan, Md Sajibul Alam Uddin, Md Islam, Md Maksudul Bipasha, Ferdaushi Hossain, Sayed. (2016). Synthesis of graphene. International Nano Letters. 6. 65-83. 10.1007/s40089-015-0176-1.

10.Yi, Min Shen, Zhigang. (2015). A review on mechanical exfoliation for scalable production of graphene. J. Mater. Chem. A. 3. 10.1039/C5TA00252D.

11.Megra, Yonas Lim, Soomook Lim, TaeGyeong Na, Seung Suk, Ji. (2021). Enhancement of the adhesion energy between monolayer graphene and SiO2 by thermal annealing. Applied Surface Science. 10.1016/j.apsusc.2021.151243.

12.Liu, ze Liu, Jefferson Cheng, Yi Li, Zhihong Wang, Li Zheng, Quan-shui. (2012). Interlayer binding energy of graphite: A mesoscopic determination from deformation. Physical Review B. 85. 10.1103/PhysRevB.85.205418.

13.Han, Yong Lai, King Chun Lii-Rosales, Ann Tringides, Michael C. Evans, James Thiel, Patricia. (2019). Surface energies, adhesion energies, and exfoliation energies relevant to copper-graphene and copper-graphite systems. Surface Science. 685. 10.1016/j.susc.2019.01.009.

14.S Ramachandra Bangari.(2021) .Exploring Electronic Properties Of Twisted Bilayer Graphene,IISc ,Benguluru,India.

15.Rokni, Hossein Lu, Wei. (2020). Direct measurements of interfacial adhesion in 2D materials and van der Waals heterostructures in ambient air. Nature Communications. 11. 10.1038/s41467-020-19411-7.

16.“The Process of Plasma Etching.” Accessed 10 th May 2023.https://tantec.com/the-process-of-plasma-etching/

17."The Complete Technical Guide for Adhesive Tape." Accessed 10th May 2023.

https://echotape.com/adhesive-tape-guides/complete-technical-guide-adhesive-tape/

18.Gao, Wei Xiao, Penghao Liechti, Kenneth Huang, Rui. (2014). Interfacial adhesion between graphene and silicon dioxide by density functional theory with van der Waals corrections. Journal of Physics D: Applied Physics. 47. 10.1088/0022-3727/47/25/255301.

19.Laturia, Akash Van de Put, Maarten Vandenberghe, William. (2018). Dielectric properties of hexagonal boron nitride and transition metal dichalcogenides: from monolayer to bulk. npj 2D

Materials and Applications. 2. 10.1038/s41699-018-0050-x.

20.Singh, Piyush Chauhan, Yogesh Agarwal, Amit Bhowmick, Somnath. (2016). Thickness and Stacking Dependent Polarizability and Dielectric Constant of Graphene–Hexagonal Boron Nitride Composite Stacks. The Journal of Physical Chemistry C. 120. 10.1021/acs.jpcc.6b05805.

21.Seyoung Kim (2012). Electron Transport in Graphene Transistors and Heterostructures: Towards Graphene-based Nanoelectronics, The University of Texas,Austin. Retrieved from

https://repositories.lib.utexas.edu/bitstream/handle

/2152/ETD-UT-2012-05-5420/KIM-DISSERTATION.pdf?sequence=1.

22.Iwasaki, Takuya Endo, Kosuke Watanabe, Eiichiro Tsuya, Daiju Morita, Yoshifumi Nakaharai, Shu Noguchi, Yutaka Wakayama, Yutaka Watanabe, Kenji Taniguchi, Takashi Moriyama, Satoshi. (2020). Bubble-Free Transfer Technique for High-Quality Graphene/Hexagonal Boron Nitride van der Waals Heterostructures. ACS Applied Materials Interfaces. 12. 10.1021/acsami.9b19191.

23.Kinoshita, Kei Moriya, Rai Onodera, Momoko Wakafuji, Yusai Masubuchi, Satoru Watanabe, Kenji Taniguchi, Takashi Machida, Tomoki. (2019). Dry release transfer of graphene and few-layer h-BN by utilizing thermoplasticity of polypropylene carbonate. npj 2D Materials and Applications. 3. 22. 10.1038/s41699-019-0104-8.

24.Xuguang Cao, Chengming Jiang, Dongchen Tan, Qikun Li, Sheng Bi, Jinhui Song, Recent mechanical processing techniques of two-dimensional layered materials: A review, Journal of Science: Advanced Materials and Devices, Volume 6, Issue 2, 2021, Pages 135-152, ISSN 2468-2179, https://doi.org/10.1016/j.jsamd.2021.01.005.

25."ADHESION OF POLYMERS." Accessed 17th May 2023.

https://www.polymerdatabase.com/polymer

26.Rullyani, Cut Sung, Chao Feng Lin, Hong-Cheu Chu, Chih-Wei. (2018). Flexible Organic Thin Film Transistors Incorporating a Biodegradable CO2-Based Polymer as the Substrate and Dielectric Material. Scientific Reports. 8. 10.1038/s41598-018-26585-0.

6.4.2 Device Fabrication

1.NPTEL-NOC IITM,"DR. MADHU THALAKULAM: mod03lec07 - Device Fabrication-Photolithography." Youtube Video, 40:28 . June 9,2021.

https://www.youtube.com/watch?v=urJ-ZoVi0uclist=WLindex=330t=7s.

2.NPTEL-NOC IITM,"DR. MADHU THALAKULAM:mod03lec08 - Device Fabrication-Electron-beam Lithography." Youtube Video, 36:45 . June 9,2021.

https://www.youtube.com/watch?v=-yNQanXZ0AI.

3.nptelhrd,"Prof. A.K. Ganguli:Mod-02 Lec-13 Lithography - I" Youtube Video, 52:52 . September 2,2014.

https://www.youtube.com/watch?v=ugif3s7a6h8.

4.nptelhrd,"Prof. A.K. Ganguli:Mod-02 Lec-14 Lithography - II" Youtube Video, 55:33 . September 2,2014.

https://www.youtube.com/watch?v=FOM7vYa-YAU.

5.Duke University - SMIF,"Dr. Nan Jokerst,Ms.Yun Chen :Introduction to EBL" Youtube Video, 16:52 . January 20,2020.

https://www.youtube.com/watch?v=Q4-HsS4eyOUlist=WLindex=273.

6.cmditr

,"Scott Braswell,E-Beam Lithography, Part 1" Youtube Video, 9:30 . April 6,2010.

https://www.youtube.com/watch?v=bvgITKqYpuYt=1s.

"Scott Braswell,E-Beam Lithography, Part 2" Youtube Video, 6:13 . April 6,2010.

https://www.youtube.com/watch?v=fZmC5xeHHawt=1s.

"Scott Braswell,E-Beam Lithography, Part 3" Youtube Video, 6:31 . June 4,2010.

https://www.youtube.com/watch?v=ktkDqofYfMYt=236s.

7.NPTEL - Indian Institute of Science, Bengaluru,"Dr.Hardik J.Pandya : 45 Details of Lithography, E-beam Lithography and Mask Aligner" Youtube Video, 43:45 . November 7,2020.

https://www.youtube.com/watch?v=p1J9cunG8Xc.

8.MIT.nano,"Dr.Mark Mondol,Dr.Juan Ferrera : A brief introduction to e-beam lithography", 1:05:06 . March 1,2023.

https://www.youtube.com/watch?v=yJF9s2MJLLMlist=WLindex=269.

9.nano@stanford,"Dr. James McVitte :Stanford Nanofabrication Facility: Dry Etching - Introduction (Part 1 of 4)" Youtube Video, 13:10 . December 8,2016.

https://www.youtube.com/watch?v=Q4-HsS4eyOUlist=WLindex=273.

nano@stanford,"Dr. James McVitte :Stanford Nanofabrication Facility: Dry Etching - Basics of Plasmas Types of Tools (Part 2 of 4)" Youtube Video, 23:17 . December 14,2016.

https://www.youtube.com/watch?v=5LZtsVI$_{R}g0list = WLindex = 331.$

nano@stanford,"Dr. James McVitte :Stanford Nanofabrication Facility: Dry Etching - Dry Etching Mechanisms (Part 3 of 4)" Youtube Video, 18:38 . December 19,2016.

https://www.youtube.com/watch?v=3CbqHWsYZ8clist=WLindex=332.

nano@stanford,"Dr. James McVitte :Stanford Nanofabrication Facility: Dry Etching - Choosing a Dry Etching Process Tool (Part 4 of 4)". Youtube Video, 18:57 . December 19,2016.

https://www.youtube.com/watch?v=dOoIHhcLWvAlist=WLindex=333.

10.Sam Zeloof,"Etching Silicon with Plasma - Reactive Ion Etching (RIE)".Youtube Video, 11:40 . June 27,2021.

https://www.youtube.com/watch?v=RoQgnC0Oz2klist=WLindex=281.

11.INUP - i2i,"Dr. Dhiman Mallick:Reactive Ion Etching". Youtube Video, 38:28 . February 8,2023.

https://www.youtube.com/watch?v=Epe-n1OfQOYlist=WLindex=334.

12.PhotofabricationEng,"The Etching Process". Youtube Video, 2:44 . August 15,2017.

https://www.youtube.com/watch?v=zkdQddMZSyMlist=WLindex=335.

13.Sungho Kim,"[|4.2] wet etching dry etching ion milling RIE Bosch process" Youtube Video , 18:41 . December 5,2022. (In Korean Language but slides in English).

https://www.youtube.com/watch?v=hh$_{V}8Gk9Zs8list = WLindex = 336.$

14.Inrfucirvine," Trion ICP / RIE Dry Etch - Standard Operating Procedures" Youtube Video , 14:37 . August 25,2015.

https://www.youtube.com/watch?v=dkMeB3CE7L8list=WLindex=337.

15.Gary Steele,"A practical introduction to some of the concepts of wire bonding". Youtube Video, 56:39 . August 31,2021.

https://www.youtube.com/watch?v=ReHQXlfWa-0list=WLindex=316.

16.WATCH LEARN 'N PLAY,"Lito Galera : WIRE BONDING (PART 1)". Youtube Video, 15:52 . January 9,2023.

https://www.youtube.com/watch?v=Xt0So1S76L0list=WLindex=317.

"Lito Galera : WIRE BONDING (PART 2)". Youtube Video, 23:20 . February 21,2023.

$https://www.youtube.com/watch?v = HyLH7hdc_W slist = WLindex = 318.$

17.Sam Zeloof,"Wire Bonding Basics - Manual Wedge Bonding ICs".Youtube Video, 11:40 . July 4,2019.

$https://www.youtube.com/watch?v = mvZ1dJuvenwlist = WLindex = 322.$

18.Practical Microfabrication,"Mr.Dan Haver : The Mysterious Secrets of Wedge Bonding".Youtube Video, 31:06 . May 5,2020.

https://www.youtube.com/watch?v=r5qehKvLo4Mlist=WLindex=324.

19.David Lindell,"Wedge Bonder Training Video".Youtube Video, 15:19 . August 10,2013.

https://www.youtube.com/watch?v=quA4INmeSbolist=WLindex=323.

20.Eric HITECH,"IC wirebonding, HITECH volume 2, 2017".Youtube Video, 17:33 . March 5,2017.

https://www.youtube.com/watch?v=4v3WfcDimsMlist=WLindex=325.

21.Eric HITECH,"IC DIE pick and place, Wire bonding recorded with high speed camera, by HI-TECH ELECTRONICS".Youtube Video, 7:38 . March 5,2017.

https://www.youtube.com/watch?v=0t7vYYejDzolist=WLindex=321.

22.Würth Elektronik Group,"Mr.Philip Conrad : Würth Elektronik Webinar: Wire bonding on PCBs, the perfect connection for unpackaged semiconductors".Youtube Video, June 3,2015.

https://www.youtube.com/watch?v=qzOpemvJG20list=WLindex=320.

23.Song, Li Balicas, L. Mowbray, Duncan Capaz, Rodrigo Storr, Kevin Ci, Lijie Jariwala, Deep Kurth, S. Louie, Steven Rubio, Angel Ajayan, Pulickel. (2012). Anomalous insulator-metal transition in boron nitride-graphene hybrid atomic layers. Physical Review B. 86. 075429. 10.1103/PhysRevB.86.075429.

6.5 Analysis,Measurements and Interpretations

1.Akshay Patil (2022)."Moire Superlattice-Twisted Bilayer Graphene". IAP,IISc Bengaluru,India.

2.David Sherrill,'Introduction to Computational Chemistry'-"Introduction to Hartree-Fock Molecular Orbital Theory Part 3" Youtube Video, 32:19 . February 10,2021.

https://www.youtube.com/watch?v=Ky1Kc9Sb54Mt=1590s.

3."Graphene." Accessed 6th June 2023.

https://en.wikipedia.org/wiki/Graphene

4."Hybrid orbitals." Accessed 6th June 2023.

https://www2.dawsoncollege.qc.ca/dbaril/NYA/Handout/$Hybrid_O rbitals/Hybrid_O rbitals.htm$

5.Supriyo Datta."Electronic Transport in Mesoscopic Systems".Chapter 2 - Conduction from Transmission.

6.Dionisis Berdebes, Tony Low, and Mark Lundstrom ."Low Bias Transport in Graphene : An Introduction",2009.Purdue University.

7.Sk Ashif Akram,"Slator Determinant Chemistry".November 13,2018.

https://www.scribd.com/document/393125260/Slater-Determinant-Chemisttry

8."Many Electron Atoms",Physical Chemistry Lecture 27,MIT.

https://ocw.mit.edu/courses/5-61-physical-chemistry-fall-2007/bdabd86227c9b892743040cc25025f8a$_{lect}$

9.David M. Hanson, Erica Harvey, Robert Sweeney, Theresa Julia Zielinski"Antisymmetric Wavefunctions can be Represented by Slater Determinants".

https://chem.libretexts.org/Courses/Pacific$_{U}nion_{C}ollege/Quantum_{C}hemistry/083A_{M}ultielectron_{A}toms/$

8.063A$_{A}ntisymmetric_{W}avefunctions_{c}an_{b}e_{R}epresented_{b}y_{S}later_{D}eterminants.$

10.Tomarken, Spencer. (2019). Thermodynamic and tunneling measurements of van der Waals heterostructures.